Designing Power Scheduling Algorithms for Electric Vehicles and Energy Storage Systems in Bi-Directional Markets Using Mixed-Integer Programming

By

Hooman Ekhteraei Toosi

A Thesis Submitted to Saint Mary's University, Halifax, Nova Scotia

in Partial Fulfillment of the Requirements for the Degree of PhD in Applied Science

May 2022, Halifax, Nova Scotia

Approved: Dr. Adel Merabet
Supervisor

Approved: Dr. Andrew Swingler
Committee Member

Approved: Dr. Jason Rhinelander
Committee Member

Approved: Dr. Hamed Aly
Committee Member

Approved: Dr. Rachid Errouissi
External Examiner

Date: May 27, 2022

Abstract

Application of Mixed Integer Programming in Designing Power Scheduling Algorithms for

Electric Vehicles and Energy Storage Systems in Bi-Directional Markets

By Hooman Ekhteraei Toosi

Optimal battery scheduling for electric vehicles and energy storage systems when cooperating with renewable energy generation in behind-the-meter applications is studied in this thesis in the framework of Mixed-Integer Programming (MIP). High capability in obtaining global optima in optimization problems has made MIP a popular tool in smart grid research and particularly for battery scheduling problems. One important issue with regards to the battery cycling, is the battery degradation which could complicate the Unit Commitment (UC) models. This is because the battery wear model can be nonlinear and difficult to be incorporated into a UC problem. To address the existing research gap, in this thesis a battery degradation model has been introduced to be incorporated into a short-term MIP battery scheduling model to estimate the capacity loss of a Li-ion battery caused by irregular charging and discharging events.

Hence, a MIP UC model is developed in this work which incorporates the introduced battery wear model. Based on that, the UC problem for a home-based microgrid is investigated and different UC strategies have been presented to minimize the operation cost as well as the capacity loss of batteries and the carbon footprint for a home equipped with a smart residential microgrid. The impact of the resolution of a home UC model on the capacity loss of batteries is another studied subject in this work, where hourly and intra-hourly granularities are compared in terms of the battery aging. A Controller-Hardware-in-the-Loop (C-HIL) setup is developed to measure the performance of the UC strategies as well as the battery degradation rates. Optimal battery scheduling in applications with multiple beneficiaries such as workplaces with electric vehicle (EV) charging stations is also investigated in this work by studying different UC strategies that take into account the interests of system operators and EV users to different extents. The results of this work show that the presented MIP UC models, that incorporate the introduced battery wear model, can be solved for real optimums in different smart grid applications.

May 2022

Designing Power Scheduling Algorithms for Electric Vehicles and Energy Storage Systems in Bi-Directional Markets Using Mixed-Integer Programming

By

Hooman Ekhteraei Toosi

A Thesis Submitted to Saint Mary's University, Halifax, Nova Scotia

in Partial Fulfillment of the Requirements for the Degree of PhD in Applied Science

May 2022, Halifax, Nova Scotia

Approved: Dr. Adel Merabet
Supervisor

Approved: Dr. Andrew Swingler
Committee Member

Approved: Dr. Jason Rhinelander
Committee Member

Approved: Dr. Hamed Aly
Committee Member

Approved: Dr. Rachid Errouissi
External Examiner

Date: May 27, 2022

Acknowledgments

I am genuinely grateful to my supervisor, Dr. Adel Merabet, for his invaluable supervision, support, and consideration during my PhD studies without which this work would not have been possible. I appreciate his continuous support and assistance as they have always been heartwarming for me in my professional and personal life.

I would like to extend my sincere thanks to my committee members, Dr. Andrew Swingler, Dr. Jason Rhinelander, and Dr. Hamed Aly for their guidance and assistance at every stage of my research project; and to Dr. Rachid Errouissi for serving as my external examiner and providing insightful comments on my work. I am also thankful to the members of the Laboratory of Control Systems and Mechatronics and the Division of Engineering at Saint Mary's University (SMU) for providing assistance with my studies and teachings at SMU.

I would like to express my deepest gratitude to my wife, Shadan, for her understanding and kind support throughout my studies. I truly appreciate her for all the efforts she has made alongside me, as well as the companionship and encouragement she has always provided for me. I am also very grateful to my parents for all their kind support during these years.

Table of Contents

List of Tables

List of Figures

List of Acronyms

MIP	Mixed-Integer Programming
UC	Unit Commitment
C-HIL	Controller-Hardware-in-the-Loop
EV	Electric Vehicle
ESS	Energy Storage System
PV	Photovoltaic
NREL	National Renewable Energy Laboratory
MG	Microgrid
EMS	Energy Management System
DR	Demand Response
BSS	Battery Storage System
DSM	Demand-Side Management
TOU	Time-of-Use
CPP	Critical Peak Pricing
RTP	Real-Time Pricing
IBR	Inclining Block Rate
HEMS	Home Energy Management System
AMI	Advanced Metering Infrastructure
DG	Distributed Generator
MILP	Mixed-Integer Linear Programming
MINLP	Mixed-Integer Nonlinear Programming
CHP	Combined Heat and Power
ROI	Return of Investment
AI	Artificial Intelligence
SoC	State of Charge
GUI	Graphical User Interface
MPP	Maximum Power Point
MPPT	Maximum Power Point Tracking
LP	Linear Programming
QP	Quadratic Programming
NP	Nonlinear Programming
CP	Convex Programming
DP	Dynamic Programming
IP	Integer Programming
PSO	Particle Swarm Optimization
GWO	Gray Wolf Optimization
GA	Genetic Algorithm
ANN	Artificial Neural Network
FL	Fuzzy Logic
GEMS	Grid Energy Management System
SST	Solid-State Transformer
ADMM	Alternating Direction Method of Multipliers
BMS	Battery Management System
LAM	Loss of Active Material
LLI	Loss of Lithium Inventory
LMO	Lithium-Manganese-Oxide
LCO	Lithium-cobalt-oxide
NCM	Nickel-Cobalt-Manganese
LFP	Lithium-Iron Phosphate
NCA	Nickel-Cobalt-Aluminum
SEI	Solid-Electrolyte Interphase
TMS	Thermal Management System
PLET	Peukert Lifetime Energy Throughput
RCA	Rainflow Counting Algorithm
PWM	Pulse Width Modulation
LCOE	Levelized Cost of Energy

Nomenclature

Parameter	Unit	Description
N	-	Number of intervals of a day
n_b	-	Interval corresponding with the beginning of the optimization horizon
n_e	-	Interval corresponding with the end of the optimization horizon
$P_{es}^{n,con}$	kW	The portion of the ESS power at the n_{th} interval which is consumed locally
$P_{es}^{n,ex}$	kW	The portion of the ESS power at the n_{th} Interval which is exported to the grid
$P_{es}^{n,dis}$	kW	The discharging power of ESS at the n_{th} Interval
η_{es}^{dis}	-	Discharging efficiency of the charging equipment
$P_{es}^{n,ch}$	kW	Charging power for charging the ESS at the n_{th} Interval
U_{es}^{n}	-	The n_{th} element of the charging array of ess
P_{es}^{ch}	kW	Maximum charging power of the ESS
P_{es}^{dis}	kW	Maximum discharging power of the ESS
SE_{es}^{n}	kWh	State of energy of ESS at the n_{th} Interval
η_{es}^{ch}	-	Efficiency of the charging process of ESS
G	$Hour$	Granularity or resolution of the model
SE_{es}^{ini}	kWh	Initial state of energy of ESS at the first interval of the model
SE_{es}^{max}	kWh	Maximum allowed amount of stored energy in the ESS
SE_{es}^{min}	kWh	Minimum allowed amount of stored energy in the ESS
n_a	-	The interval of EV's arrival
n_d	-	The interval of EV's departure
$P_{ev}^{n,con}$	kW	The portion of the EV power at the n_{th} interval which is consumed in the microgrid
$P_{ev}^{n,ex}$	kW	The portion of the EV power at the n_{th} Interval which is exported to the grid
$P_{ev}^{n,dis}$	kW	Discharging power of the EV battery at the n_{th} Interval
η_{ev}^{dis}	-	Discharging efficiency of the EV charging equipment
$P_{ev}^{n,ch}$	kW	Charging power of the EV battery at the n_{th} Interval
U_{ev}^{n}	-	The n_{th} element of the charging array of ev
P_{ev}^{ch}	kW	Maximum charging power of the EV battery
P_{ev}^{dis}	kW	Maximum discharging power of EV
SE_{ev}^{n}	kWh	State of energy of EV battery at the n_{th} Interval
η_{ev}^{ch}	-	Efficiency of the EV charging process
SE_{ev}^{ini}	kWh	Initial state of energy of the EV battery at the first interval
SE_{ev}^{max}	kWh	Maximum allowed amount of stored energy in the EV battery

SE_{ev}^{min}	kWh	Minimum allowed amount of stored energy in the EV battery
SE_{ev}^{ch}	kWh	User's desirable state of energy at the time of departure
$P_{pv}^{n,con}$	kW	PV power that is consumed locally at the n_{th} Interval
$P_{pv}^{n,ex}$	kW	The portion of the PV generation that is exported to the grid at the n_{th} Interval
$P_{pv}^{n,gen}$	kW	Total generated power of the PV array at the n_{th} Interval
η_{pv}	-	The efficiency of the PV system
P_{cl}^{n}	kW	Power of controllable load at the n_{th} interval
D_{cl}^{n}	-	The n_{th} element of the array that controls the operation status of controllable load
P_{cl}	kW	Nominal operating power of the controllable load
n_{cl}^{row}	-	Count of intervals in a row required for every operating iteration of controllable load
S_{cl}^{n}	-	The n_{th} member of the array associated with the start of the controllable load operation
F_{cl}^{n}	-	The n_{th} member of the array associated with the finish of controllable load operation
n_{cl}^{day}	-	Number of times that controllable load needs to function every day
P_{im}^{n}	kW	The power imported from the electric network
P_{ex}^{n}	kW	The power exported to the electric network
P_{l}^{n}	kW	Power consumption of regular load at the n_{th} interval
P_{im}^{max}	kW	Maximum allowed power that can be imported by the microgrid
U_{im}^{n}	-	n_{th} member of the power import array
P_{ex}^{max}	kW	Maximum power that can be exported to the grid
$T^{n,buy}$	$\$$	Buying tariff of energy unit
$T^{n,sell}$	$\$$	Selling tariff of energy unit
$P_{pv}^{n,gen}$	kW	Generated power of the photovoltaic system at the n_{th} interval
A_{array}	m^2	Area of the PV array
I^{n}	$\frac{kW}{m^2}$	Solar irradiance
η_{array}	-	Efficiency of the PV array
T	$°C$	Temperature
E_a	$Jmol^{-1}$	Activation energy of reaction
t	*Hour/Second*	Time
I	A	Discharge current of the battery
Q	kWh	Charge throughput of battery
D	-	Depth of discharge
N_D	-	Number of cycles that the battery can complete at DoD of D
Q_D	kWh	Lifetime energy throughput of the battery at DoD of D
ΔE_D	kWh	Capacity loss of battery caused by a completing a half cycle with DoD of D

V^{ini}	$\$$	Initial value of the battery
V^{sal}	$\$$	Salvage value of the battery
E^{ini}	kWh	Initial (rated) capacity of the battery
E	kWh	Available capacity of the battery
R	-	Remaining SoH at the time of replacement
Y_D	$\$$	Cost of capacity loss per every single half-cycle
ΔE^{total}	kWh	Total capacity loss during N intervals
ΔE^n	kWh	Capacity loss inflicted within the subinterval n
$\Delta E^n_{reg\ cycle}$	kWh	Capacity fade of the battery caused by completing the n_{th} regular cycle
ΔE^n_{reg}	kWh	Capacity loss of battery caused by completing the n_{th} regular half cycle
E^n	kWh	Battery capacity just before starting the n_{th} irregular half cycle
W_D	$\frac{kWh}{kWh}$	Wear coefficient corresponding with the DoD of D
α and β	-	Curve fitting parameters derived from applying exponential curve fitting to $N(D)$
ΔE^n_{ireg}	kWh	Capacity fade caused by completing the n_{th} irregular half cycle
D_b	-	DoD of the battery corresponding with its charge level at the beginning of a half cycle
D_e	-	DoD of the battery corresponding with its charge level at the end of a half-cycle
W_{D_b}	$\frac{kWh}{kWh}$	Wear coefficients corresponding with D_b
W_{D_e}	$\frac{kWh}{kWh}$	Wear coefficients corresponding with D_e
S_b	-	Soc corresponding with the beginning of the irregular half-cycle
S_e	-	Soc corresponding with the end of the irregular half-cycle
η	-	Efficiency of the charging process
SC^n_{ev}	-	Soc of the EV battery at the beginning of the n_{th} Interval
E^n_{ev}	kWh	Available energy capacity of EV battery at the beginning of the n_{th} Interval
D^n_{ev}	-	DoD associated with SC^n_{ev}
W^n_{ev}	$\frac{kWh}{kWh}$	Wear coefficient associated with D^n_{ev}
f	-	Function of the wear coefficient of the EV battery
ΔE^n_{ev}	kWh	Capacity fade of EV battery caused by the n_{th} Interval
L^n_{ev}	kWh	Absolute value of ΔE^n_{ev}
SC^n_{es}	-	Soc of ESS at the beginning of the n_{th} Interval

E_{es}^{n}	kWh	Available energy capacity of ESS at the beginning of the n_{th} Interval
D_{es}^{n}	-	DoD associated with SC_{es}^{n}
W_{es}^{n}	$\frac{kWh}{kWh}$	Wear coefficient associated with D_{es}^{n}
g	-	Function of the wear coefficient of ESS
ΔE_{es}^{n}	kWh	Capacity fade of ESS caused by the n_{th} Interval
L_{es}^{n}	kWh	Absolute value of ΔE_{es}^{n}
$L_{ev,life}$	-	Lifetime capacity fade of EV
E_{ev}^{ini}	kWh	Initial storage of EV battery
V_{ev}^{ini}	$\$$	Initial cost of the EV battery
V_{ev}^{sal}	$\$$	Salvage cost of the EV battery
$L_{es,life}$	-	Lifetime capacity fade of ESS
E_{es}^{ini}	kWh	Initial storage of ESS
V_{es}^{ini}	$\$$	Initial cost of ESS
V_{es}^{sal}	$\$$	Salvage cost of ESS
E_{ev}^{opt}	kWh	Available capacity of EV battery for the next optimization
E_{es}^{opt}	kWh	Available capacity of ESS for the next optimization
O	-	Set of the total optimization iterations
CF_H	kg	Carbon emission per one kWh of energy consumption from the grid
HE	kg	Apparent carbon emission of home
CF_U	kg	Carbon emission associated with 1kwh capacity loss
CF_M	$\frac{kg}{kWh}$	Carbon emitted by the battery maker for manufacturing one kilowatt-hour of battery capacity
SE_{es}^{end}	kWh	Expected SoE of the ESS at the end of the optimization horizon
M	-	Set of electric vehicles
m	-	Index of electric vehicle

Chapter 1: Introduction

1.1 Microgrid unit commitment problem

Clean and efficient generation, transmission, and consumption of electric energy have become an absolute necessity today to slow down the global warming issues. Development of renewable energy generation, energy storage technologies, electric vehicles (EV), and smart grid technology are some of the important steps toward cleaner and more efficient electricity and transportation industries as these two industries are responsible for 64% of the total global CO2 emission [1].

More governments are taking effective measures to increase renewable generation and lower the carbon footprints. The European Union is considering reducing the carbon emissions by 80% by the year 2050 compared to that of the year 1990 [2] and also increasing the share of EVs to at least 80% by 2050 [3]. In Japan, the government is planning to build net-zero energy houses by 2030 whose annual energy consumption will be around zero or even negative. In order to have almost 50 million houses with net-zero energy, the application of photovoltaic (PV) systems, energy storage systems (ESS), and energy management systems (EMS) is necessary [4]. Also, EVs could be considered sustainable systems only if the power that is used to charge them is generated from sustainable resources. In other words, charging EVs with fuel-based electricity only moves the source of pollution from the EV to the power plant. The development of renewable energy sources such as PV and other green resources is crucial [5].

However, poorly managed renewable energy generation could even negatively impact the power [6]. As renewable energy sources such as PV and wind generators depend on the weather, the connection of these intermittent sources to the grid could cause imbalances between the power generation and the load, which will lead to voltage and frequency fluctuations. In this regard, energy storage systems and EV batteries can be very helpful to stabilize the grid and minimize the

possibility of overload cases [7]. Optimal cooperation of renewable energy systems and battery storage systems can be very helpful in harnessing the energy resources maximally due to the intermittent nature of wind and solar energies. It is shown that between 14 to 50% of the energy demand of a city's passenger transportation vehicles can be obtained merely by using photovoltaic energy [1]. Smart application of batteries to store and release renewable energy efficiently is the key to the optimal use of renewable energy sources. Energy storage systems have several benefits including assisting the peak shaving and Demand Response (DR) strategies, helping with the intermittencies of the renewable energy systems, and applications in the power flow control and the energy storage for the grid are some of the major uses of ESSs [8].

Today, with the advancement of the smart grid and developments of the vehicle to everything (V2X) technologies such as vehicle to grid (V2G), vehicle to building (V2B), and vehicle to home (V2) EVs can participate in the power network not just as energy consumers but also as energy storage units and providers as EVs carry large amounts of storage capacities. The EV market has been growing rapidly over the recent years as its related costs have been decreasing and also because of the increase in public concern about carbon emissions [3]. In particular, the number of EVs with bidirectional chargers is expected to rise significantly in the coming years which will facilitate more widespread V2G and V2H services [9]. Since most of the privately-owned EVs are parked the majority of the time, providing smart V2G service by a large number of parked EVs can be significantly helpful for the grid in terms of providing ancillary services [10]. There are several ancillary services that EVs can offer through the V2G service, including the provision of the storage capacity to compensate for the intermittent nature of the renewable energy sources and spinning reserve, assisting with the frequency and load regulation through the use of distributed capacity, energy trading and regulation services for renewable energy sources [1], [11].

However, the unscheduled cycling of EVs can pose a major challenge for the grid, namely the grid stability and power quality, the rise of power losses and peak powers, reduction of reserve margins,

and rise in costs. A study has found that uncoordinated charging of EVs could worsen the harmonics, ruin the demand-supply balance, undermine the voltage control and lead to the necessity of changing the protection schemes [8]. Uncontrolled charging of EVs is normally coincident with the peak time demand from the grid. This can cause severe issues for the stability of the grid [12]. Especially, due to the large power and energy demand of EV batteries, where a small EV can exceed the balance of the loads in many homes [13]. As an example, a typical supercharging of an EV is almost equal to the consumption of 120 average houses for 30 minutes. While the average energy consumption of a household in the US is almost 19 kWh/day [14]. Hence, optimal charging of EVs on different scales has been a trending subject in the literature in recent years. Energy management systems, built onto the vehicles or applied externally, can be used to optimize the cycling of batteries while the vehicles are traveling or when they are stationary and connected to the grid. Regarding the optimal charging of EVs, it has been studied in the literature with two approaches of centralized and decentralized. In the centralized fashion, a single agent such as the smart grid operator controls the charging of all EVs. In this approach, the managing agent requires plenty of data to make optimal schedules. While, in the decentralized approach, EV users have the total authority overcharging their vehicles which gives them more room to participate in demand response (DR) programs [15]. Also, the EV integration has been investigated on different scales, including the vehicle, building, local distribution, and transmission grid [16].

Thus, optimal employment of batteries in the presence of renewable energy sources can be studied on different scales to benefit different entities. One example of this problem is the Behind-the-Meter (BTM) unit commitment (UC) problem for microgrids (MG) incorporating renewable energy generation, batteries, and loads which would be a common application, especially in residential and commercial sectors. Microgrids are integrated energy systems that could incorporate distributed energy resources, storage systems, and loads, and facilitate bidirectional communication between users and the operator for the transfer of data and control signals [16], [17]. In some cases,

small-scale microgrids under the scale of 100 kVA and 10 kVA are also referred to as nanogrids and picogrids, respectively [18], [19]. Today, a typical small-scale microgrid employed by residential or commercial users consists of renewable energy generation, ~~and~~ in particular photovoltaic arrays, a local energy storage system which is mostly of battery storage system (BSS) type, plug-in electric vehicles, and different types of loads (dispatchable and non-dispatchable) which can have a bidirectional power transfer with the grid to take energy and possibly sell energy to the grid in the context of an energy market. Depending on the available technologies and electronics on the EVs and their charging equipment, their interaction in the microgrid could occur in a monodirectional fashion where the EV is only charged or bidirectional fashion where EV's battery can also be discharged to provide a V2X service.

Optimal energy management in microgrids can be realized by employing unit commitment algorithms. Unit commitment is a fundamental problem in the operation and planning of power systems which aims to determine the operating schedule of power generators (including on/off status and generation levels) while satisfying different physical and operational constraints for different time horizons [20]. UC problem tends to find the reference power points over a specific period to provide high-quality power to the microgrid users [21]. UC can be implemented on different scales aiming at benefiting different entities. One way to classify the UC problems would be based on the entity that is going to directly benefit from the solution of the UC problem. In this regard, the grid operator and energy consumers could be considered as two parties that can employ UC strategies to maximize their interests or minimize their costs and losses in a power system or microgrid. Unit commitment or energy management algorithm is often a mathematical model or algorithm which is implemented on computing resources (e.g., computers, microprocessors, microcontrollers, etc.) to manage the operation of microgrid components through an interface circuitry.

The energy management system of a microgrid has two major responsibilities, including the scheduling of the generation and the Demand-Side Management (DSM) [21]. DSM or Demand response (DR) refers to the reduction of the load demand when the power demand and price are high. There are two types of demand response programs including direct load control programs and price-based programs [14]. Utility companies are shifting from posing fixed energy prices to a mixture of time-of-use and demand charges. While demand charge is based on the maximum rate of the power consumption over a period, the time-of-use charge refers to assigning different tariffs to different time frames. This latter approach can have different forms ranging from defining on/off-peak prices to market prices at each time frame. There are also three different mechanisms implemented for the load reduction, including the chemical energy storage (which is the traditional battery storage), thermal storage (such as thermal bricks) as well as the demand response. Regarding the demand response programs, they are classified into two major types, namely incentive-based programs and price-based programs. Also, price-based programs include different types including Time-of-Use (TOU), Critical Peak Pricing (CPP), Real-Time Pricing (RTP), and Inclining Block Rate (IBR) [22]. Heavy participation of households in the DR programs could lead to intensive power peak events during off-times which could jeopardize the power quality of the grid. It also causes events like transformer overloading, which leads to the aging of the grid infrastructure [23]. Heating and thermal systems, storage systems, and electric vehicles are good candidates for providing demand-side response service [10]. Home energy management systems (HEMS) and Advanced Metering Infrastructure (AMI) are major components for the implementation of DR programs in homes [13]. Advancements in computers in the past decades on one hand and the growth of the smart grid on the other hand have enabled many people to implement their local energy management systems. In this regard, BTM unit commitment has gained momentum in academia and industry in recent years. This thesis aims at addressing the BTM UC for PV/battery-based microgrids.

1.2 Microgrid control scheme

Microgrid control is a comprehensive area of study that has attracted a large number of researchers in the recent years. A brief and general review of the main microgrid control approaches is provided in this section. In general, microgrid control is carried out hierarchically, with different levels of the control hierarchy working together to provide a stable and efficient operation of the microgrid. In the microgrid control system, there are three sets of requirements that must be met. Firstly, the energy transfer between the microgrid and the grid must be managed. Secondly, the microgrid must be operated within the allowed voltage and frequency ranges and thirdly, distributed generator (DG) units' active and reactive powers must be regulated. These needs must be addressed by the control hierarchy. When a microgrid is connected to the grid, it often has extremely low voltage and frequency variations as inverters use the grid signal as a reference to achieve proper voltage and frequency control. As a result, every DG or ESS might be regarded as a current source in this mode, with the power flow regulated by altering the current reference. In islanded mode, however, there is no grid reference signal accessible from the grid end. Therefore, the reference voltage signals must be generated by the DG unit controllers. In this case, one or multiple DG units must act as voltage source(s) to maintain the voltage and frequency of the bus [24].

It is worth noting that sometimes the local controllers of the DGs are referred to as the “zero level” of the microgrid control hierarchy. Anyways, if the local control stage of the power converters is considered a part of the primary level of the microgrid control, the generic microgrid control scheme can be classified into three levels. In the first level, the preliminary power-sharing, as well as voltage and current regulation of power converters is controlled. At the second level, any probable voltage deviation that might arise in the first layer is controlled. The optimal energy management, power flow, and economic dispatch are handled by the tertiary level of the control hierarchy [25], [26]. The required speed of the control system significantly falls when moving from the primary control level towards the tertiary level, where the dynamic response of the primary

control must be on the scale of milliseconds to ensure the frequency and voltage stability of the microgrid at all times. While the tertiary level does not necessarily need to communicate with the next levels at a high speed since it deals with the economic aspects of the system. In this regard, the microgrid UC problem falls within the tertiary level of the control hierarchy, that is why it is sometimes referred to as the high-level control. On this level, the control problem is concerned with the economics and energy management of the microgrid rather than the voltage, frequency, and dynamics which are handled by the lower control levels. Hence, this work is concerned with the tertiary level of the microgrid control, therefore the voltage and frequency regulation are not within the scope of this thesis. Figure 1.1 depicts the microgrid control hierarchy and the major tasks handled by every level of it.

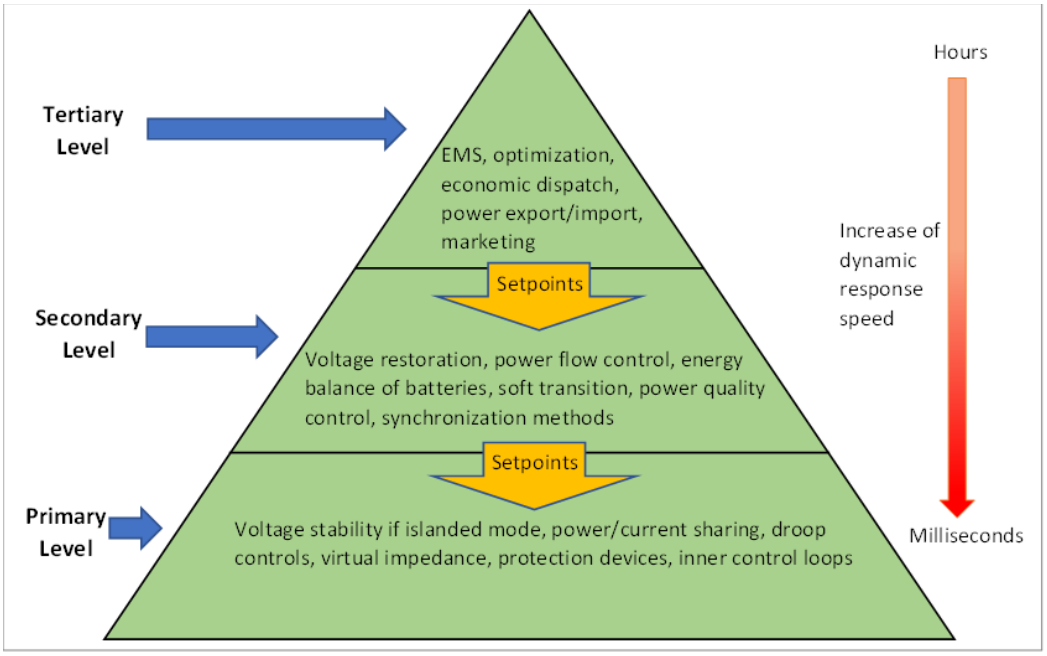

Figure 1.1: Microgrid control hierarchy [25]

Although the microgrid control hierarchy consists of different layers, as shown above, not every microgrid necessarily utilizes all the aforementioned control layers. In fact, the availability of "high-speed" communication technologies as well as the level of autonomy, that is expected from a microgrid, impact the structure of the control hierarchy. In this regard, one way to categorize the

microgrid control strategies is based on the available communication technology between the microgrid components. According to this criterion, microgrid control strategies could be categorized into communication-based and non-communication-based methods. In communication-based control, the availability of a high-speed communication link between the microgrid controller and microgrid components enables the local controllers to receive their reference signals directly from a central controller with a minimal delay. Therefore, the central controller will be able to always maintain the power balance of microgrids, ensuring the stability of the voltage and frequency during the off-grid times. In this case, managing the system during the on-grid times is of no significant difficulty from the control point of view as the grid maintains the frequency of AC buses. Thus, the availability of high-bandwidth communication links allows us to implement a control scheme with low autonomy where microgrid components rely on receiving instantaneous commands from the central controller at every moment. This approach to microgrid control could be highly efficient but it could be prone to frequent downtimes due to possible communication losses. However, in non-communication-based methods, there is no high-speed communication link in place and microgrid components need to maintain a certain level of autonomy while they still have a low bandwidth communication link with the upper levels of the control hierarchy. This type of microgrid control is often implemented by utilizing a droop-based controller. Droop control is used to specify the active and reactive power of every DG to maintain the frequency and/or the voltage of the bus. In this case, the DG units will function as regulated voltage sources, with their output sharing the load demand proportionally to their ratings, so there is no need for receiving instantaneous reference points from an upper control layer. Non-communication-based methods are generally more reliable and allow a plug-and-play feature for the MG components. Also, in these methods, there is no need for the DGs to be in proximity as they do not require fast communications. However, this control approach suffers from lower accuracy and optimality compared to the communication-based type. Some literature suggests combinations of these two methods for achieving the best performance and reliability [27].

1.3 Scope of the research

The research area of “microgrid optimization” is considerably vast. Many authors have tried to address the following question from different points of view: “How can we design, build and run microgrids for different applications in the most favorable way?”. It is worth mentioning that the word “favorable” in this context could refer to different quantities or qualities. Minimum cost, maximum revenue, minimum employment of the grid power or particular equipment, maximum comfort of the owners/users, minimum emissions, minimum stress on the power grid, etc. are some of the objectives that one could consider as the “favorable” operational condition of a microgrid. Hence, this generic problem can be investigated from different aspects which has been studied in different works. In this regard, this section is devoted to explaining what is within the scope of this research and what is not.

First, with regards to the grid connectivity as mentioned before, microgrids should be able to work in the two modes of grid-connected (on-grid) and islanded (off-grid). Technically, a microgrid must be able to function seamlessly in both states and also during the transition times from one state to another. However, the operation, control, and energy management of microgrids in off-grid mode is an extensive field of research that is not within the scope of this work. Hence, this work is merely focused on the optimal operation of grid-connected microgrids. In the islanded mode of microgrids, one power converter (usually at the battery side) or multiple converters must be able to maintain the frequency and/or the voltage of the AC/DC buses. Thus, in order for the electrical components of a modern home to form a microgrid in the exact sense, at least one of the converters must be able to have the capability of detecting the power outages and working in the grid-forming mode to maintain the frequency and/or the voltage of lines during islanded/transition times. Nowadays, some of the smart grid equipment such as AC batteries are able to work in the grid following/grid forming mode, while some devices can only operate in the grid following mode. For the sake of simplicity of vocabulary, in this work, the power system of residential or commercial buildings is

also referred to as a "microgrid". Therefore, the term "microgrid" in this thesis does not necessarily mean the system can operate in the islanded mode. Also, with regards to the energy management in the grid-connected mode, only the active power (P) has been addressed in this work, and reactive power (Q) control and management are not within the scope of this research work.

Hence, in this thesis, the behind-the-meter (BTM) unit commitment problem has been investigated for grid-connected battery-based systems (ESS, EV) as well as controllable loads in some cases. In this work, the UC problem has been studied from the perspective of energy consumers and is generated in the framework of mathematical programming which will be discussed in more detail in the next chapters. More specifically, this work aims to present BTM UC problems in the framework of Mixed-Integer Programming (MIP) including Mixed-Integer Linear Programming (MILP) and Mixed-Integer Nonlinear Programming (MINLP) to schedule the operation of battery-based units such as electric vehicles and energy storage systems in BTM microgrid applications (particularly, residential and commercial microgrids which are equipped with PV generation, ESS and EV charging facilities). Diesel generators and thermal systems such as Combined Heat and Power (CHP) equipment are not considered in the UC models provided in this work. Mathematically speaking, the UC problem is an optimization problem whose goal is to assign operation reference points to the microgrid components to minimize or maximize one or several objective function(s) while satisfying different model constraints. In the microgrid research, "optimization" is usually applied in two different fields of study, namely "system sizing" and "unit commitment". Before a microgrid is constructed, assuming there are no strict financial or logistical restrictions for selecting the size and type of the components, a comprehensive study should be carried out for finding the right sizes of components. In case the microgrid is designed for both islanded and grid-connected operation, there is even a need for another round of study before the system sizing to determine the best system topology (e.g., AC bus, DC bus, hybrid) to achieve the lowest cost and energy dissipations. The efficient microgrid topology itself depends on many

factors such as the composition of loads and available equipment. Thus, prior to the procurement of the equipment, a system sizing study would be necessary to determine the optimal sizes of components (e.g., battery size, size of PV arrays, etc.). System sizing is an optimization problem that aims to find the optimal sizes of microgrid components so they can lead to an optimality such as the lowest Return-of-Investment (ROI) term. Different publications, such as [28], [29], have focused on the optimal sizing of microgrid components. However, this field of microgrid research is entirely out of the scope of this work. In this thesis, the microgrid is assumed to be made of an AC-bus structure and solely operate in the grid-connected mode. Also, in this thesis, the "optimization" is applied for its other application in MG research which is producing the optimal operation plan for microgrid components when they are already available and ready to work.

Forecasting is another field of research associated with high-level control of microgrids. Day-ahead/hour-ahead load profile, as an important input dataset of an energy management system is usually obtained by statistical or Artificial Intelligence (AI)-based forecasting methods. Forecasting the energy prices when they are not available ahead of time, solar irradiance, EV's commuting times, and initial State of Charge (SoC) of EV batteries at the times of arrival are some other parameters that could be obtained through forecasting. In some cases, some of this information might be provided by third parties such as the utility company through the cloud space. Otherwise, they may need to be forecasted on the user end. In this regard, problems such as solar irradiance or energy price forecast are focused on by a different group of publications such as references [30], [31]. However, forecasting is also not within the scope of this work. Therefore, in this thesis, it is assumed that all the input information of the energy management algorithm is already obtained in crisp values and high precisions.

With regards to the certainty of the optimization parameters, the smart grid optimization problems may be classified into deterministic and stochastic optimization. Deterministic optimization is used when specific values are selected to represent variables associated with a model and produce

different scenarios corresponding with those cases. However, stochastic optimization is used when there are independent random variables with known distributions in the model [32]. In fact, a challenge with home energy management systems is caused by the randomness of different phenomena and values such as the idle times of EV, load profile, and renewable energy generation which is often addressed by stochastic optimization [6]. Some researchers have investigated the UC problem in the context of stochastic optimization [33], [34]. Forecasting and statistical models have been employed in the literature to model different uncertainties in EV charging stations with PV arrays, such as PV power, EV arrival, departure times, and initial SoCs [35]. However, in this thesis, the uncertainty of model parameters is not taken into consideration, and carried out optimizations are of deterministic type.

With regards to the method of optimization, a wide range of approaches has been taken in the literature. However, when it comes to optimal scheduling for microgrids, mathematical programming would be the most popular and useful optimization method due to its two major advantages. The first advantage is its ability for achieving global optima which is important to achieve the best possible solutions. The second advantage is concerned with its modular structure which makes it easily adaptable to new conditions and variables. In other words, introducing new variables, constraints, or objectives to a MIP model could be done with minimal difficulty [36]. One case study showed that MIP was able to solve a UC problem significantly faster than a metaheuristic method [37]. As there are normally different discrete or binary variables in a UC model, MILP has become the most used type of mathematical programming in smart grid research. In this regard, according to the abovementioned advantages of mixed-integer programming and also the fact that a typical modern computer is normally able to handle the complexity and size of a MILP model for a generic small microgrid in a relatively reasonable amount of time, MIP has been employed in this work for generating microgrid UC models. In the next chapter, the application of the different optimization techniques in producing UC models will be reviewed.

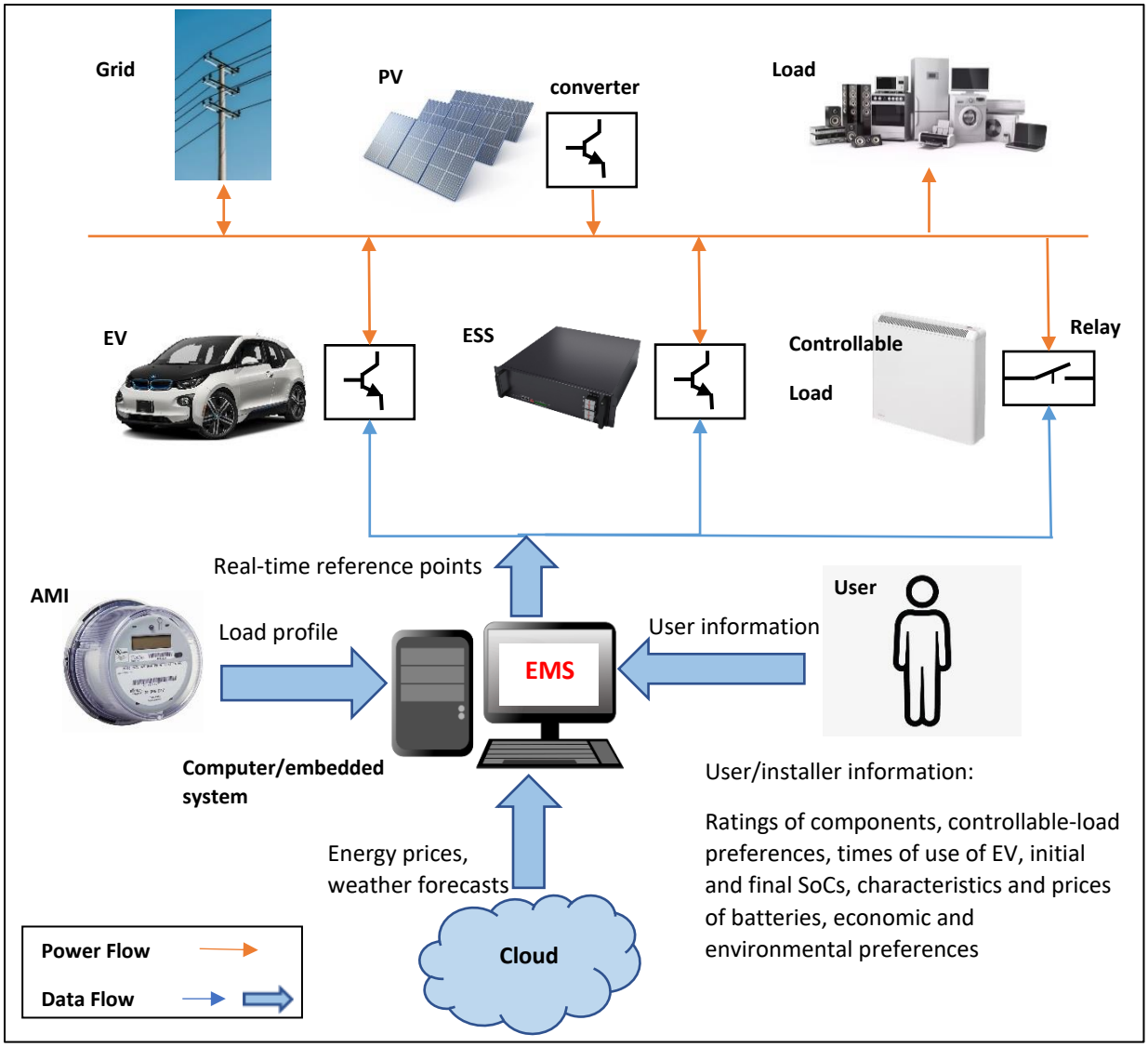

Figure 1.2: Residential microgrid and energy management system scheme

Figure 1.2 illustrates the high-level control scheme for a home or a building microgrid. The term "high-level" control refers to the fact that the energy management system falls within the high levels of the microgrid control hierarchy, where the control system is responsible for optimizing the energy transactions within the system without being involved with the dynamics of the microgrid. In this regard, the real-world energy management system is essentially a program containing a MIP model which receives input data from the user, cloud, and utility meter, executes a round of optimization and produces the optimal power schedule of the batteries as well as the

optimal operation times of the controllable loads for the next optimization horizon (e.g., 24 hours, 1 hour). Those reference points then will be sent to their respective converters/relays in real-time but at a low (minute/hour) update rate through a low-bandwidth communication link between the energy management system and converters/relays. The frequency at which the EMS receives information from different entities depends on the type of information. For example, with regards to the user-provided information, some of them such as the ratings of components, battery capacities and characteristics, battery prices, and economic/environmental preferences could be provided by the user and/or installer at the time of commissioning. However, information such as the controllable-load preferences, times of departure and arrival of EV for the weekdays and weekends as well as initial and final SoC values of EV battery, when EV is connected to the microgrid, could be uploaded anytime the user decides. Obviously, some of the data that are of a more random nature such as departure and arrival times of EV as well as its initial SoC value may not be known ahead of time with high certainty due to the unpredictable nature of humans' behavior. This issue can be addressed in two different ways. From the modeling point of view, a good way to address the random nature of some input data such as the initial SoC of EV or times of arrival and departure (as well as other uncertain values such as PV generation) is employing stochastic optimization to make sure that the solution of the optimization problem is always within an acceptable margin of optimality. However, another way to address this randomness issue is by providing more reliable data to the EMS through more sophisticated communication links. For example, provided that the technological infrastructure is in place, a modern EV may be able to send the times of arrival and expected level of SoC with a relatively good level of accuracy to the EMS and through the internet before the EV arrives at the parking place. However, as mentioned before, in this work deterministic optimization has been carried out based on the assumption that the data provided by the user are highly accurate and reliable without focusing on how the data is provided to the EMS. In this work, the information received from the cloud is assumed to be of two types, namely the energy prices and the solar irradiance forecast (although other sets of information

such as peak power limits, and warnings could be also provided by the grid operator [36]. This information can be uploaded on the cloud on certain intervals (daily, hourly, etc.) by different third parties such as the utility companies, weather stations, etc. The EMS can then calculate the estimated solar generation by using simple mathematics locally. The AMI could record the loads' consumption as well as the building's energy transactions with the grid and also provide automatic bidirectional communication between the utility company and the user [14]. The previous load-profile records can then be used locally or by a third party to predict the load profile of the next optimization horizon. Carrying out this task locally would require available forecasting algorithms that should be able to share its outcome with the UC model.

There are two different approaches for producing charge/discharge cycles plan for multiple EVs, including individual planning and aggravated planning [11]. Depending on the number of the electric vehicles and the network level which is of concern (e.g., low voltage, medium voltage, high voltage) any of these approaches may be needed in the analysis [38]. With regards to how this thesis addresses the problem of charging "multiple" EVs, it should be noted that although the UC problem in this work is solved at the individual level, it can address the scheduling problem for multiple EVs. However, they are designed to address cycling EV batteries when their idle times within the next optimization horizon (e.g., one day, one hour, etc.) is known at the time of optimization. Hence, the presented UC models would be more useful for the places where a certain number of EVs are to be scheduled for a time horizon, while the parking times of every EV are predictable, as in the parking lots of office or residential apartment buildings. However, this work would not be suitable for optimal EV scheduling in places where EVs' availability is of a random nature, they are charged within unpredicted time frames and their commuting times are not known ahead of time, such as in fast-charging stations or parking lots of the shopping centers. This is because the designed MIP models can produce optimal battery cycling schedules when they access the times of EV availability and also since the model, ~~(~~especially the battery degradation model~~)~~,

requires specific information about every single EV battery that is going to be addressed. Moreover, the presented degradation model, in this work, may not be suitable for fast charging of EVs as it does not take into account the impact of C-rate (i.e., the rate of charging or discharging a battery relative to its capacity) and temperature on the capacity loss of the battery. In fact, in these cases, where EVs' presence is random, two different approaches have been employed in different works. Either the EVs are collectively treated as loads rather than control variables and the UC problem is solved solely for scheduling the local storage system [8]. In another approach, the commuting times of EVs in a public parking lot or fast charging station are statistically modeled and the optimization problem for the EVs is roughly solved based on the available statistical forecasts [39]. However, this approach may not lead to the optimal results for every EV, and also modeling the battery degradation tailored for every EV may not be feasible for this case.

According to what is explained in this section, the energy management system, that is supposed to optimize the operation of a microgrid, may be considered a system consisting of a UC model and possibly a forecasting algorithm which are integrated under the umbrella of an energy management software package, which also executes some other potential calculative tasks such as calculating the PV power profile based on the irradiance profile. This comprehensive program can be implemented on a computer or possibly embedded systems that can support internet connection and communicate with AMI and power converters for receiving and sending data. It also needs to have a graphical user interface (GUI) so the user can input the information into the system. The communication link between the device that hosts the EMS program, and the power converters or relays is another technical issue as they need to be able to properly communicate with each other. However, these technical issues are out of the scope of this work. Finally, it should be noted that in this thesis, the terms “energy management system”, “energy management algorithm” or “unit commitment model” are used interchangeably, carry the same meaning and only refer to a mathematical optimization model which is designed to schedule the operation of microgrid

components (mostly batteries) in terms of their power values and times of operation. In other words, the term energy management system in this work has the same meaning as the UC model as this work is mainly focused on developing mathematical models for optimal battery scheduling. In practice, a "unit commitment program" could be a part of a larger "energy management software package" which could also incorporate a forecasting program. Such comprehensive energy management package could be installed on a computer to receive information from different entities and send reference point values to the microgrid components through appropriate communication links.

1.4 Literature review on the unit commitment of electric vehicles and energy storage systems in behind-the-meter microgrids

Unit commitment at residential and commercial buildings is now a possibility for the home and business owners as fast computers and internet (cloud) connection is now accessible for a significant percentage of people. A modern microgrid employed by the residential/commercial sector often consists of (but, not limited to) energy storage units and renewable energy generators (in particular, PV systems in urban areas). Gradually, more EV manufacturers are also providing their vehicles with circuitry required for the vehicle to grid service which means in a modern building, the EVs can also be components of the local microgrid which is significant due to the large storage capacity of an average EV compared to the amount of daily energy transactions in a typical residential or small commercial building. Numerous studies have investigated the optimal charge/discharge of EVs within bidirectional markets. One way of classifying these studies could be based on the connection of the EV to the grid (V2G) through a charging station or connection to a home power bus (V2H) [4].

Thus, most of the time the UC problem for an urban microgrid can be narrowed down to a battery scheduling problem. Controllable (i.e., shiftable, dispatchable) loads are also other components of a residential power system that can be addressed in the UC algorithm. When it comes to islanded

microgrids that are situated in remote areas and have no connection to the grid, the main concern is maintaining the voltage regulation in the system. While for a microgrid, which is normally connected to the grid, the main issue is usually the economic dispatch. In a grid-connected microgrid, the renewable energy systems normally work on their Maximum Power Points (MPP) unless otherwise required. Assuming that the microgrid is committed to participating in ancillary service, PV curtailment could also be considered as a parameter that is determined by the energy management algorithms. Hence, PV curtailment is the subject of some of the literature that has addressed energy management systems for buildings. When excessive PV energy is generated, such that available storage systems are not capable of storing all the excess energy, PV curtailment could be necessary to avoid the voltage peaks in the distribution system [4]. However, in this thesis, the PV system is assumed to work on the MPP as it normally does in grid-connected systems. Thermal systems and diesel generators are also included in some residential or commercial microgrids and they can be subject to a comprehensive study. However, the focus of this research is mainly on the battery scheduling problem, hence, diesel generators and thermal units are not addressed in this work.

The literature review is focused on the UC problem for the BTM microgrids with a focus on batteries (both local energy storage systems and EV batteries) as battery scheduling is focused on in this thesis. The literature review has been carried out with a methodological approach, where different methods used to study the unit commitment for electric vehicles and/or battery storage systems in microgrids have been reviewed. It aims to point out the applied methodologies and objectives in recent years for addressing UC problems for batteries. Due to the fact that this work is based on MIP optimization, research works that have employed this method have been emphasized in this literature review.

With regards to the application, residential and commercial microgrids are the subject of this thesis and the literature review section as well. Several researchers have studied the battery cycling

problem for a building with different approaches and objectives. Minimization of net energy cost, electricity cost, renewable energy curtailment, load shedding mitigation, voltage deviations, battery degradation, emission, maximization of revenues or deployment of renewable energy, and user's comfort during grid-connected or islanded conditions are the most applied objectives in these types of problems [40]-[42].

Technically, the energy management problem in microgrids falls into the category of mixed-integer nonlinear programming [43]. However, various optimization methods have been employed in different studies to solve the energy management or battery scheduling problems. Mathematical programming, metaheuristics, and AI-based methods are the main categories employed in the literature among which the first two are more commonly applied by researchers [37]. Linear and Quadratic Programming (LP, QP) [9], [10], Nonlinear Programming (NP) [44], Convex Programming (CP) [45], Mixed-Integer Linear Programming (MILP) [1], [3] ,[5], [12]-[14], [18], [23], [36], [39], [46]-[53] and Dynamic Programming (DP) [3], [6], [53] are among the mathematical programming models that could be employed in a deterministic or stochastic fashion. Particle Swarm Optimization (PSO) [40], [53], [54], Gray Wolf Optimization (GWO) [55], and Genetic Algorithm (GA) [49], [56], [57] are some of the heuristic search-based algorithms used in the literature optimization and planning of microgrids. However, these algorithms usually require large computational and storage resources. Therefore, for the real-time application, they may end up being expensive in terms of the equipment [58]. Rule-based algorithms [35], [59]-[63], game theory [17], [64], and AI-based techniques such as Artificial Neural Network (ANN) [15] and Fuzzy Logic (FL) [65]-[67] are some of the other methods that have been used for optimal scheduling of batteries (e.g., EVs) in the literature [39]. Some of these most relevant works are introduced in the following.

By implementing nonlinear programming and a rule-based algorithm, a smart charging method designed for a building with a multi-port system combining EV, PV, battery, and a heat pump was

provided in reference [44]. The smart charging algorithm of this work managed to lower the entire cost of energy by combining grid power prices, PV investment costs, EV/battery operation expenses, and revenue gained from serving as the main frequency regulation reserve, all based on PV production and load estimates. Reference [4] presents an EV charge-discharge management system in the mathematical programming framework based on information interchange between the home energy management system (HEMS) and the grid energy management system (GEMS) for optimal PV output utilization. The HEMS develops an EV charge-discharge strategy to reduce home operating costs and PV curtailment without interfering with EV driving.

A linear programming model for several households with PV generation, shiftable load, and EV has been presented in [10] and the optimal schedule of EV charging as well as heating and cooling loads has been solved. A stochastic optimization framework for smart home energy management using EV storage and PV generation has been presented in [6]. The electric power allocation in the EV battery, home load demand, PV power, and utility grid is optimized using stochastic dynamic programming. The technique explicitly considers probability distributions for EV's journey duration and length, as well as forecasting home load demand and PV electricity generation. The study in [45] proposes a convex-programming framework for optimizing the energy management of a hybrid solar-battery power source in a smart-home nanogrid with electric vehicle load. The convex program in this work is a mathematical formulation for allocating electric power between the EV battery, house battery, residential power demand, PV arrays, and the utility grid.

An energy management system for a household user is presented in [14] in the framework of MILP, which is capable of energy transactions between the consumer and the load-serving entity. The suggested household model includes shiftable and non-shiftable loads, as well as an electric vehicle that can provide V2H and V2G services to cut the household's energy costs. The study in [18] proposes a MILP for reducing the total operating cost of an interconnected nanogrid by optimizing the overall operating cost while considering the effects of V2H and V2G. The main goal is to

minimize carbon emissions, overall operating costs, and peak load demand while meeting the needs of each nanogrid's customers. An EV scheduling system that makes use of V2H technology to schedule the charging/discharging level for each timeslot is presented in [12] to reduce the payable costs of customers. This algorithm which is built in the framework of MIP can support both on-grid and off-grid working conditions.

The study in [13] has conducted an assessment of dynamic-pricing and peak power limiting-based Demand-Response (DR) schemes for EV and ESS using mixed-integer linear programming. This was carried out for a single home with a distributed small-scale renewable energy system, an EV with V2H and V2G capabilities as well as an ESS with two-way energy trading, to study several DR techniques. Alternative ways for charging a single car, connected to the power system of a single home were studied in [9] by using a rule-based algorithm and linear programming. All optimum algorithms have the same goal: to lower the vehicle's charging cost. In this regard, numerous use scenarios and four distinct daily energy price profiles were used to test the seven effective solutions. The impact of the BTM unit commitment on the grid equipment is a subject that has been addressed in [59], where the benefits of adopting a peak shaving algorithm for each house that makes up a domestic electric grid were investigated in this work. It shows positive results as the transformer's aging rate has significantly decreased as a result of the employment of a heuristic rule-based peak shaving algorithm.

With the integration of wind and solar systems, battery storage, and electric vehicles, the study in [47] provides a MILP model to optimize the energy production and consumption systems in a smart house. Also, a variety of case studies are provided in this work using the Taguchi technique to create experiments. Then, to tackle the problem of domestic energy management and reduce the consumer's electricity costs, a heuristic approach is provided. For a day-ahead UC model in microgrids, a heuristics-based optimization mechanism is provided in [21]. This model seeks to schedule electricity among the many microgrid units, which include renewable energy resources, a

storage unit, two microturbines, a fuel cell, and electric vehicles while reducing operational costs and CO2 emissions. The study in [48] aims to maximize the overall profit of a building microgrid by optimizing the operation of EVs and batteries in the day-ahead and regulated energy markets while taking the EV's driving pattern into account. This work considers electric vehicles as dynamic energy storage devices and batteries as managed demand facilities to take advantage of buildings' energy flexibility. The optimization problem of this work is a two-stage MILP.

Reference [68] describes a dual-layer predictive energy management system for a microgrid with a hybrid energy storage system that includes batteries and supercapacitors. A hierarchical dispatch model is suggested to determine the scheduling of utilities within a finite time horizon to maintain high system robustness at minimal operational cost, where the upper layer minimizes total operational cost, and the lower layer eliminates fluctuations caused by the forecast errors. A MILP has been presented in [49] for making charging decisions for multiple facilities of a single end-user with green energy generation, ESS, EV, and an internet-of-energy (IoE)-based energy trading platform to reduce energy waste and total energy usage costs. Due to the vast number of constraints and variables in the suggested model, this study also presents a genetic algorithm for this issue, to manage the solution infeasibility of constraints. The study in [15] has presented an intelligent charging technique based on Machine Learning technologies to schedule the EV charging during connection times. This is accomplished by making real-time charging decisions based on auxiliary data such as price, environment, driving, and demand time series to minimize the total energy costs of the vehicle.

A MILP-based EMS is proposed in reference [36] to produce an efficient day-ahead schedule for a smart household under hourly pricing and peak power limiting demand response schemes. This work addressed the scheduling of different types of controllable assets, including thermostatically and non-thermostatically controlled appliances. Also, EV, ESS, and distributed generating at the user location are taken into account. In reference [50], a MILP-based online UC algorithm is

proposed for microgrids with on-site batteries, renewable energy sources, and integrated EVs. Using forecasted values such as power consumption, renewable energy generation, EV connection, and disconnection timings, this problem is solved over a rolling time horizon. It also formulated the problem as a stochastic chance constraints optimization to improve the system resilience when dealing with uncertainties in demand/generation, EV state of charge, as well as connection/disconnection timings.

One way of classifying the publications that have investigated the MG unit commitment problem would be based on the number of beneficiaries of the UC algorithm that have different and probably conflicting interests in the microgrid's operation. As long as a microgrid is going to serve only one party (its owner or operator), the scale of the system and the size of its components do not have a meaningful impact on the structure of its mathematical model. However, introducing other parties with involved interests could change the model noticeably, especially in terms of the objective functions. Thus, the number of parties that are going to benefit from the operation of a microgrid impacts the system modeling and formulation. For instance, different neighbors/owners that may operate a neighborhood microgrid in a shared way or different EV owners that connect their EVs to a local microgrid are examples of the cases where a microgrid could have different beneficiaries with separate and potentially conflicting interests. Different works have studied the UC problem for joint utilization of microgrid components which are mentioned in the following. For instance, workplaces are one of the noticeable places where several entities could benefit from a tailored energy management system. Especially, when it is known that during the daytime, around 25% of vehicles are parked at the workplaces [16].

The optimal interaction of a neighborhood of smart houses that have bi-directional power flow between themselves, and the grid is investigated in [23] aiming at minimizing the overall energy cost. The problem is formulated in the framework of MILP. These houses could be equipped with EVs that provide V2H and V2G services, controlled appliances, energy storage, and distributed

generation. A heuristic operating method for commercial building micro-grids with different EVs and PV systems is suggested in [58] which is centered on real-time data collection. The technique can effectively enhance the self-consumption of PV energy and minimize reliance on the power grid by allocating the charging rate of EVs in real-time. In [5], a MILP model has been implemented for charging an EV fleet in a workplace from the photovoltaic generation. In this model, the EVs are charged from the PV array, and provide V2G service for the grid support and ancillary services in the form of reserves, while taking the distribution network capacity constraints into account. The MILP optimization model which uses a fixed period is implemented as a receding horizon model predictive control.

An EV charging model is outlined in [35], for a Solid-State Transformer (SST) in a charging station equipped with a PV array. This work suggests a rule-based EMS that allows SST-based charging stations to dynamically engage in ancillary services while ensuring the quality of charging for EV owners. A categorization method for electric vehicles has been investigated in [1], which can help a PV-powered charging station minimize the overall cost of energy trading with various energy entities in a smart grid network. The EVs in this MIP model are planned according to their priorities, which could be premium, conservative, or green. A dual-stage power flow method for a PV-battery facilitated EV charging station is proposed in [53] to obtain the minimum cost of operation. As a prediction layer, an offline particle swarm optimization is employed in the first step of the optimization method. Dynamic programming is also used as an online reactive layer in the second level. In both rounds, predicted system data is used to develop the best power schedule. A UC model capable of predicting the PV generation and optimizing power transfer between the PV array, the grid, and EVS at the workplace is presented in [51]. The goal of this work is to reduce the charging costs while lowering the grid energy demand by enhancing the PV self-consumption. A MILP framework is used to efficiently designate power to minimize the charging cost of EVs in this work.

The effect of different V2G approaches on the batteries at a workplace charging station facilitated with a PV array is investigated in [11]. In this regard, two types of V2G modes have been studied in this work namely power-coordinated and time-coordinated modes using the Round Robin scheduling method. The study in [69] proposes a four-stage UC method a charging station with PV array and ESS, that is connected to a commercial building. The proposed algorithm aims to minimize the operational cost associated with user satisfaction while balancing real-time supply and demand. This happens by optimal scheduling of EVs, battery storage, grid supply, and dispatchable load in the context of chance-constrained optimization. The optimum operation of a PV-equipped charging station is addressed in [70] through multi-objective problem formulation to schedule the EVs and local battery storage system. This work aims to achieve the highest revenues as well as the lowest capacity loss of battery while taking into account the grid's power restrictions. This multi-objective problem is then solved by the Enhanced Augmented-Constrained (AUGMECON2) Algorithm.

In [71], a rule-based UC technique has been proposed for real-time control of multi-source charging stations with distributed energy resources, ESS, and V2G service capability while the stochastic character of the sources is taken into account. This energy management algorithm is made up of different cascaded problems to reach the lowest operating cost. For a parking station with a Photovoltaic system, a battery cycling model is developed by [39] in the framework of MILP to arrange the charging or discharging rates of EVs and ESS. In this work, the EVs are categorized and prioritized according to their initial SoC levels; some may be considered suitable for V2G service, and some are in need of urgent charging. This article aims at maximizing the EV users' satisfaction as well as the parking station's profit. An energy management strategy for microgrids with an EV charging station, PV system, and dynamic loads is presented in [3]. This strategy uses the PV and demand forecasts to implement a dynamic programming method that optimizes the EV

cycling regime. This algorithm offers the consumers different charging alternatives while lowering the reliance on the grid.

~~Reference~~ [40] has employed particle swarm optimization to implement nonlinear, degradation-incorporated energy management algorithms for a DC microgrid with PV, ESS, and charging station aiming at minimizing the costs. In [52], MILP and model predictive control have been applied to produce an EMS for an apartment building with a parking lot that offers V2H service, renewable energy generation, and storage system to achieve the minimum cost. Gray wolf optimization is used in [55] to solve the linear UC problem of the parking lot of a building which also includes photovoltaic generation and ESS. The study in [17] presents a decentralized demand-side management technique that uses two layers to reduce the difference between forecasted and real-time load in a microgrid composed of several households. The suggested technique is based on the game theory where its first layer calculates the projected demand, and the second layer calculates the deviation of the forecasts. In [72], a framework has been developed for controlling and optimizing the operation of a microgrid with PV, dispatchable load, EV charging stations, and a local battery unit using model predictive control and Alternating Direction Method of Multipliers (ADMM) to minimize the cost of operation.

1.5 Research gaps and contributions

This thesis aims to address some of the existing gaps and shortcomings of the literature that has studied the UC problem in microgrids. More specifically, it focuses on the research gaps of the works that have implemented mixed-integer programming as the framework of battery scheduling problem. First and foremost, this thesis addresses the battery degradation issue in the behind-the-meter UC problems. A battery scheduling model requires to take into consideration the battery degradation caused by the irregular cycling of batteries to be able to provide realistic outcomes. (The irregular cycling takes place between random SoC values unlike the regular cycling which takes place between 0 and 100%SoC). Otherwise, the inflicted cost associated with the capacity

loss of batteries could undermine the profitability of any cycling regime. As a result of introducing the battery degradation model, a UC model will be introduced for a home-based microgrid to minimize the real costs and carbon footprint for a user. In this regard, the next contribution of this work is investigating the impact of the resolution of the MIP model on the capacity loss of batteries in the intra-hourly markets. A Hardware-in-the-Loop (HIL) experimental setup has been employed to study this subject in depth. Optimal battery scheduling in a commercial building with charging station where multiple parties (microgrid owner and EV owners) could have conflicting interests is another subject of study in this work. In brief, the main contributions of this work can be categorized into the following areas.

- Investigating the battery degradation for irregular cycling in microgrids in the context of MIP.
- Examining the impact of the resolution of the MIP unit commitment model on batteries in microgrid.
- Studying the MIP-based UC strategies in applications with multiple beneficiaries.

In the following sections, every one of these areas are explained in more detail as well as the research gaps associated with them.

1.5.1 Battery degradation problem

One common shortcoming among the relevant published literature is the lack of consideration of battery degradation or just oversimplifying this issue, given the fact that battery degradation can largely affect the optimization results [56]. Several manuscripts have produced sophisticated UC models, however, failed to address the crucial issue of battery degradation such as [1], [17], [23], [35], [48], [50], [55]. However, those works that employed MIP to build UC models and addressed battery wear in a way, suffer from some important shortcomings. These shortcomings mainly consist of assuming static factors or constants as the wear rate of different cycling regimes or

missing some important parameters that impact the capacity loss of batteries in smart grid/microgrid applications. The study in [73] states that most of the literature has considered battery wear as a simplified and additional cost factor rather than addressing it as a main objective.

The battery degradation problem and its associated factors will be investigated in the next chapters. However, in this section, some of the main shortcomings of the relevant literature concerning battery wear are pointed out. Some of the literatures have used oversimplified mostly static degradation models that may not be able to model the wear with a decent precision [66], [74]-[76]. Attributing constant degradation factors to different cycles cannot reflect the impact of different effective factors such as Depth of Discharge (DoD) and State of Charge (SoC). Some works have overlooked the impact of DoD on the capacity fade or just oversimplified this effect [44]. Some authors that have taken into account the impact of DoD on the capacity loss, neglected the dependence of DoD-related capacity loss on the initial and final SoC of charging and discharging attempts [77]-[79]. Some of the research works are produced based on special datasets, charts, etc. that may not be provided by the manufacturers normally [44]. Computing the capacity loss separate from the original objective function of the problem is another issue that could undermine the optimality of results [80], [81]. This could lead to the emergence of competing objectives which may affect the optimality of results. Some of the research works rely on specific battery chemistry and they cannot be applied to the other battery technologies directly [44], [82], [83]. Low precision or high complexity due to the application of metaheuristics or iterative structures [77], [78], [82], [84] is another shortcoming in the existing literature.

To the best of the author's knowledge, among the published literature that has provided a battery wear model in the context of UC problems, some of them have more similarities to this work in terms of the methodology used for producing the battery wear model. The shortcomings of those works are explained as follows. Reference [82] which has been used as the basis for the wear model in this work has proposed a capacity loss model based on the cycle life-DoD of the battery. This

model was proposed for irregular cycling in V2G scenarios. By using a single global wear coefficient corresponding with every charging/discharging event, this study seeks to simplify the wear rates associated with every irregular half-cycle. However, the global wear coefficient was based on the cycle life-DoD curve of a specific battery. Therefore, it may not be directly applicable to all battery technologies. Furthermore, the form of the wear model presented in this paper needs the use of an iterative framework to ensure the convergence of the algorithm. Other works such as [85] and [86] that employed the approach of [82] suffer from the same shortcomings.

Reference [87] provides an empirical battery degradation model for the short-term cycling of batteries in the energy market. It provides a novel method for addressing SoC and charging rate by extracting the wear data from a contour map of a battery that maps battery degradation versus SoC of two consecutive time intervals at a particular C-rate. Although this work manages to address the SoC of cycling and C-rate, it suffers from some deficiencies. First and foremost, it builds the degradation model based on the SoC-degradation contour map of a particular battery type, while this map is not normally provided by the battery manufacturers. Also, in order to address C-rate, it assumes the effect of the C-rate of the battery wear changes linearly which is not an accurate assumption according to [88]. Moreover, the degradation model of this work is minimized along with the cost function in the context of a multi-objective optimization problem and a good solution is tried to find through the Pareto front of these objectives. Therefore, the degradation and cost function compete with each other which will avoid obtaining the exact optimum result where battery degradation and energy costs lead to a total minimum cost [87].

Reference [89] has proposed a semi-empirical wear model that is based on the cycle life-DoD curve and provides a wear cost as the return value to incorporate it into the optimization models. It implements the wear model for an EV that provides V2G service and operates along with PV generation. However, this work has used particle swarm optimization to solve the EV charging problem which would not be able to produce a global solution within a reasonable time as MIP

does. Reference [90] presented a wear model based on a linearized version of a capacity loss vs SoC curve. However, the linearization attempt could notably lower the accuracy of the model. Also, it cannot guarantee the maximum revenue as the user has to set a minimum value for the lifetime of the battery and then attempt to carry out the optimization to maintain that initial lifetime, rather than search for the optimum solution (maximum revenue) among all the possible states.

In order to tackle the deficiencies of the MIP-based UC models for BTM microgrids, this work represents several contributions as follows.

First and foremost, a technology-agnostic battery wear model is provided in this work to address the real-world battery cycling practices in microgrids where batteries are cycled irregularly between random SoC levels. The wear model is built based on the cycle life-DoD curve of batteries and is applicable in MIP structures for online minimization of UC costs. Hence, it takes into consideration the fact that DoD-related capacity fade depends on the initial and final values of SoC during every cycle/half cycle. Due to the reliance of the proposed wear model on the cycle life-DoD curve of the battery and concerning the fact that this curve itself is normally provided for specific C-rates, one technique is also introduced to employ the best cycle life-DoD curve for every problem. As a consequence of calculating the capacity wear of batteries during their operation, the real costs associated with the battery operation and also the environmental footprint of the microgrid are addressed in this thesis. It is demonstrated how scheduling the batteries without taking into account the battery wear as practiced traditionally could significantly increase the costs and carbon footprint of microgrids.

1.5.2 Impact of model granularity

After a MIP unit commitment is produced and incorporates a tailored battery degradation model to schedule the day-ahead operation of a microgrid, a raised question would be, what is the optimal time resolution to schedule the microgrid components. In general, more frequent battery scheduling

seems promising in achieving better energy costs, while at the same time could overwhelmingly increase the cost of battery degradation. Hence, in the energy markets where the prices change on an intra-hourly basis, we normally have to deal with two sets of competing interests. On one hand, cycling the batteries with maximum frequency to minimize the net cost of energy, and on the other hand, prohibiting the excessive battery wear that is caused by high cycling frequency. Hence, to participate in an intra-hourly bidirectional market, the users should be aware of the potential battery degradation costs associated with different model granularities to make a proper choice regarding the desirable battery scheduling frequency. Different publications have addressed the BTM unit commitment problem in the context of mathematical programming (LP, MILP, etc.) in different time resolutions, most of them considering hourly resolution with daily horizons [6], [10], [13], [14], [18], [47], [91], while some others have employed intra-hourly resolution (5 minutes, 15 minutes, 30 minutes) for their case studies, such as references [12], [36], [44], [52], [68]. However, the impact of the time resolution or granularity of the UC model on the capacity loss of batteries has not been properly addressed in the literature. In this regard, this issue is investigated in this work by presenting a dual-stage energy management strategy for intra-hourly scheduling of EV and ESS that addresses the hourly scheduling in the first layer and produces the intra-hourly schedule in the second layer. This strategy can provide useful information about the impact of model resolution on the capacity fade of batteries. In order to improve the precision of battery degradation estimations, a hardware-in-the-loop simulation is then employed to measure the capacity loss associated with real-world battery cycling conditions. This approach enables us to have a more realistic estimation of the battery wear due to its capability to calculate the nonlinear wear rates in real-time and with higher precision.

1.5.3 Unit commitment with multiple beneficiaries

Investigating the optimal unit commitment for applications where multiple parties (beneficiaries) have conflicting interests demands consideration of battery degradation issue for all the involving

entities. Without consideration of battery wear, chances are some or all parties be in loss due to the excessive degradation of their batteries. In this regard, different publications that have investigated the UC problem for multiple parties ignored the degradation issue as in [1], [39], [50], [52], [55]. However, some other references that have considered battery wear in a way, suffer from shortcomings such as fixed DoD [8] or constant wear rate [5], [51]. In this regard, the UC problem for the microgrid of a public building (an office) that can charge and discharge multiple EVs is investigated in the framework of mixed-integer programming. Similar to the residential building, the office is also considered to benefit from a local energy storage unit, photovoltaic arrays, and bidirectional power transfer with the grid. Investigating optimal UC models that could benefit both the microgrid operator (office) and the EV owners can be realized by employing the battery degradation model that could estimate the capacity loss of every battery during any given optimization horizon. Hence, different strategies are provided by this work to manage the unit commitment in an office in an efficient and fair fashion. Due to the fact that the presented battery wear model addresses the capacity loss of batteries individually, the studied UC strategies can be specifically tailored to minimize the costs for EV owners, MG operators, or all parties to different extents. This approach also can predict the profitability of participating in a V2B service for the EV owners.

Chapter 2: Application of mixed-integer programming in a unit commitment problem

2.1 Introduction to mixed-integer programming

In this chapter, mixed-integer programming as the framework of optimization in this thesis is briefly introduced. “Mathematical programming” in general and its subsets such as “mixed-integer programming” are used for modeling systems and optimizing (e.g., maximizing or minimizing) a function of different variables derived from systems. The limitations of the system (i.e., model constraints) are expressed by restricting functions of decision variables via equations or inequations. By nature, some variables are of discrete type while some others are continuous. The size of a model and subsequently the processing power required for solving it rises exponentially with the number of variables. This modeling method is now very popular in the electricity industry due to its applications in UC problems on different scales. In recent years, to formulate the UC problems, the power system operators in the US have transitioned from using heuristics to MIP models which are solved by commercial branch-and-cut engines such as Gurobi and CPLEX. From an economic viewpoint, this transition is estimated to have saved up to 5 billion dollars a year [20].

In order to introduce mixed-integer programming, first the concept of “linear programming” should be introduced. “Linear program” (LP) is a problem of the form below whose constraints and objective functions are linear. Linear programming problems or simply linear programs include a set of decision variables that are unknown values or are subject to optimization. The objective function in linear programs should be a linear function of the decision variables which is to be maximized or minimized. To enforce the restrictions that limit the decisions, we use constraints in the model which must be written as linear functions of the decision variables. As a general

condition, decision variables cannot be negative values. In this regard, assuming that x_1 to x_n are the decision variables, we can present a linear programming problem as follows.

$$\text{Maximize or minimize } (c_1x_1 + c_2x_2 + c_3x_3 + \cdots + c_nx_n) \tag{2.1}$$

$$\text{Subject to: } a_{11}x_1 + a_{12}x_2 + a_{13}x_3 + \cdots + a_{1n}x_n \ \geq/\leq/= \ b_1 \tag{2.2}$$

$$a_{21}x_1 + a_{22}x_2 + a_{23}x_3 + \cdots + a_{2n}x_n \ \geq/\leq/= \ b_2 \tag{2.3}$$

$$a_{31}x_1 + a_{32}x_2 + a_{33}x_3 + \cdots + a_{3n}x_n \ \geq/\leq/= \ b_3 \tag{2.4}$$

$$a_{m1}x_1 + a_{m2}x_2 + a_{m3}x_3 + \cdots + a_{mn}x_n \ \geq/\leq/= \ b_m \qquad x_j \geq 0 \ \forall j = 1,2,3, \dots, n \tag{2.5}$$

In the model above, normally, c_j values are called objective coefficients, b_j values represent the magnitude of available resources and requirements, and a_{ij} values show the number of resources or requirements i that are utilized or satisfied by decision j. It should be noted that nonlinear terms (e.g., a product of decision variables, the absolute value of variables, or the largest value among different variables) cannot be used in a linear model. Moreover, there is no strict inequality in a linear model.

"Integer Programming" (IP), also referred to as "Integer Linear Programming", is another subset of Mathematical Programming that can be described similar to linear programming (LP) with the exception that in IP as its name implies, all the decision variables take integer values. Furthermore, a "mixed-integer program" (MIP) is similar to a linear problem with the exception that some of the variables must be of integer type. Regarding the types of solutions to MIP problems, if a solution satisfies all the constraints of the model, it is named a "feasible solution". The feasible solution that also leads to the most optimum value for objective function (maximum or minimum depending on the model) is referred to as the "optimal solution". However, if the MIP model has no solution, it is called "infeasible". However, there is a possibility that a mixed-integer program would be feasible but without an optimal solution, and those programs are called "unbounded". This is because in unbounded programs, it is possible to obtain infinitely decent values for objective functions.

In order to model any system by mixed-integer programs, one needs to have an in-depth knowledge of the system's nature. In general, a MIP model could be produced in three steps as follows, where steps 2 and 3 could be switched:

1. Defining the decision variables which constitute the terms that are to be optimized.
2. Defining the model constraints.
3. Defining the objective function.

In many cases, the MIP model may not be correctly and completely built-in entirety in the first attempt, and it may be required to add more variables and constraints and examine the model again multiple times. In this regard, the production process of MIP models can be considered as a loop [92]. To solve a practical mathematical programming problem, it is crucial to take into consideration the potential changes needed to be made to the primary model from the beginning. In fact, during the production process of the mathematical model, some modifications may turn the initial model into a different class of models. For instance, an LP model could turn into a MIP by adding some simple discrete constraints [93], also a MILP could turn into a mixed-integer nonlinear program (MINLP) by adding some nonlinear constraints that cannot be replaced with linear alternatives.

A mixed-integer program (MIP) can be expressed as follows:

$$max\{c^T x: b_1 \leq Ax \leq b_2, d_1 \leq x \leq d_2, x_j \in \mathbb{Z}\ for\ j \in S\} \tag{2.6}$$

where, $b_1, b_2 \in \mathbb{R}^m$, $d_1, d_2 \in \mathbb{R}^n$, $S \subseteq \{1,2,\dots,n\}$, A is a real $m \times n$ matrix, x is an n vector of variables and S is the array of integer variables

In integer programs where all variables are of integer type, $|S| = n$, also in linear programs as there is no integer variable, $S = \emptyset$. The fact that MIP includes discrete variables, makes them more complex and one of the most difficult mathematical programs from the algorithm viewpoint despite their simple formulation [93]. In the model above, $b_1 \leq Ax \leq b_2$ represents a linear constraint and

$d_1 \leq x \leq d_2$ represents a bound constraint. The x_j variables that must take integer values are integrality constraints. The integrality constraints allow a program to model the discrete nature of a decision such as turning on or off a generator.

In the MIP above, a vector such as $y \in \mathbb{Q}^n$ is called a feasible solution provided that it satisfies linear constraints, bound requirements, and integrality restrictions of the model. A solution such as y^{opt} is considered an optimal solution if it satisfies $y^{opt} = c^{opt}$. If there are no integrality restrictions, the MIP is considered a linear program (LP). Hence, the LP-relaxation of a MIP program is obtained by neglecting the integrality restrictions. Solving the LP-relaxation to optimality provides the lower bound on the optimal objective of the model [94].

Nonlinearity is the factor that can turn a MILP into an MINLP and make it significantly hard to solve for computers. Simplifying nonlinearities or modifying the nonlinear terms to make them less complex while representing the same mathematical concept is often used in MIP modeling. One way to address the nonlinearities in MIP constraints is by modeling them using integer variables. In fact, by introducing additional integer variables to a MIP model, it is possible to model many nonlinearities by employing linear constraints. For example, in the following constraint, *x* must be an integer to satisfy the equation.

$$sin(\pi x) = 0 \tag{2.7}$$

Also, the following equation enforces the fact that *x* is a binary number.

$$x^2 - x = 0 \tag{2.8}$$

Hence, various optimization problems can be formulated as "Quadratic Programming" (QP) problems that incorporate quadratic terms. In other words, a MIP problem could be simplified down to a quadratic model. Although integer programming could be considered different in the sense that integer values are handled at the algorithmic level by implementing branching and cuts.

In order to handle the nonlinearity in MIP models, a nonlinear function can be simplified by piecewise linear approximation. Let us assume $f(x)$ is a function defined between [a,b] where,

$$a = \overline{x_1} < \overline{x_2} < \cdots < \overline{x_r} = b \tag{2.9}$$

By connecting the adjacent breakpoints on this nonlinear function with lines, a piece-wise linear approximation of $f(x)$, which is denoted with $\tilde{f}(x)$, can be obtained as illustrated in figure 2.1.

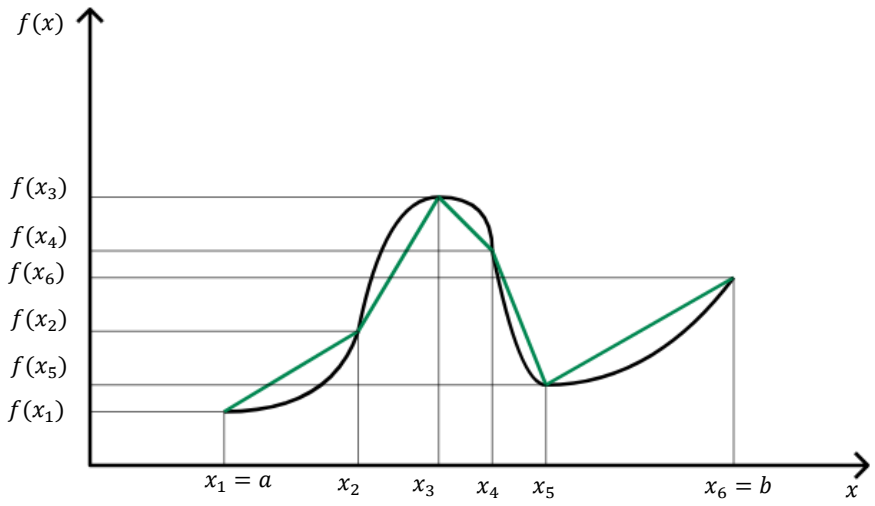

Figure 2.1: Piecewise linear approximation of a nonlinear function [93]

Thus, $\tilde{f}$ can be represented by the following model:

$$x = \sum_{k=1}^{r} \lambda_k \bar{x}_k \tag{2.10}$$

$$y = \sum_{k=1}^{r} \lambda_k \bar{y}_k \tag{2.11}$$

$$\sum_{k=1}^{r} \lambda_k = 1 \tag{2.12}$$

$$\lambda_k \leq \delta_k, \qquad k = 1,2,\dots,r \tag{2.13}$$

$$\delta_i + \delta_j \leq 1, \qquad j = 3,\dots,r, \quad i = 1,2,\dots,j-2 \tag{2.14}$$

$$\lambda_k \geq 0, \qquad \delta_k \in \{0,1\}, \quad k = 1,2,\dots,r \tag{2.15}$$

The first three equations enforce that the point (*x*, *y*) belongs to the convex hull of the points $(\bar{x}_1, \bar{y}_1)$,…., $(\bar{x}_r, \bar{y}_r)$. The second three inequations enforce the fact that at most, two λ_k variables can be nonzero values and also those nonzero values must be consecutive numbers. In fact, these conditions are the mathematical representation of the fact that the point (*x*,*y*) must lie on a line segment that connects to adjacent breakpoints [93].

To obtain an intuitive understanding of how a mathematical program and in particular MIP works, one needs to notice that mathematically, a "program" is solved altogether. Therefore, there is no sequential process for addressing the model components. In order to solve a MIP model, all the constraints and objective functions must be considered at once to explore the best solutions that lead to the desirable optimality. Hence, even though the computers solve problems during multiple machine cycles, there is no precedence in addressing the model components during the solution process.

Probably, the best way to learn how to produce a mixed-integer program is to study the existing MIP models [93]. MIP can be applied in a wide range of industries such as energy, transportation, health, automotive, etc. In this regard, a classic and relevant application of MIP in the energy industry, which is electricity generation planning, is reviewed in this section. One of the use cases

of MIP in real-life applications is in UC problems. The goal of a UC problem is to produce a power generation schedule for a certain horizon (e.g., a day or a year) with a certain resolution (e.g., hourly or intra-hourly). In other words, the outcome of a UC problem shows how much power should be delivered by which generators. Hence, it has been used to schedule the operation of traditional diesel generators or balance the use of different generators with different capacities. More recently, it has also gained interest in scheduling renewable energy-based generators and energy storage systems.

Assume that the problem is to minimize the operation cost of n generators that are going to work for T periods and feed the load demand which is equal to d_t in each period t. To be on the safe side, the maximum power of generators in each period must be at least q times the load demand in the same period. Now, the MIP objective function is meant to minimize the total cost of the operation for all the generators during the entire horizon and includes the start-up costs. It is defined by:

$$min \sum_{i=1}^{n} \sum_{t=1}^{T} (g_i z_{it} + f_i x_{it} + p_i y_{it}) \tag{2.16}$$

Where, g_i denotes the start-up cost for the generator i from the off state in period t, f_i is the fixed operation cost in period t, p_i is the variable cost of the operation in period t (operation cost at level v in a period is $f_i + vp_i$), z_{it} is a binary value representing the switching status of the generator i in period t (1: switched, 0: not switched), x_{it} is a binary value representing the generation status of the generator i in period t (1: generating, 0: not generating), y_{it} is the generated power of the generator i in period t. Moreover, the model constraints are presented as follows.

$$\sum_{i=1}^{n} y_{it} = d_t, \quad t = 1,2, \dots, T \tag{2.17}$$

$$\sum_{i=1}^{n} u_i x_{it} \geq q d_t, \quad t = 1,2,\dots,T \tag{2.18}$$

$$l_i x_{it} \leq y_{it} \leq u_i x_{it}, \quad i = 1,2,\dots,n, \quad t = 1,2,\dots,T \tag{2.19}$$

$$-r_i^1 \leq y_{it} - y_i, \big((t-2+T)\ mod\ T\big) + 1 \leq r_i^2, \quad i = 1,2,\dots,n, \quad t = 1,2,\dots,T \tag{2.20}$$

$$x_{it} - x_i, \big((t-2+T)\ mod\ T\big) + 1 \leq z_{it}, , \quad i = 1,2,\dots,n, \quad t = 1,2,\dots,T \tag{2.21}$$

$$z_{it} \leq x_{it}, \quad i = 1,2,\dots,n, \quad t = 1,2,\dots,T \tag{2.22}$$

$$x_{it}, z_{it} \in \{0,1\}, \quad i = 1,2,\dots,n, \quad t = 1,2,\dots,T \tag{2.23}$$

$$y_{it} \in \mathbb{R}_+, \quad i = 1,2,\dots,n, \quad t = 1,2,\dots,T \tag{2.24}$$

where, u_i represents the maximum power of the generator i, l_i is the minimum operating power of the generator i, r_i^1 is the maximum power decrease (ramping) of the generator i between two consecutive periods and r_i^2 expresses the maximum power increase (ramping) of generator i between two consecutive periods [93].

Equation (2.17) enforces the fact that the total generation of generators at each interval must be equal to the load demand. Inequation (2.18) guarantees that the maximum power of the operating generators is sufficiently large. Inequation (2.19) confines the generation of the generator i to the values between the maximum and minimum range. Inequation (2.20) ensures that the ramp up and ramp down rates of generators do not exceed their ramping specifications, where the interval $\big((t-2+T)\ mod\ T\big) + 1$ is followed by the interval t. Inequations (2.21) and (2.22) enforce the fact that the generator i is operating at the interval t provided that it has switched on in this interval or the prior intervals. Equations (2.23) and (2.24) declare that x_{it} is a binary value (on/off) while z_{it} could take any positive value.

2.2 Solving methods of MIPs

There are two popular approaches for solving MIP problems, namely the cutting plane methods, and the branch and bound methods [95]. Some other alternatives also exist for solving a MIP

problem such as metaheuristic methods. However, branch & bound, and cutting planes are the dominant methods that are also used in the majority of solvers including Gurobi, which is used for this work [96]. These methods are briefly introduced in the following section.

2.2.1 Branch and bound

MILP problems are often solved by an LP-based branch-and-bound algorithm. In this regard, as the first step of the algorithm, all the integrality restrictions of the model are removed which leads to a linear program also referred to as LP-relaxation of the original MIP, and then this LP is solved. Although this is unlikely in most cases, however, in case the results of the LP could satisfy the integrality restrictions, they can be considered as the solution of the original MIP which means the optimization is over. However, in most cases, the LP-relaxation results will not satisfy the integrality restrictions. Hence, the next step is to select some variable that is restricted to be an integer but has a fractional value in the LP relaxation. Let us assume x is such a variable whose value in the LP relaxation is 5.6. Therefore, this value can be excluded by setting new restrictions such as $x \leq 5$ and $x \geq 6$. If the original MIP is P_0, then P_1 could be a subproblem with restriction $x \leq 5$ and P_2 could be another subproblem with restriction $x \geq 6$. In this case, x is called a branching variable. At this stage, if the optimal solution can be obtained for P_1 or P_2, the better of those two solutions would be the optimal solution to the P_0. In the next step, the same process can be done for every one of the branches by solving their corresponding LP relaxations and selecting the branching variables if needed. This process will result in what is referred to as a search tree. In a search tree, as shown in figure 2.2, MIPs produced by the branching procedure are called nodes where P_0 represents the root node. Those nodes, from which the branching is not performed, could be considered the leaves of the tree. Reaching a point where we can either solve or remove all the leaf nodes means the original MIP, P_0, has been solved [97].

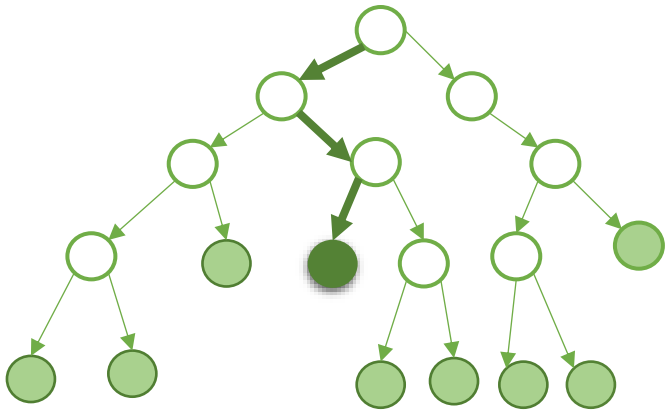

Figure 2.2: Branching in the branch and bound algorithm

In the branch-and-bound algorithm, optimization problems are divided into smaller pieces recursively to create search trees, such as the one in figure 2.2, and enumerate the potential assignments of integers. In fact, branching and splitting the problems into smaller subproblems is repeated until the individual subproblems can be solved. Every node on the search tree is the representation of one subproblem [94].

Following the introduction of the branch and bound algorithm, it is worth explaining the concepts of fathomed and incumbent nodes. In this regard, a case is assumed where the target is to minimize an objective and the LP relaxation of some node in the search tree has been solved. In case every integrality constraint, in P_0, is satisfied at this node, it means that a feasible solution to the original problem has been obtained. At this stage, we could refer to this node, which is also a permanent leaf, is referred as fathomed. Hence, it is not essential to branch on this node. The incumbent can be defined as the best integer solution obtained at any point during the search. Thus, it can be said that at the beginning of the search, there is no available incumbent. In case the obtained integer solution leads to a better objective function value compared to the current incumbent or if there is no incumbent at all, the current solution can be regarded as the new incumbent. Otherwise, the search can be proceeded without updating the incumbent [97].

Best bound and gap are two other relevant factors that should be introduced here. Let us assume that there is a minimization MIP problem. Now, if we have an incumbent, the objective value corresponding with that incumbent is a valid upper bound on the optimal answer to the MIP problem. It means that the integer solution of any value will be lower than this value. Furthermore, during the searching process, there is also a valid lower bound which is called the best bound. This bound is also the minimum of the optimal objective values among the leaf nodes. The difference between the lower and upper bounds at each moment is called the gap. Therefore, once the gap is equal to zero the search has reached optimality [97].

2.2.2 Cutting planes

The idea of cutting plane is basically restricting the formulation of a problem by disposing of the undesirable fractional solutions during the solution process without inflicting undesirable side effects such as introducing additional subproblems [97]. Once a mixed-integer program has been formulated, we could improve it by the addition of new inequalities that have two characteristics. First, they must be valid for all the feasible solutions, and second, they must be invalid for the relaxation polyhedron, where polyhedron is the set of solutions in a system of linear inequalities [93]. These inequalities are referred to as cuts and they can be added at the time of formulating or during the solution process of the problem. It would be better to explain the cutting planes algorithm by an example. Let us assume the following integer program.

$$\text{Maximize } x_1 + 2x_2 \tag{2.25}$$

$$s.t.\ \ 3x_1 + 2x_2 \leq 9 \tag{2.26}$$

$$x_2 \leq 2 \tag{2.27}$$

$$x_2, x_2 \in \mathbb{Z}_+ \tag{2.28}$$

The first step is to solve the LP relaxation of this IP by allowing the integer variable to take real values as well. Figure 2.3 demonstrates the feasible prototype (P_0) of the LP relaxation as well as

the optimal solution ($x^{(0)} = (\frac{5}{3}, 2)^T$). However as $x^{(0)}$ is not an integer, it cannot be considered as a solution to the IP. Now, an inequality that cuts off $x^{(0)}$ from the set of feasible solutions is called "cut" or "cutting plane".

$$X = \{x \in \mathbb{Z}_+^2 : 3x_1 + 2x_2 \leq 9, x_2 \leq 2\} \tag{2.29}$$

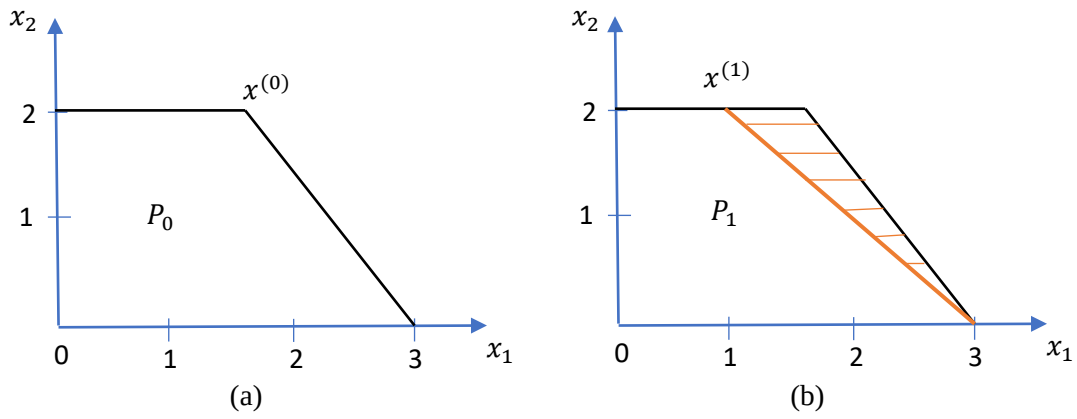

Figure 2.3: Example of Cutting planes algorithm

These cuts can be built in different ways. In this example, the point $x^{(0)}$ was removed based on the following observation. Both inequalities of the IP model cannot be satisfied simultaneously at the points from X. Thus, the following inequality is true for X but not for $x^{(0)}$ as $(3 \times 1.66 + 3 \times 2 > 10)$.

$$3x_1 + 2x_2 + x_2 \leq 9 + 2 - 1 \quad or \quad 3x_1 + 3x_2 \leq 10 \tag{2.30}$$

Therefore, we can simplify the cut as follows.

$$x_1 + x_2 \leq \left\lfloor \frac{10}{3} \right\rfloor = 3 \tag{2.31}$$

This inequality can now be added to the model constraints. It is worth noting that the cut-off region does not include integers and subsequently no feasible point from X. Also, X is included in the

feasible prototype of the new LP relaxation. Now, the point $x^{(1)} = (1,2)^T$ is an optimal solution to the LP, and as it is an integer $x^{(1)}$ is an optimal solution to the IP [93].

Apart from the introduced search algorithms, the field of MIP has advanced significantly in recent years and several other capabilities and techniques have been developed most of which aim at lowering the size of the search tree. Presolve, heuristics, parallelism, symmetry detection, etc., are some of these techniques. However, introducing these techniques is out of the scope of this work [97]. Different commercial software packages such as CPLEX, Gurobi, and Xpress and several non-commercial or open-source solvers such as MINTO, SCIP, and SYMPHONY are available for solving mixed-integer programs. These packages use variants or combinations of cutting planes and branch and bound methods and are accessible by different modeling languages such as C, C++, Java, MATLAB, and Python [98].

2.3 Modeling a day-ahead unit commitment problem for a residential microgrid in the framework of MIP

In this section, a MILP unit commitment model for a residential building (home energy management system (HEMS)) is produced and solved in the context of a case study. HEMS is one of the key parts of a smart home that controls the optimal cooperation of multiple systems such as smart meters, EVs, ESS, different types of power generators, and loads [45] under any market scenario.

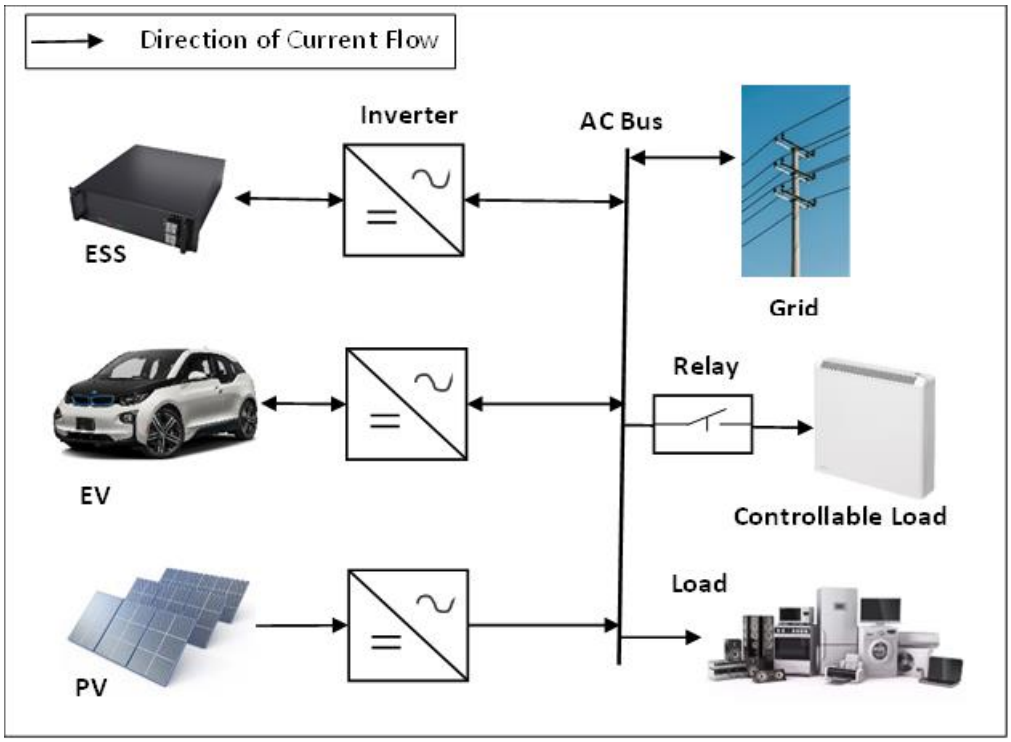

Figure 2.4: Schematic of the studied AC-bus microgrid

When it comes to the energy market, we could classify the energy pricing schemes into static and dynamic types. Where static pricing schemes (e.g., fixed prices) are normally determined in advance and do not change with the grid condition. However, dynamic pricing schemes (e.g., real-time pricing) depend on the regional marginal prices and are normally determined a day or hours ahead, which enables the consumers to plan ahead of time to minimize their costs or maximize benefits [68].

In this regard, a day-ahead UC problem for a typical residential building under dynamic pricing has been laid out in this section. The building was considered to be facilitated with the common components of a modern home, including photovoltaic arrays, a battery-based energy storage system, charging equipment for an electric vehicle, and an electric vehicle, controllable loads and regular (non-controllable) loads. These components are interconnected on an AC bus and could constitute an AC-bus microgrid. Considering a residential/commercial-based microgrid situated in

urban areas is supposed to operate grid-connected most majority of the time, it is assumed that the frequency and voltage of the main bus are maintained by the grid. Hence, in a practical application, a low bandwidth communication link between the EMS and the components is sufficient to send the reference points that lead to optimal energy management.

In a real-world scenario, the practical system configuration for the studied microgrid would be as follows. The ESS is essentially an AC battery equipped with a battery management system (BMS) that could protect the battery from overcharging and discharging. The battery is then connected to a battery inverter that can operate in P/Q mode to inject and absorb power to and from an AC bus. The battery inverter must be able to provide and take continuous amounts of power based on the reference values it receives from a microgrid controller (EMS). The EV must be able to provide bidirectional power flow through the V2X circuitry. Regarding the EV charging facilities, residential buildings are normally equipped with type 1 or 2 charging systems that provide different levels of charging power. However, regardless of the charging power, the EV charging equipment in this work is supposed to have two major features. First, the power converter which is responsible for charging the EV battery should be able to work bi-directionally so it can also discharge the EV battery. Also, similar to the ESS inverter, it is assumed that the EV's power converter is able to charge and discharge the EV battery with continuous amounts of power based on the reference signals received from the microgrid controller.

In the grid-connected operation of a microgrid, PV inverters work on the MPPT mode most of the time to produce the maximum possible amount of power. Hence, the user normally avoids controlling the current/power of the PV inverter in the grid-connected mode unless there is a need for providing ancillary services by the microgrid. In this regard, as this thesis is focused on producing UC models for grid-connected systems, the PV power is not considered a control variable in the MIP models, and it is addressed as a model parameter that should be provided through prediction or by a third-party.

Concerning the controllable loads, they are of two types, including thermostat loads such as water heaters and air conditioners which can be flexible and controlled but always have to be supplied. The other type is deferrable loads that need to be powered for a specific but shiftable duration such as dishwashers and washing machines [69]. Controllable loads in this work are of the deferrable type that can be operated at alternative times. In fact, these loads can be operated at the optimal times by the microgrid controller via relays and/or timers. However, the regular or non-controllable loads are the type of loads that cannot be scheduled or shifted such as lighting, TV, etc. The microgrid is then operated and monitored by a microgrid controller which includes the energy management or UC algorithm for scheduling the batteries and controllable load. In order to manage the operation of a microgrid in the grid-connected mode, the MG controller could communicate with power converters, relays, etc., via a low bandwidth communication link.

Now, the mixed-integer programming model required for the day-ahead unit commitment of the introduced microgrid is provided as follows. This model is to schedule the operation of ESS and EV battery chargers as well as controllable-load relay throughout a certain horizon (e.g., a day) with a certain resolution (e.g., one-hour). This mathematical model could be incorporated into the energy management program of a microgrid controller. In this regard, the following equations lay out the MIP model constraints and objective functions to minimize the operation cost of the microgrid.

2.3.1 MIP constraints of ESS

Equations (2.32)-(2.38) provide the MIP constraints associated with the ESS component where (2.32) shows that the applicable part of the discharging power of ESS is composed of a portion that is consumed in the microgrid and a portion which is exported to the grid. Equation (2.33) sets a maximum amount for the charging power of ESS at every interval and equation (2.34) defines the maximum discharging power of ESS. Equation (2.35) enforces the fact that the state of energy or the amount of energy stored in ESS at every interval is a function of the state of energy at the

previous interval as well as the charged or discharged energy in the previous interval. Equations (2.36) to (2.38) define the initial, maximum, and minimum states of energy for ESS respectively [13].

$$P_{es}^{n,con} + P_{es}^{n,ex} = P_{es}^{n,dis} \times \eta_{es}^{dis} \qquad \forall n \in N \tag{2.32}$$

$$P_{es}^{n,ch} \leq U_{es}^{n} \times P_{es}^{ch} \qquad \forall n \in N \tag{2.33}$$

$$P_{es}^{n,dis} \leq (1 - U_{es}^{n}) \times P_{es}^{dis} \qquad \forall n \in N \tag{2.34}$$

$$SE_{es}^{n} = SE_{es}^{n-1} + \left(\eta_{es}^{ch} \times P_{es}^{n-1,ch} \times G\right) - (P_{es}^{n-1,dis} \times G) \qquad \forall n \in [n_b + 1, n_e + 1] \tag{2.35}$$

$$SE_{es}^{n} = SE_{es}^{ini} \quad for\ n = n_b \tag{2.36}$$

$$SE_{es}^{n} \leq SE_{es}^{max} \qquad \forall n \in [n_b\ , n_e + 1] \tag{2.37}$$

$$SE_{es}^{n} \geq SE_{es}^{min} \qquad \forall n \in [n_b\ , n_e + 1] \tag{2.38}$$

The superscript n in these equations and this thesis refers to the n_{th} time interval of the day and N is the set of intervals of the day, therefore its size depends on the resolution of the model. n_b and n_e are the intervals corresponding with the beginning and end of the optimization horizon. In other words, these two intervals are the first and last elements of the N respectively. In a day-ahead optimization with an hourly model resolution, N is a set of 24 elements that represent the 24 hours of the day. In these equations, $P_{es}^{n,con}$ represents the portion of the ESS power at the n_{th} interval which is consumed locally. $P_{es}^{n,ex}$ denotes the portion of the ESS power at the n_{th} interval which is exported to the grid. $P_{es}^{n,dis}$ denotes the discharging power of ESS at the n_{th} interval, η_{es}^{dis} refers to the discharging efficiency of the charging equipment which is a value between 0 and 1. $P_{es}^{n,ch}$ is the charging power for charging the ESS at the n_{th} interval, U_{es}^{n} represents the n_{th} element of an array (referred to as "charging array of ESS") which has N binary members which could be either 0 or 1. P_{es}^{ch} denotes the maximum charging power or charge rating of the ESS which depends on the charging equipment. P_{es}^{dis} represents the maximum discharging power or discharge rating, SE_{es}^{n}

denotes the state of energy of ESS at the n_{th} interval, and accordingly SE_{es}^{n-1} denotes the same variable at the $(n-1)_{th}$ interval. η_{es}^{ch} represents the efficiency of the charging process of ESS which depends on the charging equipment and is a factor between 0 and 1. G is the granularity or resolution of the model whose dimension is time (hour). SE_{es}^{ini} denotes the initial state of energy of ESS at the first interval of the model. SE_{es}^{max} and SE_{es}^{min} represent the maximum and minimum allowed amounts of stored energy in the ESS respectively. It is considered charging and discharging the ESS beyond these levels could significantly increase their wear rate. In this thesis, all the power variables and parameters are considered to be in kilowatt. Also, all the energy (or state of energy) variables and parameters are assumed to be in kilowatt-hours.

2.3.2 MIP constraints of EV

The following constraints address the EV battery in the MIP model. Equation (2.39) shows that the applicable part of the discharging power of an EV battery includes a portion that is consumed in the microgrid and a part that is exported to the grid. Inequation (2.40) specifies a maximum amount for the charging power of the EV battery at every interval and inequation (2.41) sets the maximum discharging power for the EV battery. Equation (2.42) enforces the fact that the state of energy of an EV battery at every interval depends on its state of energy at the previous interval plus the charged or discharged energy during the previous interval. Equations (2.43) to (2.46) enforce the initial, maximum, minimum, and final states of energy for the EV battery respectively. Equation (2.47) enforces the fact that during the EV's absence times, all the power and energy variables associated with it are equal to zero.

$$P_{ev}^{n,con} + P_{ev}^{n,ex} = P_{ev}^{n,dis} * \eta_{ev}^{dis} \quad \forall n \in [n_a, n_d] \tag{2.39}$$

$$P_{ev}^{n,ch} \leq U_{ev}^{n} \times P_{ev}^{ch} \quad \forall n \in [n_a, n_d] \tag{2.40}$$

$$P_{ev}^{n,dis} \leq (1 - U_{ev}^{n}) \times P_{ev}^{dis} \quad \forall n \in [n_a, n_d] \tag{2.41}$$

$$SE_{ev}^{n} = SE_{ev}^{n-1} + \left(\eta_{ev}^{ch} \times P_{ev}^{n-1,ch} \times G\right) - \left(P_{ev}^{n-1,dis} \times G\right) \quad \forall n \in [n_a + 1, n_d + 1] \tag{2.42}$$

$$SE_{ev}^{n} = SE_{ev}^{ini} \quad for\ n = n_a \tag{2.43}$$

$$SE_{ev}^{n} \leq SE_{ev}^{max} \quad \forall n \in [n_a, n_d + 1] \tag{2.44}$$

$$SE_{ev}^{n} \geq SE_{ev}^{min} \quad \forall n \in [n_a, n_d + 1] \tag{2.45}$$

$$SE_{ev}^{n} \geq SE_{ev}^{ch} \quad for\ n \geq n_{ch} \in [n_a, n_d] \tag{2.46}$$

$$P_{ev}^{n,con} = P_{ev}^{n,ex} = P_{ev}^{ch} = P_{ev}^{n,dis} = SE_{ev}^{n} = 0 \quad \forall n \notin [n_a, n_d] \tag{2.47}$$

Where n_a is the interval of EV's arrival and n_d is the interval of EV's departure. These two intervals are provided by the user. $P_{ev}^{n,con}$ represents the portion of the EV power at the n_{th} interval which is consumed in the microgrid. $P_{ev}^{n,ex}$ denotes the portion of the EV power at the n_{th} interval which is exported to the grid. $P_{ev}^{n,dis}$ represents the discharging power of the EV battery at the n_{th} interval, η_{ev}^{dis} refers to the discharging efficiency of the EV charging equipment which is a value between 0 and 1. $P_{ev}^{n,ch}$ denotes the charging power for charging the EV battery at the n_{th} interval, U_{ev}^{n} represents the n_{th} element of an array referred to as charging array of EV which has *N* binary members which could be either 0 or 1. P_{ev}^{ch} denotes the maximum charging power of the EV battery which depends on its charging equipment. P_{ev}^{dis} represents the maximum discharging power, SE_{ev}^{n} denotes the state of energy of EV battery at the n_{th} interval. η_{ev}^{ch} is the efficiency of the charging process which depends on its charging equipment and is a factor between 0 and 1. SE_{ev}^{ini} denotes the initial state of energy of the EV battery at the first interval. SE_{ev}^{max} and SE_{ev}^{min} denote the maximum and minimum allowed amounts of stored energy in the EV battery respectively and SE_{ev}^{ch} is the user's desirable state of energy at the time of departure.

2.3.3 MIP constraints of PV system

The following equation enforces the fact that the applicable portion of the photovoltaic power is partly consumed at home and partly exported to the network [13].

$$P_{pv}^{n,con} + P_{pv}^{n,ex} = P_{pv}^{n,gen} \times \eta_{pv} \qquad \forall n \in N \tag{2.48}$$

In this equation, $P_{pv}^{n,con}$ is the PV power that is consumed locally at the n_{th} interval, $P_{pv}^{n,ex}$ denotes the portion of the PV generation that is exported to the power network and $P_{pv}^{n,gen}$ is the total generated power of the PV array at the n_{th} interval. However, as some part of the PV generation is wasted in the power interfaces, η_{pv} is also defined as the efficiency of the PV system.

2.3.4 MIP constraints of controllable loads

Controllable load is the other type of component whose operation is planned by the presented UC algorithm. The UC model is laid out for a deferrable controllable load that works at fixed amount(s) of power while its operation times can be shifted to different times of the day. In this regard, equation (2.49) shows that the power which is assigned to the controllable load at any interval is the product of a binary number and the nominal power of the controllable load. Equation (2.50) specifies the count of intervals that controllable load must work consecutively whenever it is operated. For example, in a model with an hourly resolution, a dryer that works for one hour each time it is operated, works for one interval every time. Equations (2.51) and (2.52) determine the number of times associated with the start and stop of operation over a day. The operation period(s) of the load is enforced through (2.53) and (2.54), where two arrays of binary numbers associated with the start and finish intervals of load operations are defined and the sum of their elements is equated with the number of times that the load needs to operate in a day. Equation (2.53) enforces that the first and last intervals of every working period of load carry the same corresponding binary values in their start and finish arrays. Equation (2.54) provides the condition between the associated

array elements that must be satisfied to schedule to controllable load properly. It is worth noting that the controllable load could possibly be modeled in other ways as well.

$$P_{cl}^{n} = D_{cl}^{n} \times P_{cl} \qquad \forall n \in N \tag{2.49}$$

$$\sum_{N} D_{cl}^{n} = n_{cl}^{row} \tag{2.50}$$

$$\sum_{N} S_{cl}^{n} = n_{cl}^{day} \tag{2.51}$$

$$\sum_{N} F_{cl}^{n} = n_{cl}^{day} \tag{2.52}$$

$$S_{cl}^{n} = F_{cl}^{n+\, n_{cl}^{row}} \qquad \forall n \in N \tag{2.53}$$

$$S_{cl}^{n} + F_{cl}^{n} + S_{cl}^{n-1} \times F_{cl}^{n+1} = D_{cl}^{n} \qquad \forall n \in N \tag{2.54}$$

Where, P_{cl}^{n} represents the power of controllable load at the n_{th} interval. If we consider D to be an array with N binary elements that controls the operation status of controllable load (1 causing the load to operate and 0 causing it to not operate), D_{cl}^{n} is defined as the n_{th} element of D. This shows that controllable load is operated in a binary fashion in this model. P_{cl} denotes the nominal operating power of controllable load, n_{cl}^{row} is the count of intervals in a row required for every operating iteration which depends on the resolution of the problem and operation length of the load. Considering S and F as arrays associated with the start and finish of load operation, each with N binary elements, S_{cl}^{n} is defined as the n_{th} member of the S, and F_{cl}^{n} is defined as the n_{th} element of F. n_{cl}^{day} denotes the number of times that controllable load needs to function every day which is specified based on the user's demand.

2.3.5 MIP constraints for power balance

After defining the constraints associated with each component, the governing equations of the microgrid should also be determined. In an AC-bus operational microgrid, the total power that is delivered to the AC bus at every moment equals the total power that is drawn from the bus. This

simple rule which demonstrates the power balance is enforced by (2.55). In fact, at any given moment, the sum of imported power from the grid, the consumed and exported power from EV battery, ESS, and PV system is equal to the sum of feed-in (exported) power, charging power of EV battery, ESS and the power of all the loads [13].

$$P_{im}^{n} + P_{ev}^{n,con} + P_{ev}^{n,ex} + P_{es}^{n,con} + P_{es}^{n,ex} + P_{pv}^{n,con} + P_{pv}^{n,ex} = P_{ex}^{n} + P_{ev}^{n,ch} + P_{es}^{n,ch} + P_{cl}^{n} + P_{l}^{n} \quad \forall n \in N \tag{2.55}$$

Where P_{im}^{n} denotes the power that is imported from the electric network, P_{ex}^{n} is the power that is exported to the electric network and P_{l}^{n} is the power consumption of regular load at the n_{th} interval.

2.3.6 MIP constraints for Power exchange

The power which is fed to the grid from the microgrid is composed of three components, the exported power from EV battery, ESS, and photovoltaic system. This rule is enforced via equation (2.56). However, the power transaction between the microgrid and the grid has a limit which depends on the ratings of the protection equipment, the utility meters, and potential DR services offered by the microgrid. In general, there must be a limit for the imported and exported power from and to the grid which is enforced by inequations (2.57) and (2.58).

$$P_{ex}^{n} = P_{ev}^{n,ex} + P_{es}^{n,ex} + P_{pv}^{n,ex} \quad \forall n \in N \tag{2.56}$$

$$P_{im}^{n} \leq P_{im}^{max} \times U_{im}^{n} \quad \forall n \in N \tag{2.57}$$

$$P_{ex}^{n} \leq P_{ex}^{max} \times (1 - U_{im}^{n}) \quad \forall n \in N \tag{2.58}$$

Where, P_{im}^{max} represents the maximum allowed power that can be imported by the microgrid. If U_{im} is considered as an array with N binary elements associated with the occurrence of power import in every interval, U_{im}^{n} is the n_{th} member of U_{im}. Also, P_{ex}^{max} represents the maximum power that can be exported to the grid.

2.3.7 Conventional objective function

Typically, the MIP unit commitment models in smart grid problems are solved for achieving the minimum monetary cost of energy or maximum potential profits. In a bi-directional market with time-of-use or dynamic energy pricing where users can buy and sell energy from and to the grid through a single or separate utility meters, the UC problem can be designed to minimize the cost of energy, maximize the revenue from energy selling or achieve each objective to some extent. Alternatively, the objective could be achieving the minimum algebraic net cost of transferred energy which could be a positive or negative value. A positive net energy cost reflects the fact that the total cost of energy consumption throughout the optimization term exceeds the total revenue from energy selling. Whereas a negative net value shows that the total revenue is larger than the total cost. Selecting the objective function boils down to the user preferences and to some extent, the energy measurement (AMI) configuration. For instance, a user might utilize two different utility meters for selling and buying energy which will undermine the structure of MIP and objective functions. In this work, the objective is to minimize the net cost of transferred energy over a given time horizon. The outcome of this objective function is the fee that the user must pay to the energy provider if the value is positive or the fee that the user must be paid to if the value is negative. Achieving the minimum paid energy fee seems to be a decent objective for scheduling the batteries in a smart grid problem. However, this objective does not take into consideration the important fact that batteries become worn out as they are employed in the microgrid. This costly wearing process can be intensified by more frequent or deeper cycling regimes which may be required to achieve the minimum energy cost. In fact, the degradation cost of batteries could possibly exceed the apparent monetary profit that could be obtained from their operation in a microgrid. However, this important fact is neglected when considering the energy cost as the sole objective of the problem and this has been traditionally practiced in many studies. Moreover, environmental aspects of the microgrid operation such as the carbon footprint is another factor that is neglected in a traditional

cost function. In this section, apparent energy cost as the conventional (basic) objective function is presented in (2.59) [13]. Although we may be able to consider the capital, operation, and maintenance expenses of chargers and feeders as the costs associated with EV charging [99], however, those costs cannot be treated as control variables. Hence, the energy cost and battery wear cost are variables that can be minimized by solving an optimization problem. In the next chapters, this problem will be investigated by addressing the battery degradation and carbon footprint of the user as other important objectives.

$$Min \sum_{N} \left(P_{im}^{n} \times T^{n,buy} \times G\right) - \left(P_{ex}^{n} \times T^{n,sell} \times G\right) \tag{2.59}$$

In this objective function, $T^{n,buy}$ is the buying tariff of energy unit (from the grid) and $T^{n,sell}$ is the selling tariff of energy unit (to the grid) at the n_{th} interval. If power variables are considered in kW and granularity (G) in hour, the tariffs could be stated in cent/kWh.

2.4 Case study: A MIP UC problem for a residential microgrid

In order to study the explained UC model, a case study has been investigated in this section for a residential unit. This case study serves as a preliminary step for studying more sophisticated UC models in the next chapters. Later in this work, the results of this case study will be compared with the results of more realistic models that can estimate battery wear. That comparison will show the deficiencies of the current model as a "basic" or "conventional" model which is used by several works of literature [1], [17], [23], [35], [48], [50], [55].

In this regard, the studied example is a home facilitated with the following equipment. A 3kW PV system including a 3kW PV array and a 3kW MPPT PV inverter, a 2.5kWh battery-based energy storage system with a grid-connected battery inverter. With regards to the capacity of the EV battery, reference [2] reports that a 16kWh battery is sufficient for 80% of transportation needs. Hence, for this work, an electric vehicle with a 22kWh battery storage (as in BMW i3-60Ah) was

selected. In this configuration, the ESS and EV batteries are supposed to be charged and discharged by bi-directional grid-connected battery inverters which are capable of receiving continuous power references from an external source. In this context, depending on the availability of technologies, the power converters that receive the reference points of EV battery and ESS could be installed onboard the EV and ESS or exist external to these devices. From a model perspective, the power conversion stages of all batteries are merely interfaces for sending the reference values to the batteries and are only modeled with an efficiency factor (η). As for the controllable load, it is considered that a 3 kW home thermal storage unit is used and set to operate for two consecutive hours over a day. These devices can be used for load shifting in the time-of-use markets by storing heat during the off-peak hours and releasing it during peak hours. The power profile for the typical or non-controllable load was acquired from [100], and the energy tariffs for the purchased energy were obtained from [101]. Usually, the general practice for assuming the feed-in tariffs is taking a percentage of the corresponding purchase tariffs as in [44]. In this work, it was considered that the feed-in price for every time interval was 0.8 of that of the purchase tariff. Also, it was assumed that the EV departs home at 8 AM and returns at 18. The initial SoC of EV battery and ESS were considered 40% and 50% respectively. Therefore, the EV is connected to the microgrid and is expected to be charged up by the next morning. The solar irradiance was obtained from [102] and the generated photovoltaic power was calculated from the following equation.

$$P_{pv}^{n,gen} = A_{array} * I^n * \eta_{array} \tag{2.60}$$

In this equation, $P_{pv}^{n,gen}$ represents the generated power of the photovoltaic system at the n_{th} interval, A_{array} expresses the area of the PV array [m^2], I^n is the solar irradiance [$\frac{kW}{m^2}$] and η_{array} denotes the efficiency of the PV array. Figure 2.5 illustrates the load power and energy prices (purchase) for the studied 24 hours. It shows that the load peak occurs around 7-9 PM when the user and EV are at home.

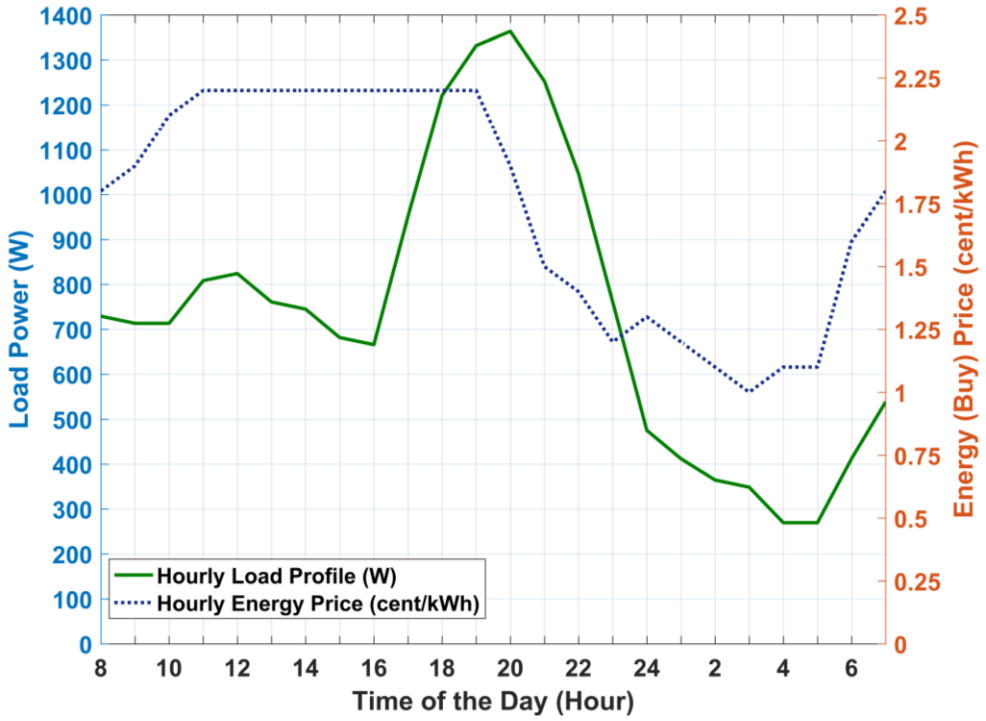

Figure 2.5: Load power and energy price profiles for the case studies of chapters 2 and 3

Table shows the input parameters of the MIP models provided in the case studies of the chapters 2 and 3.

Table 2.1: Input parameters of the MIP model of chapters 2 and 3

Input Parameter	Value
$\eta_{es}^{ch}/\eta_{ev}^{ch}$	96%/96%
$\eta_{es}^{dis}/\eta_{ev}^{dis}$	96%/96%
P_{es}^{ch}/P_{ev}^{ch}	0.75kW/1.75kW
$P_{es}^{dis}/P_{ev}^{dis}$	0.75kW/1.75kW
G	1 hour
$SE_{es}^{ini}/SE_{ev}^{ini}$	1.225kWh/8.8kWh
$SE_{es}^{max}/SE_{ev}^{max}$	2.375kWh/22kWh
$SE_{es}^{min}/SE_{ev}^{min}$	0.1875kWh/1.65kWh
SE_{ev}^{ch}	20.9kWh
η_{pv}	100%
P_{cl}	3kW
n_{cl}^{row}	2
n_{cl}^{day}	1
P_{im}^{max}	10kW
P_{ex}^{max}	10kW
$E_{es}^{ini}/E_{ev}^{ini}$	2.5kWh/22kWh
$V_{es}^{ini}/V_{ev}^{ini}$	\$2005/\$5500
$V_{es}^{sal}/V_{ev}^{sal}$	\$125/\$1122
CF_M/CF_U	175 kg/kWh /175 kg/kWh
R_{es}/R_{ev}	0.5/0.8

The resulting model was a mixed-integer linear program which was produced using Python language and solved by the Gurobi solver [96] which uses a combination of Branch & Bound and Cutting Planes techniques to solve MIPs. With regards to the hardware, a personal computer with core i7, 1.8GHz CPU, and 8 GB RAM was used for this work. According to the report produced by the solver, the optimization model of this case study includes 768 continuous and 144 integer

variables and 22 quadratic constraints. The best objective (global optima) was found to be -9.83 in 0.18 seconds with a gap of 0.0%.

The simulation results are depicted in figure 2.6 where the power distribution of all the involving units throughout the 24 hours is presented. It shows that after the EV arrives at home, it starts charging in a relatively uniform way during the nighttime. However, noticeably is also discharged over three hours to contribute to the minimum net energy cost of the building. The ESS's charge and discharge attempts are also scattered throughout the day to help minimize the net energy cost, although at a lower power compared to the EV. The controllable load is scheduled to operate early in the morning when the energy prices are minimum. During the daytime, the PV system covers the consumption, and its excess power is fed to the grid for making revenue from selling energy to the grid. During the evening time, however, the grid and batteries address the energy demands. It also shows that only in 11 hours there was a need for drawing power from the grid and during the remaining hours, PV, EV battery, and ESS managed to provide the entire energy demand of the building and more.

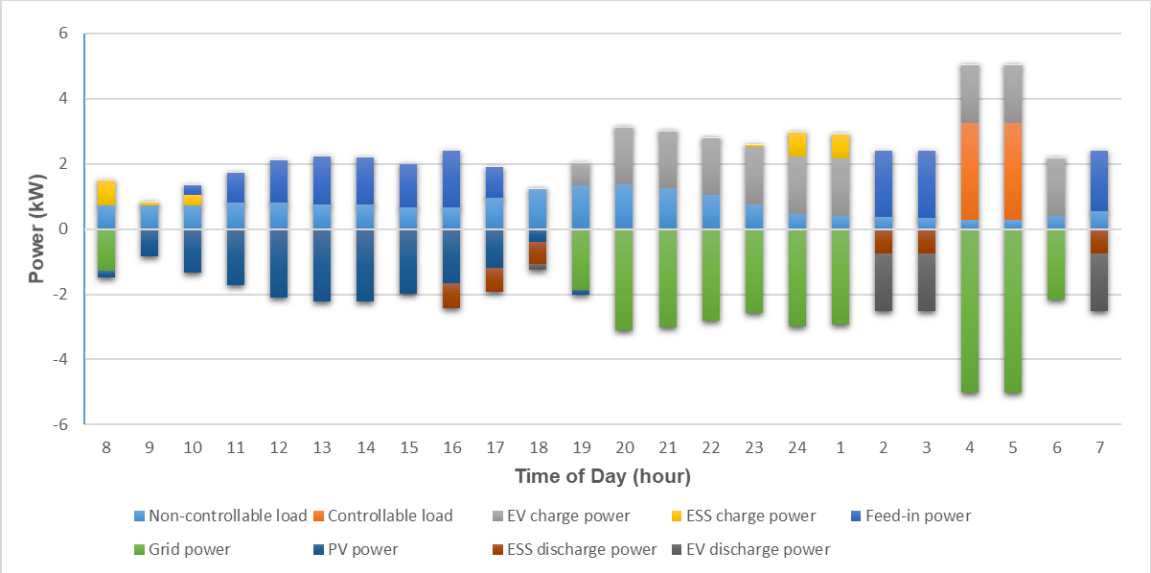

Figure 2.6: Power profile of the microgrid components-objective function: energy cost

To observe the UC results on various days, the case study was carried out for a month-long period. To obtain the input datasets for the monthly simulation, solar irradiance was obtained from [102] and electricity tariffs were acquired from [101]. The monthly load profile was obtained by changing the original daily load profile as a mean value with a Gaussian distribution with a 10% standard deviation. The initial SoCs of the EV battery and ESS for the days were obtained by varying their original values with a Gaussian distribution and 10% standard deviation. With regards to the departure and arrival times of the EV, it was assumed that it departs at 8 AM every day and arrives home at 6 PM on weekdays and 8 PM on weekends. The results of the payable energy prices are shown in figure 2.7. It can be seen that the daily energy prices vary between 8 and 42 cents, totaling $6.82 over the month. Significant variations in energy costs could be attributed to different reasons especially large differences in daily energy tariffs and solar irradiance levels. In general, relatively low energy costs can be attributed to different reasons, including the use of PV array, ESS, and EV battery for local energy consumption, and selling energy to the grid. Also, relatively low energy tariffs and finally, applying the UC model which attempted to minimize the payable cost led to the low payable energy cost for the home.

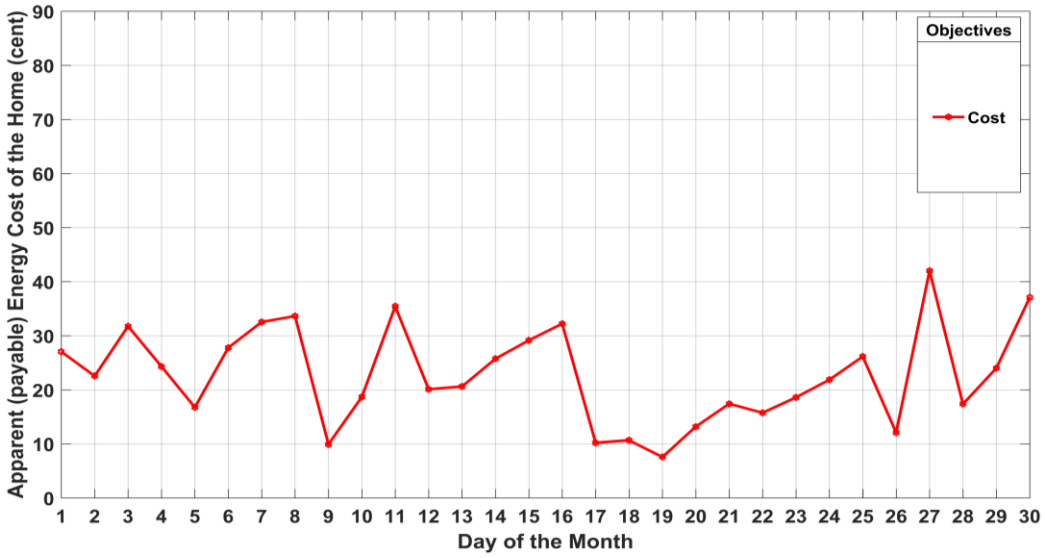

Figure 2.7: Daily energy cost of the home for one month, under the basic objective function (energy cost)

The peak power chart is illustrated in figure 2.8. The daily peak power of a building is the maximum amount of power that is drawn from the grid by the building throughout the day. Larger peak powers are associated with larger stress on the grid infrastructure which could lower the lifetime of the grid equipment and particularly the transformers. The graph shows that the daily peak power varies between 3.3 and 6.7 kW depending on different reasons such as the variations of daily load profile and energy prices. In fact, these factors impact the most important reason for peak power which is the controllable-load operation. Usually, due to the large consumption of these loads, they could largely affect the peak power during the day. To avoid large peak power values, (e.g., in the context of DR service) we could apply further restrictions to the grid power in the model constraints or try to include the grid power in the objective functions as a subject of minimization. This approach will be studied in the next chapter.

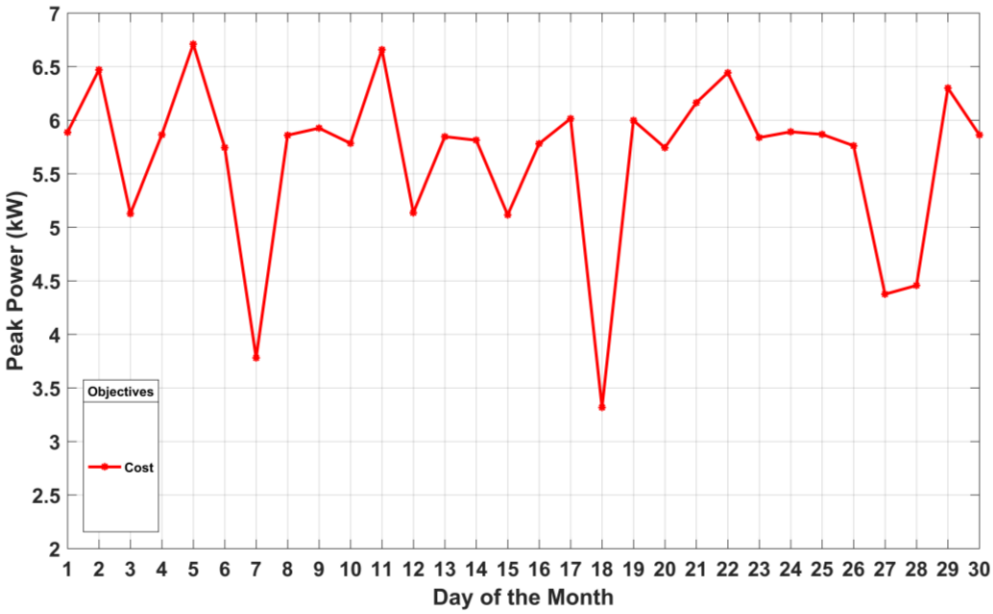

Figure 2.8: Daily peak power of home for one month, under the basic objective function (energy cost)

Chapter 3: Incorporation of battery degradation model into the MIP problem

A MIP-based UC problem was formulated and solved in the previous chapter. However, as explained in chapter 1, neglecting the important issue of battery degradation could lead to suboptimal or potentially wasteful unit commitment. However, this work aims to present a useful battery wear model which can be incorporated into MIP UC models. In this chapter, after a review of the battery degradation problem, the proposed wear model is explained and used.

3.1 Overview of battery degradation problem in Li-ion batteries

Battery degradation is a phenomenon caused by electrochemical and material fatigue in battery cells, as these two factors can degrade the cell's chemical, electrical, and mechanical characteristics. This phenomenon causes a change in the structural characteristics of the cell, a change in the electrolyte composition, loss of active material, or a composition of these three events, leading to a reduction in the performance of the battery. During a degradation process, the cathode and anode of batteries go through different wear mechanisms while the former is probably more prone to aging. The aging mechanisms can be divided into different classes, most importantly, the rise of internal resistance, the loss of active materials on anode and cathode (LAM), and the loss of lithium inventory (LLI) [40], [103]. The electrochemical aging of batteries is a complicated phenomenon caused by several factors affecting the electrodes and electrolytes. Despite this intricacy, the observable results include a loss of energy capacity and a reduction of output power. As a result, an aging model must strive to replicate these two effects [103]. As an example, in an electric vehicle, the degradation mechanism of the battery leads to the increase of the internal resistance of it which impacts the EV's power draw capability when it is traveling. Also, it lowers the capacity of the EV battery which corresponds to a lower driving range [73].

Despite the large variety of batteries' chemistries, due to the dominance of Lithium-ion batteries in the transportation and smart grid industries, this thesis is focused on Li-ion batteries. Li-ion batteries can be categorized based on the chemistry of their cathode to Lithium-Iron-Phosphate ($LiFePO_4$), Lithium-Manganese-Oxide (LMO), Lithium-Cobalt-Oxide (LCO) and Nickel-Cobalt-Manganese (NCM) types [103]. Among the Li-ion batteries, different materials impact the degradation in different ways. For instance, Lithium-Iron Phosphate or LFP batteries are largely sensitive to the number of cycles while Lithium-Nickel-Cobalt-Aluminum (NCA) batteries are impacted by both number of cycles and DoD [104].

The capacity fade of Li-ion batteries mainly stems from two major factors, namely the calendric aging which is independent of usage, and the cyclic aging which is caused by usage. The shelf-life of a battery is limited by its calendric life, due to the decomposition of the cell composites such as the electrolyte. However, calendric aging is normally small compared to the cycling aging which is caused by driving (in EVs) and charging/discharging of battery [73]. The calendar life of the battery represents the irreversible process of self-discharge loss. The rates of calendar loss are obtained by observing the capacity loss of the batteries that are kept at a constant voltage [105]. The calendric aging is independent of utilization and determines the battery's shelf life. However, it depends on the battery's SoC, temperature, and the length of time itself [106] during the periods that it is not under cycling, as shown in (3.1). As for the SoC, higher rates increase the decomposition rate of battery cell composites and consequently lead to higher degradation. Also, the degradation dependence on the temperature is modeled with the Arrhenius law [73] which will be provided later in this chapter.

$$C_{calendar} \propto f\left(\exp\left(\frac{-E_a}{RT}\right), f(SoC), t^{k_1}\right), (0< k_1 \leq 1) \tag{3.1}$$

Where T represents the temperature, R denotes the universal gas constant and E_a is the activation energy of reaction, t stands for the time and k_1 is a constant which is reported in the literature to be equal to 0.5 and 0.75. Calendar aging becomes notable at high temperatures. For example, the

results of [73] show that at 35°C it is comparable to cyclic aging. The calendric wear factor has a declining nature, meaning that at the early stages of the battery life the rate of degradation is higher, and it gradually decreases over time. However, an increase in SoC and temperature increases the rate of calendric degradation. For instance, according to the Arrhenius law, 10 degrees increase in temperature can decrease the battery lifetime by 50%, and at 35°C, the calendric rate can even exceed the cyclic rate of degradation.

Although reference [103] reports that there is a possibility that the calendar wear of an EV battery is larger than its cycle wear even when the EV is regularly used for driving, however, normally the cyclic aging is larger for batteries that are regularly used. Therefore, as the total capacity loss of battery within any period is determined by the larger of cycling and calendric aging [107], cycling aging is the determining factor in the cases where batteries are operated regularly. The cycling aging depends on the usage and usually leads to larger degradation rates compared to the calendric aging. It also highly depends on the chemical composites of the battery cells. On the system level, it largely relies on the DoDs of the cycling events. Obviously, the higher rates of DoDs can increase the battery wear. It has been shown that maintaining the DoD levels at moderate levels such that the average SoC will be around 50% can increase the battery life considerably [73]. The effective parameters of calendar aging are represented by (3.2). On a systemic scale, high DoD levels, as well as very low and very high average SoCs (around 0 and 100%) during cycling, amplify the aging process. The other parameter which proportionally impacts the cycling aging is the charge and discharge current [73].

$$C_{cycle} \propto f\left(f(\overline{SoC}), f(DoD), f(I), Q^{k_2}\right), (0< k_2 \leq 1) \tag{3.2}$$

Where, $\overline{SoC}$ refers to the average SoC of a cycle, I is the discharge current, Q represents the charge throughput, and the constant k_2 has been reported to be 0.5 and 0.87 in the literature.

The battery degradation is modeled in the literature using three different approaches, namely physically-based electrochemical models, semi-empirical models, and empirical models. Put

simply, these modeling approaches aim to provide the relationship between the capacity loss and resistance of batteries with different aging factors. Semi-empirical and empirical types focus on the wear mechanism rather than the physics of the phenomena and are commonly used for the online calculation of batteries' State of Health (SoH). Hence, they are more utilized in the system-level design as they benefit from simple structures and relatively accurate outcomes. However, the accuracy and applicability of these two types depend on the type of data used for the calibration of models, where those datasets are normally obtained through extensive experimental tests. On the other hand, electrochemical models normally address the diffusion and charge flow of ions in a battery and express the degradation on a physical basis. Thus, they can be applied in a wider range of cases, but at a higher complexity [108], [109]. In semi-empirical models, observable wear mechanisms are represented by low-order models and the parameters of these models are fitted to the experimental data. Whereas, in empirical models, available experimental data is utilized to forecast the behavior of batteries without knowledge of the electrochemical characteristics of the battery. Polynomial, exponential and trigonometric are some of the functions used as empirical models [109].

There is also another way to categorize the battery wear models which classifies them into performance-based and energy throughput models. Performance-based models which include electrochemical models, equivalent circuit models, analytical models, and ANNs are known to have good precision but could be complicated and require large amounts of data to address the range of battery operational conditions.

Energy throughput is the total cycled energy by the battery in one year. Therefore, the energy throughput models, relate the capacity loss to the level of charge transfer, considering the total amount of energy that can be processed by the battery. These models may have relatively lower accuracy but higher practicality [110].

Normally, the datasheets provided by the battery manufacturers provide the safety specifications such as voltage, current, and temperature ranges without providing significant performance metrics for the batteries [88]. Hence, although the physics-based models could be accurate, they are rarely useful at a higher system level, such as the pack simulations. Furthermore, these models are very dependent on numerous physical parameters of the cell, such as size and porosity of electrode, accurate mass, and properties of materials which require comprehensive measurements [111]. Furthermore, a notable issue of physical wear models is that they do not predict the nonlinear relationship between cycle life and DoD as shown in figure 3.1. If we assume *N* as the number of cycles that the battery can complete at the DoD of *D*, the cycle-life function can be represented as *N(D)*. In physical models, the capacity loss is roughly a linear function of the charge throughput. Whereas, the empirical wear models could provide the capacity loss as a nonlinear function of DoD [112].

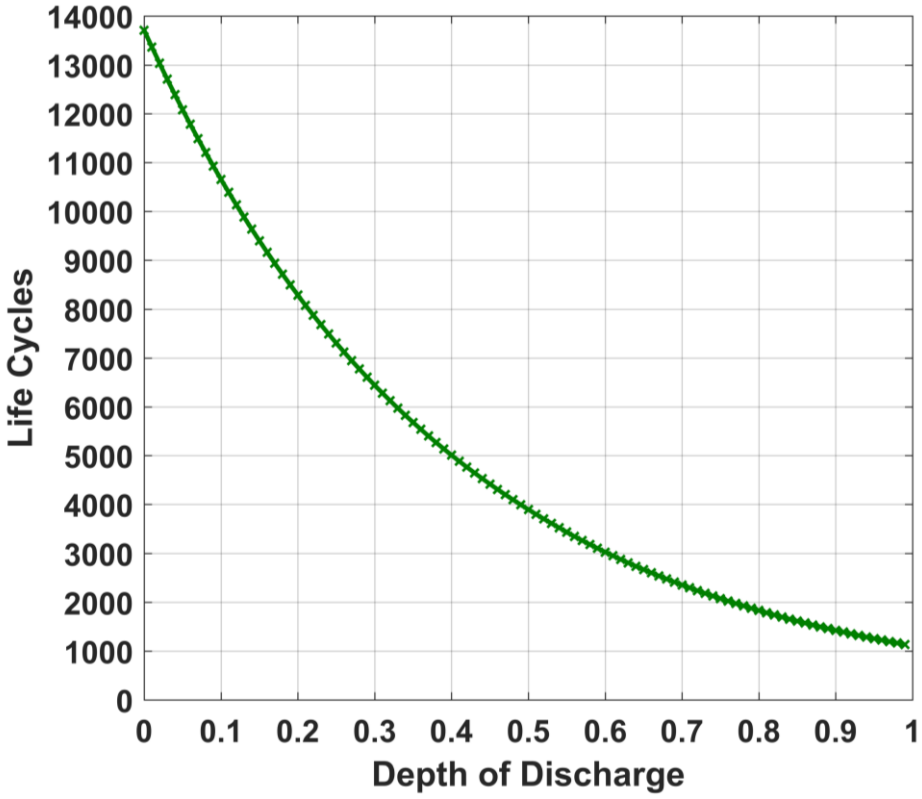

Figure 3.1: Life cycles of a Li-ion battery against its depth-of-discharge (N(D))

Most of the degradation models employ one of the following two approaches, curve fitting of the experimental data and using the extracted parameters from the chemistry of the battery which are also derived from experimental data. However, there are different challenges associated with using these methods. One of the issues is the fact that sometimes the battery wear is expressed as a physical quantity such as resistance which cannot be conveniently managed in a battery cycling model. Let us assume in order to lower the degradation rate of a battery, we would like to maintain the resistance of the battery cells at a low level by maintaining the SoC in a certain range. However, as the battery wear is expressed as a physical parameter (resistance), it could be difficult to incorporate that as a cost within a cost function for the problem. Another challenge with producing battery wear models is that they are normally built upon experimental data, which are difficult, time taking, and costly to obtain and are usually not provided by the manufacturers [89].

Figure 3.2 demonstrates the causes and results of different degradation modes that lead to capacity loss, power loss, or both of them, obtained from reference [103]. It demonstrates how the main causes of the battery aging such as extreme temperatures, SoC, DoD, C-rate, and physical imperfections of the battery cells could impact the battery cells chemically (stated as degradation modes) such as decomposition of electrolyte and corrosion which then manifest in the changes that can be regarded as battery degradation symptoms, such as the rise of internal resistance and loss of cyclable lithium. With regards to the aging mechanism of these factors, it could be said that the lower availability of lithium and decrease in the surface of anode and cathode lead to capacity loss. Whereas, the rise in internal resistance leads to the power loss of the battery [103].

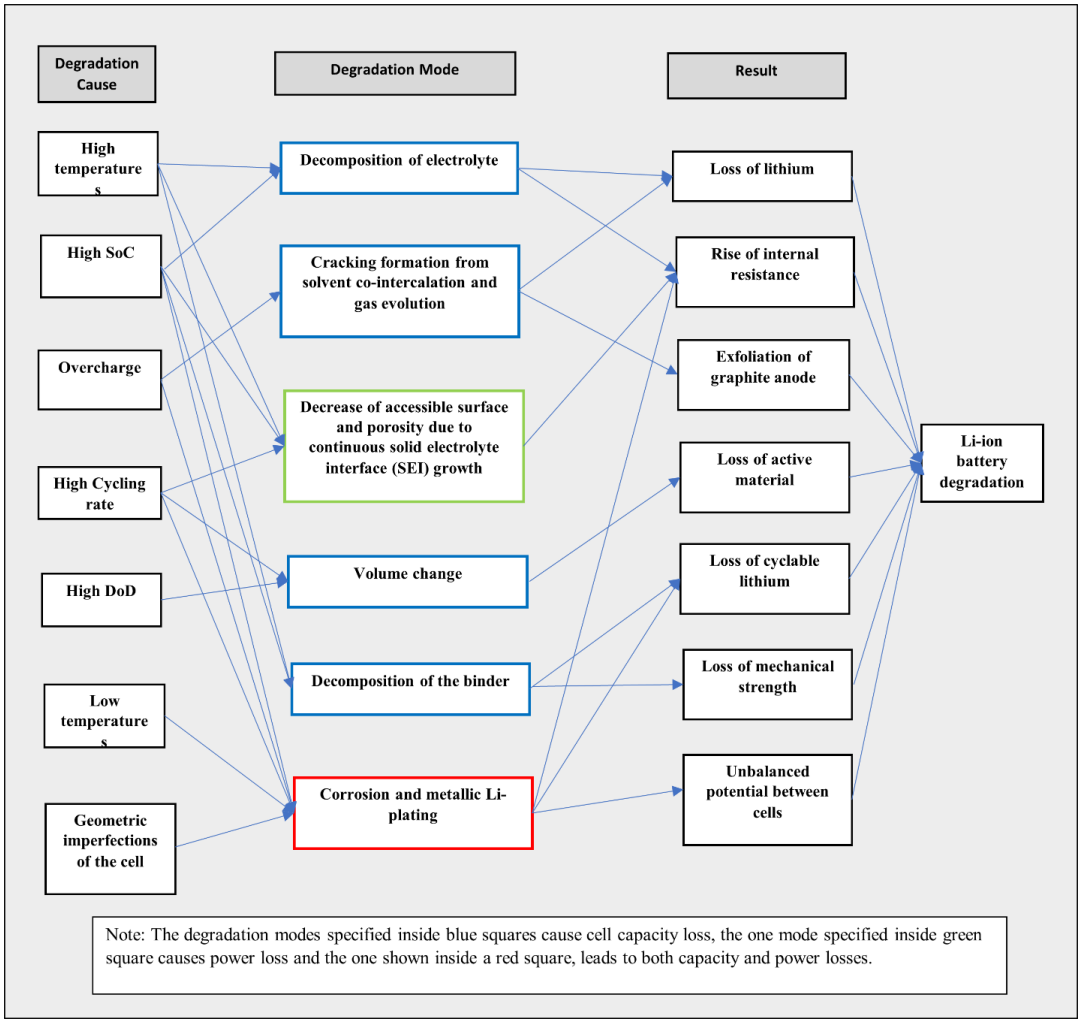

Figure 3.2: Degradation scheme of Li-ion batteries including causes, modes, and results [103]

Reference [113] categorizes the causes of battery aging into internal and external types where parameters associated with battery chemistry fall within the former group, while temperature, SoC, DoD, and charging regime are considered external parameters. In this regard, DoD, SoC, mean SoC, C-rate, charge throughput, and temperature are the factors that could impact the battery degradation and be included in the semi-empirical models. Therefore, semi-empirical models could be comprised of a single factor or multiple factors. Among these factors, battery temperature cannot be managed directly and it is controlled through other variables [40], [73].

As a matter of fact, the exact impact of DoD, C-rate, and temperature on the capacity loss is chemistry-specific. For every battery chemistry, the capacity loss could show nonlinear trends over a range of temperatures, DoDs, and C-rates. For example, [88] has investigated the aging of LFP, NMC, and NCA cells in the range of 15 to 35°C. In this particular range, for the LFP technology, the cycle aging increases with the rise of temperature, while it decreases for NMC batteries and NCA showed no significant correlation between temperature and cycle aging. This can be related to the fact that the degradation mechanism changes at different temperatures. For example, this article reports that for temperatures below 25°C, the dominant degrading mechanism is Li plating, while for temperatures over 25°C it is the SEI (Solid-Electrolyte Interphase) growth. However, with regards to the calendar aging, all the three battery technologies showed increasing capacity loss with the temperature rise. Regarding the impact of DoD, this reference has studied three cycling ranges (40-60%), (20-80%), and (0-100%) and observed that for all the batteries, the degradation directly increased with an increase in DoD. This is attributed to the more created cracks that increase the reactions between Lithium and electrolyte followed by further SEI creation, loss of Li inventory, and capacity loss. However, NCA and NMC chemistries show more dependence on the DoD. Regarding the impact of SoC, larger SoCs directly increase the calendar aging for all the studied battery types. This can be attributed to the increased loss of electrolyte and Li involvement in developing SEI which occur at lower anode potentials. However, with regards to the cycle aging, NMC and NCA batteries show large capacity losses around SoC of 100%. As for the discharge rate, larger discharge rates cause higher degradation in the three battery types because of the larger stress on the battery electrodes caused by fast volume change [88].

In this regard, although meticulous experimentations on every Li-ion chemistry demonstrate complex nonlinear relationships between the capacity loss and the degradation causes (e.g., DoD or C-rate), some general rules could be extracted from several research works that have focused on battery degradation of Li-ion batteries [40], [73], [88], [89], [105], [111], [113]-[116]. For example,

with regards to the impact of SoC, most Li-ion batteries show high degradation levels at very small and large amounts of SoC and smaller at the medium values of SoC. This is due to the larger internal resistance at both ends of the SoC. It is worth noting that the impact of SoC on battery aging could be studied from two different viewpoints. When it comes to the calendric aging, the SoC at which the battery is kept or stored affects its degradation. However, with regards to the cycling aging, the initial and final values of SoC levels during every charging/discharging process impact the inflicted degradation during that process [40], [89]. Authors in [2] reported that small cycles (around 20%) around an average SoC (roughly 50%) are more beneficial and less likely to cause battery degradation. It has also been observed from the EVs that different ranges of SoC will affect the state of health of batteries to different extents, where wide ranges of SoC cause more capacity loss in the batteries [114].

As an example, authors in reference [114] have investigated the impact of different SoC ranges (with 25% DoD for every case) on the capacity loss of a $LiFePO_4$/graphite cell when the cell is cycled with 1000 iterations. The results of this work show that cycling this cell in the mid-SoC ranges (25% to 75%SoC) will lead to better cycle life compared to cycling at both ends of the SoC range. Interestingly, the capacity loss inflicted by cycling at a large DoD of 60% but within (20 to 80%SoC) shows a smaller capacity loss compared to the case with a smaller DoD (20%) but at (0 to 20%SoC) or (80 to 100%SoC). This is due to the larger polarization impedance at the end of SoC which is caused by the reactions between electrodes and electrolytes as well as the structural variations of anode and cathode materials in these SoC ranges [114]. These results show that in order to have a realistic estimation of the battery wear due to a charging/discharging process, not only should we address the DoD of the process but also the initial and final SoCs of the battery should be considered throughout the process.

As a general fact regarding the impact of DoD, the battery degradation rises at higher levels of DoD [105]. For instance, it is recommended in the study, presented in [2], that for the V2G service, the

DoD be kept under 60% and SoC between 30% and 90%. In this regard, two types of approaches have been employed commonly in the battery scheduling research works to address the DoD-related wear rate. The first approach is to put a restriction on DoD to guarantee a certain amount of lifetime, and the second method is to designate a cost to DoD which impacts the operating cost [113]. However, taking restrictive measures like limiting the usable range of SoC to 80% [16] and depriving a battery of operating in a large range of charge such as 0 to 30% and 90% to 100% would not be the best approach. Because, in this case, a significant portion of the battery capacity will be unusable.

The rate of charging and discharging the battery also has a significant impact on its rate of capacity loss. The study, carried out by [105], shows that the rate of capacity loss versus the C-rate for a Li-ion battery that is cycled at 10°C is an exponential function which is shown in figure 3.3. The graph shows that low C-rate levels (<1) cause a minimal capacity loss in the Li-ion batteries.

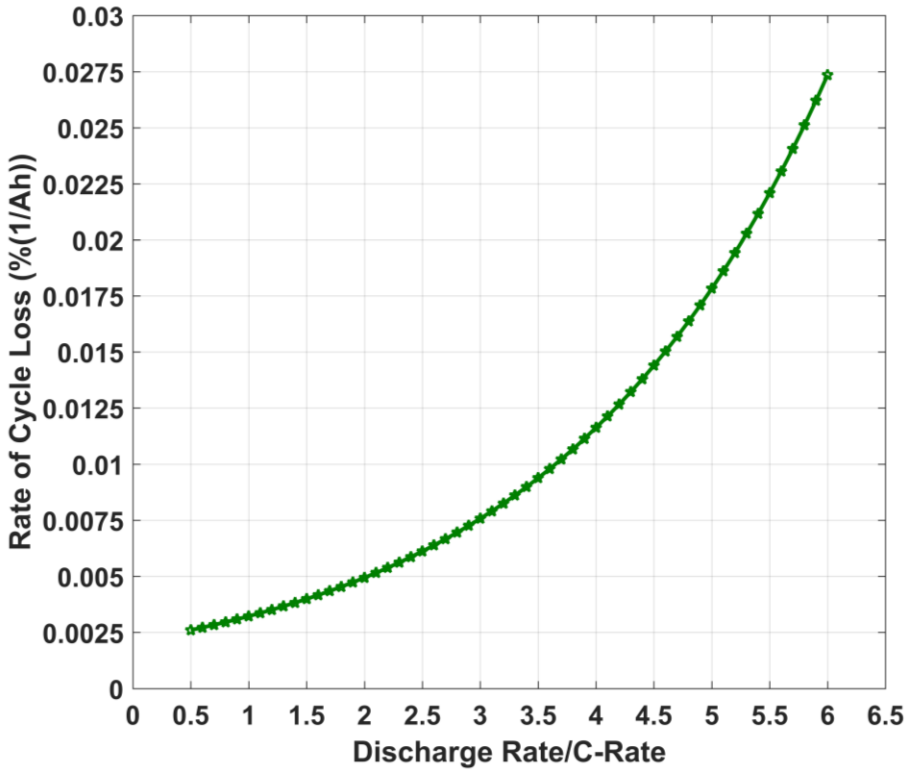

Figure 3.3: Rate of cycle loss of a Li-ion battery as a function of its C-rate [105]

Battery temperature is another effective factor in the wear rate which depends on different factors, especially the ambient temperature and the C-rate. Ambient temperature is not a control variable of the battery. However, controlling the C-rate of the battery could largely impact its temperature. We could state that at low temperatures, the degradation accelerates when C-rate rises and at low C-rates the battery wear rises with higher temperatures. However, at high temperatures, there is high battery wear regardless of the value of the C-rate [105]. Thus, as a rule of thumb, larger C-rates lead to larger battery temperatures which cause higher capacity fade rates. In this regard, the study, presented in [115], has measured the temperature of a pouch Li-ion cell when cycled with different C-rates (1C, 3C, and 5C) over 1500 seconds and from an initial temperature of 297 kelvin. The results show that after the testing time, the battery's temperature change was insignificant when it cycled at the rate of 1C. However, when the C-rate was 3C the temperature increased to around 303-305 K depending on the point of measurement on the battery. Also, cycling at 5C raised the temperature to 312-320 K.

The study, presented in [116], has investigated the temperature changes for a Li-ion cell under 1C, 1.5C, and 2C cycle rates. This work also shows that depending on the point of measurement, the temperature could show larger rises (on the positive electrode tab), small changes (on the negative electrode tab), or uniform changes (on the surface of the battery). Also, it shows that not only do higher C-rates increase the battery temperature, but also make it happen in a shorter amount of time. Applying a thermal management system (TMS), which is usually a component of sophisticated battery management systems (BMS), is an effective measure to maintain the cells' temperature and subsequently temperature-related degradation at a low level [111]. Thermal management systems could be of the active or passive type. Active TMS preserves the battery temperature at a specific rate, while the passive type uses the ambient air circulation for heat dissipation [117]. In [118], it is recommended to maintain the temperature of Li-ion batteries between 15 and 35°C for better longevity. In this regard, assuming the Li-ion battery is not

preserved in a place with extreme ambient temperatures and also is equipped with onboard TMS, provided that it is not cycled at high C-rates, the temperature-associated degradation could be maintained at a low level.

3.2 Semi-empirical battery degradation models

Due to the large applicability of semi-empirical models in online wear estimation, this work is focused on this type of wear model. Hence, in this section, the popular semi-empirical wear models are introduced. Cycle aging has been modeled in the literature based on different causes or stress factors. As mentioned before, these factors include C-rate, temperature, SoC, DoD, and charge throughput of battery. A semi-empirical wear model could be laid out based on single or multiple stress factors. The battery temperature is not a directly controllable factor; hence it is managed through the other stress factors and in particular, C-rate. Three common semi-empirical wear models for obtaining cycling loss of batteries are the linear model, NREL model, and Arrhenius model which will be introduced in the following. There are also other wear models available in the literature such as the Peukert Lifetime Energy Throughput (PLET) model or more complex multi-actor models [40] which use different combinations of inputs to address the wear rate.

It is worth noting that these models are usually constructed based on the results of experimentations that have cycled batteries regularly (e.g., from and to 100%SoC [90]). Hence, they might not be directly applicable to online estimation of dynamic battery degradation caused by irregular cycling attempts where batteries are cycled between random SoCs.

3.2.1 Linear Model

To define the linear degradation model of batteries, it is assumed that the cycle life of batteries only depends on the depth of discharge. Then, cycle life can be represented by the total amount of energy that can be transferred by the battery as follows.

$$Q_D = EDN_D \tag{3.3}$$

In (3.3), D denotes the depth of discharge, N_D denotes the number of cycles that the battery can complete at DoD of D, E represents the nominal capacity of the battery and Q_D expresses the lifetime energy throughput of the battery at DoD of D. Averaging the lifetime throughput for every DoD provides the general lifetime throughput as follows, where i is the count of DoD quantities.

$$Q_{lifetime} = \frac{1}{i}\sum_{D=0}^{D=1} Q_D \tag{3.4}$$

Then, the linear model provides the capacity loss as follows:

$$Q_{loss}^{linear}(T) = \sum_{t=1}^{T} C_L P(t)\Delta t \tag{3.5}$$

Where, $C_L = \frac{1}{Q_{lifetime}}$ is the equivalent capacity fade of battery per kWh, calibrated through experimentation, and $P(t)$ denotes the average battery power during the interval of the problem (Δt).

3.2.2 NREL Model

NREL weighted Ah wear model is built based on the assumption that the battery can go through a certain number of effective Ampere hours and after that, it reaches the end of life. In this regard, the rated charge life (Γ_R) is defined as:

$$\Gamma_R = C_R D_R L_R \tag{3.6}$$

Where C_R represents the rated capacity of the battery under the rated current, D_R denotes the rated DoD associated with the rated battery life, L_R represents the life cycles associated with the discharging rate and D_R. Capacity loss can be calculated according to the accumulated discharged Ampere hours (d_{eff}) as follows.

$$Q_{loss}^{NREL}(T) = \frac{1}{\Gamma_R}\sum_{t=1}^{T} d_{eff}(t) \tag{3.7}$$

And,
$$d_{eff} = (\frac{D_A}{D_R})^{u_0} e^{u_1\left(\frac{D_A}{D_R}-1\right)} \frac{C_R}{C_A} d_{actual} \tag{3.8}$$

Where, D_A and C_A represent the actual DoD and battery capacity under the actual condition, u_0 and u_1 are the fitting coefficients obtained from the *N(D)* curve of the battery and d_{actual} represents the actual discharge value.

3.2.3 Arrhenius Model

Arrhenius aging model of battery provides the relationship between the electrolyte film growing and Ampere hour throughput of battery as laid out below. The beauty of this wear model is that it can provide the impact of temperature on the battery wear. Another advantage of this model over the time-based wear models is that it could also model the relationship between C-rate and capacity loss.

$$Q_{loss}^{Arrhenius} = A\ exp(\frac{-E_a}{RT})Ah^z \tag{3.9}$$

In this equation, A is a pre-exponential coefficient, E_a denotes the activation energy ($Jmol^{-1}$), R represents the gas constant, T expresses the absolute temperature and z represents the power-law factor which is considered to be constant under different charging rates. However, to use this model for the dynamic operation of batteries in microgrid applications, it needs to be discretized to calculate the capacity loss within a given period. Therefore, the following two equations provide the discrete version of the Arrhenius model.

$$Q_{loss}^{Arrhenius}(T) = Q_{loss}^{Arrhenius}(T-1) + zA^{\frac{1}{z}}\exp(\frac{-E_a}{zRT})\Delta Ah Q_{loss}^{Arrhenius}(T-1)^{\frac{z-1}{z}} \tag{3.10}$$

$$\Delta Ah = \int_{t-1}^{t} |I(t)| dt \tag{3.11}$$

In these equations, $Q_{loss}^{Arrhenius}(T-1)$ represents the accumulated value of capacity fade at the end of time $T-1$, ΔAh is a variable denoting the Ampere hour throughput during the period from $T-1$ to T, and $I(t)$ represents the average current during the same period [40].

3.3 Introducing the battery degradation to the MIP UC problems

In this chapter, a technology-agnostic semi-empirical battery degradation model is presented for applying in the unit commitment of batteries in applications such as residential and commercial microgrids where batteries go through irregular charging and discharging half cycles with relatively low levels of power (C-rate ≤ 1) without experiencing extreme temperatures. This battery wear model can be incorporated into a mathematical programming model such as a MIP model for online minimization of real costs associated with the operation of a microgrid including the cost of battery wear.

Unless a UC algorithm is employed by an energy-system developer for a proprietary configuration, a generic short-term (daily planning) battery scheduling algorithm that could be used globally for residential or commercial buildings in bi-directional markets is anticipated to carry some important characteristics. First of all, it should be technology-agnostic so that it could be used for different batteries regardless of their chemistry and technology. In this regard, the applied battery degradation model plays a major role in making the UC algorithm accommodating. The battery degradation model is expected to take into consideration the factors that impact the battery life in a meaningful way. DoD, SoC, C-rate, and temperature are the three factors that play a major role in battery degradation in general. However, due to the complicated correlation between these factors themselves, a comprehensive wear model that could model capacity loss caused by all of those factors simultaneously could be highly nonlinear and complex. Thus, it may be required to compromise some of the wear factors depending on the case to keep the model fairly reasonable in

terms of size and complexity. For instance, when the battery temperature is controlled by the battery's thermal management system, it may be possible to neglect the temperature and still have a wear model with decent accuracy. Alternatively, if battery charging/discharging facilities are merely capable of cycling the battery with low C-rates (e.g., < C/2), it may be worthwhile to overlook C-rate as it barely can cause meaningful capacity loss. Computational resources is another subject that should be taken into account when developing a wear model. Processing and memory hardware are normally of great importance for mathematical programming and metaheuristics respectively. With regards to the software resources, it should be known what tools and programs are required for implementing a UC algorithm. Developing proprietary solvers and programs could take large amounts of time, energy, and cost. Utilizing commercial programs and solvers is another alternative that entails its limitations and costs. In either case, it is important to make sure that the UC model can be properly implemented with the available resources. This is because solving a complex optimization model in the research and development phase using commercial solvers and computers is one thing while solving a similar model in a practical application could require sophisticated and costly proprietary software and hardware. For instance, it is difficult or possibly impossible for most of the existing MIP solvers to handle severe nonlinearities in MIP models. In short, a good wear model should be able to model the battery degradation rate caused by the effective wear factors with a level of complexity that can be handled by available computational resources within an acceptable time and in an economic fashion.

In this thesis, the optimal UC problem for residential and commercial buildings in bi-directional markets has been addressed in the framework of mixed-integer programming. In order to address the battery degradation problem in this work, a battery wear model will be presented which can be used as a generic wear model compatible with different MIP short-term battery scheduling models. The presented wear model is a semi-empirical technology-agnostic model which is developed based on the *N(D)* curve of batteries. The wear model is capable of estimating the magnitude of the

capacity loss of the battery caused by irregular cycles. Also, this wear model can be written in the discretized-time format and directly incorporated into a mixed-integer programming model to minimize a cost function. This is significant in the sense that embedding the battery wear (as a cost factor) directly into the UC model can help us achieve the real minimum cost of a system with consideration of energy and battery wear cost. While implementing a battery wear model along with (and not embedded into) a UC model could prevent achieving the best possible unit commitment approach since different objectives will compete with each other. However, incorporating the wear model into the UC model with the same dimension (e.g., cost) could lead to obtaining the global optima of the problem.

By considering the fact that residential and workplace EV chargers work at low power compared to the capacity of an average EV battery, we may be able to neglect the impact of the charging rate on the battery degradation. Residential and commercial typical charging is normally implemented by type 1 or type 2 chargers (less than 20 kW of power). Moreover, typical EVs normally come with two types of charging connectors, namely AC and DC connectors. The AC inlet is used for level 1 and 2 chargers up to 20 kW power at the standard distribution voltage level. The DC connectors can be used for DC fast charging in places like fast-charging stations. EV batteries usually benefit from onboard AC-DC and DC-DC chargers [119] to facilitate these different types of charging. On the other hand, today an average EV has a battery capacity of over 20 kWh. Hence, the offered C-rate of residential charging equipment is normally under 1C which makes the effect of the C-rate insignificant in the wear rate in comparison with the DoD of cycles. Battery temperature is the other factor that could affect its lifetime and it could be caused by high cycling currents or the ambient temperatures. However, low C-rates have minimal impact on the battery temperature, leaving the battery temperature mainly affected by the ambient temperature. Authors in [82] state that the lifetime of Lithium-Ion batteries is not notably affected by temperature as long as these batteries are operated within normal temperatures. Assuming that EV batteries benefit from

TMS and normally do not experience extreme ambient temperatures at residential or commercial parking lots, in this work also the impact of temperature on the battery degradation has been omitted [120].

In this regard, to address the impact of DoD (for both charging and discharging actions) on the capacity loss in a Li-ion battery we need to have access to the specifications and characteristics of the battery which are normally provided by manufacturers. However, battery manufacturing companies normally provide limited specifications for every battery as providing different electrical or physical parameters for batteries would require extensive, time taking, and costly testing procedures. Cycle count vs capacity, discharge capacity vs voltage, storage time vs capacity, and charge time vs voltage are some of the common plots provided by manufacturers. Hence, many of the important specifications of batteries are normally not provided in the battery's datasheets. On top of that, these relationships have complex correlations that make them very difficult to be discovered by the battery makers. For example, not only does the cycle life of a battery depend on the DoD of the charging/discharging actions (as represented by the N(D) curve), but also that function depends on the other factors such as temperature and C-rate. Thus, in order to lay out a battery degradation model, apart from the importance of model accuracy, one needs to consider the fact that the inputs of the degradation model should be accessible.

One of the major specification plots that are provided by some of the manufacturers is the *N(D)* of the battery (figure 3.1) which is related to the cycle count vs capacity plot. As a matter of fact, the cycle count vs capacity curve provides the number of cycles that a battery can complete at one specific DoD (normally 100%), C-rate, and temperature, before its capacity drops by 20 or 30% [120]. Figure 3.4 illustrates the approximate relationship between cycle count and capacity for a Li-ion battery [121].

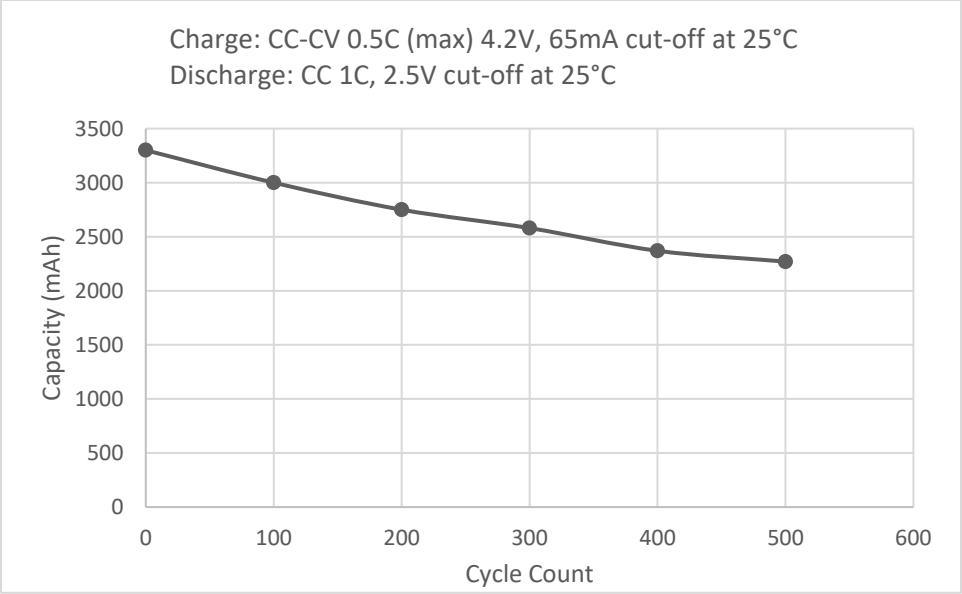

Figure 3.4: Capacity of a Panasonic Li-ion battery (NCR18650B) as a function of completed cycles [121]

However, batteries are normally cycled at DoDs other than 100%. Therefore, the cycle life-DoD (*N(D)*) plot is provided by some of the battery makers to show how many cycles a battery can complete with different DoD values before its usable capacity falls by 20%. This graph accommodates very important information about the battery's cycle life, and it can be used as a useful dataset for building the battery wear model as it relates a health index of the battery (cycle life) to the DoD which is controllable by the user. As a matter of fact, the N(D) graph provides the number of cycles that the battery can get through before it reaches the end of life.

Therefore, in an application where the battery goes through cycles/half "regular cycles" with a fixed DoD, we can simply calculate the amount of capacity that is lost per every single half-cycle and its corresponding cost as in (3.12) and (3.13). The term ½ in (3.12) is because capacity loss caused by every half cycle can be considered half of the that of a full cycle. Based on (3.12), it is assumed that under similar circumstances, capacity loss caused by charging a battery from SoCx to 100% SoC is equal to that of discharging from 100% SoC to SoCx.

$$\Delta E_D = \frac{1}{2}\left(\frac{E}{N(D)}\right) \tag{3.12}$$

$$Y_D = \Delta E_D\left(\frac{V^{ini} - V^{sal}}{E^{ini}(1-R)}\right) \tag{3.13}$$

Where, D denotes the DoD of half-cycle, ΔE_D is the capacity loss of battery caused by a completing a half cycle with DoD of D. E is the available capacity of the battery, V^{ini} is the initial value (price) and V^{sal} is the salvage value of the battery, E^{ini} is the initial (rated) capacity of the battery and R denotes the remaining SoH at the time of replacement which is a value between 0 and 1. It is worth emphasizing that the equations above can be used to calculate the capacity loss in applications in which the battery is cycled from and to 100%SoC. This is since the *N(D)* curve is acquired from discharging and charging the battery from and to 100%SoC. However, not every battery is cycled under that condition. In fact, a practical battery cycling strategy would schedule batteries for charging, discharging, and idle modes in different time frames, leading to various SoC changes within the range of 0-100%.

Thus, a more feasible wear model would be able to address random cycling actions or "irregular cycles" in which SoC varies between random levels. On the other hand, when it comes to the effect of DoD on the battery degradation, it is vital to remember that the wear induced by the depth of discharge varies depending on the SoC values [82]. The DoD-related degradation is influenced by the battery voltage or SoC at the beginning and end of any charging/discharging attempt. For example, discharging a battery with a fixed DoD of 5% between SoCs of 6% and 1% could lead to much larger degradation rates compared to discharging with the same DoD between SoCs of 65% and 60%. Regardless of the cycling strategy, every charging or discharging attempt degrades the battery's health relative to the amount of DoD as well as the initial and final SoCs of the cycle/half cycle [120]. A method called Rainflow Counting Algorithm (RCA) has been employed by some of the literature to address the random variations of DoD to calculate the wear rate [78], [79], [84], [122]-[124]. This method estimates the degradation cost according to the count and amplitude of

battery cycles. However, this technique suffers from some problems. First, it is difficult to incorporate it into analytical models to be solved by a mathematical solver, therefore it may need to be used in parallel with optimization problems which could undermine the global optima. Moreover, it fails to consider the fact that the initial and final SoCs of a cycle also impact the capacity loss associated with it [120].

Hence, the objective of this chapter is to provide a mathematical solution to model the degradation of a Li-ion battery caused by the DoD of irregular cycles with consideration of the initial and final SoCs of cycles. The presented wear model is built upon a wear model proposed in [82] which has visualized the relationship between the initial and final SoCs versus the capacity loss of a cycle for a Li-ion battery which is shown in figure 3.5. The figure is symmetrical due to the fact that capacity loss is considered to be independent of the direction of SoC changes. It means that the capacity loss caused by a charging or discharging attempt can be approximated to be equal, provided that they are executed between an identical pair of SoCs in identical conditions as long as the charge or discharge event does not occur at very large DoD and temperature simultaneously [125]. This graph incorporates the capacity loss information for different amounts of DoD. In this regard, if we assume a random charging or discharging attempt is done during N time intervals, the total DoD-associated capacity loss of the battery within this duration can be written as the total capacity loss caused by every single subinterval within the range N.

$$\Delta E^{total} = \sum_{n=1}^{N} \Delta E^{n} \tag{3.14}$$

Where, ΔE^{total} is the total capacity loss during N intervals and ΔE^{n} is the capacity loss inflicted within the subinterval n.

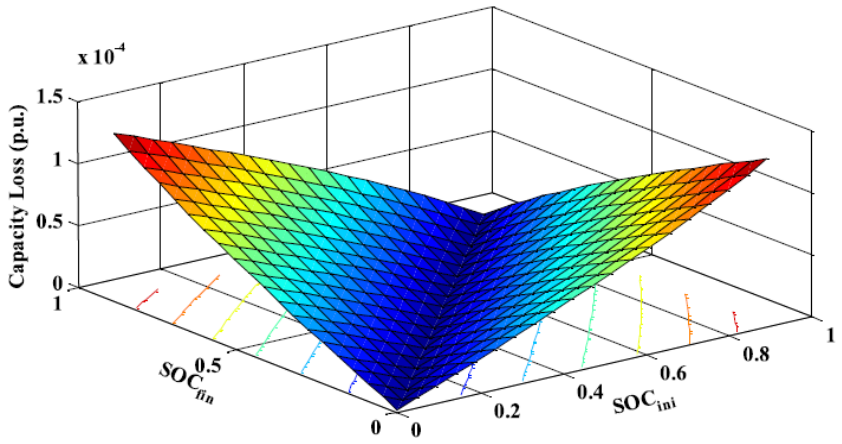

Figure 3.5: Capacity loss of a Li-ion battery as a function of initial and final SoCs of cycle obtained from [82], Copyright IEEE

However, despite the symmetry of the graph, its flat sides do not precisely model the nonlinear relationship between the SoC changes and the capacity loss in a Li-ion battery. Hence, a more precise version of this graph is required as both sides of it need to evolve to more complex and nonlinear forms from the existing linear form. A more complex demonstration of this graph is presented in [87] which is provided along with its contour map in figure 3.6, demonstrating a more detailed relationship between SoC variations (DoD) and capacity loss of a battery. It shows that at a fixed initial SoC, the capacity loss of Li-ion battery changes nonlinearly with respect to the amount of DoD. It also demonstrates that completing a half-cycle between a given pair of SoCs with a rate of C2 causes more damage to the battery than completing the same half-cycle with 1C. However, these figures still do not seem to accurately model the relationship between DoD-associated capacity loss as a function of initial and final SoCs for all the Li-ion batteries. As can be seen from the contour map, the capacity loss caused by cycling the battery with a small DoD (e.g., 3%) around a very large SoC (e.g., 97%) or very small SoC (e.g., 3%) will inflict a lower capacity loss compared to a cycling attempt with the same DoD but around a moderate SoC such as 70%, which is against the expectations. This proves the need for further research and more comprehensive experimentations in the field of Li-ion batteries as a more precise graph is expected to show larger capacity losses around very small and very large SoCs [114].

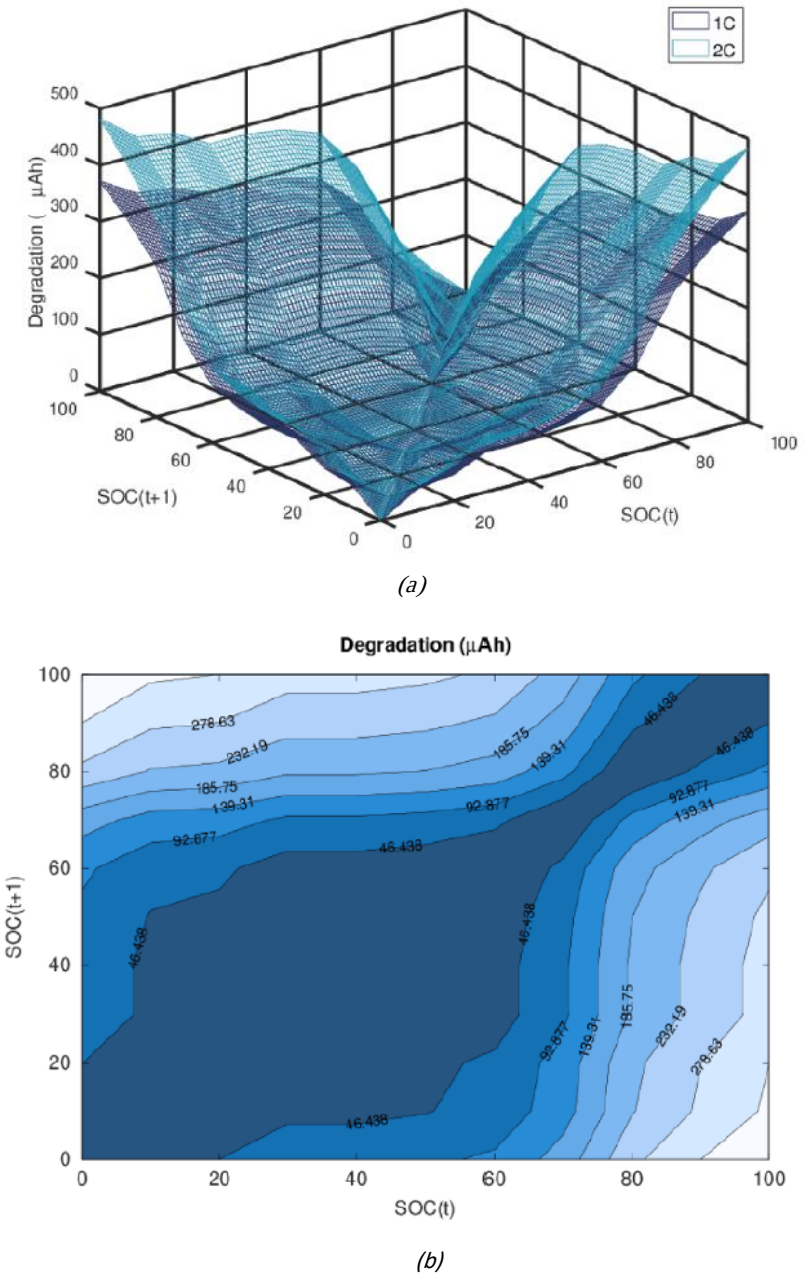

Figure 3.6: (a): Capacity loss of a Li-ion battery as a function of initial and final SoCs of cycles. (b): Contour map of the capacity loss graph, both images obtained from [87], Copyright Elsevier

In order to obtain the capacity loss of battery caused by an "irregular half-cycle", first the capacity loss caused by a "regular half-cycle" must be obtained. According to the wear formulation provided in reference [82], the capacity loss caused by a regular full cycle is derived from equation (3.15).

As mentioned before, an irregular half cycle takes place between two random SoCs while a regular half cycle takes place between 100%SoC and a lower SoC or vice versa. This equation shows that the capacity loss of a battery caused by a cycling process could be expressed as a function of its capacity, the cycle's depth-of-discharge, and a coefficient (W_D) that entails the cycle life information of the battery. In this context, this coefficient which is called the "wear coefficient" in this work, expresses the "capacity loss per transferred energy" based on the cycle life-DoD (*N(D)*) function of the battery. Hence, in a sense, D is the key variable of this equation which also determines W_D. More precisely, W_D represents the amount of capacity loss per unit of transferred energy if the battery is regularly cycled to the end of life with the DoD of D. Hence, this factor which is associated with "regular cycling" is used for obtaining the degradation of "irregular cycling". Coefficient 2 refers to the fact that each full cycle of battery consists of two half-cycles. Therefore, this equation is rearranged as in (3.16) for a regular half-cycle event. From this, we can derive (3.17) which expresses the battery capacity after going through *n* regular half cycles as a function of initial capacity, depth-of-discharge, and wear coefficient. We could assume that the battery can go through $n = N(D)$ half cycles before its life comes to an end at SoH= R. R is the end-of-life or remaining capacity of the battery at the time of replacement and it is normally a value between 50% and 80% depending on the user's decision and the application of the battery. Usually, for EV batteries R is considered 80%, while for ESS we could take a lower value. For instance, reference [40] considered the R of an ESS equal to 50%. Therefore, we will be able to derive equation (3.18) from (3.17) to obtain the wear rate function. On the other hand, the *N(D)* function of the battery can be modeled as in equation (3.19). We know that *the N(D)* curve is obtained through conducting experimental analysis on batteries and it is usually provided by the battery manufacturers. These curves normally have an exponential shape and can be modeled by an exponential function [126] obtained from applying curve fitting. By substituting (3.19) in (3.18) we can directly calculate the wear rate of a regular half-cycle as a function of DoD which is

presented in equation (3.20). Moreover, it is known that the battery wear caused by irregular cycling between two given SoCs, is equal to the difference of wear for regular cycling from the initial and final SoCs [90]. Thus, the capacity loss caused by implementing an irregular half cycle can be expressed as in equation (3.21). According to this equation, capacity loss caused by an irregular half-cycle depends on the DoD values associated with the SoC levels at the beginning and end of the half-cycle. To clarify, if a half-cycle starts at 20%SoC and ends at 60% SoC, its corresponding beginning DoD (D_b) and end DoD (D_e) would be 80% and 40% respectively. Hence, (3.22) and (3.23) provide the relationship between the SoCs and DoDs at the beginning and end of the half-cycle.

$$\Delta E^n_{reg\ cycle} = E^n - E^{n+1} = 2W_D E^n D \tag{3.15}$$

$$\Delta E^n_{reg} = W_D E^n D \tag{3.16}$$

$$E^n = E^{ini}(1 - W_D D)^n \tag{3.17}$$

$$W_D = \frac{1}{D}(1 - R^{\frac{1}{N(D)}}) \tag{3.18}$$

$$N(D) = \alpha e^{\beta D} \tag{3.19}$$

$$W_D = \frac{1}{D}(1 - R^{\frac{1}{\alpha e^{\beta D}}}) \tag{3.20}$$

$$\Delta E^n_{ireg} = E^n \left| W_{D_b} D_b - W_{D_e} D_e \right| \tag{3.21}$$

$$D_b = 1 - S_b \tag{3.22}$$

$$D_e = 1 - S_e \tag{3.23}$$

In equations (3.15) to (3.23), $\Delta E^n_{reg\ cycle}$ is the capacity fade of the battery caused by completing the n_{th} regular cycle as these are the equations of the continuous wear model. ΔE^n_{reg} is the capacity loss of battery caused by completing the n_{th} regular half cycle. E^n denotes the battery capacity just before starting the n_{th} irregular half cycle and subsequently E^{n+1} denotes the battery capacity just

before starting the $(n+1)_{th}$ irregular half cycle. D represents the depth-of-discharge (DoD) and W_D represents the wear coefficient corresponding with the DoD of D. This coefficient shows how much battery capacity is faded due to one-kilowatt-hour energy transfer (either through charging or discharging) upon completion of a regular half-cycle which takes place at DoD of D. Hence, the unit of this variable is [kWh/kWh]. E^{ini} denotes the initial energy capacity of the battery, R is the state-of-health (SoH) of the battery at the end of its lifetime which depends on how much the user wants to exploit the battery. SoH is the ratio of available capacity to the rated capacity of the battery which is always a value between 0 and 1. $N(D)$ is the cycle life function which shows how many cycles the battery can complete before it reaches the end of life. Therefore, $N(D)$ in (3.19) must be obtained for an end-of-life state of health of R. For example, if it is decided that the user will replace the battery at SoH of 50%, the $N(D)$ curve and its function must have been obtained for the same battery when the end-of-life SoH is 50%. This is because the capacity loss of battery per every cycle/half cycle at any DoD can be derived from the $N(D)$. On the other hand, every curve of $N(D)$ is obtained for a specific state of health at the end of life (R). Hence, using a $N(D)$ which has been produced for a specific R and calculating the capacity losses based on that, while attempting to change the battery at a different R will lead to mismatches and inaccuracies in the wear calculations. α and β are the curve fitting parameters that are derived from applying an exponential curve fitting to the $N(D)$. ΔE_{ireg}^{n} denotes the capacity fade caused by completing the n_{th} irregular half cycle. Subscripts b and e express the beginning and end of a half-cycle, therefore D_b and D_e are the DoD of the battery corresponding with its charge level at the beginning and end of a half cycle. As a result, W_{D_b} and W_{D_e} represent the wear coefficients corresponding with D_b and D_e respectively. S_b and S_e are also the SoCs corresponding with the beginning and end of the irregular half-cycle respectively.

In this context, the SoC of the battery at every time frame is a function of the SoC at the previous time frame and the battery power within the previous time frame as shown in equation (3.24). Then,

battery power can be a control variable which determines the SoCs as the inputs of the wear equations. As a result, equations (3.17) to (3.21) implicitly provide a relationship between the battery power which can be controlled, and the capacity loss caused by an irregular cycling action. Therefore, they can be used to calculate the capacity loss of a battery during a cycle/half cycle in an off-line way or be incorporated into a dynamic battery scheduling model and estimate the degradation caused by a series of cycles online.

$$S^n = S^{n-1} + \left(\frac{\eta \times P^{n-1,ch} \times G}{E^n}\right) - \left(\frac{P^{n-1,dis} \times G}{E^n}\right) \tag{3.24}$$

Where η denotes the efficiency of the charging process, also, $P^{n-1,ch}$ and $P^{n-1,dis}$ are the charging and discharging powers within the previous time frame respectively.

Different publications and manufacturers have reported various *N(D)* functions for different Li-ion cells, mostly exponential waveforms. The *N(D)* employed by this work has been produced based on the datasets acquired from [127] for R of 0.8. Implementing exponential regression on the data provided the *N(D)* as follows which includes the α and β coefficients [120].

$$N(D) = 13704e^{-2.51616486} \tag{3.25}$$

Figure 3.7 demonstrates the key parameters of the UC model and how they are defined on the time axis. It can provide a more intuitive picture of how the UC model has been built in this work and how different variables relate to one another in the context of the time.

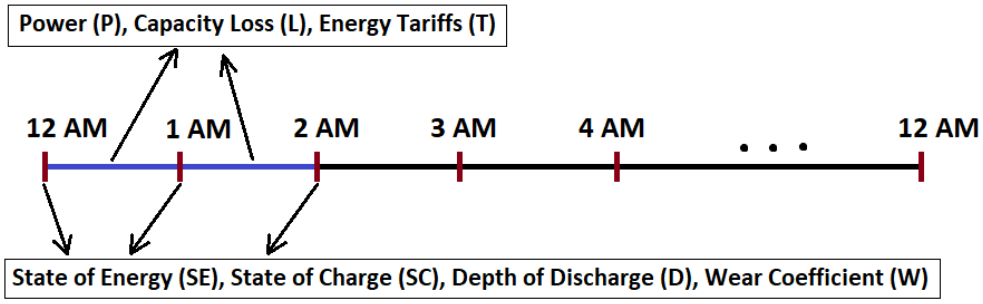

Figure 3.7: Distribution of the major parameters of the UC model on the time axis

It can be seen that in this battery degradation model, the wear coefficient and subsequently the capacity loss is obtained based on the information embedded in the *N(D)* function. Therefore, it is important to obtain this function for every battery which is going to be scheduled based on this wear model. The *N(D)* function depends on the battery chemistry and testing condition including C-rate and temperature [128]. However, generally, it could be said that batteries that have the same technology have similar *N(D)* functions under the same conditions. However, it is worth noting that not all the *N(D)* curves are produced in the same conditions. Different manufacturers may provide the cycle life curve of their batteries for different C-rates and temperatures. Figure 3.8 illustrates the variations of the cycle life curve for a Lithium-ion Phosphate battery cell under different C-rates. It is seen that larger C-rates mildly lower the cycle life of the battery across the range of DoDs.

Regardless of which C-rate the cycle life curve has been produced for, one should know how to employ the best possible *N(D)* curve for a battery wear model. As mentioned before, to avoid complications, the C-rate factor is neglected in the battery wear presented in this work. However, it is still important to know how we can accommodate the available *N(D)* function with our use case. For instance, in a case where the battery's charging/discharging power does not exceed C/5, employing an *N(D)* that has been produced for C2 may lead to suboptimal results. It is suggested that a good while conservative *N(D*) for employing in the wear model is the one that is produced for the largest cycling power in the studied battery. For example, in a case where the maximum cycling power of a battery is C/2, it could be a relatively good choice to build the wear model based on an *N(D)* generated under C/2. To provide a general technique for accommodating the available *N(D)* curve with the case under study, we need to know how the cycle-life curve varies with C-rate. At the time of writing this thesis, it seems that this is an understudied subject, and not enough data is available on the dependence of *N(D)* on the C-rate. It could take comprehensive experimental measurements to study this issue in more depth which could be costly and time taking. However,

figure 3.8 which has been acquired from a battery manufacturer [129] shows the variations of *N(D)* with three different C-rates. Roughly speaking, this graph suggests that *N(D)* for C-rates equal to C1 and lower rates shifts upwards and downwards as the C-rate decreases and increases respectively. A precise model for this relationship might be a nonlinear function that requires exact datasets for these graphs which were not available. However, at least for C-rates equal to and less than C1, the mentioned "shifting" hypothesis seems to be legit. In this regard, once we have the *N(D)* of a battery for a particular C-rate, we could approximate a more favorable *N(D)* by applying a fixed shift upwards or downwards as shown in (3.26). In this equation, Cx is the C-rate of the desirable *N(D)*, hence $N(D)_{Cx}$ represents *N(D)* for the C-rate of Cx, $N(D)_{C1}$ denotes *N(D)* for the C-rate of C1. K_{Cx} could be a positive or negative constant that depends on the Cx. Obtaining K_{Cx} requires more comprehensive *N(D)* datasets for different C-rates and this is out of the scope of this work. In this work, it has been assumed that the available *N(D)* is the best possible option ($K_{Cx} = 0$). This equation is merely provided to point out that it could be possible to obtain more precise *N(D)* curves for a particular case study.

$$N(D)_{Cx} = N(D)_{C1} + K_{Cx} \tag{3.26}$$

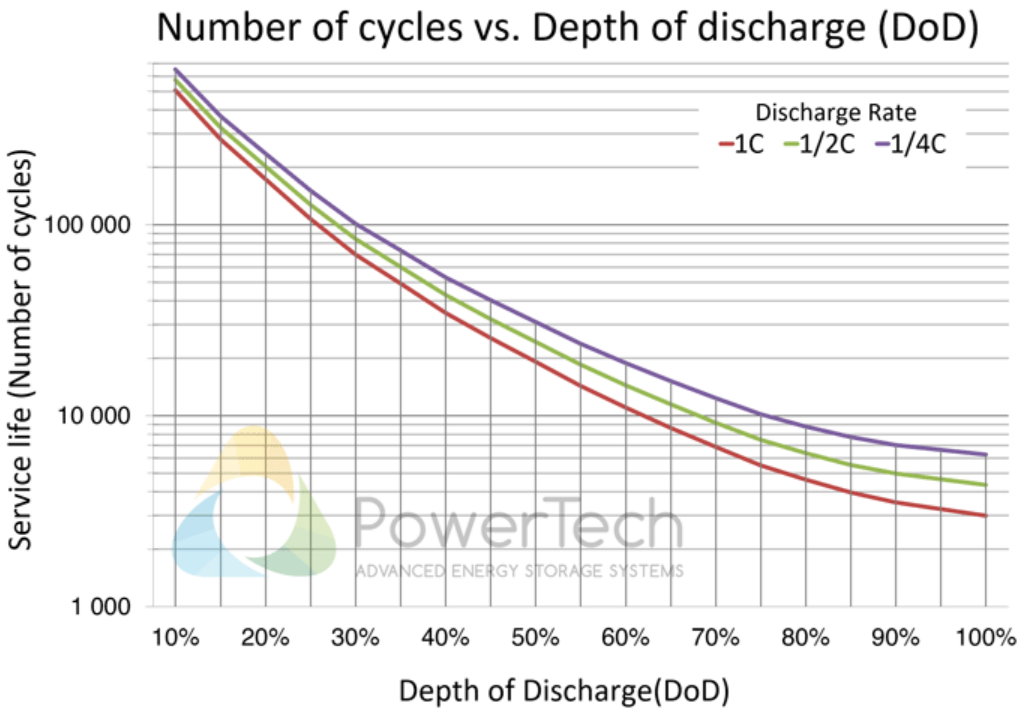

Figure 3.8: Impact of the C-rate on the N(D) curve of a Li-ion battery, obtained from [129], Copyright PowerTech Advanced Energy Storage Systems

Furthermore, the *N(D)* curve also depends on the temperature. Due to the dependence of the battery life on the temperature, higher average temperatures lead to more severe capacity losses and consequently lower life cycles. This is especially more visible in the low DoDs as illustrated in figure 3.9. This figure whose dataset was acquired from [130] shows the variations of the *N(D)* at three different temperatures (25, 35, and 45°C). Applying exponential regression to the data points produced the curve lines. This figure suggests that in order to achieve the best precision in producing the wear model based on *N(D)*, the temperature at which *N(D)* has been produced as well as the existing battery temperature should be taken into consideration. For example, using an *N(D)* curve that is created for 25°C for building the wear model of a battery that is normally operated at higher temperatures (e.g., >35°C) could lead to suboptimal results. Providing the *N(D)* for the room temperature (25°C) might be more prevalent among the battery manufacturers. Moreover, in this work, the impact of the temperature on the wear model has also been neglected as it has been assumed that employed batteries at residential or commercial buildings are equipped

with thermal management systems which prevent the battery temperature from exceeding specific ranges. Hence, to avoid complications, in this work, it is assumed that *N(D)* is provided for 25°C, and all the batteries are also operated at the same temperature.

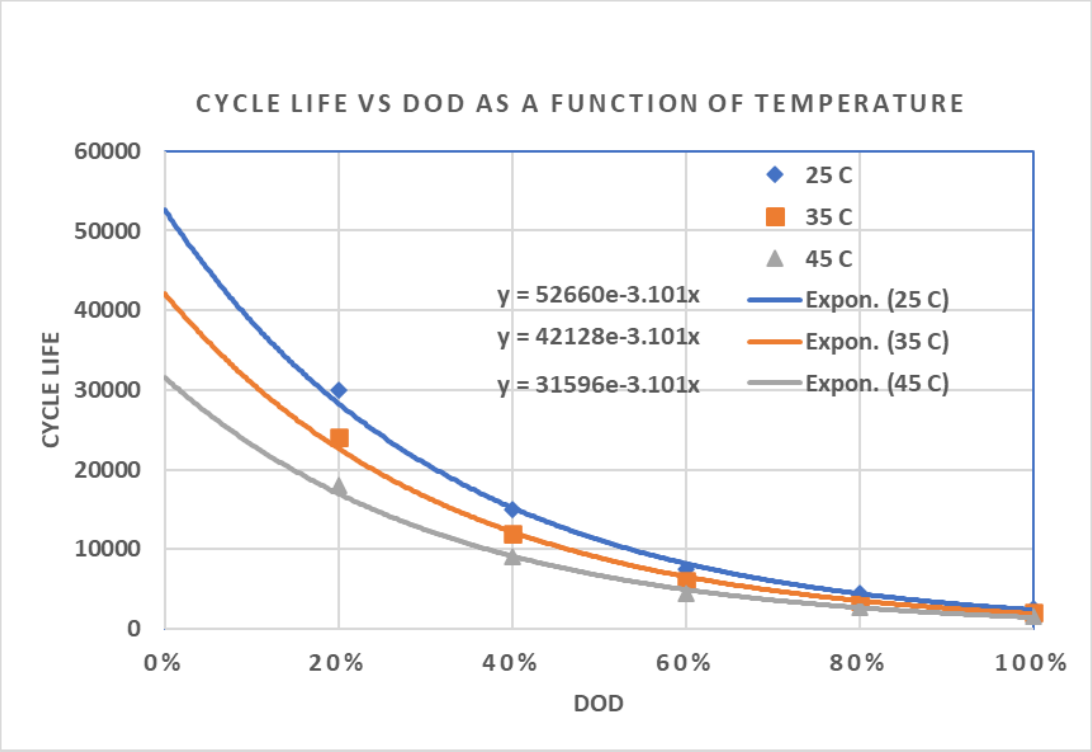

Figure 3.9: Impact of the temperature on the N(D) curve of a Li-ion battery [130]

After the battery degradation model has been formulated, the next step is to present the degradation model in the context of mixed-integer programming so it can be solved for dynamic UC problems. In this regard, the discretized MIP constraints associated with the wear model have been presented as follows. The MIP wear model aims at calculating the cost of capacity loss in every interval of the problem. Incorporating this model into the original UC model provided in chapter 2 provides it with the information on battery degradation costs so the model will be solved for the real minimum costs including the energy costs and the wear cost. To do this, the SoC of the battery is calculated during every optimization cycle as in equation (3.27). Then, the DoD associated with the current SoC is calculated as in (3.28). This factor expresses how much the battery needs to be discharged

to reach from 100%SoC to the current SoC. Now, the wear coefficient which is a function of DoD is presented in equation (3.29). The function *N(D)* is directly included in this equation so it can estimate the wear coefficient for any arbitrary value of DoD. Next, the capacity loss of the battery for an irregular half cycle at interval n is expressed in (3.30). It is seen that for the n_{th} half-cycle, the values of wear coefficient and DoD at the beginning of interval n are considered as the initial values of those two variables, while at the beginning of interval $n+1$ they are considered as the final values of the variables. Now, finally, as D_{ev}^{n} could be greater or smaller than D_{ev}^{n+1}, ΔE_{ev}^{n} could take a positive or negative value. However, the proposed wear model has been made on the basis that the capacity loss inflicted from completing a charging and discharging half-cycle between a pair of SoC values is the same. Moreover, it would be considered common sense that battery wear is always a positive value. Thus, in (3.31), the absolute value of the capacity loss is generated for the MIP model. Although the dimension of L_{ev}^{n} is battery capacity (energy), however, this parameter can simply be used in other parts of the UC model to generate the cost or emission associated with the battery wear. This can be done by multiplying the L_{ev}^{n} by the appropriate "cost per capacity" or "emission per capacity" factor.

$$SC_{ev}^{n} = \frac{SE_{ev}^{n}}{E_{ev}^{n}} \qquad \forall n \in [n_a, n_d + 1] \tag{3.27}$$

$$D_{ev}^{n} = 1 - SC_{ev}^{n} \quad \forall n \in [n_a, n_d + 1] \tag{3.28}$$

$$W_{ev}^{n} = f(D_{ev}^{n}) = \frac{1}{D_{ev}^{n}}\left(1 - R_{ev}^{\frac{1}{\alpha e^{\beta(D_{ev}^{n})}}}\right) \qquad \forall n \in [n_a, n_d + 1] \tag{3.29}$$

$$\Delta E_{ev}^{n} = E_{ev}^{opt} \times [W_{ev}^{n} \times D_{ev}^{n} - W_{ev}^{n+1} \times D_{ev}^{n+1}] \qquad \forall n \in [n_a, n_d] \tag{3.30}$$

$$\mathrm{L}_{ev}^{n} = |\Delta E_{ev}^{n}| \qquad \forall n \in N \tag{3.31}$$

As before, the superscript n refers to the index of interval in the discrete wear model. In (3.27)-(3.31), SC_{ev}^{n} denotes the SoC of the EV battery at the beginning of the n_{th} interval, E_{ev}^{n} expresses the available energy capacity of EV battery at the beginning of the n_{th} interval, D_{ev}^{n} represents the

DoD associated with SC_{ev}^n, W_{ev}^n denotes the wear coefficient associated with D_{ev}^n and f denotes the function of the wear coefficient of the EV battery. ΔE_{ev}^n expresses the capacity fade of EV battery caused by the n_{th} interval. And, L_{ev}^n shows the absolute value of ΔE_{ev}^n.

The MIP constraints for the wear model of ESS are also laid out similar to the EV as shown in the following equations. Therefore, (3.32) to (3.36) enforce the constraints for SoC, DoD, wear coefficient, capacity loss, and the absolute value of capacity loss for the energy storage system at the n_{th} interval, respectively. However, ESS and EV batteries differ in terms of the ranges, as the constraint ranges of EV batteries are defined for the times of day that EV is present at the parking spot, while constraint ranges of ESS are defined for the entire intervals of the day as ESS should be operational 24 hours of the day.

$$SC_{es}^n = \frac{SE_{es}^n}{E_{es}^n} \qquad \forall n \in \{n_b, n_e + 1\} \tag{3.32}$$

$$D_{es}^n = 1 - SC_{es}^n \quad \forall n \in \{n_b, n_e + 1\} \tag{3.33}$$

$$W_{es}^n = g(D_{es}^n) = \frac{1}{D_{es}^n}\left(1 - R_{es}^{\frac{1}{\alpha e^{\beta(D_{es}^n)}}}\right) \qquad \forall n \in \{n_b, n_e + 1\} \tag{3.34}$$

$$\Delta E_{es}^n = E_{es}^{opt} \times [W_{es}^n \times D_{es}^n - W_{es}^{n+1} \times D_{es}^{n+1}] \qquad \forall n \in N \tag{3.35}$$

$$L_{es}^n = |\Delta E_{es}^n| \qquad \forall n \in N \tag{3.36}$$

In the equations above, SC_{es}^n denotes the SoC of ESS at the beginning of the n_{th} interval, E_{es}^n shows the available energy capacity of ESS at the beginning of the n_{th} interval, D_{es}^n represents the DoD associated with SC_{es}^n, W_{es}^n is the wear coefficient associated with D_{es}^n and g denotes the function of the wear coefficient of ESS. ΔE_{es}^n expresses the capacity fade of ESS caused by the n_{th} interval. Finally, L_{es}^n shows the absolute value of ΔE_{es}^n.

However, as can be seen in equations (3.29) and (3.34), the wear coefficient (*W*) is a severely nonlinear function with respect to the DoD. Many MIP solvers may not be able to handle this highly

nonlinear function as a part of a model constraint. In order to address this problem, it is suggested to use a curve-fitted version of the wear coefficient-DoD function instead of the original function. In fact, using curve fitting to simplify this function to a simpler function with a lower nonlinearity degree could enable the typical MIP solvers to handle the complexity of the curve-fitted curve. Depending on the capabilities of the employed solver in supporting different mathematical functions and also depending on the shape of the wear coefficient function (which itself depends on the shape of *N(D)*), one may find different functions more suitable for the curve fitting. Cotangent, reciprocal and polynomial functions are some of the functions that can be used for curve fitting as shown in figure 3.10, although each of them could have its shortcomings in presenting the detailed information incorporated into the *W* curve. Moreover, the polynomial function seems to do a better job at showing the increasing wear rate at the higher DoDs.

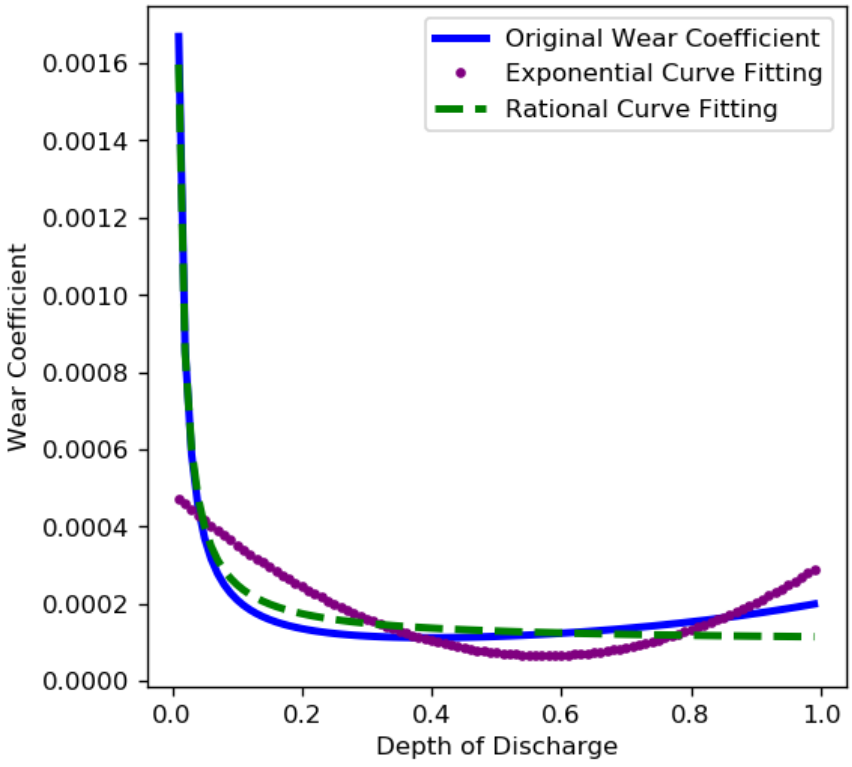

Figure 3.10: Wear coefficient function of a Li-ion battery

However, according to the accuracy of every fitting function and other considerations, one can decide on the best fitting function for every case. For example, reference [131] reports that EVs normally provide a range of 10-15%SoC to 90%SoC of their batteries for cycling. In this case, the data of the *W* curve for DoD values of under 10% and over 90% will be insignificant because the battery is banned from being cycled by less than 10%DoD and more than 90%DoD from an initial SoC of 100%. In this case, the user might find it useful to use a fitting function that can model the range of 10%DoD-90%DoD in the most accurate way. It is worth mentioning that a low DoD on this figure is associated with a high SoC and vice versa. For instance, the SoC of the battery associated with DoD of 0.2 is 0.8, which means that by discharging the battery by 20% from the initial SoC of 100%, the resulting SoC will be 80%. In this work, a polynomial curve fitting function has been employed to mimic the wear coefficient vs DoD curve as shown in figure 3.11. Despite its deviations from the original curve, the polynomial curve fitting seems to fairly model the fact that wear rate is larger at low and high DoDs. However, depending on the capabilities of the MIP solver in taking complex constraints, employing more accurate fitting functions may model the wear rate with less error.

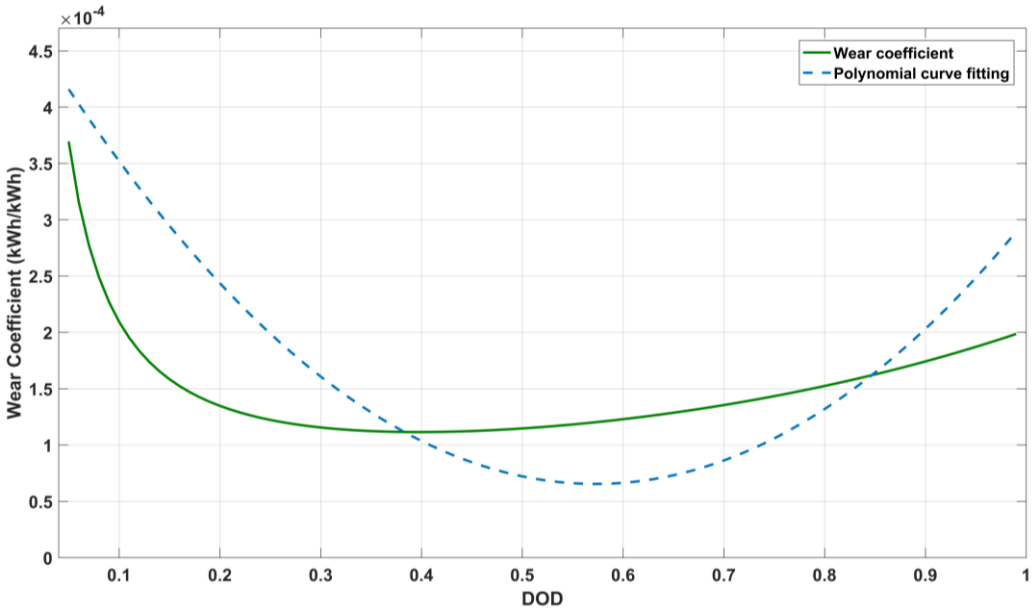

Figure 3.11: Original nonlinear wear coefficient function and its polynomial approximation

A decent function to fit the curve would approximate the wear function properly and can be embedded as a constraint in an available MIP solver simultaneously. That's why the polynomial function was selected in this work as the used solver was able to handle polynomial constraints. The batteries that benefit from the same technology have the same wear function and subsequently can benefit from the same simplified versions of the wear function. Thus, In this work, W_{ev}^{n} and W_{es}^{n} are approximated as in equations (3.37) and (3.38) with an identical curve fitting function, where the polynomial coefficients are $a_1 = a_2 = 0.0012837373$, $b_1 = b_2 = -0.0014698375$ and $c_1 = c_2 = 0.0004861267$.

$$W_{ev}^{n} = f(D_{ev}^{n}) = \frac{1}{D_{ev}^{n}}\left(1 - R_{ev}^{\frac{1}{\alpha e^{\beta(D_{ev}^{n})}}}\right) \approx a_1(D_{ev}^{n})^2 + b_1(D_{ev}^{n}) + c_1 \tag{3.37}$$

$$W_{es}^{n} = g(D_{es}^{n}) = \frac{1}{D_{es}^{n}}\left(1 - R_{es}^{\frac{1}{\alpha e^{\beta(D_{es}^{n})}}}\right) \approx a_2(D_{es}^{n})^2 + b_2(D_{es}^{n}) + c_2 \tag{3.38}$$

After introducing the constraints of the MIP model, in this part, the objective functions are presented. A proper objective function should be able to precisely model the parameter that is to be optimized. In this regard, when producing an objective function, it is important to notice who is going to benefit from it directly. For instance, when it comes to a home, the objective function could be made to benefit the homeowner, the grid operator, and so on by minimizing the cost, energy consumption, emission, battery degradation, etc. In this work, the focus is on minimizing the real cost of the homeowner (including the cost of battery degradation) as well as the carbon footprint of the homeowner. Thus, the "real cost" objective function of the MIP model that incorporates the net energy cost and degradation cost of the battery is presented in (3.39).

$$\begin{aligned} Min \sum_{N} \left(P_{im}^{n} \times G \times T^{n,buy}\right) + \left(\frac{\mathrm{L}_{ev}^{n}}{L_{ev,life} \times E_{ev}^{ini}}\right) \times \left(V_{ev}^{ini} - V_{ev}^{sal}\right) \\ + \left(\frac{\mathrm{L}_{es}^{n}}{L_{es,life} \times E_{es}^{ini}}\right) \times \left(V_{es}^{ini} - V_{es}^{sal}\right) - \left(P_{ex}^{n} \times G \times T^{n,sell}\right) \end{aligned} \tag{3.39}$$

In the objective functions above, $L_{ev,life}$ represents the lifetime capacity fade of EV which equals (1-R_{ev}), E_{ev}^{ini} denotes the initial storage of EV battery, V_{ev}^{ini} expresses the initial cost of the EV battery, V_{ev}^{sal} is the salvage cost of the EV battery, $L_{es,life}$ represents the lifetime capacity fade of ESS which equals (1-R_{es}), E_{es}^{ini} expresses the initial storage of ESS, V_{es}^{ini} denotes the initial cost of ESS and V_{es}^{sal} shows the salvage cost of ESS. Regarding the "cost" parameters in this work whose dimension is price, it should be mentioned that the unit of these parameters must be in accordance with the unit of energy fees. If energy fees are for example expressed in cents per kWh, the battery cost and cost functions must be considered in cents. Whereas in case energy fees are provided in dollars per kWh, the battery cost and cost functions must be considered in dollars. In the case studies of this work, all the battery costs, energy fees, and cost functions are considered in cents.

After completing an optimization attempt for each day, the available battery capacities for EV and ESS need to be recalculated to obtain the updated battery capacities for a new optimization attempt. Hence, the available capacity of EV battery and ESS after every optimization iteration can be obtained from (3.40) and (3.41). These equations are valid for all the UC models presented in this thesis. Needless to mention these equations are not components of the MIP model and are merely used offline to find the remaining battery storage for the next optimization attempt.

$$E_{ev}^{opt} = E_{ev}^{ini} - \sum_{O}\sum_{N} \mathrm{L}_{ev}^{n} \tag{3.40}$$

$$E_{es}^{opt} = E_{es}^{ini} - \sum_{O}\sum_{N} \mathrm{L}_{es}^{n} \tag{3.41}$$

Where E_{ev}^{opt} and E_{es}^{opt} represent the available capacity of EV battery and ESS for the next optimization, O is the set of the total optimization iterations (which must be equal to the number of days in a day-ahead UC model) since the first day that batteries were employed by the microgrid.

3.4 Carbon emission study

In the previous sections, the UC problem of a smart home was investigated for the aim of minimizing the costs associated with energy consumption and battery degradation. However, the carbon footprint of users is another target that has been addressed in this work. This is important as residential and commercial buildings consume 32% of the total produced energy globally and emit 30% of the total carbon into the environment [69]. Also, reference [51] reports that 48% of the people that are interested in procuring an EV want to do so mainly for sustainability reasons, which shows carbon footprint could be a major objective function in a smart building as in (3.42). This objective function aims at minimizing the energy intake of the building to minimize its corresponding emission. Thus, carbon footprint and cost objective functions can be treated altogether in the framework of a multi-objective MIP model as most MIP solvers could handle multi-objective models. It may be desirable to tune the impact of every objective function in the commercial solvers by decreasing or increasing the impact of one objective function in a multi-objective problem such as this one. For instance, in this work, the "weight" of the emission objective can be tuned to figure out how it can impact the costs and emissions. The carbon footprint of a user can be considered as the sum of the carbon footprint associated with the battery wear and the carbon footprint caused by the energy consumption. Hence, to minimize the battery degradation, which is the other major cause of carbon footprint, we could use the objective function of (3.43).

$$Min \sum_{N} P_{im}^{n} \tag{3.42}$$

$$Min \sum_{N} (\mathrm{L}_{ev}^{n} + \mathrm{L}_{es}^{n}) \tag{3.43}$$

The value of the carbon footprint associated with energy consumption relies on the cleanness of the home energy providers. Obviously, the electricity is generated from different sources in different regions. These sources could be clean and renewable such as solar and wind energy or could be polluting such as gas and coal. Hence, in different regions, different amounts of carbon are released per generation of a unit of electric energy which should be taken into consideration when calculating the carbon footprint of a local energy consumer. In this regard, the CO2 emission per kilowatt-hour of generated energy is assumed to be 449 grams which is equal to the average rate in the United States in 2018 [132]. Although other pollutant gasses may be released in the process of power generation, in this work only CO2 is taken into consideration. Thus, in this thesis, it is assumed that per every kilowatt-hour of energy drawn from the grid, CF_H =449 grams of CO2 is emitted into the environment. Hence, the total carbon emission caused by the home energy consumption is derived from (3.44), where HE denotes the amount of home emission.

$$HE = CF_H \times \sum_{N} P_{im}^{n} \tag{3.44}$$

The other source of carbon footprint is the battery degradation phenomena. The manufacturing and recycling process of batteries releases large amounts of harmful emissions into the environment. Inefficient employment of batteries could expedite their wear rate which leads to a more frequent need for battery replacement**.** As demonstrated before, neglecting the battery degradation could considerably increase the wear rate which leads to a larger carbon footprint for the user even when the problem is seemingly optimized for the best energy efficiency. The carbon emission caused by the battery manufacturing process depends on several factors such as the manufacturing method and material of the battery as well as the energy sources of the battery plant.

A lifecycle assessment process could assess the carbon footprint of batteries during their manufacturing procedure using a top-down or bottom-up approach. The former technique first

specifies the total emissions of a plant and then determines the emissions of each procedure, while the latter starts with analyzing the impact of each component. Between these two approaches, the top-down method normally leads to obtaining larger amounts for the emission [133]. Hence, the method of performing the lifecycle assessment could largely impact the results of battery environmental studies. Different studies have carried out the lifecycle assessment for the Li-ion batteries and reported various values for the carbon emission of the battery production process. Due to the different employed assessment methods, different values have been reported for the CO2 emissions ranging between 56 and 494kg CO2 per kilowatt-hour of manufactured battery cell [134]. According to [134], on average, Asian battery manufacturers emit between 150 and 200 kilograms of CO2 per kilowatt-hour of manufactured battery capacity. In this thesis, the median of this range (175 kg/kWh) is assumed as the CO2 emission of the battery manufacturing process. If we assume that the battery will have a second life before recycling, it will add a large amount of uncertainty to the problem. Hence, in this work, the second life is not taken into consideration [120]. To calculate the CO2 footprint caused by losing one kilowatt-hour of the battery capacity, equation (3.45) is used in this work.

$$CF_U = \frac{CF_M}{(1-R)} \tag{3.45}$$

In this equation, CF_U is the CO2 footprint (kg) associated with 1kWh capacity loss, CF_M is the CO2 footprint (kg) that is emitted by the battery maker for manufacturing one kilowatt-hour of battery capacity which is assumed to be 175 kg/kWh in this work [120]. Therefore, assuming that both EV and ESS batteries have been made by the same manufacturer, the CO2 footprint caused by the battery degradation is obtained by (3.46).

$$BE = CF_U \times \sum_N (\mathrm{L}_{ev}^n + \mathrm{L}_{es}^n) \tag{3.46}$$

Figure 3.12 demonstrates the used algorithm for producing and solving the presented UC model.

Algorithm 1 Unit Commitment Algorithm for Smart Home-Hourly Time Resolution

1: Updating or calculating model parameters and data including departure and arrival times of EV, initial and final SoCs of EV, initial and salvage prices and current capacities of EV and ESS batteries, day-ahead PV generation, energy tariffs, load profile and user's demand for controllable load.
2: Updating the $N(D)$ for EV battery and ESS according to their power ratings.
3: Calculating the $W(D)$ function and performing curve fitting on it to make it implementable as a model constraint in the used mathematical solver.
4: **procedure** "PRODUCING THE MIXED-INTEGER PROGRAMMING MODEL WHICH INCLUDES THE FOLLOWING COMPONENTS AND PERFORMING THE OPTIMIZATION FOR THE NEXT 24 HOURS"
5: General constraints of the model including EV, ESS, PV and controllable load
6: Battery Degradation constraints for EV and ESS
7: Objective functions for minimizing cost, degradation and emission or combinations of them
8: Obtain the control variables of EV power, ESS power and operation schedule for controllable load, as well as state variables of SoC arrays, battery degradation values, consumed energy and costs for the next 24 hours from the solved MIP problem.
9: Calculate the battery degradation for the scenarios that neglect battery degradation by applying the wear model to the obtained SoC arrays of EV and ESS.
10: Calculate the carbon footprint caused by energy consumption and battery wear.

Figure 3.12: Unit commitment algorithm for a residential microgrid built in the framework of MIP with hourly resolution

3.5 Impact of the degradation model on the optimization results

In order to study the functionality of the proposed battery degradation model, the case study that was carried out in chapter 2 is repeated in this chapter, however, this time with the battery degradation model incorporated into the MIP model. Regarding the fact that the proposed battery degradation model incorporates the battery price into the UC model, the battery's monetary value has a significant impact on how it is scheduled to be cycled by the energy management system. A costly battery could shift the outcomes of the UC problem to less frequent and shallower cycles while cheaper battery prices could lead to more frequent and deeper cycles. Reference [89] reports that considering higher battery costs leads to the flattening of the SoC graph, this is because the degradation cost could surpass the potential revenues achieved by the battery when the battery price is high. As a matter of fact, what matters about the battery price is the net price of the battery which results from the initial and salvage prices of the battery. These two prices themselves depend on several factors. For example, the initial price depends on the technology, market, and manufacturer

of the battery. Fortunately, as time goes on, the prices of Li-ion batteries are declining as the technology is maturing and the market is expanding continuously. The salvage price is proportional to the price of a new battery with similar capabilities with consideration of health, cost of collection, refurbishment, and certifying the old battery [135]. The initial and salvage prices of this thesis have been acquired from [107] which are 250 $/kWh and 51 $/kWh respectively. The second lifetime of the battery and consequently the salvage price (selling price) of a used EV battery heavily depend on the DoD at which the battery is used during its second lifetime. However, for a battery with the initial price of 250 $/kWh, per DoD of 50% in the second life, its salvage value will be 131 $/kWh, while per DoD of 60%, the salvage value will be 51 $/kWh [107]. One beauty of the proposed wear model is that it allows the battery capacity to be used in its entirety as it can estimate the capacity loss caused by any half cycle. However, as a general practice, the EV and ESS manufacturers normally limit the usable capacity of their batteries. For stationary energy storage systems, this could be mainly because they generally lack sophisticated battery cycling algorithms and for electric vehicles, this could be to prevent their users from using up the entire stored energy of battery while driving as it could lead to high wear rates. Hence, regardless of the merit of the battery wear model, the available ESS and EV batteries do not provide 100% of capacity for usage. In this regard, in this section, the usable SoC range of batteries has been assumed to be between 7.5% and 95% [136]. This approach will also prevent the inaccuracy of the used (polynomial) curve-fitting function to impact the results significantly. One of the factors that are included in the UC model is the batteries' capacity at the end of life. This could differ depending on the application of the battery as well as the user's choice. For example, EV batteries are less capable of being used in low state-of-health conditions. This is because lower SoH for EV batteries will undermine the vehicle's driving capabilities. While stationary batteries (e.g., ESS) could be exploited more in one or more lifetimes. In this regard, various articles have stated different values for the state of health of a battery at the end of life (R) such as 50%, 65%, and 80%. In this thesis, the R-value of ESSs and EVs are assumed to be 50% and 80% respectively. This means it is assumed that by the time EV

battery loses 20% of its capacity and ESS loses 50% of its capacity they will be replaced. It should be noted that after the battery degradation model is laid out, to use it for a case study it is necessary to maintain the battery cycling regime under conditions that do not initiate degradation processes that are not predicted in the wear model. In this regard, as a general recommendation, Li-ion batteries of EVs should be cycled at the rates under 5C and temperatures within -20°C and +45°C [112]. Hence, in this thesis, the C-rate of the cycling events is assumed to be C-rate ≤ 1, and the temperature is assumed to be 25°C.

To investigate the effectiveness of the battery degradation model in the MIP unit commitment model, in this chapter the general MIP model constraints provided in chapter 2 (equations (2.32) to (2.58)) will be used along with the additional battery wear constraints and new objective functions provided in this chapter (equations (3.27) to (3.39)) using the general input datasets provided in chapter 2 and battery datasets provided earlier in this chapter. To compare the results of the basic case where apparent cost is the only objective function with more sophisticated degradation-equipped models, seven different cases have been investigated where the optimization model is subject to different single or multi-objective functions. In all these cases, all the constraints are similar, however, the objective functions vary from case to case. These cases consider combinations of apparent cost, battery degradation, and apparent emission as objective functions. Thus, the objective functions are considered as follows:

- Net energy cost of the building (aka cost)
- Capacity loss of EV and ESS batteries (aka degradation)
- Apparent CO2 footprint emission of the building led by the electricity consumption (aka emission)
- Cost & degradation
- Cost & emission
- Degradation and emission

- Cost & degradation & emission

These objective functions can show how neglecting or considering battery wear and emission in the UC problem could impact the real costs, carbon footprint, and battery capacity loss for a homeowner. Similar to the basic case, all these scenarios have been simulated for a month-long period. Equations (3.47), (3.48), (3.49), and (3.50) which can be formed from the results of an optimization attempt, provide capacity loss of batteries, apparent carbon footprint, real (total) carbon footprint of user, and peak power of home, respectively.

$$\sum_{N} (\mathrm{L}_{ev}^{n} + \mathrm{L}_{es}^{n}) \tag{3.47}$$

$$\sum_{N} CF_H \times P_{im}^{n} \tag{3.48}$$

$$\sum_{N} (CF_H \times P_{im}^{n}) + (CF_U \times (\mathrm{L}_{ev}^{n} + \mathrm{L}_{es}^{n})) \tag{3.49}$$

$$max\ \{P_{im}^{n}\} \tag{3.50}$$

After an optimization problem has been solved, if it has incorporated the battery degradation model, the capacity loss of batteries can be extracted from the outcome of the optimization. However, in order to obtain the capacity loss of batteries for those cases that omit the battery wear, the SoC profile of batteries is given to the battery wear model (equations (3.20) to (3.23)) in an offline fashion to have it calculate the capacity loss caused by the battery activity [120].

To investigate the performance of the proposed UC strategies in a residential building, each strategy is first simulated for a single sample day and the results are produced. Next, each strategy is simulated for a one-month period to provide more comprehensive results. The figures below show the variations of the power for all the involved units during 24 hours under different sets of objective functions. This graph was presented in chapter 2 for the case where the apparent energy cost of the home was the only objective function. However, the following figures show how

incorporating the battery wear model and optimizing the problem with more optimal objective functions change the unit commitment results.

In this regard, figure 3.13 demonstrates the power rates when the cost is considered as the objective function along with the battery degradation for both EV battery and ESS, therefore the objective function consists of (3.39). Clearly, in this case, to avoid the degradation cost caused by inefficient battery cycling, ESS and EV battery are discharged less often and only when their discharging revenue overcomes the degradation cost associated with discharging. The EV battery provides relatively less energy through discharging and in the other time intervals it is charged with low amounts of power. Controllable load is also operated early in the morning to keep the costs low.

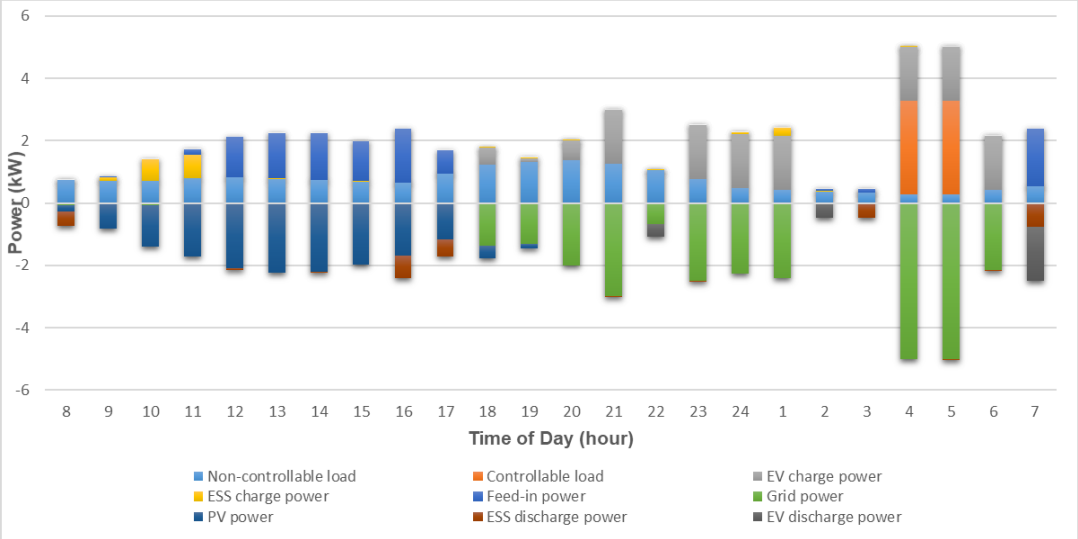

Figure 3.13: Power profile of the microgrid components-objective functions: energy cost and battery degradation

For the next scenario, cost and apparent emission are assumed as two different objective functions provided in (2.59) and (3.48). In this case, it is desirable to find a solution where both cost and apparent emission have their lowest possible level simultaneously, but it does not take battery degradation into account. Therefore, this set of objectives will not provide real cost and carbon footprint directly. However, regarding the apparent emissions of the home, this case is considerably better that the conventional approach where energy cost is the only objective function. Hence, it is

seen in figure 3.14 that EV battery and ESS discharge events are performed during the daytime, afternoon and nighttime and controllable load is operated early in the morning for a lower cost of operation.

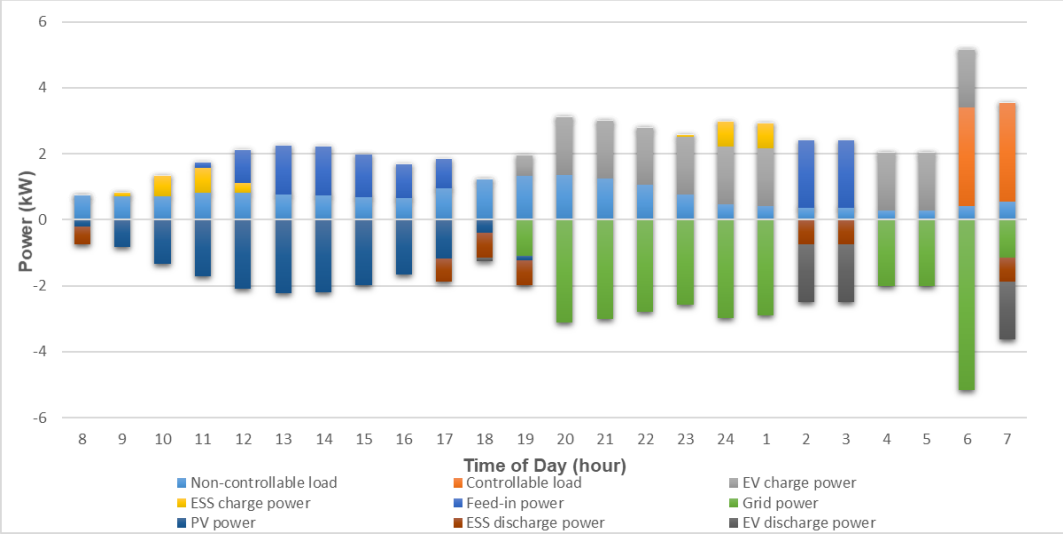

Figure 3.14: Power profile of the microgrid components-objective functions: energy cost and apparent emission

Degradation is another objective function to be investigated which is provided in (3.47) and the results are shown in figure 3.15. Even though taking degradation as the only objective would not be desirable in practice, it was studied to provide a better understanding of how minimizing the degradation as a sole objective compares to the other objectives in terms of cost, degradation, and emissions. Although, in a case where the energy price is a static constant rate and there is no available feed-in option, minimizing the mere battery degradation may seem a practical approach. Obviously, in this case, EV and ESS are discharged minimally. Also, the EV battery is charged with low power to keep the wear rate low. Moreover, as the scheduling is performed without consideration of the costs, the controllable load is dispatched at a time which is not optimal in terms of the energy tariffs.

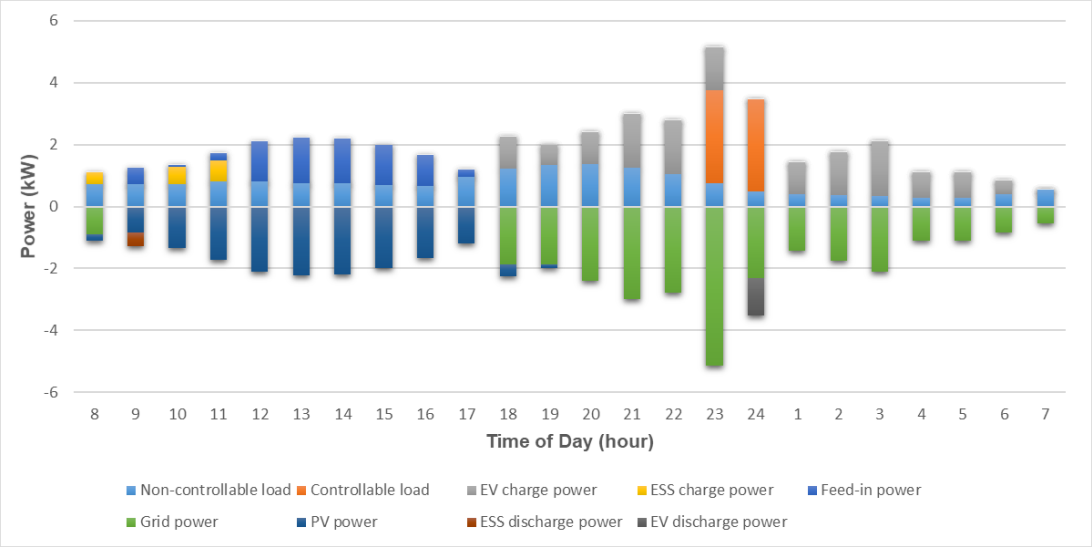

Figure 3.15: Power profile of the microgrid components-objective function: battery degradation

To study the case where minimizing the apparent emission is the only objective, (3.48) is considered as the objective function of the problem. Since apparent emission is correlated with the grid-supplied energy, this objective aims at minimizing the energy drawn from the grid. As a result, it is seen in figure 3.16 that the grid power is relatively lower as compared to the previous scenarios. In this case, the EV's contribution to the energy provision is minimal, ESS is merely charged from the PV generation and controllable load is dispatched in the middle of the day when it is mostly supplied by the solar power.

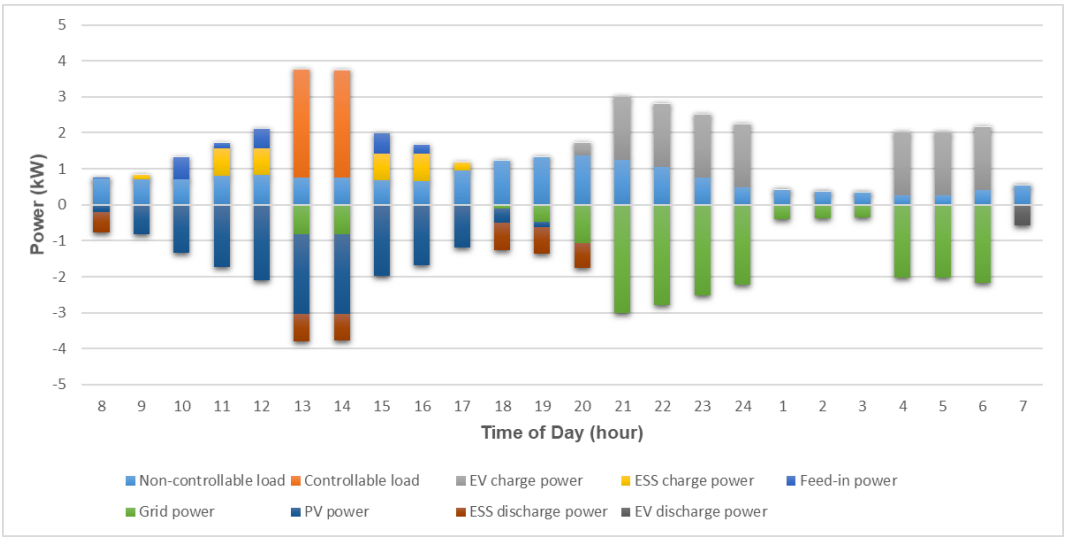

Figure 3.16: Power profile of the microgrid components-objective function: apparent emission

To observe the effect of the minimization of both factors that impact the real carbon footprint of the home, this time, both apparent emission and battery degradation of EV and ESS ((3.47) and (3.48)) are considered as objectives of the model. In this case, the grid-supplied energy has been reduced to lower the emission associated with the grid power, and EV charging is performed with relatively smaller power rates. According to the battery wear model, lower cycling powers correspond to the lower DoD rates which cause less degradation. Also, the EV battery is not discharged in this case to avoid further degradation which is against the model objectives. In this case, the ESS charging and discharging activities are only to help lower the grid-supplied energy, not contributing to the cost minimization. The controllable load is also activated in the middle of the day which is not the most cost-efficient as appeared in figure 3.17.

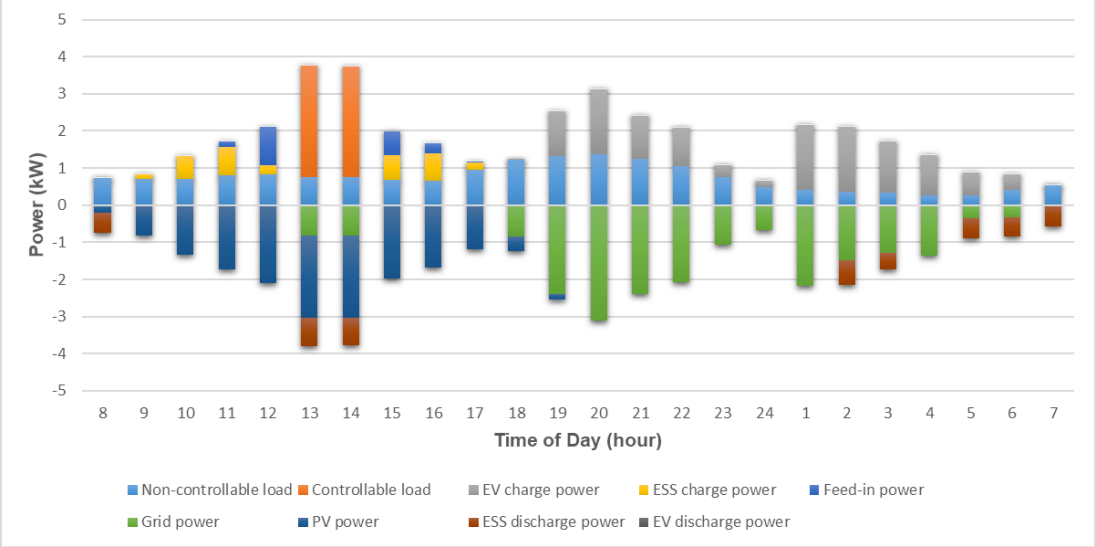

Figure 3.17: Power profile of the microgrid components-objective functions: apparent emission and battery degradation

Finally, real cost (including the energy and degradation cost) and apparent emission have been assumed as the objectives of the model as provided in equations (3.39) and (3.48) as an attempt to minimize all the three major factors (energy cost, battery wear (which reflects on cost and emission) and apparent emission) at once. In this case, the cycling of both batteries is carried out in a moderate way to make sure they are employed efficiently to increase the revenues and limit the grid-supplied

energy while avoiding excessive operations which cause a high wear rate. The results show that EV discharging is performed only once so that it will help with costs without adversely impacting the degradation and emission. Also, the controllable load is dispatched early in the morning to consume energy at the cheapest times of the day as seen in figure 3.18.

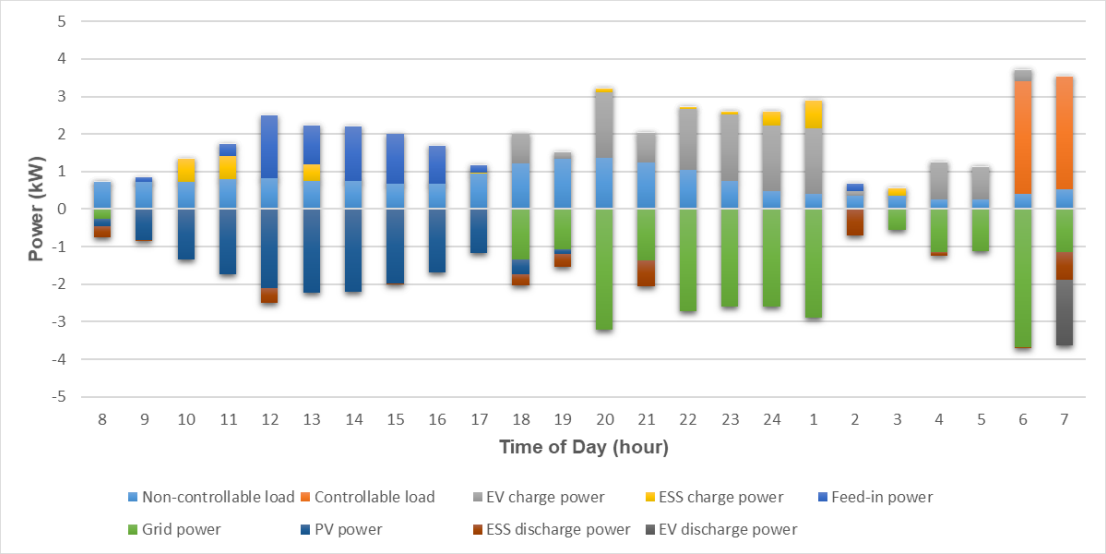

Figure 3.18: Power profile of the microgrid components-objective functions: real cost (including degradation) and apparent emission

Probably the most tangible outcome of an energy system (e.g., microgrid, home, etc.) for a user is the energy price that they need to pay the utility company which in this work is also referred to as the "apparent cost". In a bidirectional market where the energy consumption and generation of users are measured by using advanced metering infrastructure (AMI), the (apparent) net energy price at every period is the difference between the consumed energy price and the generated energy price. However, it is important to note that in a modern energy system that includes energy storage and renewable generation, minimum energy cost is not necessarily equal to the "real minimum costs" of the system, as "real cost" could be considered to include other components such as the battery degradation cost. Thus, it is worthwhile to study how apparent cost and real costs are correlated in a home microgrid. To do this, the net energy cost of the home was studied for the sample month (based on the same datasets used in chapter 2), this time under seven sets of

objectives, and the results are demonstrated in figure 3.19. Table 3.1 also provides the numeric values of the monthly energy fees resulting from the seven scenarios. The results show that the minimum energy cost was obtained when the objective was set to specifically minimize the energy price. As we incorporate emission or degradation to the cost in the objectives set, the monthly cost will rise as "cost" will need to compete with another objective in the optimization problem. Degradation specifically has a more detrimental effect as it also confines the battery's performance. As expected, incorporating both emission and degradation on top of the cost will further increase the costs as this time cost needs to compete with two other objectives. Removing cost from the objectives will increase the energy expenses where "emission" and "emission + degradation" are the costlier cases. Also, the largest amount of energy cost occurs when the objective is merely minimum degradation. This is because this objective will control the battery's performance to achieve the minimum wear without any consideration of the direct monetary interests of the user.

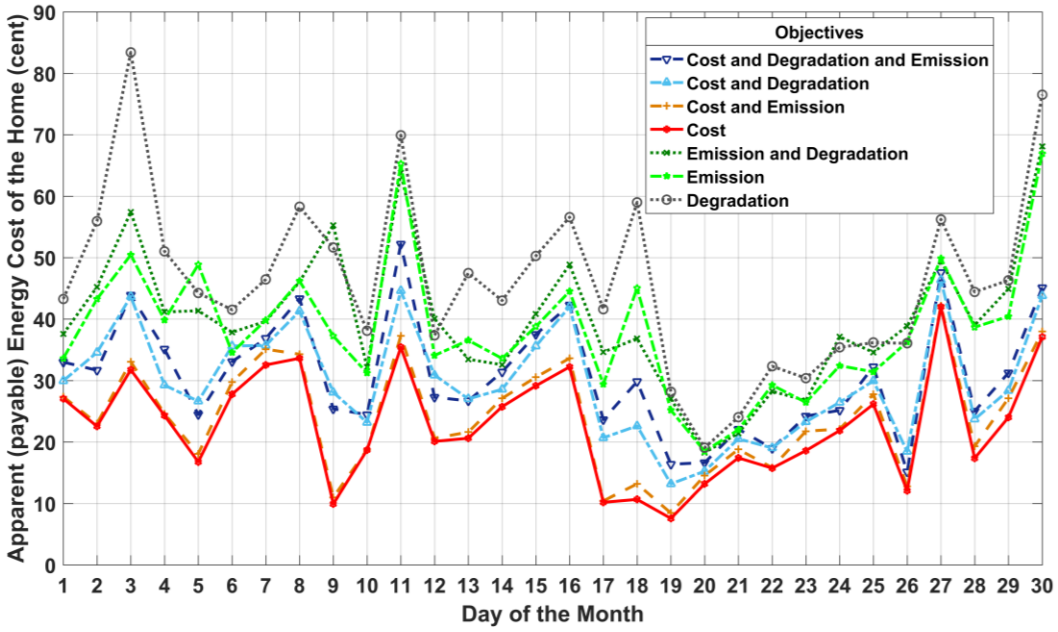

Figure 3.19: Daily energy cost of home for one month, under seven different sets of objective functions

Table 3.1: Energy cost of home for one month

Objective Set	Cost	Cost & Deg	Cost & Emission	Cost & Emission & Deg	Emission	Deg	Emission & Deg
Net Monthly Cost of Energy ($)	6.82	8.88	7.18	9.22	11.49	13.84	11.98

The capacity fade of the EV battery over the 30 sample days is sketched in figure 3.20 and the values are provided in table 3.2. As can be seen, the largest capacity fade corresponds to the basic objective which leads to around 0.1 kWh capacity fade in the EV battery. This is due to the high contribution of the EV battery to the energy transactions in that case. The addition of emission to the cost as another objective function lowers the capacity fade as it lowers the battery's operation to some extent. Once emission is considered as the only objective it leads to average capacity fades, but if we add degradation, it almost halves the monthly capacity loss. All the cases that include degradation as an objective show minimal capacity fade with insignificant differences. This is due to the significant impact of "degradation" on the battery wear as compared to the other objectives.

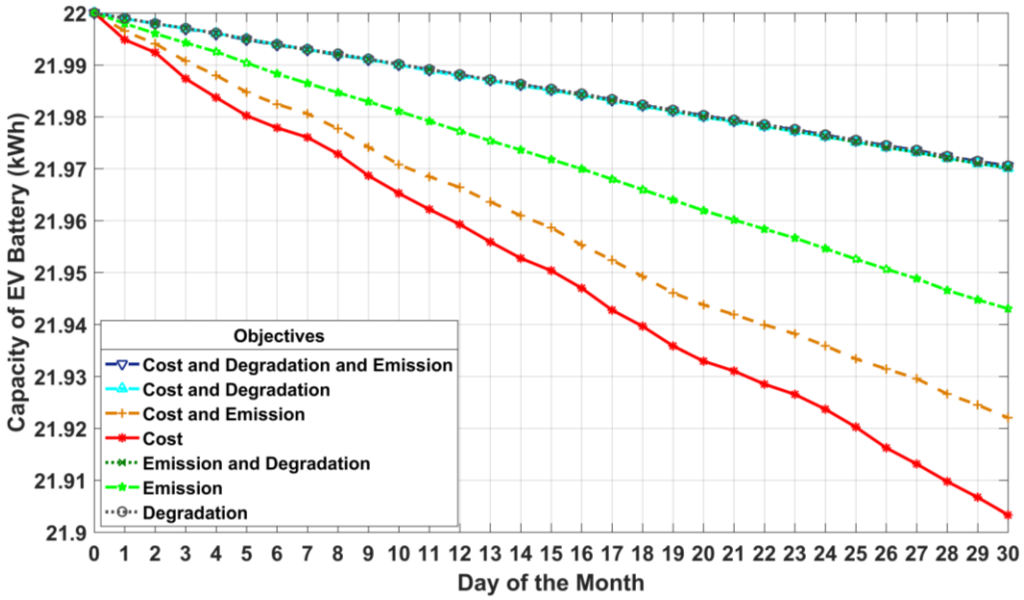

Figure 3.20: Daily capacity loss of EV battery for one month, under seven different sets of objective functions

Table 3.2: Capacity loss of EV battery for one month

Objective Set	Cost	Cost & Deg	Cost & Emission	Cost & Emission & Deg	Emission	Deg	Emission & Deg
Monthly Capacity Loss of EV Battery (kWh)	0.0966	0.0299	0.0779	0.0294	0.0569	0.0294	0.0298

The capacity fade of ESS relatively follows a similar trend to EV battery which can be seen in figure 3.21 and table 3.3. Basic objective function again leads to the highest amount of degradation. The addition of emission as an objective function will slightly lower the battery wear which is not as significant as in the case of EV. In other words, the addition of emission to the cost is not able to lower the battery wear as much as it can for an EV battery. This is possibly because ESS is merely scheduled to help lower the costs throughout the day, while EV has a priority of being fully charged while it is parked at home. Hence, the EV battery is more prone to be prevented from too

much cycling compared to the ESS. When emission is the sole objective function, it leads to mediocre levels of degradation, and adding degradation to that will naturally further reduce the wear rate. However, concerning this case is equipped with “degradation” as an objective function, it still leads to more than expected capacity loss compared to the other cases. This is because in this case, the ESS has to increase its operation to store the PV energy to lower the energy consumption of the building. The other cases that incorporate the degradation objective show minimal wear rates with small differences.

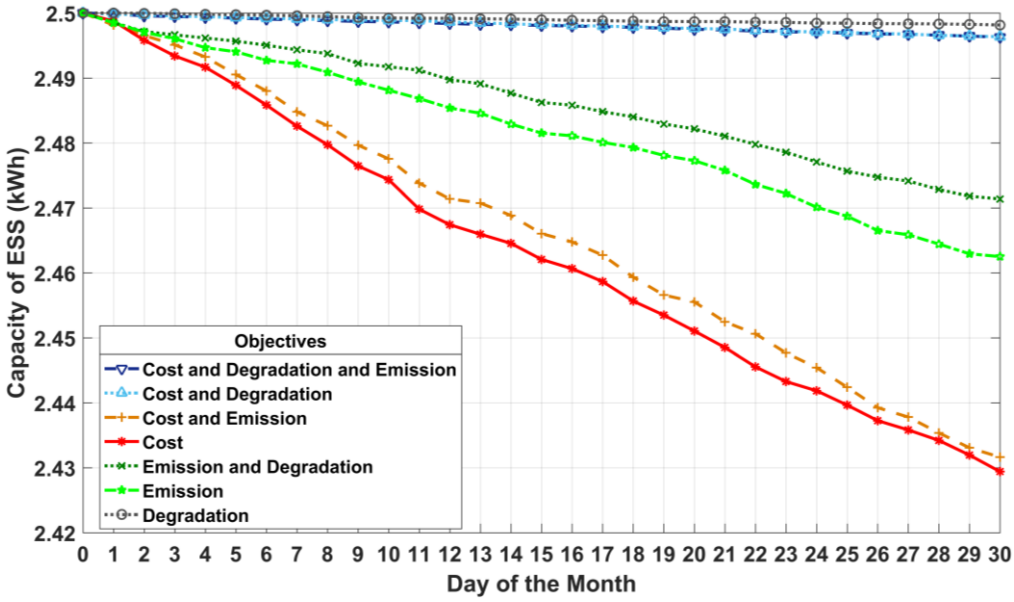

Figure 3.21: Daily capacity loss of ESS for one month, under seven different sets of objective functions

Table 3.3: Capacity loss of ESS for one month

Objective Set	Cost	Cost & Deg	Cost & Emission	Cost & Emission & Deg	Emission	Deg	Emission & Deg
Monthly Capacity Loss of ESS (kWh)	0.0705	0.00362	0.0683	0.00368	0.0374	0.00185	0.0286

The total capacity loss of EV battery and ESS during a month is plotted in figure 3.22 with their values provided in table 3.4. It shows that among these seven cases, the case that "cost" is the sole objective function leads to the highest capacity loss of batteries. This is due to the fact that batteries are exploited maximally in that case to minimize the net energy expense of the building. The addition of degradation to the objective functions improves the capacity loss due to the more optimal operation of batteries in that case. When emission is the sole objective function, it leads to a moderate amount of degradation as it lowers the energy input of the building. Also, as the degradation objective is added to that it will further lower the battery wear. All the other cases (degradation, cost & degradation, cost & degradation & emission) show a minimal capacity loss as they incorporate degradation into the objective functions. However, the case of "degradation & emission" shows relatively larger battery wear. This could be because of the more frequent activity of ESS in that scenario. These results show the significant impact of the inclusion of battery degradation in the objectives of a problem as it leads to shifting the average SoC of the battery towards the middle of the range and prevents unnecessary cycling of batteries which is not financially efficient.

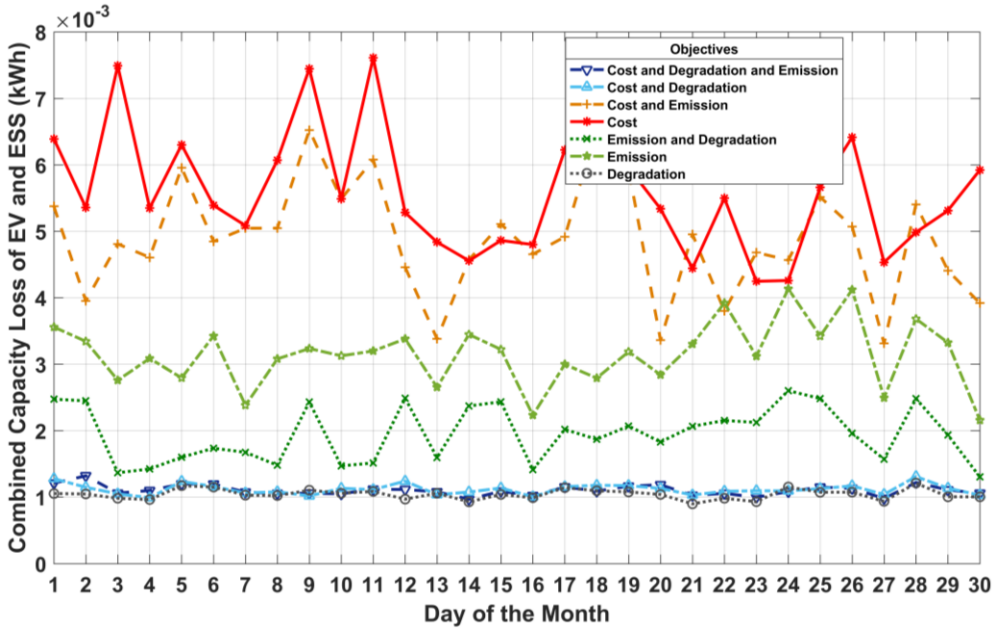

Figure 3.22: Total capacity loss of batteries for one month, under seven different sets of objective functions

Table 3.4: Total capacity loss of batteries for one month

Objective Set	Cost	Cost & Deg	Cost & Emission	Cost & Emission & Deg	Emission	Deg	Emission & Deg
Total Monthly Capacity Loss of EV and ESS (kWh)	0.1672	0.0335	0.1463	0.0331	0.0944	0.0312	0.0584

Once the wear rate or capacity loss of a battery within a period is obtained, the carbon footprint associated with that period can also be calculated. Larger battery wear leads to faster deterioration of the battery and expedites the need for battery replacement. Thus, we expect to see a similar trend for CO2 footprint as we see for degradation of every battery. The total carbon footprint of a user is the sum of apparent emissions caused by energy intake from the grid as well as the carbon footprint associated with the degradation of batteries. Figure 3.23 and Table 3.5 illustrate the total carbon

footprint of the user over the sample month. It is seen that maximum carbon emission is caused by the basic or conventional objective function where cost is the only factor to be minimized. As anticipated, with the inclusion of the emission objective, the emission is notably decreased. However, the incorporation of emission itself is not able to decrease emissions as much as a degradation objective does. This shows the large impact of battery degradation on the carbon footprint even compared to the emission associated with energy consumption. However, the case that considers minimizing the sole degradation leads to mediocre amounts of emission as it omits the consumption-led emission. Emission itself as a sole objective leads to relatively low wear rates, but when it is stacked with degradation it leads to considerably low emission rates. In conclusion, in order to minimize the real carbon footprint of the building, we need to minimize both degradation and apparent emission simultaneously.

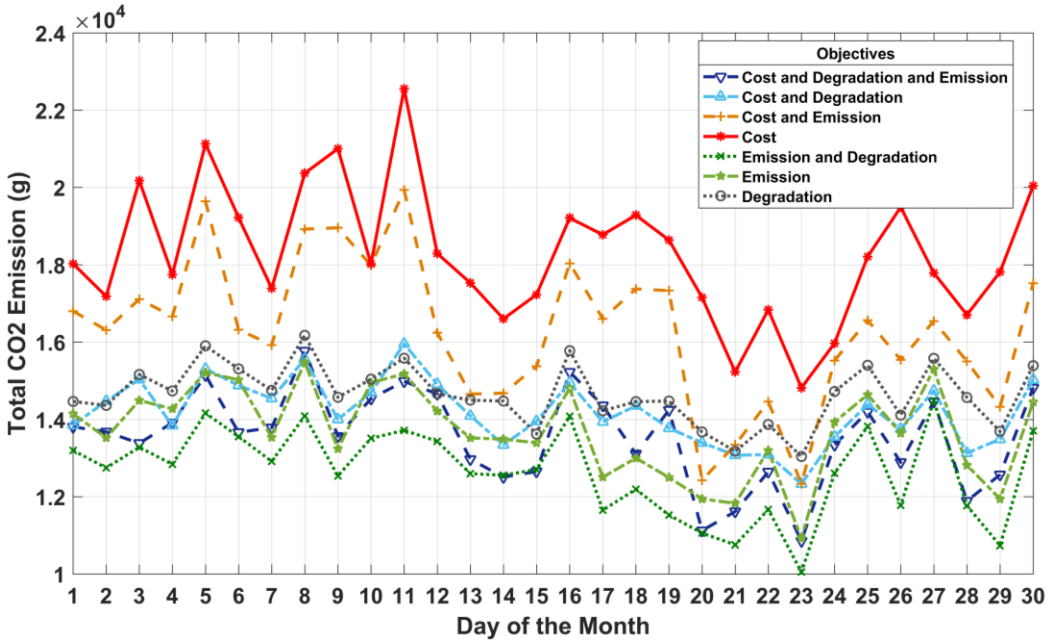

Figure 3.23: Daily carbon footprint for one month, under seven different sets of objective functions

Table 3.5: Carbon footprint of home for one month

Objective Set	Cost	Cost & Deg	Cost & Emission	Cost & Emission & Deg	Emission	Deg	Emission & Deg
Total CO2 Emission of the User (g CO2)	548.4	425.3	488.9	406.3	411.0	439.4	379.6

The peak power of the building is another important factor that was studied for this chapter. Peak power is a proper index to measure the amount of stress that a unit causes for the power grid. Larger peak power values cause more stress on the grid and particularly transformers and could adversely impact the lifetime of the grid infrastructure and increase the costs and carbon footprint on a broader scale. Although the impact of the home peak power on the lifetime and carbon footprint of grid equipment is out of the scope of this work, the average monthly peak power of the unit has been observed as a helpful index for evaluating different objective functions. The results which are depicted in figure 3.24 and table 3.6 show that the basic case again led to the highest and worst results which could have the most detrimental effect on the grid. If other objectives such as emission, degradation, or both are added to the model, however, the average peak power is reduced. This stems from lower power intake of batteries and consequently lower power intake of the building when apparent energy cost is not the only objective of the model. The “Degradation” objective shows the average peak power ranges, and the lowest peak power belongs to the cases where “emission” is set to be minimized. Because in these cases, the building is planned to receive the minimum amount of energy or power from the grid. Considering the large power of typical controllable loads at residential buildings, the timing of their operation is a major factor to impact the peak power of a unit. Those objective sets that schedule the controllable loads to operate at peak times of the day are naturally more likely to experience significant peak powers. These outcomes

demonstrate that the peak power of the home could be lowered by 45% depending on the type of objective function.

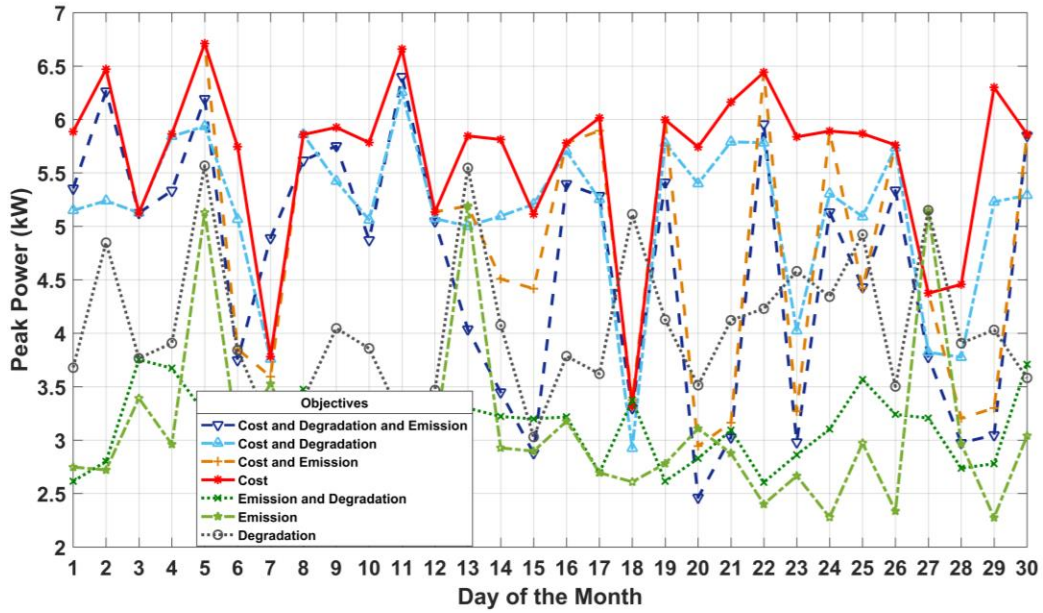

Figure 3.24: Daily peak power of home for one month, under seven different sets of objective functions

Table 3.6: Average daily peak power of home for one month

Objective Set	Cost	Cost & Deg	Cost & Emission	Cost & Emission & Deg	Emission	Deg	Emission & Deg
Average Daily Peak Power of Home (kW)	5.650	5.133	5.021	4.644	3.102	4.062	3.144

A general overview of the discussed results has been provided in the three following charts. Figure 3.25 illustrates the total monthly costs of energy and battery wear corresponding with each objective set. It was demonstrated before that applying cost as the only objective function can minimize the apparent energy costs of the home which could seem appealing. However, in this work, it is shown that not only is cost (as the only objective function) not able to minimize the real

costs associated with an energy system, but also it could largely increase the real costs due to the excessive operation of batteries in this case. In fact, in the seven studied cases, cost as the only objective led to the maximum real cost of $209 over a month. As demonstrated before, the inclusion of other objectives in the MIP model lowers the total price by lowering the wear-associated cost. In this regard, the total monthly cost of "cost & emission" is $187 and for "emission" it is $124. The next costly scenario was "emission & degradation" at $84. The other scenarios that incorporate battery degradation led to minimal total costs due to minimal battery wear rates. In this regard, "degradation", "cost & emission & degradation" and "cost & degradation" led to $45.91, $44.06 and $44.09 respectively.

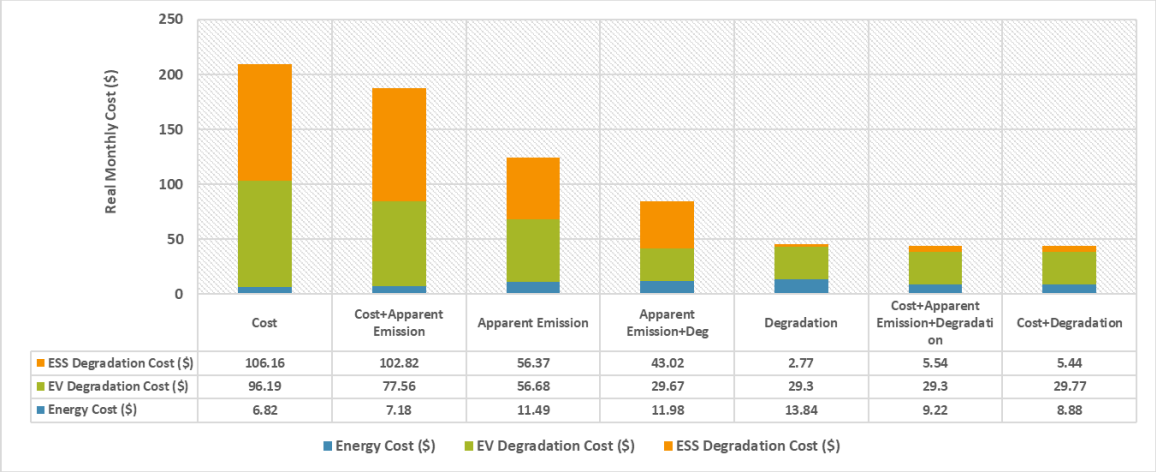

	Cost	Cost+Apparent Emission	Apparent Emission	Apparent Emission+Deg	Degradation	Cost+Apparent Emission+Degradation	Cost+Degradation
ESS Degradation Cost ($)	106.16	102.82	56.37	43.02	2.77	5.54	5.44
EV Degradation Cost ($)	96.19	77.56	56.68	29.67	29.3	29.3	29.77
Energy Cost ($)	6.82	7.18	11.49	11.98	13.84	9.22	8.88

Figure 3.25: Monthly costs of the user, under seven different sets of objective functions

The overview of the battery degradation under the studied scenarios is presented in figure 3.26. This figure clearly shows the impact of the inclusion of battery degradation in lowering the capacity loss of batteries. As before, the basic objective function led to the least favorable results in terms of battery degradation. Including emission as the second objective lowered the capacity loss by 13% as it prevents some of the unnecessary operations of batteries. "Emission" alone leads to even better results as it does not enforce batteries to contribute to monetary profits. Among the scenarios that incorporate battery wear "emission & degradation" led to relatively larger wear rates. This is

because, in that scenario, the ESS has more activity to compensate for the lower energy input from the grid. All the other scenarios that include battery wear as an objective function, cause minimal capacity losses where all of them cause less than 20% wear rate of the basic case. This figure demonstrates that by lowering the unnecessary operation of batteries by employing appropriate objective functions, we can lower the capacity loss of batteries to a large extent.

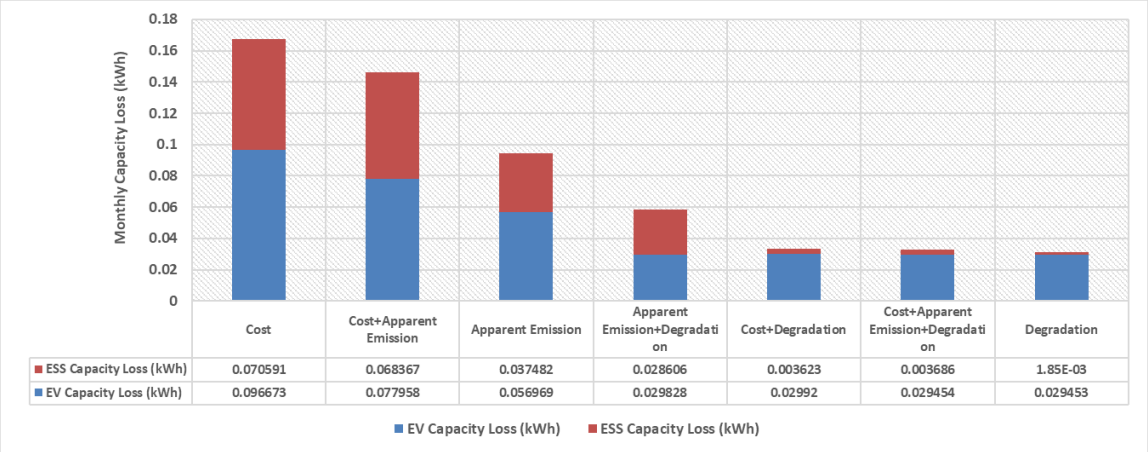

Figure 3.26: Monthly capacity loss of EV and ESS batteries, under seven different sets of objective functions

Carbon footprint is the last parameter to be reviewed in this section and its bar chart is depicted in figure 3.27. Again, mere "cost" showed to be the worst possible objective function as it leads to unjustified and unnecessary battery activities to gain the maximum apparent benefits. This case led to a staggering amount of emissions (548 kg) in one month. The rest of the scenarios which tried to improve this in a way managed to lower the total carbon footprint by lowering the battery degradation, apparent emission, or both of them. In this regard, "cost & emission" led to an 11% decrease in carbon footprint as it lowered energy consumption. In general, the incorporation of battery wear and emission in objective functions caused a 56% and 14% reduction in total emissions respectively. It simply shows the significant impact of battery health on the environmental impact of a home. One interesting outcome of this research is that even when battery wear is not taken into consideration, only by adding emission to the cost as a second objective function, the emission was lowered by around 11% while the real cost was also reduced by 10% and the apparent cost was

increased by only 5%. Finally, table 3.7 provides a review of the total monthly values of cost, emission, and capacity loss for the studied home.

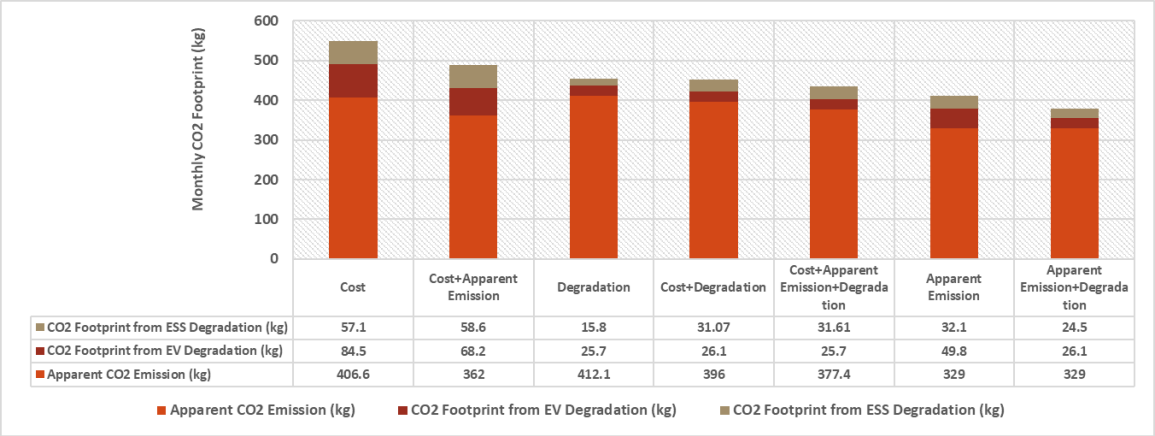

Figure 3.27: Monthly carbon footprint associated with battery wear and energy consumption, under seven different sets of objective functions

Table 3.7: Total monthly cost, carbon footprint, and capacity loss of batteries

Objective Set	Cost	Cost & Deg	Cost & Emission	Cost & Emission & Deg	Emission	Deg	Emission & Deg
Total Monthly Cost of the Home ($)	209.17	44.09	187.56	44.06	124.54	45.91	84.67
Total Carbon Footprint of the Home(kg)	548.2	453.17	488.8	434.7	410.9	453.6	379.6
Total Capacity Loss of Batteries (kWh)	0.167264	0.033543	0.146325	0.03314	0.094451	0.031303	0.058434

One important advantage of incorporating the battery degradation model is the fact that it can provide the user with realistic estimations of the UC outcomes. Different users have different

priorities concerning running their power systems. Some users may give priority to lowering the total cost or even the apparent energy cost while some others may have environmental concerns and prefer to shrink their carbon footprint. In a UC problem, cost and emission objectives could contradict and compete with each other. Hence, once a sophisticated UC model is implemented for a power system, the user should be given enough information and freedom to determine what objectives they want to achieve by using the energy management system. Preferably, the users should be informed of all the monetary costs and emissions caused by every set of objective functions. Moreover, they should be aware of the extent of compromises that they could make in terms of costs to lower their carbon footprint. In this case, they will be able to make their desirable choices for employing unit commitment objectives. As a matter of fact, depending on different factors such as the *N(D)* curve of batteries, initial and salvage prices of batteries, energy tariffs, and battery's state-of-health (SoH) at the time of replacement, different objectives may seem more appealing to the users. In some cases, the user might be able to significantly lower their carbon footprint by a very small compromise (increase) in their cost. Lack of this information could avoid many users from saving a lot of unnecessary carbon emissions. Hence, in this work, it is studied how cost and emission objectives compete in the UC model of a home microgrid. To do this, the contribution of emission to the objective set of "Cost & Degradation & Emission" was tuned by varying its corresponding weight (denoted with *W*, where, $0<W<1$) parameter with a step of 4% in the objective function. The weight tuning capability was offered by the used solver program. Figure 3.28 shows the results of this practice with their Pareto front showing the best results in terms of cost and emission. It is worth noting that in the state of Pareto optimal, none of the objective functions can be improved without deteriorating other objectives [21]. This graph shows how the model objectives compete, also it helps to find the user's desirable outcome in terms of cost and emission through fine-tuning of *W*. For example, in the case under study, it is possible to reduce the CO2 footprint by 13.5% (1.91 kg) per day with only 18 cents increase in the apparent cost, while the total cost shows even no notable changes. If we compare this with the basic case, the

results will be more dramatic since the decrease in emissions will be 16.4% (2.4 kg). In a practical scenario, such information could help users to cut their emissions at a possibly low extra cost [120].

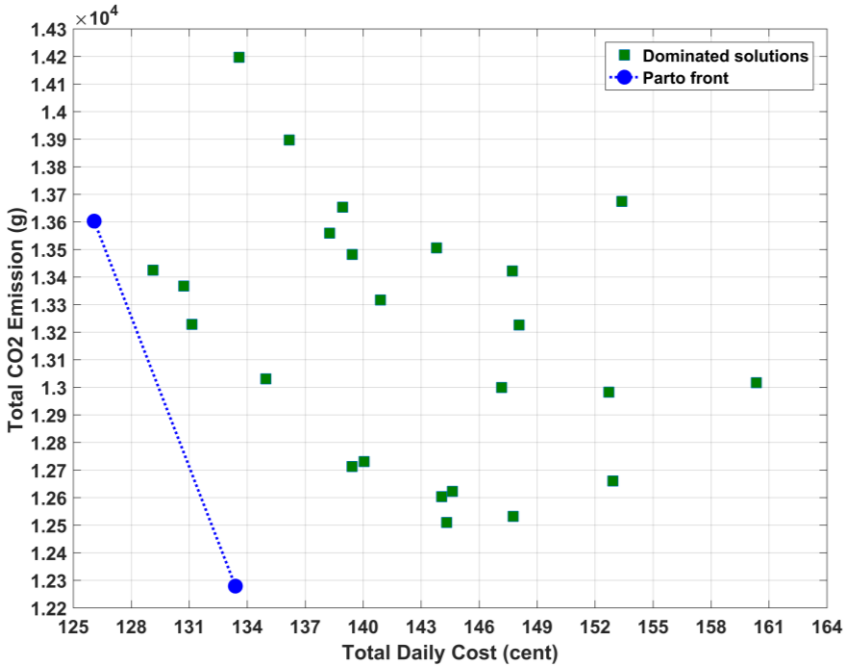

Figure 3.28: Pareto front of cost and emission objectives

Chapter 4: Impact of the granularity of the MIP model on the battery degradation

4.1 Modelling the intra-hourly MIP UC problem for residential microgrid

Granularity or model resolution is a considerable factor in UC problems which could impact the efficiency of the system. In simple words, the resolution determines the frequency of unit commitment in a power system. Most of the time, the model resolution relies on external factors and particularly the frequency of energy tariff variations or possibly the smallest resolution among the input datasets (tariffs, renewable energy generation, load, etc.). For instance, for day-ahead markets with one-hour price resolution, the UC model is normally built with hourly resolution. However, when it comes to the unit commitment in the intra-hourly markets where prices change on an intra-hourly basis (30 minutes, 15 minutes, etc.), one important question is whether dispatching the batteries at pace with the market's price variations is efficient with regards to the battery's health. It is of notable concern that dispatching the battery with high frequency in an intra-hourly market to extract the maximum energy yield, could lead to excessive degradation that could exceed any potential financial profits. To address this matter and in order to investigate the impact of the model granularity on the capacity loss of batteries in the studied microgrid, a dual-stage UC algorithm has been proposed in this chapter in the context of mixed-integer programming. To build this model, it was assumed that the user has access to the energy tariffs every day in hourly resolution from the day before. Also, it was assumed that the load profile and photovoltaic generation profile (via solar irradiance prediction) are accessible from the previous day. It is worth mentioning that the day-ahead tariffs, solar irradiance, and load profile could be obtained in different ways (e.g., using historical data, carrying out a prediction, or receiving from a third party). However, the process of data procurement is out of the scope of this work. Thus, in the first stage of the UC algorithm, a day-ahead UC problem including the wear model is produced with one-hour

granularity and solved similar to what was presented in the previous chapter. Once the day-ahead optimization has been solved, it provides the estimated power schedule, SoE and SoC profile of EV and ESS batteries for the next day which includes 24 intervals. However, to produce a UC model with an intra-hourly resolution we need to consider two facts. First of all, high precision intra-hourly data for grid tariffs are usually provided in the hour-ahead market where the energy prices of every hour are set around one hour earlier after the operator has received all the bids from different producers. Also, regarding the intermittency of solar energy which largely depends on the weather condition, relatively precise irradiance predictions with intra-hourly resolution would not be available from a day before and it needs to be acquired shortly (e.g., one hour) before any given period. In this regard, the optimization process with intra-hourly granularity should be carried out in an hour-ahead fashion to have a decent level of precision. Needless the mention that the intent of performing optimization with intra-hourly granularity is achieving the maximum possible profits and efficiency due to employing the system optimally in the shortest accessible periods. Secondly, when it comes to hour-ahead optimization, we should notice that carrying out optimization on an hourly basis without considering their results on the daily horizon could lead to suboptimal results. For example, the EV battery needs to reach a certain level of SoC by the time of departure and this requirement can be addressed in the scheduling algorithm. In this regard, in the second stage of the proposed dual-stage UC algorithm, another MIP model is produced; this time with intra-hourly resolution. This model needs to be solved for every hour using the high-precision intra-hourly energy prices, load, and solar irradiance for the coming hour. This time, the initial and final SoCs of batteries are constrained to the hourly SoC values obtained by the day-ahead optimization stage. In other words, the hour-ahead optimization needs to be carried out 24 times a day, every time with updated intra-hourly input data as well as initial and final SoC values from the first stage. This algorithm can guarantee that the SoC of batteries will track the optimal intra-hourly trends within every hour and EV SoC will reach the desirable levels by the time EV leaves. As mentioned before, the first stage is exactly designed as explained in chapters 2 and 3. However, to build the MIP

model for the intra-hourly simulation (second stage) it should be pointed out that although intra-hourly constraints are mostly similar to the hourly constraints, there are some exceptions as explained below. Regarding the ESS constraints, (4.1) needs to be added to the set of ESS constraints for the intra-hourly case. This equation enforces the final state of energy of ESS for every interval which is obtained from the primary day-ahead optimization.

$$SE_{es}^{n} = SE_{es}^{end} \qquad for\ n = n_e \tag{4.1}$$

In this equation SE_{es}^{end} denotes the expected SoE of the ESS at the end of the optimization horizon.

The EV constraints in hour-ahead optimization have different ranges from the day-ahead optimization. This is due to the fact that in day-ahead optimization the EV is present at home during a portion of the entire optimization horizon. However, in the hour-ahead case, every time optimization action is carried out the EV is either considered present during the entire optimization horizon or is entirely absent. Moreover, a new constraint as in (4.9) is added to the set of EV constraints to limit the final SoE of the EV battery at every hour to the value specified primarily by the hour-ahead optimization attempt. In this regard, the EV constraints for those hours that EV is parked at home is laid out as follows.

$$P_{ev}^{n,con} + P_{ev}^{n,ex} = P_{ev}^{n,dis} \times \eta_{ev}^{dis} \qquad \forall n \in N \tag{4.2}$$

$$P_{ev}^{n,ch} \leq U_{ev}^{n} \times P_{ev}^{ch} \qquad \forall n \in N \tag{4.3}$$

$$P_{ev}^{n,dis} \leq (1 - U_{ev}^{n}) \times P_{ev}^{dis} \qquad \forall n \in N \tag{4.4}$$

$$SE_{ev}^{n} = SE_{ev}^{n-1} + \left(\eta_{ev}^{ch} \times P_{ev}^{n-1,ch} \times G\right) - \left(P_{ev}^{n-1,dis} \times G\right) \qquad \forall n \in [n_b + 1, n_e + 1] \tag{4.5}$$

$$SE_{ev}^{n} = SE_{ev}^{ini} \qquad for\ n = n_b \tag{4.6}$$

$$SE_{ev}^{n} \leq SE_{ev}^{max} \qquad \forall m \in [n_b, n_e + 1] \tag{4.7}$$

$$SE_{ev}^{n} \geq SE_{ev}^{min} \qquad \forall m \in [n_b, n_e + 1] \tag{4.8}$$

$$SE_{ev}^{n} = SE_{ev}^{end} \qquad for\ n = n_e \tag{4.9}$$

Where, SE_{ev}^{end} is the expected SoE of the EV battery at the end of the optimization horizon. However, for those hours that EV is not parked at home, all of its associated power variables are set to zero as in (2.47). Consequently, the wear constraints of EV for the intra-hourly scheduling have different ranges as presented below.

$$SC_{ev}^{n} = \frac{SE_{ev}^{n}}{E_{ev}^{n}} \qquad \forall m \in [n_b, n_e + 1] \tag{4.10}$$

$$D_{ev}^{n} = 1 - SC_{ev}^{n} \quad \forall n \in [n_b, n_e + 1] \tag{4.11}$$

$$W_{ev}^{n} = f(D_{ev}^{n}) = \frac{1}{D_{ev}^{n}}\left(1 - R_{ev}^{\frac{1}{\alpha e^{\beta(D_{ev}^{n})}}}\right) \approx a_2(D_{ev}^{n})^2 + b_2(D_{ev}^{n}) + c_2 \qquad \forall m \in [n_b, n_e + 1] \tag{4.12}$$

$$\Delta E_{ev}^{n} = E_{ev}^{opt} \times [W_{ev}^{n} \times D_{ev}^{n} - W_{ev}^{n+1} \times D_{ev}^{n+1}] \qquad \forall n \in N \tag{4.13}$$

$$\mathrm{L}_{ev}^{n} = |\Delta E_{ev}^{n}| \qquad \forall \mathrm{n} \in N \tag{4.14}$$

Now, a case study is carried out to investigate how the hour-ahead intra-hourly battery scheduling can impact the capacity loss of batteries in comparison with the conventional day-ahead hourly scheduling in 24 hours. To do this, the same setup that was used in chapters 2 and 3 was employed for this case study except for controllable load. For this case study, the input data (irradiance, tariffs, and load) needed to be available in hourly and intra-hourly resolutions. In this regard, the solar irradiance data in hourly and 5-minute resolutions was acquired from [137], and the load profiles in hourly and 5-minute resolutions were obtained from [138]. Moreover, the energy tariffs with these two resolutions were derived from [101]. The feed-in energy prices were assumed to be 0.8 of those of buying tariffs in the same hourly or intra-hourly intervals. The EV's availability at home is considered to be between 6 PM and 8 AM. The proposed UC strategies that are laid out in the

context of mixed-integer programming models written in Python and solved by Gurobi are then tested for this case study and the results are provided in the following. Figure 4.1 illustrates the algorithm of the dual-stage intra-hourly UC model which was explained in this section and Table 4.1 lists the input parameters of the case study provided in this chapter.

Algorithm -2 Unit Commitment Algorithm for Smart Home-Intra-hourly Time Resolution

1: Updating or calculating model parameters and data including departure and arrival times of EV, initial and final SoCs of EV, initial and salvage prices and current capacities of EV and ESS batteries, day-ahead PV generation, energy tariffs and load profile for the next 24 hours with hourly time granularity.
2: Updating the $N(D)$ for EV battery and ESS according to their power ratings.
3: Calculating the $W(D)$ function and performing curve fitting on it to make it implementable as a model constraint in the used mathematical solver.
4: **procedure** "PRODUCING THE MIXED-INTEGER PROGRAMMING MODEL WHICH INCLUDES THE FOLLOWING COMPONENTS AND PERFORMING THE OPTIMIZATION FOR THE NEXT 24 HOURS"
5: General constraints of the model including EV, ESS and PV
6: Battery Degradation constraints for EV and ESS
7: Objective functions for minimizing cost, degradation and emission or combinations of them
8: Obtaining the SoC arrays of EV battery and ESS for the next 24 hours
9: **procedure** "OPTIMIZING THE MIP MODEL WITH INTRA-HOURLY GRANULARITY PRIOR TO EVERY SINGLE HOUR FOR THE COMING HOUR DURING THE TARGET DAY, MAKING IT 24 OPTIMIZATION ITERATIONS FOR 24 TIME INTERVALS. EVERY OPTIMIZATION ITERATION IS COMPOSED OF THE FOLLOWING STEPS: "
10: Updating the PV generation forecast, energy tariffs and load profile for the next hour with intra-hourly time granularity.
11: Enforcing the initial and final SoCs of EV battery and ESS in that particular interval according to the SoCs obtained previously from the day-ahead optimization.
12: General constraints of the model including EV, ESS and PV
13: Battery Degradation constraints for EV and ESS
14: Objective functions for minimizing cost, degradation and emission or combinations of them
15: Obtaining the intra-hourly control variables of EV power, ESS power, as well as state variables of SoC arrays, battery degradation values, consumed energy and costs for the next hour from the solved intra-hourly problem.
16: Calculating the battery degradation for the scenarios that neglect degradation by applying the wear model to the obtained SoC arrays of EV and ESS.
17: Calculating the carbon footprint caused by energy consumption and battery wear.

Figure 4.1: Dual-stage UC algorithm for a residential microgrid built in the framework of MIP with intra-hourly resolution

Table 4.1: Input parameters of the case study of chapter 4

Input Parameter	Value
$\boldsymbol{\eta_{es}^{ch}/\eta_{ev}^{ch}}$	100%/100%
$\boldsymbol{\eta_{es}^{dis}/\eta_{ev}^{dis}}$	100%/100%
$\boldsymbol{P_{es}^{ch}/P_{ev}^{ch}}$	0.75kW/1.75kW
$\boldsymbol{P_{es}^{dis}/P_{ev}^{dis}}$	0.75kW/1.75kW
$\boldsymbol{G}$	1 hour/$\frac{1}{12}$ hour
$\boldsymbol{SE_{es}^{ini}/SE_{ev}^{ini}}$	1.25kWh/11kWh
$\boldsymbol{SE_{es}^{max}/SE_{ev}^{max}}$	2.375kWh/22kWh
$\boldsymbol{SE_{es}^{min}/SE_{ev}^{min}}$	0.125kWh/1.1kWh
$\boldsymbol{SE_{ev}^{ch}}$	20.9kWh
$\boldsymbol{\eta_{pv}}$	100%
$\boldsymbol{P_{im}^{max}}$	10kW
$\boldsymbol{P_{ex}^{max}}$	10kW
$\boldsymbol{E_{es}^{ini}/E_{ev}^{ini}}$	2.5kWh/22kWh
$\boldsymbol{V_{es}^{ini}/V_{ev}^{ini}}$	\$2005/\$5500
$\boldsymbol{V_{es}^{sal}/V_{ev}^{sal}}$	\$125/\$1122
$\boldsymbol{R_{es}/R_{ev}}$	0.5/0.8

Figure 4.2 shows the load power and energy price (buy) graphs for the studied day. These datasets are provided in both hourly and intra-hourly (5-minute) resolutions which are needed for their respective optimization attempts.

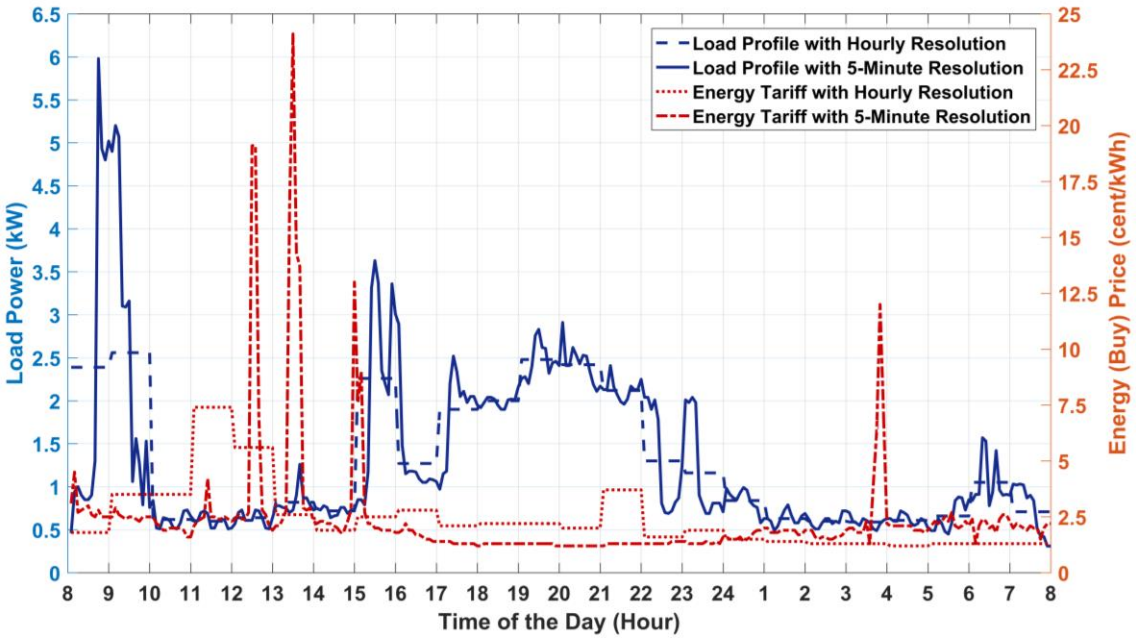

Figure 4.2: Load power and energy price profiles with hourly and 5-minute resolutions for the case study of chapter 4

The estimated SoC trend of ESS when it is scheduled by a day-ahead model with an hourly granularity and also when it is scheduled by an hour-ahead model with a 5-minute granularity are depicted in figure 4.3. These graphs show that ignoring the battery wear in the UC model could lead to an intense charging/discharging regime where the battery is cycled with large depth-of-discharge levels from and to extreme state-of-charge levels. Whereas incorporation of the proposed battery wear model caused the SoC of the battery to avoid going towards the extremes to a large extent. As a matter of fact, the UC model which is equipped with the wear model is able to recognize whether charging or discharging the battery to the extreme SoCs is worth it financially with regards to the cost of energy and battery wear. It can also be seen that when battery wear is neglected, the hour-ahead SoC tends to follow its day-ahead trend. However, the inclusion of battery wear makes the battery power and consequently SoC fluctuate constantly around the day-ahead optimization outcomes to achieve the optimal results. The SoC fluctuation domain for the intra-hourly cases directly depends on the variance of intra-hourly input data with respect to the hourly data.

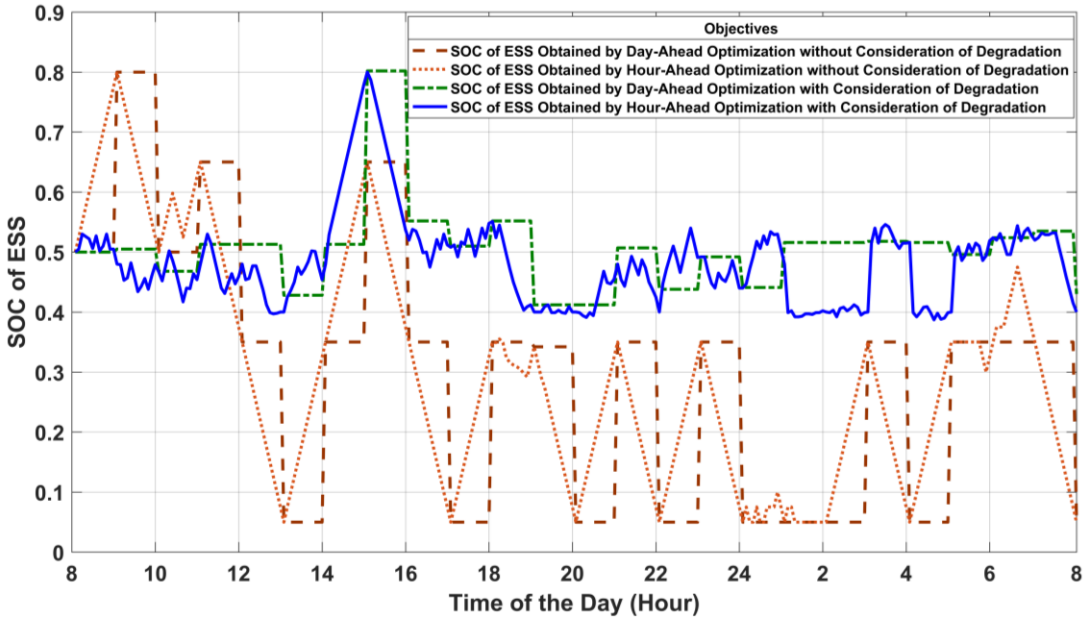

Figure 4.3: SoC variations of ESS for one day, resulted from hourly and intra-hourly battery scheduling with and without consideration of degradation

The trend and rates of capacity loss associated with the operation of ESS are presented in figure 4.4 and table 4.2 respectively. According to the employed battery wear model, it was expected that the capacity loss of a cycled battery would depend on two factors. The DoD of charging/discharging attempt and the initial and final SoCs of every cycle/half cycle. The degradation results for the ESS also prove that idea, as small SoC fluctuations which correspond with small DoDs lead to small degradation rates, especially if they are located in the mid-range. No SoC variation corresponds with no charging or discharging events which lead to no capacity loss. However, larger SoC variations (larger DoDs) lead to larger wear rates, especially if they lead to extreme rates of SoCs. The results show that for both cases that consider and ignore battery wear, capacity loss caused by intra-hourly optimization almost tracks a similar trend as in hourly optimization. It shows that the energy storage system lost up to more than half a Watt-hour capacity per hour as a result of ignoring the battery wear. While considering the wear in the problem could keep the maximum hourly capacity loss under 10% of that. The close similarity of the wear trends in hourly and intra-hourly

simulations especially when battery wear is not addressed in the model is because SoC in the intra-hourly case follows a similar trend as in the hourly case.

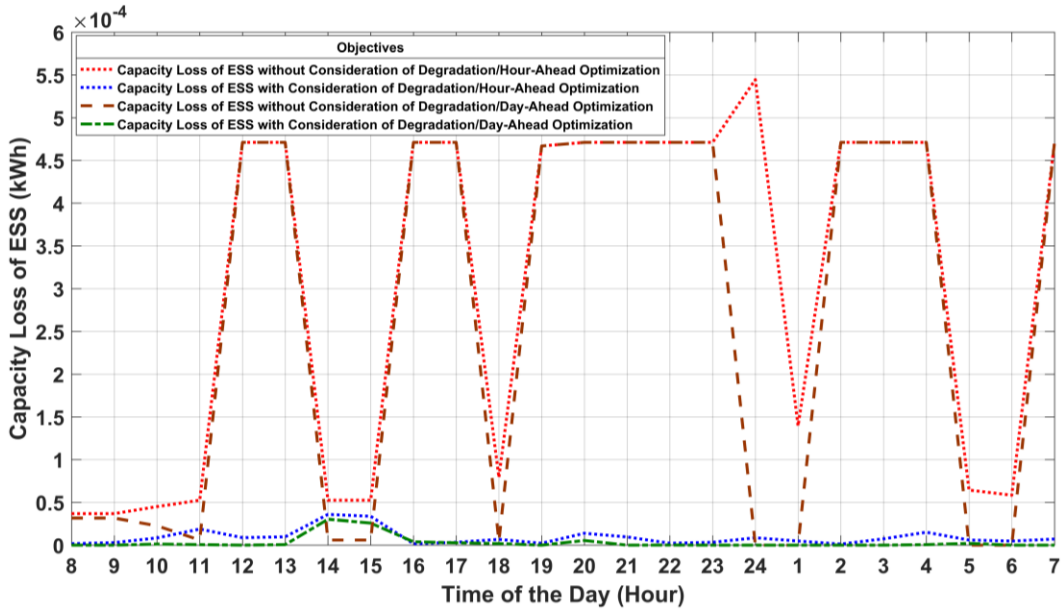

Figure 4.4: Capacity loss of ESS for one day, resulted from hourly and intra-hourly battery scheduling with and without consideration of degradation

Table 4.2: Impact of granularity and consideration of battery degradation on the capacity loss of ESS over one day

Optimization Horizon	Optimization Granularity	Employed Degradation Method	Capacity loss of ESS (kWh)
Day-ahead	1 hour	None	0.00622
Day-ahead	1 hour	DoD-associated wear from irregular cycling	0.00007
Hour-ahead	1 hour / 5 minutes	None	0.00728
Hour-ahead	1 hour / 5 minutes	DoD-associated wear from irregular cycling	0.000218

The SoC trends for the EV battery under the four simulated scenarios have been illustrated in figure 4.5. In these cases, we can see that a basic objective function that merely aims at minimizing the apparent energy cost leads to discharging attempts to SoCs under 20% for both hourly and intra-

hourly cases with minimal differences between the two. As a matter of fact, in a real-life scenario where battery wear is not studied, the differences in SoC trends in day-ahead and hour-ahead optimizations solely stem from the deviations of the hour-ahead predictions of solar irradiance, load profile, and energy tariffs from their day-ahead predictions. After integrating battery wear into the model, the battery avoids what the algorithm considers as “unnecessary discharging” which causes unjustified capacity losses. As a result, the state of charge of the battery varies around the mid-range almost half of the day. Also, the SoC amounts in the hour-ahead optimization do not follow the exact trend of the day-ahead optimization. This is since hour-ahead optimization with intra-hourly resolution and updated input data might show that decision of day-ahead optimization for cycling the battery within every hour is not necessarily optimal. To conclude, apart from lowering the capacity fade of batteries, incorporating the battery degradation into the UC model also leads to the maximum employment and involvement of batteries in an optimal fashion. Whereas neglecting it leads to sub-optimal employment of battery capacity, especially in models with intra-hourly resolution.

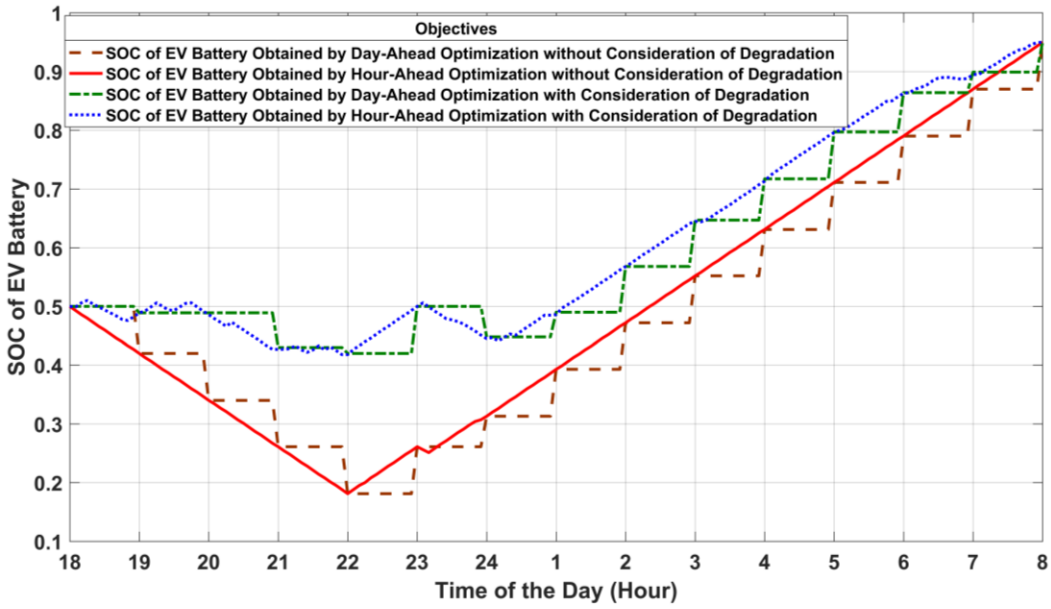

Figure 4.5: SoC variations of EV battery for one day, resulted from hourly and intra-hourly battery scheduling with and without consideration of degradation

The trends and magnitudes of capacity loss associated with the operation of the EV battery are provided in figure 4.6 and table 4.3 respectively. According to these results, the capacity fade of EV battery when battery degradation is neglected could surpass 0.9 Wh in an hour due to deep discharging events. The maximum wear rate occurs when the battery is being discharged at the lowest SoC. Avoiding unnecessary discharging attempts when the energy management algorithm addresses the wear rate leads to significantly lower amounts of capacity loss (under 0.1 Wh/hour) in the first hours of the EV's stay. Nevertheless, within the last seven hours that EV is parked at home, due to the necessary charging attempts, the capacity loss rises for all the cases.

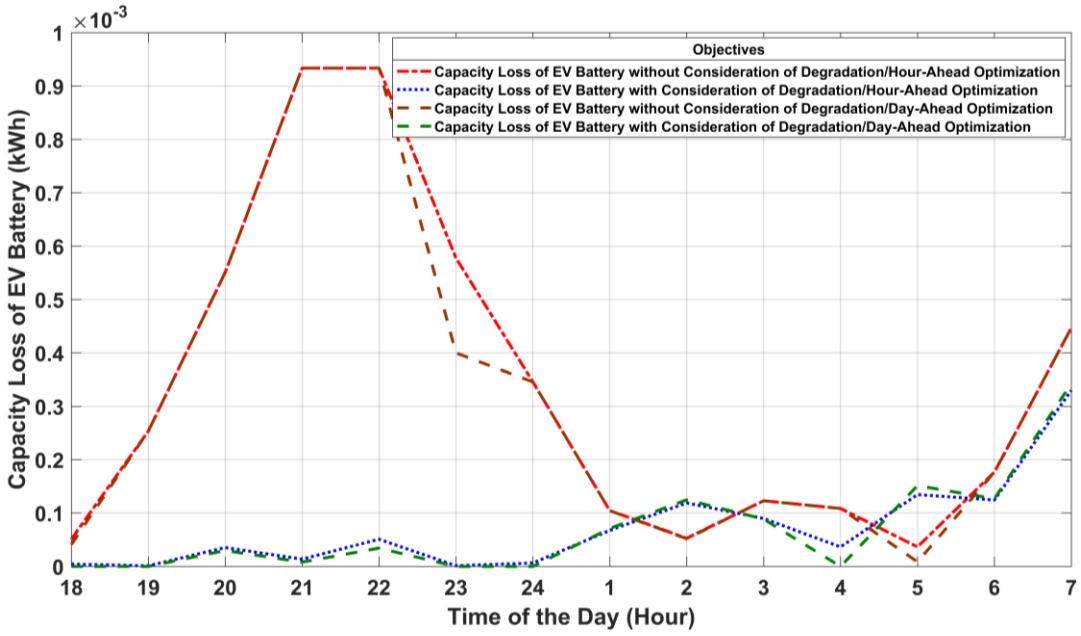

Figure 4.6: Capacity loss of EV battery for one day, resulting from hourly and intra-hourly battery scheduling with and without consideration of degradation

Table 4.3: Impact of granularity and consideration of battery degradation on the capacity loss of EV battery over one day

Optimization Horizon	Optimization Granularity	Employed Degradation Method	Capacity loss of EV Battery (kWh)
Day-ahead	1 hour	None	0.00526
Day-ahead	1 hour	DoD-associated wear from irregular cycling	0.00097
Hour-ahead	1 hour / 5 minutes	None	0.00469
Hour-ahead	1 hour / 5 minutes	DoD-associated wear from irregular cycling	0.00101

Finally, the peak power of the home is provided in figure 4.7 as an index for the home's impact on the grid under the different studied scenarios. In this graph, negative values represent the power drawn from the grid and positive values represent the power delivered to the grid. During most of the morning time, due to the abundance of solar generation, power is delivered to the grid in all the scenarios. However, the daily peak power takes place at the time of load peak around 9 AM.

Although studying the peak power for a single day would not be sufficient to make a certain conclusion about the impact of the model structure on the peak power and also the differences between the peak of the day are small among the cases, however, the two cases that have hourly resolution led to the larger peak power compared to the intra-hourly cases.

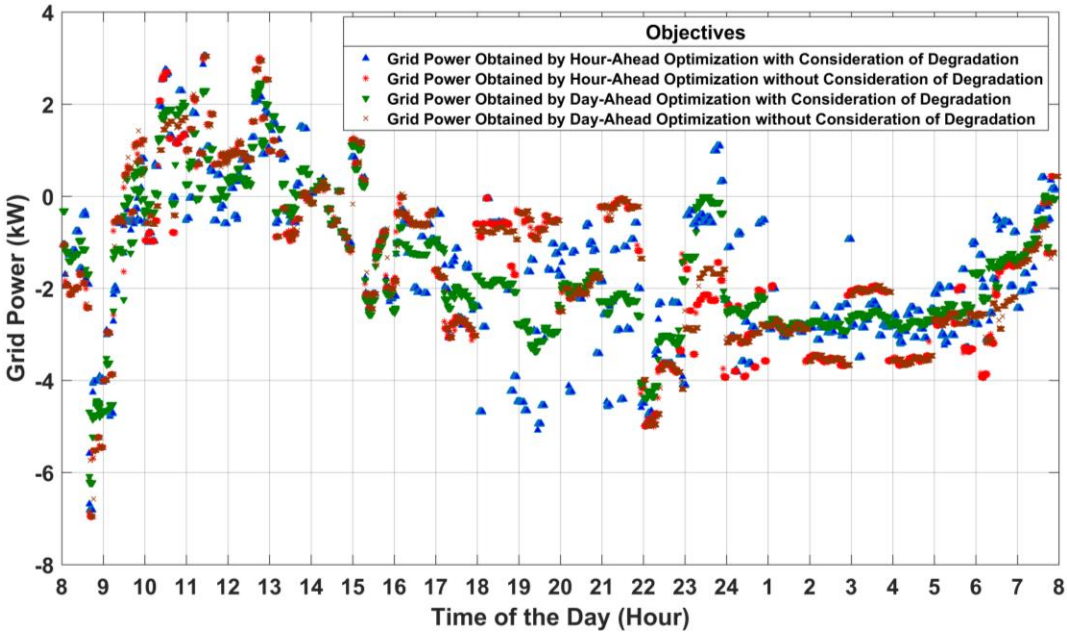

Figure 4.7: Peak power of home for one day, resulted from hourly and intra-hourly battery scheduling with and without consideration of degradation

Now that the UC model has been solved with hourly and intra-hourly resolutions, it should be mentioned that the results of battery degradation especially for the intra-hourly simulation may suffer from a lack of high accuracy due to different reasons. First and foremost, as explained in chapter 3, the wear model which is incorporated into the MIP UC problem is a simplified version of a more complicated model which was represented in equations (3.20) to (3.23). The simplification was done to reduce the nonlinearity of wear equations so they can be implemented by a typical commercial MIP solver. This simplification comes with a price which is deteriorating the precision of the wear model when it is incorporated into the MIP model. Moreover, when solving a UC problem equipped with the battery wear model for short terms and using the real data, some of the parameters such as wear coefficients and capacity loss in short periods could become

so small relative to the size of the battery capacity. This could cause difficulties for a typical mathematical solver to solve the model and lead to producing inaccurate results or numerical flaws and inconsistencies. In this regard, proper configuration of mathematical solver would be an important step in obtaining reliable results. However, solvers may not be able to handle very small values (e.g., $<10^{-5}$) in a MIP problem. In these cases, it could possibly be helpful to scale up the entire variables and parameters and scale them down again after the solutions have been produced. However, regardless of the inaccuracies of a simplified incorporated degradation model in estimating the degradation of batteries throughout cycling procedures, this work has demonstrated how effective the proposed wear model could be in reducing the capacity loss and saving cost and carbon emission. Nevertheless, after the UC problem has been solved and the charging/discharging power of batteries has been produced, the capacity loss of batteries can be calculated with higher precision by applying the original wear model to the SoC trend of batteries. In this case, as the calculations could be done in an offline fashion separate from the main MIP model, the original highly nonlinear wear model could be applied to the SoC variations to find the predicted capacity losses with better accuracy. This trend could also be applied in a real-time testing scenario, where batteries are first scheduled by a MIP unit commitment model, and then operated in real-time according to their produced schedule. Then, during the operation of batteries, the capacity losses could be calculated by applying the original wear model which could be implemented and run in the same simulation platform.

4.2 A controller-hardware-in-the-loop approach to investigate the battery degradation

In the previous chapters, the simulations were carried out in an offline fashion using a MIP solver, where the model is optimized, and it provides different control and state variables including the battery power schedule for the next day as well as the battery wear estimations. However, to test the presented unit commitment and battery wear models in real-time and under operational

conditions, a hardware-in-the-loop simulation setup was developed for this work in the Laboratory of Control Systems and Mechatronics of Saint Mary's University. The developed system is a controller-HIL (C-HIL) setup based on a Typhoon-HIL platform [139] and is comprised of hardware and software components. The software part includes the "Schematic Editor" and the "HIL SCADA" environments which are accessible through the "Typhoon-HIL Control Center" package. The hardware part includes the HIL 402 device, control cards, and an interface card used to provide signal processing between the control cards and the HIL device. Figure 4.8 shows the hardware components of the employed C-HIL testbed.

Figure 4.8: The C-HIL testbed, including the HIL402 device, control cards, and interface boards

The power stage of the system is developed in the Schematic Editor and the control and monitoring stage is developed in the HIL SCADA environment. In this work, EV and ESS are modeled with the Li-ion batteries without any additional battery or thermal management systems, and they are available from the Schematic Editor library. These battery models mimic the electrical

characteristics of real Li-ion batteries such as nominal voltage, capacity, full-charge voltage, nominal discharge current, internal resistance as well as the voltage-SoC curve of the battery. However, this battery model itself does not include any degradation model. The following figure 4.9 demonstrates the schematic of the power stage of the C-HIL model built inside the Schematic Editor.

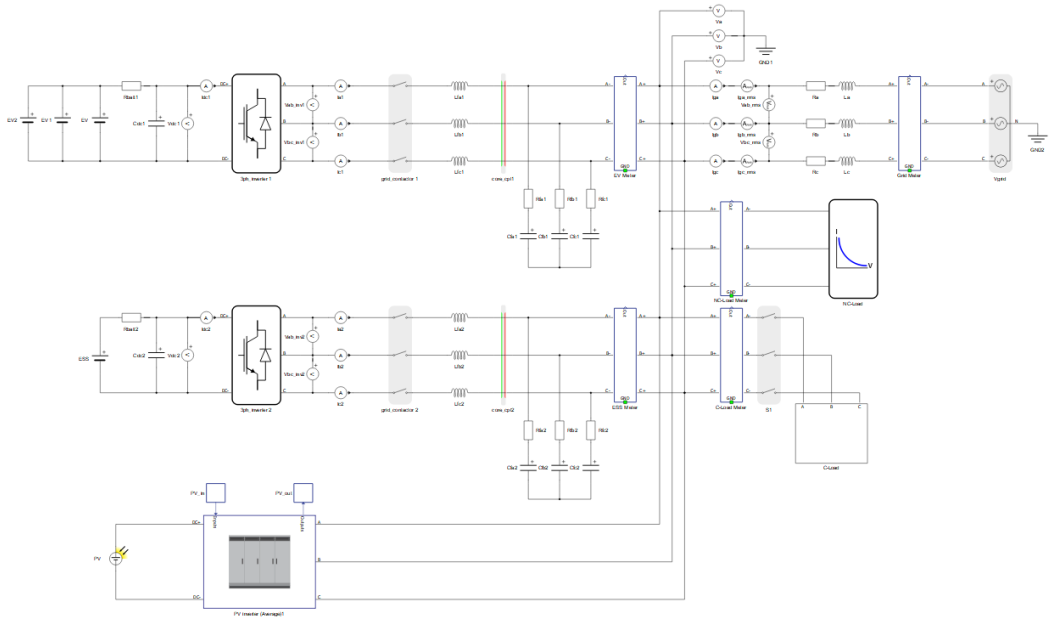

Figure 4.9: Schematic of the power stage of the employed C-HIL setup inside Schematic Editor

With regards to the grid-connected inverters, there are two major types of them used in this platform that are different in control and characteristics. These two types of inverters are “Switch Inverters” which are composed of the real switch models and “Average Inverters” which model the functionality of switch inverters, however without using switches. In order to operate switch inverters, their switches need to be triggered in a controlled way by an internal or external source. In this work, the two inverters that are used for batteries are of switch type and they can provide a bi-directional power flow for charging and discharging batteries. These two inverters are controlled externally by using real control cards that function as the “hardware” part of the simulation in the context of the “hardware-in-the-loop” simulation. This control card provides the PWM signals for

the gates of the six inverter switches. Figure 4.10 shows the schematic of the inverter's power stage as well as the exchanged signals between the battery inverters and their control circuit, and figure 4.11 shows the schematic of the control stage of the battery inverters. The corresponding power reference values are sent to the inverters from EMS by the P^{ref} input.

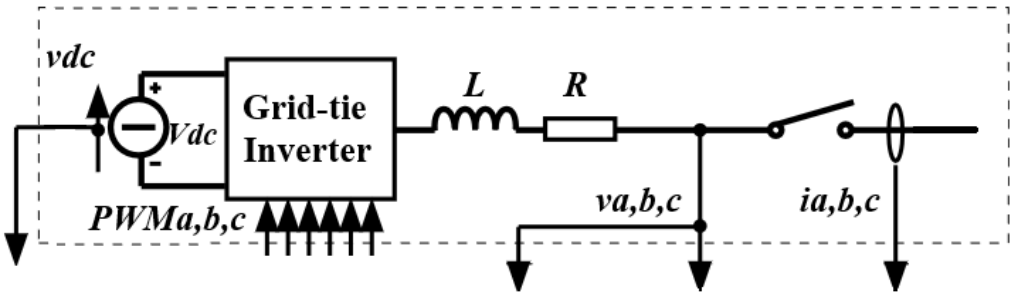

Figure 4.10: Grid-connected battery inverter and its corresponding input and output signals in relation to its local controller [139]

The battery inverters are controlled by a PID-based grid-following control algorithm as shown below. The active and reactive power references are sent to the controller by an upper stage control level (energy management algorithm). It is worth noting that in this work the reactive power control is not taken into consideration and only active power is addressed. As can be seen from this figure 4.11, after calculating the proper trigger signal, the SVPWM module provides the trigger to the switch gates.

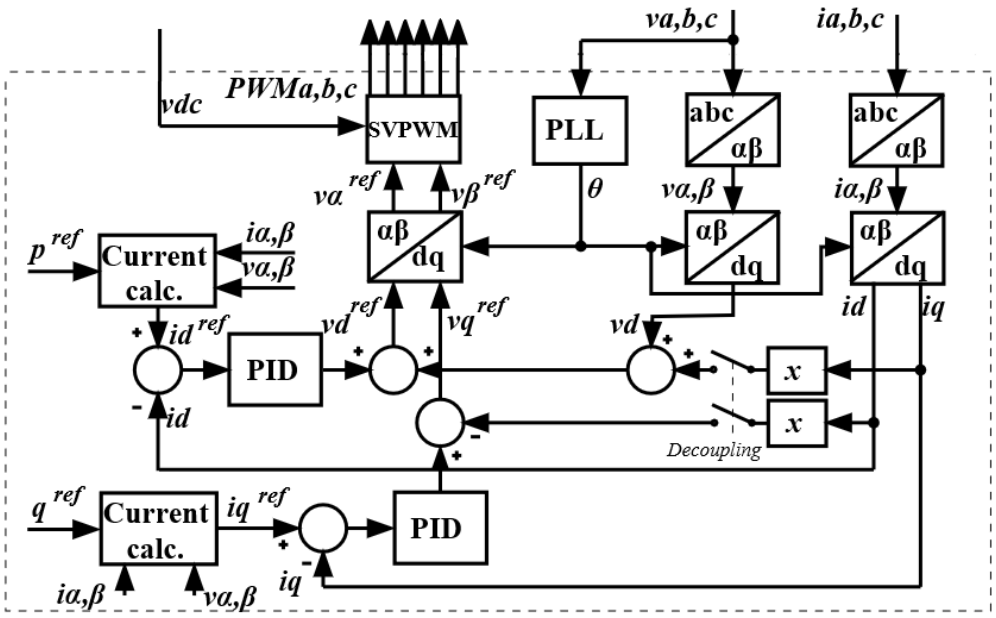

Figure 4.11: Schematic of the local control of the grid-connected battery inverters [139]

Regarding the photovoltaic components of the system, the PV array is introduced by the I-V characteristic of a desirable PV array. This characteristic can be produced inside the "Waveform Generator" of the Typhoon-HIL control Center package. Since in this grid-connected system, the PV inverter is supposed to always work at the maximum power point (MPP) and there is no need for PV power control and curtailment, the "Average PV Inverter" was used for this application which runs the PV array using MPPT algorithm. Opposite to the switch inverters that are controlled externally via a control card, the Average PV Inverter is controlled locally by an integrated control algorithm which is embedded inside the inverter's package in the Schematic Editor environment. The schematic of the PV inverter is depicted in figure 4.12.

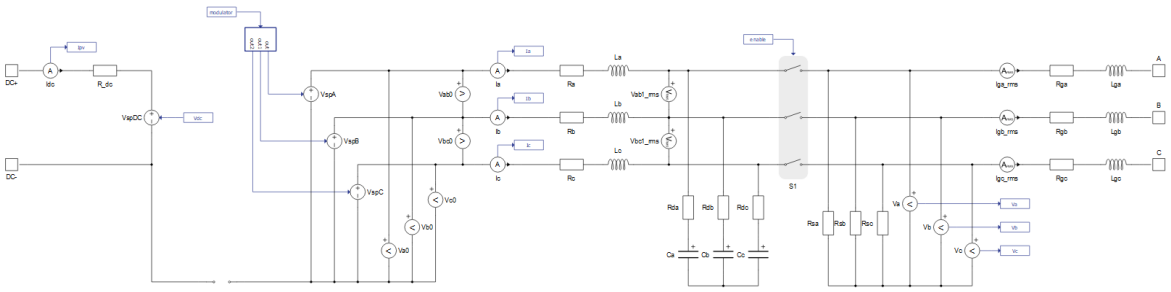

Figure 4.12: Schematic of the Average grid-connected PV inverter

As the studied microgrid is of the AC-bus type, the battery and PV inverters are connected to a three-phase AC bus. Also, connected to the AC bus, there is the grid that maintains voltage and frequency for the system as well as (typical) loads which can be estimated by load prediction and provided as a profile (array) to the model.

Once the microgrid is operating in the Schematic Editor environment, the control and monitoring processes can be done on different levels of the control hierarchy inside the HIL SCADA environment. One significant feature of the utilized platform is that users can plan any desirable action using Python coding and Python facilitates the employment of all the available resources of Typhoon-HIL. Several widgets in HIL SCADA provide the option of coding and implementing comprehensive energy management programs. Also, the Analog and digital electric signals of the microgrid can be monitored in real-time on this window. Alternatively, these signals can be recorded for offline analysis in other tools such as MATLAB. Thus, the developed energy management system including its corresponding battery degradation model was implemented through Python in the HIL SCADA environment. Starting, managing, and stopping the power units are carried out in this window. The nominal and seamless operation of a microgrid demands the precise deployment of hardware and software components in the right sequence. Figure 4.13 shows the SCADA window of the system. The inputs of the power system such as the grid voltage, solar irradiance, and temperature are specified in this environment. These values could be given as a

fixed amount or a profile that could be built or imported from outside.

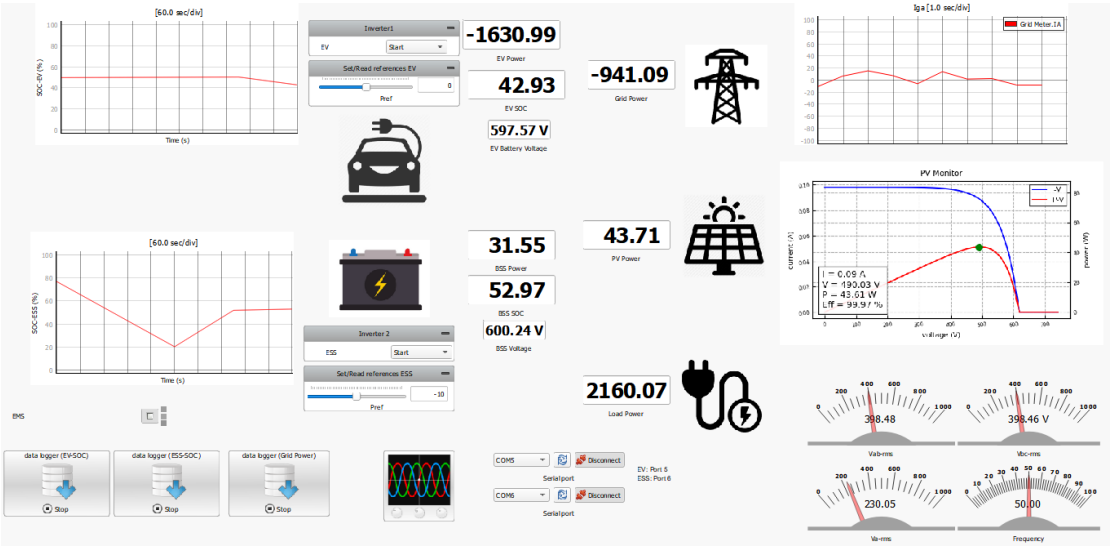

Figure 4.13: SCADA panel of the developed C-HIL setup

With regards to the hardware components of the utilized C-HIL platform, it is composed of three types of components. A Typhoon HIL 402 machine is used for emulating the power stage of microgrids which could provide a bi-directional connection between the simulated power system and an external controller. Two TMDSCNCD2808 control cards from Texas Instruments (TI) are used to control the battery inverters. In order to facilitate the connection of the TI control cards to the HIL machine, there is a need for an interface device. Therefore, a uGrid DSP interface 2.1 board from Typhoon-HIL is used as an interface for the control cards and HIL machine which also serves for downloading the codes into the control cards. The development of the inverter control algorithm which is programmed into the control cards can be done through different third-party platforms such as MATLAB Simulink. The communication between the HIL SCADA environment which generates the reference power signals for the control cards and the control cards is done through a serial link which runs from the computer to the interface board. The developed C-HIL system was set up for implementation of the proposed UC algorithms and observing the results (e.g., battery SoC variations, battery degradation, peak power, etc.) in a realistic experiment. Figure 4.14 shows the entire C-HIL simulation testbed including the power and control stages.

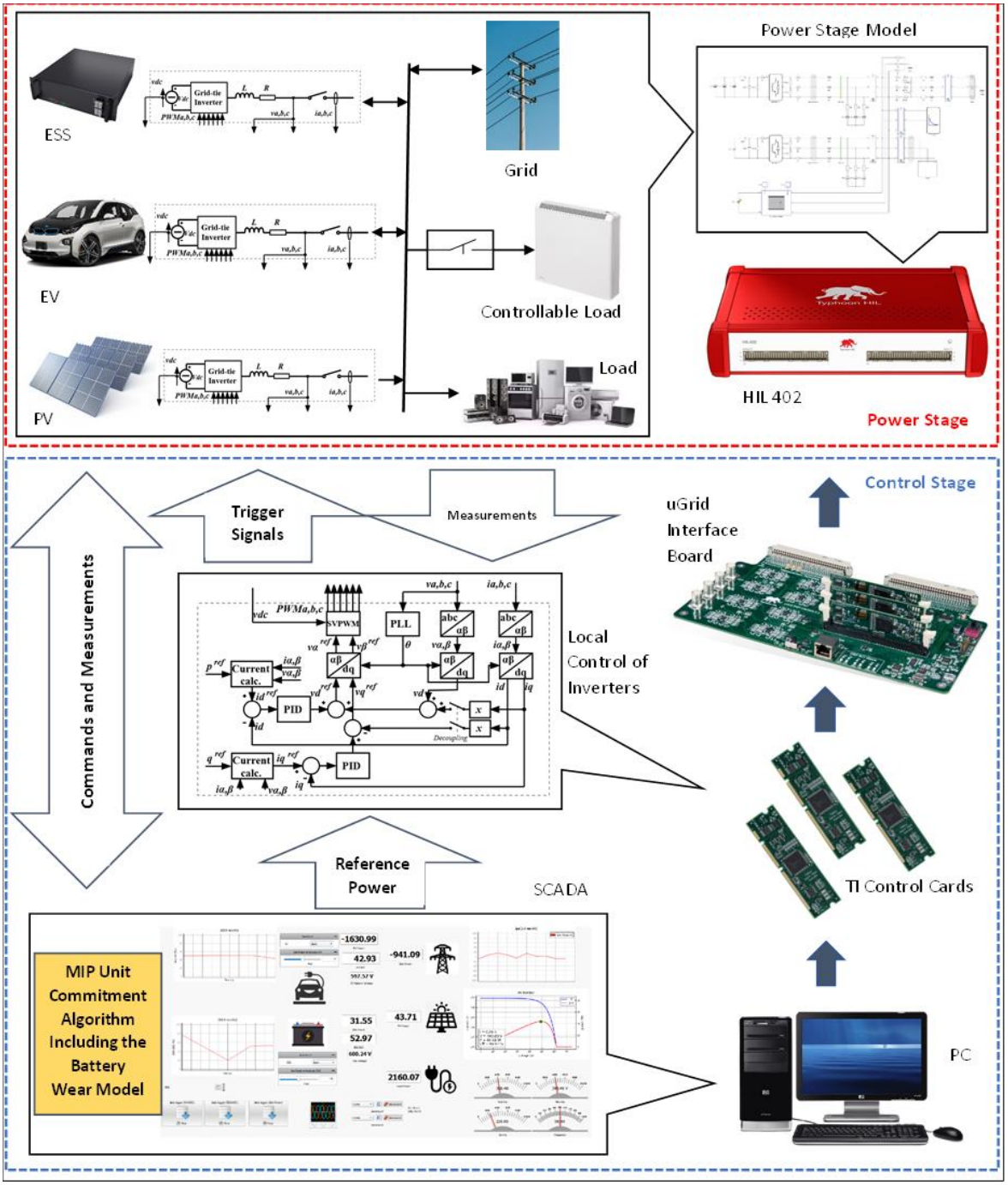

Figure 4.14: The C-HIL simulation setup

To sum up, to carry out the experimentation stage, first the MIP model is built and optimized as explained in the previous chapters. After the optimal results are produced by the MIP solver and the reference (battery power) values for the next optimization horizon are obtained, they can be

applied to the batteries in real-time. Hence, in the simulation stage, the obtained reference points of batteries are provided to the control cards of their respective inverters during the real-time simulation process. The power stage of the microgrid is operated on the HIL device and the entire system's operation is monitored and controlled in the HIL SCADA window. Any desirable signal from the system such as batteries' SoCs or the capacity loss values which are calculated online through integrated wear model formulations can be monitored in this environment. The HIL testing can demonstrate the accuracy and reliability of the optimization results when they are then compared with the offline-calculated results obtained from mathematical models of systems. For example, the HIL simulation results determine if batteries can be cycled to the desirable SoCs as anticipated from the optimization results. Hence, it can show if developed energy management algorithms can be applied in real-life cases. The MIP unit commitment model in this work was tested for both hourly and intra-hourly time granularities when they incorporate and omit the battery degradation model. For all cases, the system was operated using the irradiance, load, and energy tariffs obtained from [137], [138], and [101], respectively. Figure 4.15 shows the microgrid waveforms including the grid-supplied current, EV battery current, ESS current, PV inverter current and load current.

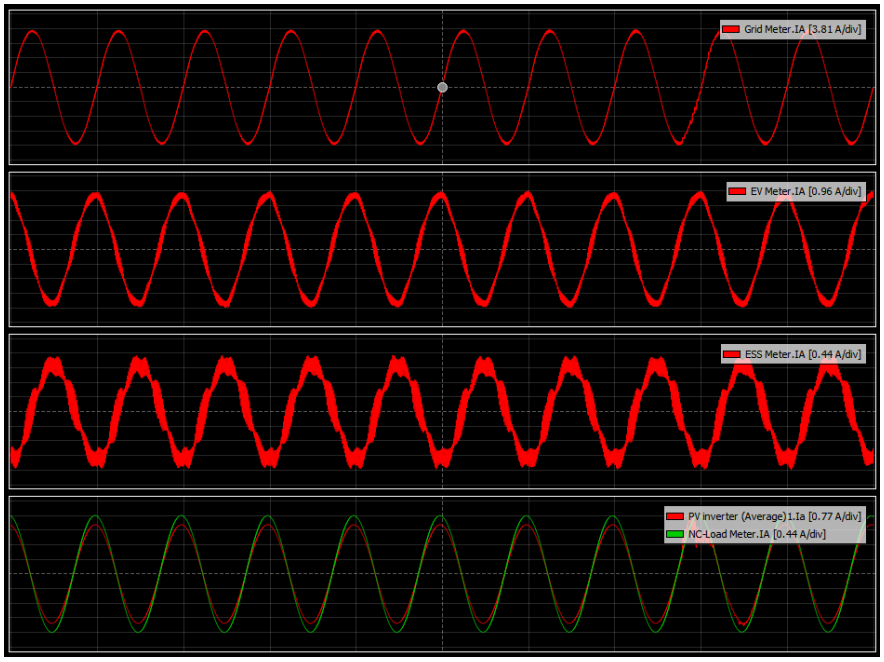

Figure 4.15: Real-time output waveforms of the microgrid components, from top to bottom: grid current, EV inverter current, ESS inverter current, PV inverter current and load current

4.3 Results of the C-HIL simulation

The SoC trends and capacity losses of the ESS and EV battery measured by the HIL setup are now presented in this section. Regarding the SoC variations of ESS which are demonstrated in figure 4.16, expectedly it was seen that lack of consideration of battery wear in the model led to large SoC variations (large DoDs) for both hourly and intra-hourly model granularities. However, by incorporating the wear model, the SoC trend shifted towards the larger SoCs to avoid causing high-capacity losses due to deep discharging attempts. Moreover, the domain of the fluctuations shrunk which shows lower DoDs in this case. Intra-hourly optimization for the case that takes into account the battery degradation leads to much more SoC fluctuations compared to the case that neglects it. Comparing the hourly and intra-hourly scenarios shows that in intra-hourly simulation, the SoC levels at every hour could deviate from their corresponding values in hourly simulation. This is because of the imperfections of the experimental testbed such as latencies and losses. For instance, in the experimental real-time simulation, the batteries show nonidealities, while in the numeric

simulation they are assumed as ideal components. Power converters and measurement components also cause energy losses in the experimentation, while in the numeric simulation they are ignored. In practice, mismatches between the day-ahead predictions and real-time levels of solar irradiance or load profile can also lead to this anomaly.

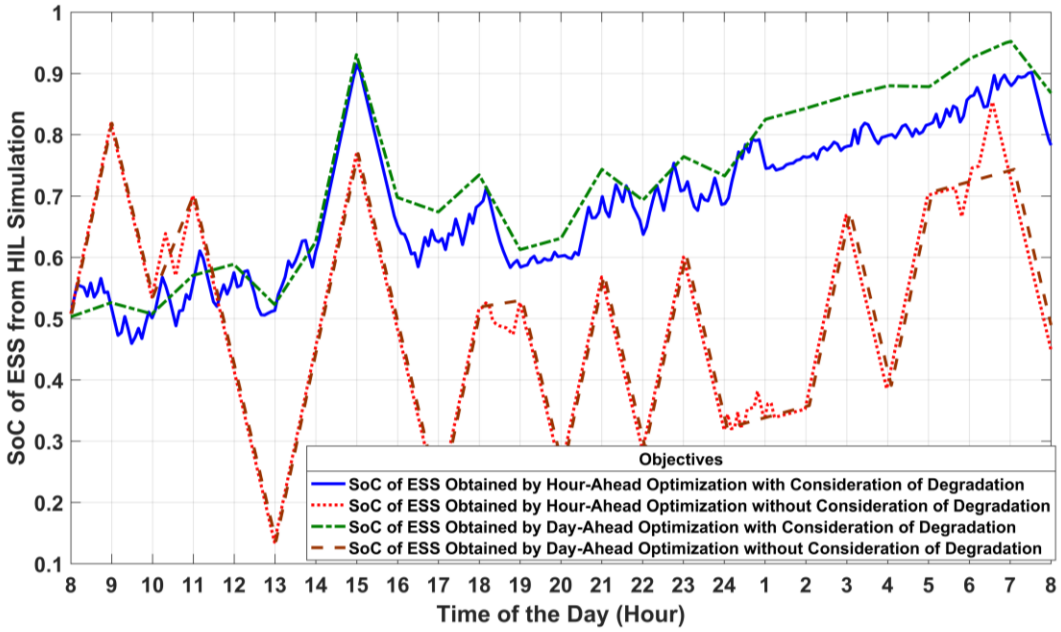

Figure 4.16: SoC variations of ESS for one day, resulted from hourly and intra-hourly battery scheduling with and without consideration of degradation and obtained from C-HIL simulation

Figure 4.17 and Table 4.4 show the trend and amount of capacity fade in the energy storage system measured in the real-time HIL simulation for four different UC strategies. It shows that large fluctuations of ESS SoC when the capacity loss is omitted lead to large capacity fade associated with high DoDs. In fact, deep discharging attempts at the lowest levels of SoC lead to the largest degradation rates as shown in the graphs. The hourly and intra-hourly scenarios showed similar capacity fade trends for all the periods that had similar SoC variations. The incorporation of battery wear expectedly reduced the wear rate as battery cycles were carried out with low DoDs at the larger half of the SoC spectrum. The intra-hourly scheduling also showed larger capacity losses as the battery functions more frequently in that case which is considerable. It shows that more frequent

battery dispatching although may seem promising in providing high energy efficiency, may lead to more severe battery wear that could possibly exceed its benefits.

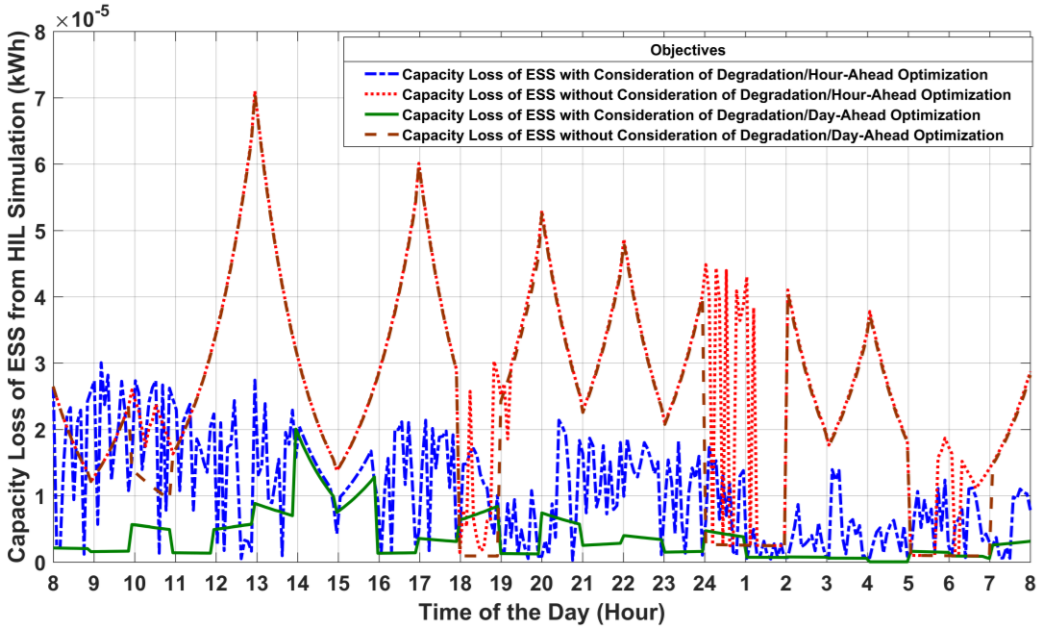

Figure 4.17: Capacity loss of ESS for one day, resulted from hourly and intra-hourly battery scheduling with and without consideration of degradation and obtained from C-HIL simulation

Table 4.4: Impact of granularity and consideration of battery degradation on the capacity loss of ESS over one day obtained from HIL simulation

Optimization Horizon	Optimization Granularity	Employed Degradation Method	Capacity loss of ESS from HIL Simulation (kWh)
Day-ahead	1 hour	None	0.007701
Day-ahead	1 hour	DoD-associated wear from irregular cycling	0.001050
Hour-ahead	1 hour / 5 minutes	None	0.006842
Hour-ahead	1 hour / 5 minutes	DoD-associated wear from irregular cycling	0.003129

The SoC variations of the EV battery obtained from the real-time HIL simulation are provided in figure 4.18. As expected, in the two cases that neglect the battery degradation, the battery was

discharged during the initial four hours of the EV's stay. After that, as the battery has become 80% empty, it needs to be charged continuously for 10 hours to make sure it will reach the desirable final SoC before departure. Similar to the ESS, the SoC caused by the hour-ahead simulation tracks the same path as that of the day-ahead simulation. However, the two cases that took into account the battery wear refused to discharge the battery considerably in the first hours to avoid unnecessary degradation costs. In these cases, the SoC mostly remained around the mid-range with mild charging/discharging attempts (more obvious in the intra-hourly case) which were justified in terms of profitability. In these cases, as the EV battery is not discharged largely during the first hours of stay, it can be charged up in the last 8 hours.

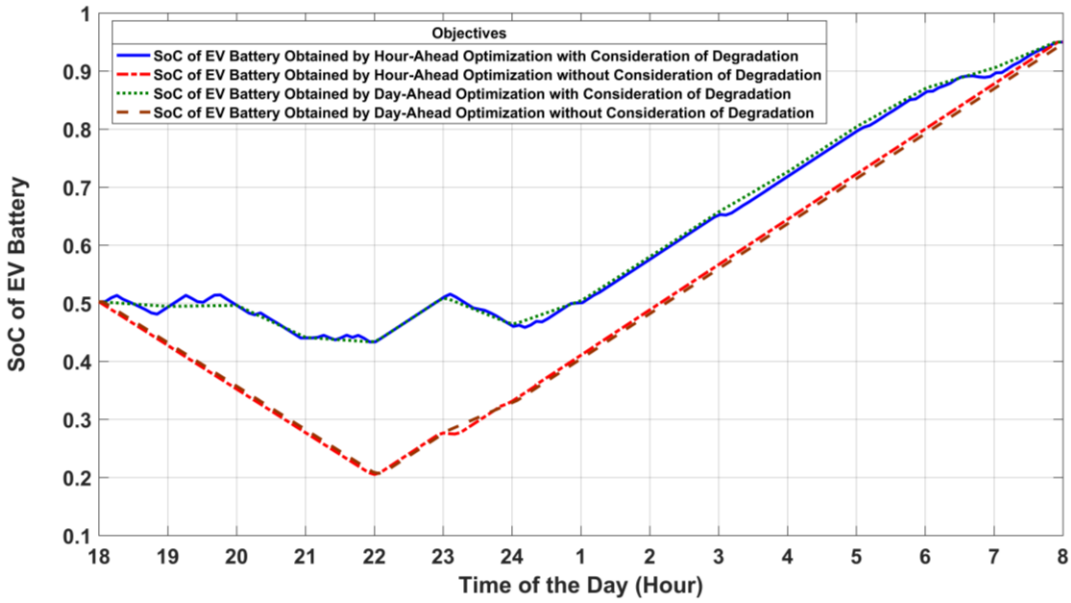

Figure 4.18: SoC variations of EV battery for one day, resulted from hourly and intra-hourly battery scheduling with and without consideration of degradation and obtained from C-HIL simulation

Finally, the trends and values of capacity fade of EV battery derived from the HIL simulation is represented in figure 4.19 and table 4.5. Again, not considering the battery wear led to larger capacity fade with their maximum (worst) values taking place around the times that the battery is discharged at the minimum SoCs. The close similarity of SoC graphs in hourly and intra-hourly cases led to the similarity of their corresponding wear rates. The Conservative approach for cycling

the EV battery in the first few hours when battery wear is taken into account leads to largely lower wear rates during those hours of the day. Smaller model granularity showed that it is capable of causing more capacity loss due to the more SoC fluctuations. As an implication of this simulation, it could be said that picking the right model resolution for a UC problem requires an initial investigation of the potential wear-associated costs as well as the resulting energy costs for every possible resolution. It is important to note that the larger wear rate caused by intra-hourly unit commitment in this case study does not necessarily show that hourly battery scheduling is superior to the intra-hourly type. In fact, battery degradation costs and energy costs themselves depend on other factors such as the energy fees, battery costs, system size, renewable energy generation, etc. Hence, depending on these factors, a comprehensive case study may identify an hourly or intra-hourly resolution, as more favorable. Moreover, it is worth mentioning that the difference in battery wear between the cases that consider, and neglect battery wear showed to be much smaller than the difference of the same set of parameters generated from the numerical simulation. This shows the importance of real-time testing in obtaining results with better accuracy.

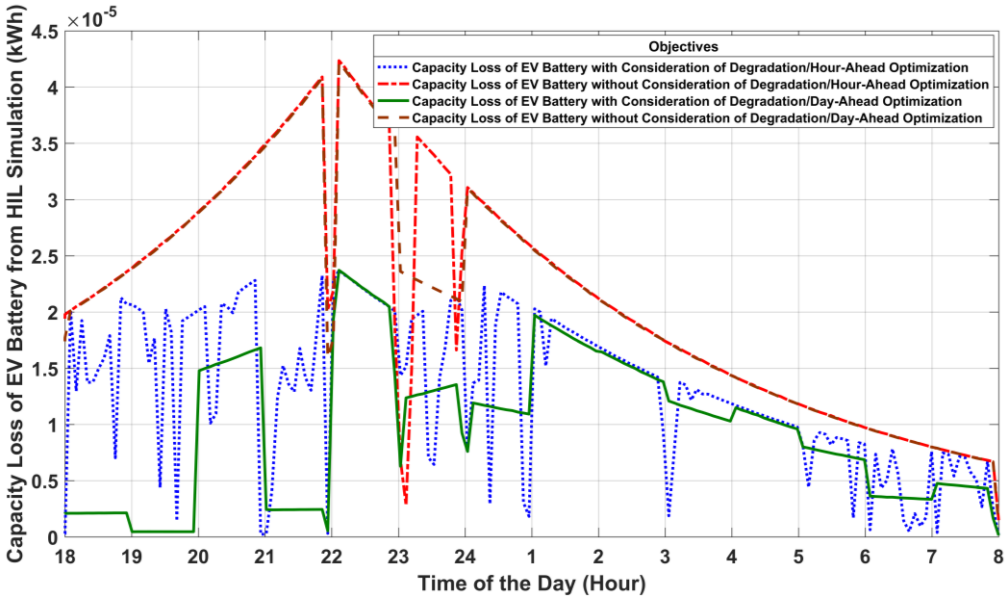

Figure 4.19: Capacity loss of EV battery for one day, resulted from hourly and intra-hourly battery scheduling with and without consideration of degradation and obtained from C-HIL simulation

Table 4.5: Impact of granularity and consideration of battery degradation on the capacity loss of EV battery over one day obtained from HIL simulation

Optimization Horizon	Optimization Granularity	Employed Degradation Method	Capacity loss of EV Battery from HIL Simulation (kWh)
Day-ahead	1 hour	None	0.003643
Day-ahead	1 hour	DoD-associated wear from irregular cycling	0.001617
Hour-ahead	1 hour / 5 minutes	None	0.003602
Hour-ahead	1 hour / 5 minutes	DoD-associated wear from irregular cycling	0.002218

Chapter 5: MIP unit commitment in microgrids with multiple beneficiaries

With the development of smart grid technology and the expansion of microgrids and distributed generation, generation and management of power are going to be handled increasingly by microgrid operators and users. In a generic microgrid, it would be probable to have different users with different interests and objectives. For instance, when a microgrid is owned and operated by a group of users in a building or neighborhood [23], or when it is employed by an organization (e.g., company, university, etc.) in a public place [5] where it benefits the organization or business owner itself and the people who may use the microgrid facilities for their personal use. For example, when a company employs a microgrid including EV charging facilities at its office building, the microgrid will be utilized by the company itself and the staff who charge their electric vehicles at the workplace. In the context of optimization, these cases where different parties have different interests in a single microgrid can be addressed by applying multi-objective models. However, when different parties have different interests that could be contradictory, it will be very important to have a concise knowledge of the system operation to have all the parties, benefit fairly. One crucial subject to address in these problems is the battery degradation issue as neglecting this issue could lead to unpredicted financial losses and environmental pollution which could be even worse compared to the cases where microgrid is possessed by a single entity. In fact, in a microgrid with multiple beneficiaries, neglecting the battery wear problem could potentially damage all the users. Therefore, this could lead to large financial losses and users' dissatisfaction which could adversely undermine the public's opinion on the joint utilization of microgrids or charging EVs in public places. Hence, it is important to address the battery degradation issue in every UC problem that aims at serving the interests of different entities. This chapter aims to study the fair and optimal

operation of a microgrid in a public place where different people with different interests want to benefit from the microgrid.

5.1 Building MIP model for a commercial building with an EV charging station

When it comes to studying the multi-beneficiary microgrid optimization problems, probably one of the most common cases is microgrid-equipped public buildings where different users and particularly EV users commute to and benefit from the microgrid in a direct way such as charging their EVs or gaining any revenues. Workplaces such as office buildings, university campuses, or health clinics with parking lots are highly capable of employing PV/battery-based microgrids and providing charging services to the EVs. Charging EVs at workplaces using locally generated PV power has several advantages, including:

1. EV batteries provide a storage capacity for excess PV energy.
2. As EVs are typically parked for long times, it is a good opportunity for providing V2X services including offering energy and ancillary services.
3. Lower cost of charging from PV compared to the grid as well as zero-carbon emission.
4. PV and EVs can diminish the adverse impact that they could have on the grid through their mutual operation [5].

The load demand of public charging facilities can be divided into two types, namely uncoordinated and statistical. The former type refers to the EVs that have no specific charging pattern such as the taxies, whereas the latter can be modeled statistically depending on several parameters such as working hours and day of the week [8]. Although both types of loads have been addressed in the literature, however, the second group that has a specific commuting pattern is more likely to receive an optimal charging regime because there is no need to consider any uncertainty or randomness in their scheduling algorithms. For instance, the employees of workplaces that have specific commuting times or even designated parking spots can have their EVs integrated into the local

microgrid to have them charged optimally or potentially make revenues from offering V2X services. Hence, as this chapter is focused on optimal unit commitment in microgrids with multiple beneficiaries, only those EVs have been addressed in this work that has a specific commuting routine. Another point to consider is concerned with the charging power. As the proposed battery wear in this work does not take into account the C-rate and the temperature, DC (fast) charging stations and such places where batteries are exposed to high charging rates and possibly high temperatures are not subject to this study.

Traditionally, there are three types of "non-optimal" strategies for charging EVs in parking lots. These strategies are immediate charging in which the EV is charged immediately with the nominal power rating of charging equipment once it arrives at the parking spot. This is the simplest and fastest charging type and does not require any communication and information about the user and EV, however, this method causes the most stress on the grid/microgrid. The other type of charging is the average rate, where the EV is charged with the minimum possible power rating during its stay time in such a way that it can be fully charged by the time of departure. In this mode, the user's arrival, departure, and required energy are needed for making the charging plan. Employing this method helps spread the EVs demand throughout the day and poses less stress on the grid/microgrid. The third method would be to start charging the EV with a delay and with the nominal rating of the equipment. This method also prevents the accumulation of EV demand around a certain time of day [5]. However, a sophisticated "optimal" battery scheduling program should be able to determine "when" to charge or discharge "which" EV and with "how much" power. However, this level of scheduling precision requires the microgrid controller system to have the luxury of accessing detailed information about every EV and their owner preferences, future (e.g., next day, next hour) renewable energy generation, future energy tariffs, and future load profile. Moreover, there must be sophisticated battery cycling facilities in place that are capable of receiving reference signals from a central controller and charging or discharging EVs with

continuous amounts of power. In this regard, the optimal UC problem for a workplace building facilitated with PV, ESS, and EV chargers has been addressed in this section. The studied microgrid of this chapter is depicted in figure 5.1.

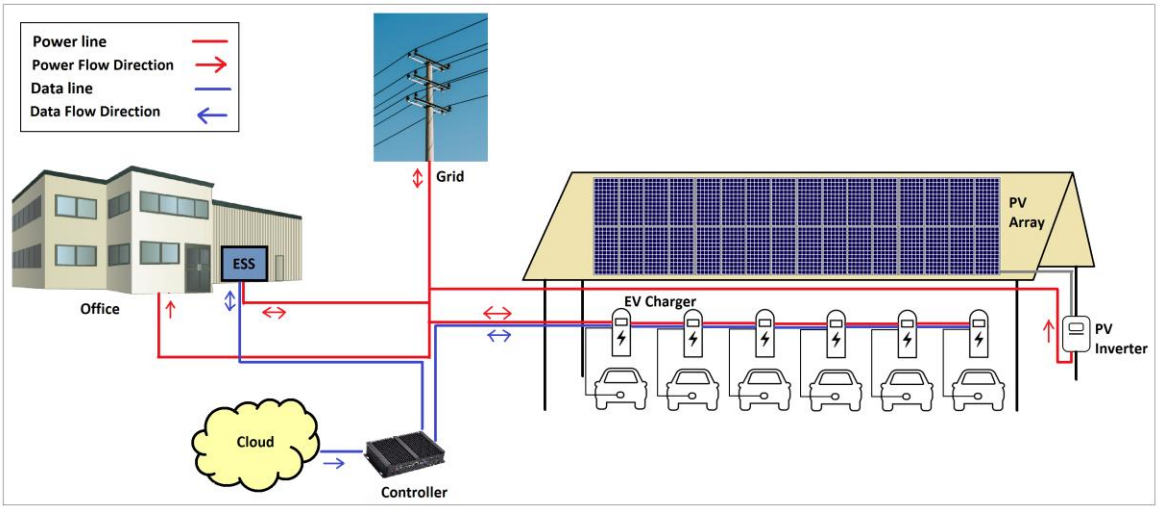

Figure 5.1: Workplace AC-bus microgrid

To study the UC problem and the impact of battery degradation in a commercial building, the battery scheduling problem for a workplace is addressed in this section. Similar to the previous chapters, a MIP-based UC model is presented and used for a case study. In this regard, a small-sized commercial building with 10 kW nominal photovoltaic generation, a 40-kWh energy storage system, and a parking lot equipped with six EV chargers have been considered for the case study. The solar irradiance, load profile of the office, and energy tariffs were derived from [102], [140], and [141] respectively. As for the EVs, some of the prevalent vehicles from the major manufacturers were selected for this case study, including Smart ED, BMW i3, Nissan Leaf, Opel Corsa, Tesla Model 3, and Tesla Model S. The battery capacities of these vehicles range from 16.5 to 90 kWh. The battery specifications of every EV (size and ratings, *N(D)*, prices) are supposed to be provided by their owners to the MG controller. In this case study, apart from *N(D)*, the other specifications of the EV batteries have been obtained from their corresponding datasheets. However, the *N(D)* data that was employed in the previous case studies have been used for all the

EVs in this case study as well, as they are hypothetically assumed to benefit from Li-ion batteries with the same chemistry. Also, the arrival and departure times of every single EV must be provided by their owners and incorporated into the model. However, in this work, the arrival time of all vehicles is considered to be the beginning of the work hours (9 AM) and their departure time is considered to be the end of the work hours (5 PM).

In this regard, first, the MIP model of the problem is formulated by presenting the MIP constraints associated with the system and the constraints associated with the battery degradation [142]. Apart from those model constraints that involve EV parameters, the rest of the constraints are similar to those of the smart home model which were provided in constraints (2.23)-(2.38), (2.48), (2.57)-(2.58) of chapter 2 and the wear-associated equations (3.27)-(3.39) of chapter 3. This is because regardless of the different scale of load profile, PV generation, and ESS size, the general equations that model these components in a smart home and a smart office could be similar. Regarding the EVs, just like the smart home problem where the information and specifications of the EV and its battery (e.g., initial capacity, initial price, salvage price, charge rating, battery type, arrival, and departure times) should be provided by the user for the microgrid control system, for the case of office, also this information needs to be provided by the EV owners (office employees) for the system controller. That's why this algorithm is not suitable for charging random EVs as it needs to have some information about the technical specifications of every EV. It should also be emphasized that the proposed UC model addresses the EVs in an individual fashion rather than considering them as a flock of storage components. Therefore, the MIP constraints associated with EVs are laid out individually. The advantage of this approach is that every EV can be scheduled in the most optimal way which is desirable for the EV owners. Also, every EV can be modeled as a separate module in the implementation process of the algorithm which makes it straightforward. However, the downside of this approach is that addressing EVs individually could make the MIP model large and potentially hard to solve in cases of larger EV numbers. Hence, it will be a more complex and

harder model to solve which may necessitate the employment of more powerful computing equipment for the system. As an example, the study in [69] reports that finding the result for each EV at each stage of optimization in multi-stage algorithms takes between 1 to 10 seconds. One common way to reduce the computational time of optimization problems is by sacrificing the accuracy of the optimization results by changing the MIP gap [69].

As a result, this algorithm is useful for cases where the number of EVs is not large (such as in large apartment/office buildings, industrial complexes, shopping malls, etc.) and it is proportional to the available computational resources. Hence, a small office building is a good applicable example for this algorithm as it does not have numerous EV chargers, the EV owners regularly commute to that place so there is a possibility to obtain the EVs' information from their users. And also, there is some sort of mutual benefit for all parties (company and EV owners), therefore, EV owners would be willing to come into an agreement to have their EV batteries cycled during the stay times. In this regard, all the constraints that differ from the previously provided ones are provided as follows. Equation (5.1) enforces the fact that the available discharge power of every EV during its stay time is partly consumed locally at the office and partly delivered to the grid. Equations (5.2) and (5.3) limit the maximum charging and discharging power of every EV according to its characteristics for its stay period. The stored energy in the battery of every electric vehicle at every interval is modeled by equation (5.4), the primary state of energy, as well as maximum, minimum and final states of energy for every EV, are enforced by (5.5) to (5.8). Equation (5.9) enforces the fact that the charging or discharging power for every EV outside its parking period is zero.

$$P_{ev}^{n,m,con} + P_{ev}^{n,m,ex} = P_{ev}^{n,m,dis} \times \eta_{ev}^{dis} \quad \forall n \in [n_a, n_d], \forall m \in M \tag{5.1}$$

$$P_{ev}^{n,m,ch} \leq U_{ev}^{n,m} \times P_{ev}^{m,ch} \qquad \forall n \in [n_a, n_d], \forall m \in M \tag{5.2}$$

$$P_{ev}^{n,m,dis} \leq (1 - U_{ev}^{n,m}) \times P_{ev}^{m,dis} \quad \forall n \in [n_a, n_d], \forall m \in M \tag{5.3}$$

$$SE_{ev}^{n,m} = SE_{ev}^{n-1,m} + \left(\eta_{ev}^{ch} \times P_{ev}^{n-1,m,ch} \times G\right) - \left(P_{ev}^{n-1,m,dis} \times G\right) \ \forall n \in [n_a + 1, n_d + 1] \ \forall m \in M \quad (5.4)$$

$$SE_{ev}^{n,m} = SE_{ev}^{m,ini} \qquad n = n_a, \forall m \in M \quad (5.5)$$

$$SE_{ev}^{n,m} \leq SE_{ev}^{m,max} \qquad \forall n \in [n_a, n_d + 1], \forall m \in M \quad (5.6)$$

$$SE_{ev}^{n,m} \geq SE_{ev}^{m,min} \qquad \forall n \in [n_a, n_d + 1], \forall m \in M \quad (5.7)$$

$$SE_{ev}^{n,m} \geq SE_{ev}^{m,ch} \quad n \geq n_{ch} \in [n_a, n_d], \forall m \in M \quad (5.8)$$

$$P_{ev}^{n,m,con} = P_{ev}^{n,m,ex} = P_{ev}^{n,m,ch} = P_{ev}^{n,m,dis} = SE_{ev}^{n,m} = 0 \qquad \forall n \notin [n_a, n_d], \forall m \in M \quad (5.9)$$

In the office case, n_a and n_d correspond to the arrival and departure intervals of EVs and can be received from the EV owners. Similar to the previous models, n represents the interval. Moreover, in this model, m denotes the number of EVs in the set of M EVs. Hence, $P_{ev}^{n,m,con}$ represents the consumed portion of the battery power at the n_{th} interval for the m_{th} EV. $P_{ev}^{n,m,ex}$ denotes the exported portion of battery power at the n_{th} interval for the m_{th} EV. $P_{ev}^{n,m,dis}$represents the discharging battery power at the n_{th} interval for the m_{th} EV, η_{ev}^{dis} may be assumed the same for all EVs as it represents the discharging efficiency of EV charging equipment. $P_{ev}^{n,m,ch}$ denotes the charging power for charging the m_{th} EV at the n_{th} interval, $U_{ev}^{n,m}$ represents the n_{th} element of the charging array of the m_{th} EV which has N binary members. $P_{ev}^{m,ch}$ denotes the maximum charging power of the m_{th} EV which depends on its charging equipment. $P_{ev}^{m,dis}$ represents the maximum discharging power of the m_{th} EV, $SE_{ev}^{n,m}$ denotes the state of energy of the m_{th} EV battery at the n_{th} interval. η_{ev}^{ch} also may be assumed the same for all the EVs as it denotes the charging efficiency of EVs. $SE_{ev}^{m,ini}$ denotes the initial state of energy of the m_{th} EV battery at the first interval of the model. $SE_{ev}^{m,max}$ and $SE_{ev}^{m,min}$ express the maximum and minimum allowed amounts of stored energy in the of the m_{th} EV battery respectively and $SE_{ev}^{m,ch}$ is the desirable SoE of the m_{th} EV at the time of departure which should be provided by the EV owners.

The MIP constraints associated with battery degradation of EVs are also incorporated individually for every EV as presented below, where equation (5.10) gives the SoC of every EV at every interval that the EV is parked and connected to the microgrid. Equation (5.11) enforces the relationship between SoC and DoD of every battery at every interval. Also, equations (5.12) and (5.13) represent the wear coefficient function and capacity loss constraint, respectively.

$$SC_{ev}^{n,m} = \frac{SE_{ev}^{n,m}}{E_{ev}^{m}} \qquad \forall n \in [n_a, n_d + 1] \tag{5.10}$$

$$D_{ev}^{n,m} = 1 - SC_{ev}^{n,m} \qquad \forall n \in [n_a, n_d + 1] \tag{5.11}$$

$$W_{ev}^{n,m} = f_m(D_{ev}^{n,m}) \approx a_m(D_{ev}^{n,m})^2 + b_m(D_{ev}^{n,m}) + c_m \quad \forall n \in [n_a, n_d + 1] \tag{5.12}$$

$$L_{ev}^{n,m} = E_{ev}^{m,opt}\left[W_{ev}^{n,m} D_{ev}^{n,m} - W_{ev}^{n+1,m} D_{ev}^{n+1,m}\right] \qquad \forall n \in [n_a, n_d] \tag{5.13}$$

where, $SC_{ev}^{n,m}$ denotes the SoC of the m_{th} EV at the beginning of the n_{th} interval. E_{ev}^{m} is the battery capacity of the m_{th} EV at the beginning of the current day. $D_{ev}^{n,m}$ represents the DoD of the m_{th} EV at the beginning of the n_{th} interval. $W_{ev}^{n,m}$ is the wear coefficient associated with $D_{ev}^{n,m}$. f_m is the function that relates the wear coefficient of the m_{th} EV battery against its depth-of-discharge, and it differs from a battery to a battery depending on its chemistry. Once f_m is curve fitted to a polynomial function for more simplicity, a_m, b_m and c_m are its polynomial coefficients. $L_{ev}^{n,m}$ denotes the capacity loss of the m_{th} EV battery caused by the n_{th} irregular half cycle and $E_{ev}^{opt,m}$ is the battery capacity of the m_{th} EV at the beginning of the optimization process.

Equation (5.14) enforces the power balance constraint to the model where the charging and discharging powers of EVs are addressed collectively. Equation (5.15) also introduces the fact that the exported power is the sum of exported components of ESS, PV, and EVs. Finally, after EVs depart at the end of a workday, the remaining capacity of the m_{th} EV for the next optimization attempt can be calculated from (5.16) which is not a model constraint.

$$\sum_{m} P_{ev}^{n,m,con} + \sum_{m} P_{ev}^{n,m,ex} + P_{im}^{n} + P_{es}^{n,con} + P_{es}^{n,ex} + P_{pv}^{n,con} + P_{pv}^{n,ex} \tag{5.14}$$

$$= \sum_{m} P_{ev}^{n,m,ch} + P_{ex}^{n} + P_{es}^{n,ch} + P_{l}^{n} \quad \forall n \in N, \forall m \in M$$

$$P_{ex}^{n} = \sum_{m} P_{ev}^{n,m,ex} + P_{es}^{n,ex} + P_{pv}^{n,ex} \quad \forall n \in N, \forall m \in M \tag{5.15}$$

$$E_{ev}^{m,opt} = E_{ev}^{m,ini} - \sum_{O} \sum_{N} \mathrm{L}_{ev}^{n,m} \tag{5.16}$$

where, $E_{ev}^{m,opt}$ is the battery capacity of the m_{th} EV at the beginning of the optimization process and $E_{ev}^{m,ini}$ is the initial battery capacity of the m_{th} EV.

Figure 5.2 demonstrates the algorithm of the studied UC model for a workplace.

Algorithm -3 Unit Commitment Algorithm for Work Place-Hourly Time Resolution

1: Updating or calculating model parameters and data including $N(D)$ curve and maximum C-rate of every EV battery, departure and arrival times of EVs, initial and final SoCs of every EV battery, initial and salvage prices and current capacities of EV and ESS batteries, day-ahead PV generation, energy tariffs and office load profile.
2: Updating the $N(D)$ for EV batteries and ESS according to their power ratings.
3: Calculating the $W(D)$ functions and performing curve fitting on them to make them implementable as model constraints in the used mathematical solver.
4: **procedure** "PRODUCING THE MIXED-INTEGER PROGRAMMING MODEL WHICH INCLUDES THE FOLLOWING COMPONENTS AND PERFORMING THE OPTIMIZATION FOR THE NEXT 24 HOURS"
5: General constraints of the model including EVs, ESS and PV
6: Battery Degradation constraints for EVs and ESS
7: Objective functions for minimizing cost and degradation for the system operator and EV owners
8: Obtain the control variables of power for every single EV and ESS, as well as state variables of SoC arrays, battery degradation values, consumed energy and costs for the next 24 hours from the solved MIP problem.
9: Calculate the battery degradation for the scenarios that neglect battery degradation by applying the wear model to the obtained SoC arrays of EVs and ESS.
10: Calculate the carbon footprint caused by energy consumption and battery wear.

Figure 5.2: Unit commitment algorithm for a workplace microgrid built in the framework of MIP with hourly resolution

5.2 Unit commitment strategies for a microgrid with a charging station

The UC strategies are concerned with the objectives, priorities, and interests of the entities that are going to benefit from the UC practice. From the user perspective, in a commercial building, there are two ends of beneficiaries, namely the organization or company that owns the building and microgrid and the employees of the organization that own electric vehicles and have their EVs charged at the workplace on a regular basis. When it comes to the cost of the system, energy consumption, and emission, different organizations could have different priorities and goals which reflect on the strategies they could implement for unit commitment. Some companies may prefer to keep their costs at the lowest possible rates regardless of their carbon footprint, while some organizations may decide to lower or possibly minimize their carbon footprint or energy intake from the grid. In some regions, there might be specific regulatory measures to limit the power drawn from the grid or the emissions of commercial buildings. Furthermore, the policies of companies could be different in terms of providing energy to the EVs of their employees. Some firms may decide to provide free electric energy to the EVs to encourage the use of EVs among their staff. Other companies may charge their staff for charging their EVs based on fixed or dynamic tariffs. In case the existing equipment can offer vehicle to building or vehicle to grid services, some corporations may offer agreements to their employees based on which their EVs will be charged and discharged locally for benefiting EV owners as the company simultaneously. By taking this approach, the companies will be able to use the locally available energy and pay their employees instead of drawing the energy from the grid and paying the utility companies. Therefore, depending on several factors such as the availability of technologies and DR programs as well as companies' preferences about expenses, emissions, and personnel, a wide range of approaches could be taken by companies for cycling EVs and ESSs. In this case study, the office and EVs are supposed to benefit from bi-directional charging equipment that can charge and discharge EV batteries with continuous rates of power. It is assumed that the company can buy and sell energy from and to the

grid in a dynamic day-ahead market. In order to investigate the optimal unit commitment from the user's perspective, three different UC strategies have been proposed in form of different sets of objective functions. These strategies prioritize the interests of the business owner and EV owners to different extents [142].

5.2.1 Case 1: conventional strategy

Similar to the case of residential buildings, the conventional strategy is to minimize the apparent net cost of the building for the business owner. In this strategy neither the cost of battery degradation nor the interest of the EV owners is taken into consideration and the interest of the business owners is merely considered to be the difference between apparent energy cost and revenues obtained from selling energy back to the grid as provided in equation (2.59) [142].

5.2.2 Case 2: minimal costs for MG operator

An optimal UC model from the perspective of the business owner requires the employment of the battery wear model to take into account the cost of ESS degradation. In this strategy, the real cost of the office building is minimized by including the net cost as well as the battery degradation cost of the local energy storage system [142]. The objective function is provided in (5.17).

$$Min \sum_{N} \left(P_{im}^{n} \times T^{n,buy}\right) + \left(\frac{L_{es}^{n}}{(1-R_{es})E_{es}^{ini}}\right)\left(V_{ess}^{ini} - V_{ess}^{sal}\right) - \left(P_{ex}^{n} \times T^{n,sell}\right) \tag{5.17}$$

5.2.3 Case 3: serving MG operator and EV owners- type 1

In the two previous cases, the UC strategy was only supposed to benefit the business owner. However, depending on the values and policies of different organizations they may decide to incorporate the interest of EV owners into their energy management strategies. For instance, some

EV owners may come to agreements with the business owner to participate in a vehicle-to-building service for monetary premiums. However, EV owners would not be willing to participate in a V2X service if their vehicle batteries are going to be heavily exploited and worn out due to the V2X service. In this regard, not only would EV owners like to know how their vehicle batteries will be impacted by a vehicle to building service, but they would also like to have their batteries degraded minimally. Therefore, the UC approach provided in this section is a multi-objective strategy involving the real cost of the business owner and the battery degradation of every single EV. Due to the structure of the proposed degradation model, the objective function that aims at minimizing the battery wear of EVs can be implemented individually for every EV. This approach can ensure that all EVs are treated equally and in a fair fashion. According to this strategy, EVs will be fully charged by the time of departure. However, not only is the real cost of the business owner minimized, all the EVs are also cycled such that they experience minimal battery wear. Using this approach, the EV owners will be ensured that their vehicle batteries will not be extensively deployed which might not be worth the incentives they receive for the V2B service [142]. This multi-objective strategy consists of (5.17), and (5.18) for every EV.

$$Min \sum_{N} (L_{ev}^{n}) \quad \forall m \in M \tag{5.18}$$

5.2.4 Case 4: serving MG operator and EV owners- type 2

Although addressing the battery degradation for EVs which was suggested in the previous strategy can minimize the costs associated with battery wear for EV owners, however, it cannot guarantee that EV owners will pay the minimum costs for charging their vehicles or make the maximum profit from having their vehicles participate in a V2B service. Therefore, as the next strategy, the monetary interest of EV owners is taken into consideration where the net cost of charging for every single EV is also incorporated into the objective functions. For the implementation of this strategy, it is assumed that the business owner charges and pays the EV owners for charging and discharging

their vehicles with the same rates of grid and feed-in tariffs. Obviously, in this case, the EV owners are given special consideration. This could be done at a higher cost for the business owner as incorporating the monetary interest of EV owners undermines the impact of the objective function that minimizes the costs of the business owner. The objective set of this strategy is composed of (5.17), (5.18), and (5.19) for every EV.

$$Min \sum_{N} \left(P_{ev}^{n,ch} \times T^{n,buy} \times G\right) - \left(P_{ev}^{n,dis} \times T^{n,sell} \times G\right) \quad \forall m \in M \tag{5.19}$$

It is worth mentioning that apart from the first case which presented the conventional and inefficient way of unit commitment, it is not possible to select any of the other proposed strategies as the "best" scenario. This is due to the fact that several factors such as variations of the *N(D)* curve, initial and salvage prices of batteries, energy tariffs, and battery's state-of-health (SoH) at the time of replacement (*R*) which depends on the user, could change the results in favor of one strategy or another. Hence, this research work aims to introduce the "methodology" for investigating the unit commitment in the workplace, thoroughly. Once sufficient computing hardware and software are available, by using the proposed methodology, the business owners will be able to evaluate all these strategies in a relatively short amount of time, discover the effectiveness of each strategy depending on their specific conditions and make decisions about the strategy they would like to implement [142].

5.3 Results and discussion

Similar to the study of unit commitment in a residential building, to observe the performance of the proposed UC strategies in a commercial building, each strategy is first simulated for a single sample day and the results are generated. Then, each strategy is simulated for a one-month term to provide more reliable results. The load power and energy price profile used in this case study are shown in figure 5.3, and the input parameters of this case study are listed in Table 5.1.

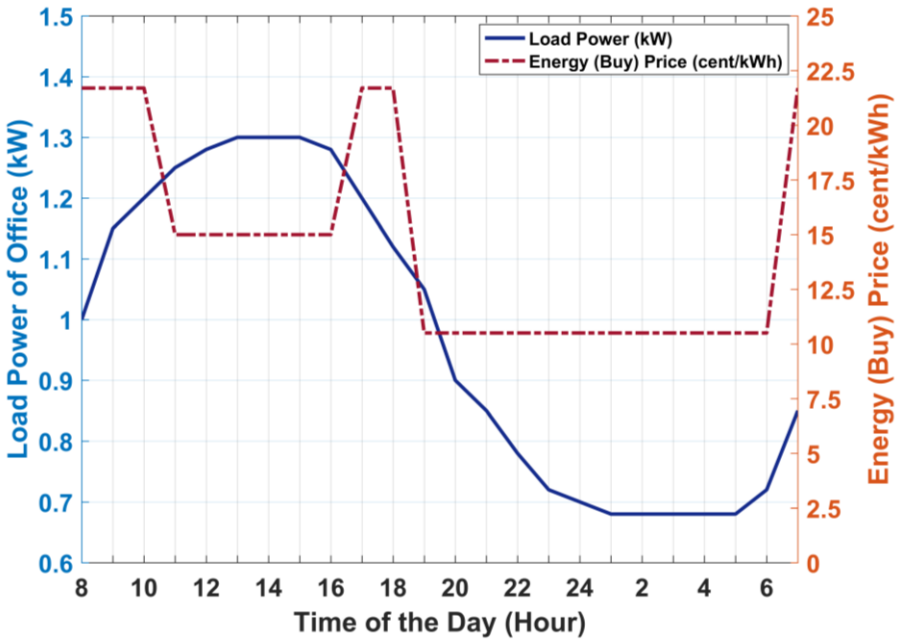

Figure 5.3: Load power and energy price profiles for the case study of chapter 5

Table 5.1: Input parameters of the case study of chapter 5

Input Parameter	Value
$\boldsymbol{\eta_{es}^{ch}/\eta_{ev}^{ch}}$	96%/96%
$\boldsymbol{\eta_{es}^{dis}/\eta_{ev}^{dis}}$	96%/96%
$\boldsymbol{P_{es}^{ch}/P_{ev}^{m,ch}}$	20kW/7, 7.4, 6.6, 7.4, 11, 16.5kW
$\boldsymbol{P_{es}^{dis}/P_{ev}^{m,dis}}$	20kW/7, 7.4, 6.6, 7.4, 11, 16.5kW
$\boldsymbol{G}$	1 hour
$\boldsymbol{SE_{es}^{ini}/SE_{ev}^{m,ini}}$	24kWh/8.25, 11, 15, 25, 37.5, 45kWh
$\boldsymbol{SE_{es}^{max}/SE_{ev}^{m,max}}$	38kWh/15.6, 20.9, 28.5, 47.5, 71.2, 85.5kWh
$\boldsymbol{SE_{es}^{min}/SE_{ev}^{m,min}}$	3kWh/1.2, 1.6, 2.2, 3.7, 5.6, 6.7kWh
$\boldsymbol{SE_{ev}^{m,ch}}$	15.6, 20.9, 28.5, 47.5, 71.2, 85.5kWh
$\boldsymbol{\eta_{pv}}$	100%
$\boldsymbol{P_{im}^{max}}$	100kW
$\boldsymbol{P_{ex}^{max}}$	100kW
$\boldsymbol{E_{es}^{ini}/E_{ev}^{m,ini}}$	40kWh/16.5, 22, 30, 50, 75, 90kWh
$\boldsymbol{V_{es}^{ini}/V_{ev}^{m,ini}}$	\$10000/\$4125, \$5500, \$7500, \$12500, \$18750, \$22500
$\boldsymbol{V_{es}^{sal}/V_{ev}^{m,sal}}$	\$2040/\$841, \$1122, \$1530, \$2550, \$3825, \$4590
$\boldsymbol{R_{es}/R_{ev}}$	0.5/0.8

In this regard, the following are the bar charts that demonstrate the power distribution of the involved units throughout a day obtained from every one of the optimization strategies. Figure 5.4 shows the UC chart for the conventional or basic case where power distribution has been done for achieving the minimum net price of energy, with consideration of grid tariffs and without addressing the efficient operation of stationary or automotive batteries. According to figure 5.5 which demonstrates the results of case 2, as ESS degradation cost is also taken into account, the ESS is also cycled at relatively lower power rates which reflects in lower DoDs and consequently lower degradation rates. In this case, the EV batteries are cycled in favor of the office to minimize the real costs of the system operator.

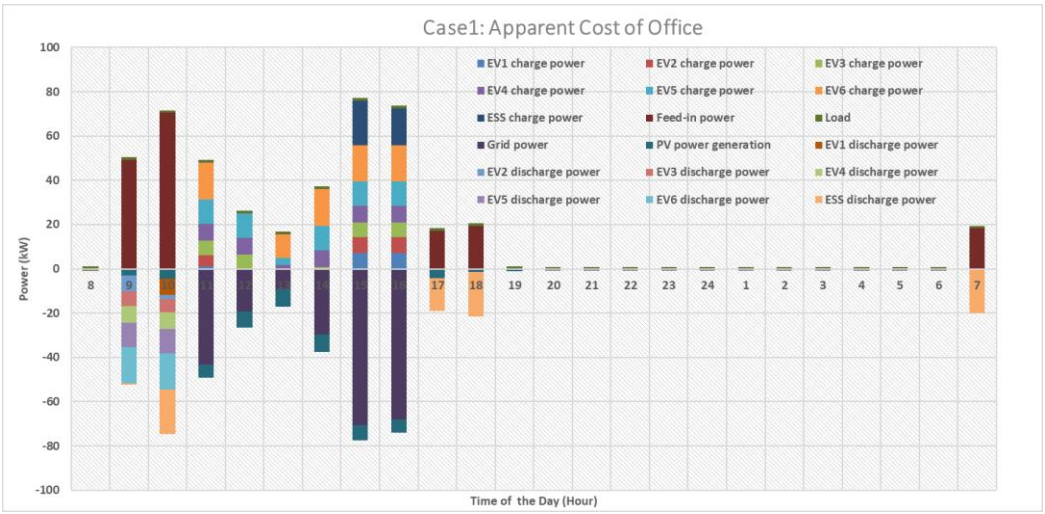

Figure 5.4: Power profile of the microgrid components-objective function: energy cost of office

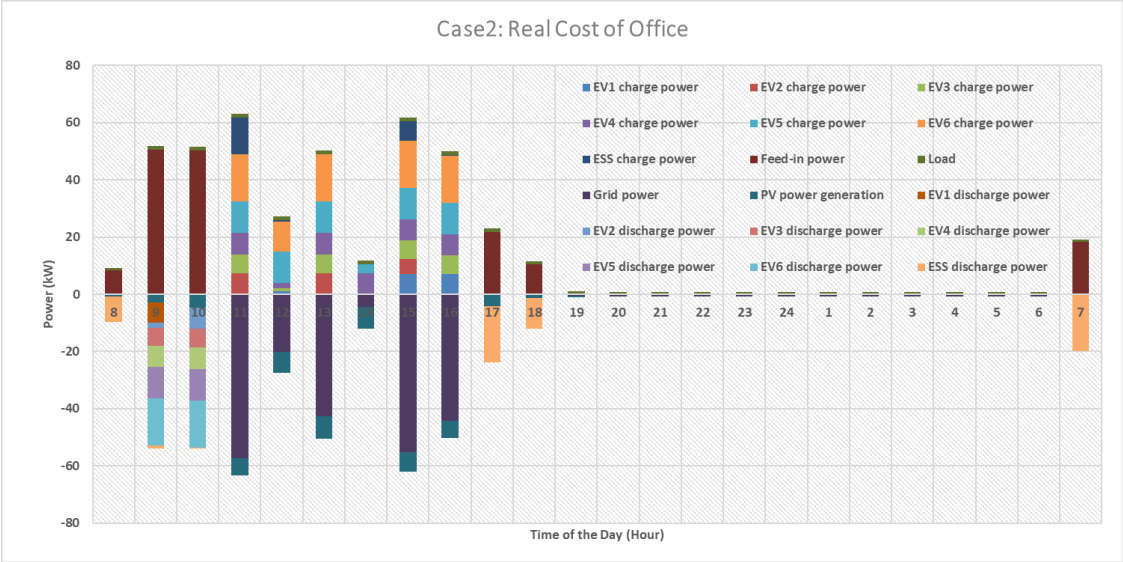

Figure 5.5: Power profile of the microgrid components-objective functions: the real cost of office (including energy cost and ESS degradation)

By taking into account the state of health of the EVs in case 3, which is illustrated in figure 5.6, EVs are charged with relatively lower powers and in a more uniform fashion throughout their stay time. This way, the SoC changes of EV batteries are smoothened to lower the degradation associated with charging attempts. Case 4 adds the charging cost of the EVs to the objective functions. This is to make sure that EV owners will not have to pay unreasonably high prices for

charging up their vehicles. In this case, which is illustrated in figure 5.7, the EV batteries are inclined towards charging with lower powers as time passes during the day. This is because energy prices are gradually increased towards the end of the day.

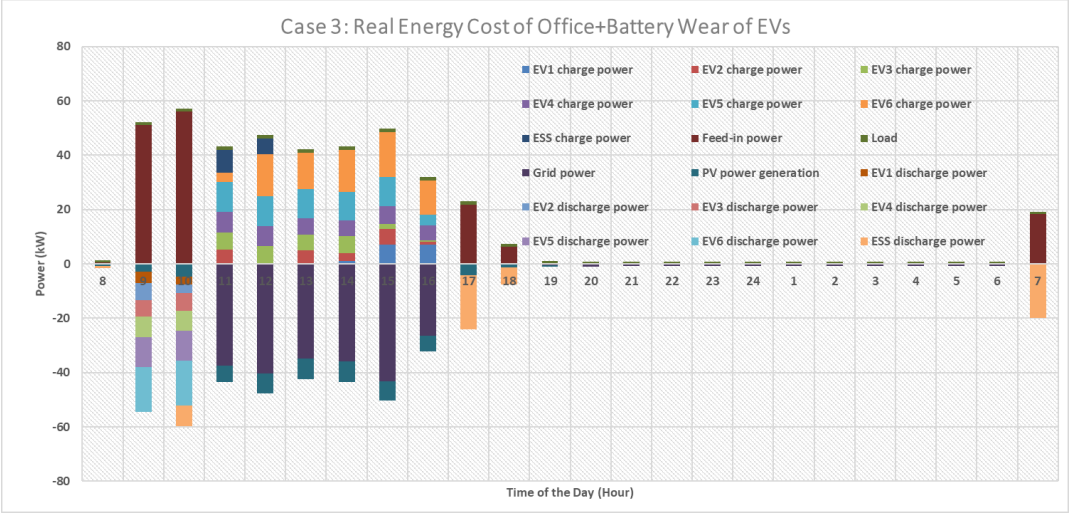

Figure 5.6: Power profile of the microgrid components-objective functions: the real cost of office and EV battery degradation

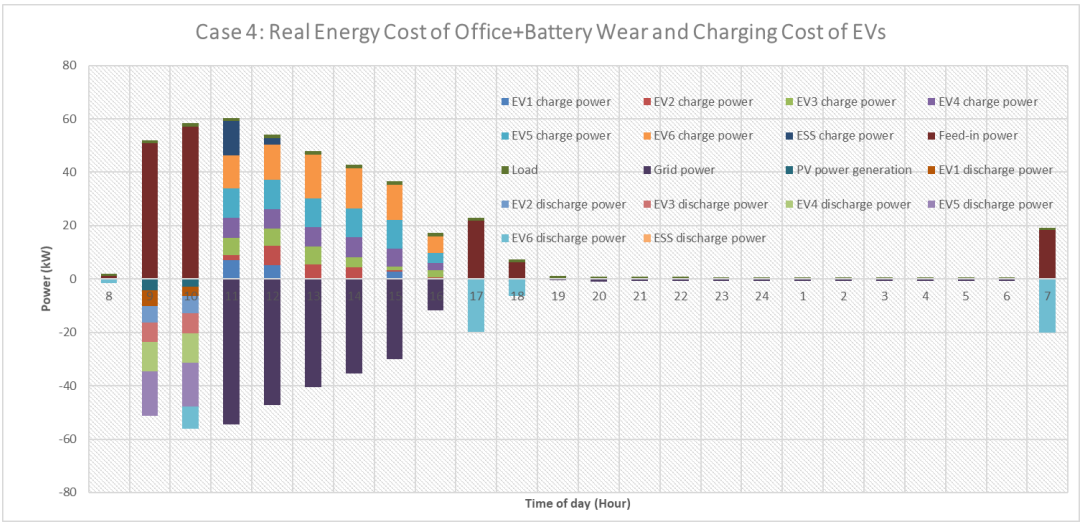

Figure 5.7: Power profile of the microgrid components-objective functions: the real cost of office, EV battery degradation, and charging cost of the EVs

Figure 5.8 shows the SoC variations of the ESS during the sample day. It shows that in the conventional case, the ESS is fully discharged to the minimum allowed limit and stays there for

four hours which could be highly detrimental to its state of health. However, in the other scenarios, as all of them take into account the degradation of ESS, the SoC trends do not show meaningful differences and they remain around the higher mid ranges most of the time during the day.

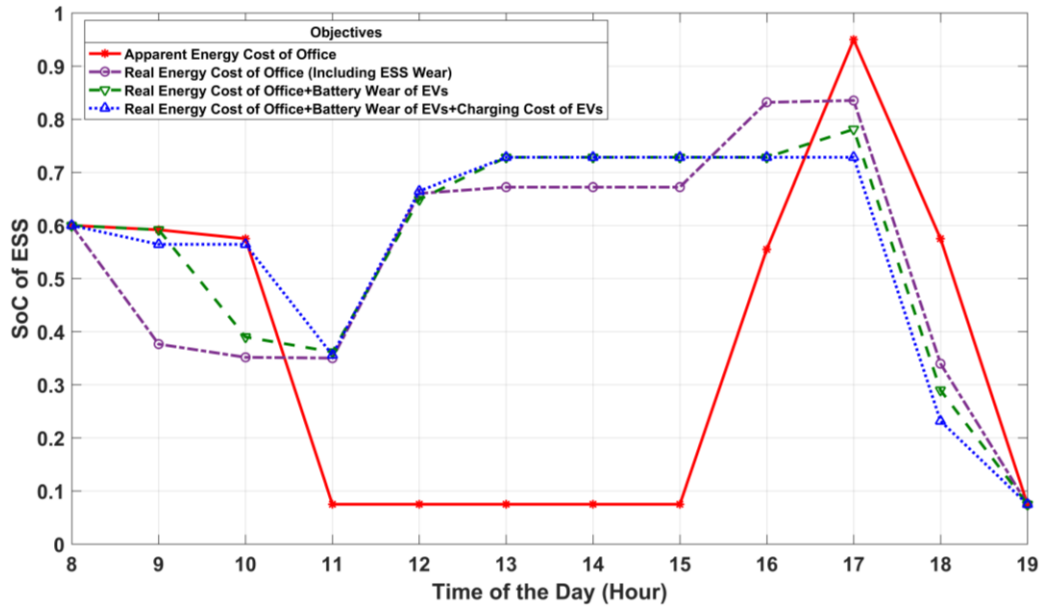

Figure 5.8: SoC variations of ESS for one day, under four different battery scheduling strategies

Figure 5.9 shows the SoC variations for one of the EV batteries (Smart ED) during the time of the workday. It shows that in the conventional case and the case that only takes into account the wear rate of ESS, the SoC of the EV battery spends four hours at the lowest level, and then within the last two hours it rises at a high speed to reach the desired level which leads to high DoDs during those hours. These trends can significantly impact the battery's lifetime. However, in the case that takes into account the battery wear of EVs (green line), the battery is discharged relatively slower and spends only one hour around low SoC levels and that is to contribute to the other objective which is the company's revenue. Then, it spends two hours around mid-range SoCs and in the last hours gradually reaches the final value. The last case which also takes into account the monetary interest of EV owners on top of the previous objectives (blue line) follows almost a similar trend, but it rises earlier during the hours when the energy price is cheaper to avoid having to charge

during the last hours when prices are higher. This approach helps lower the charging cost of the EV.

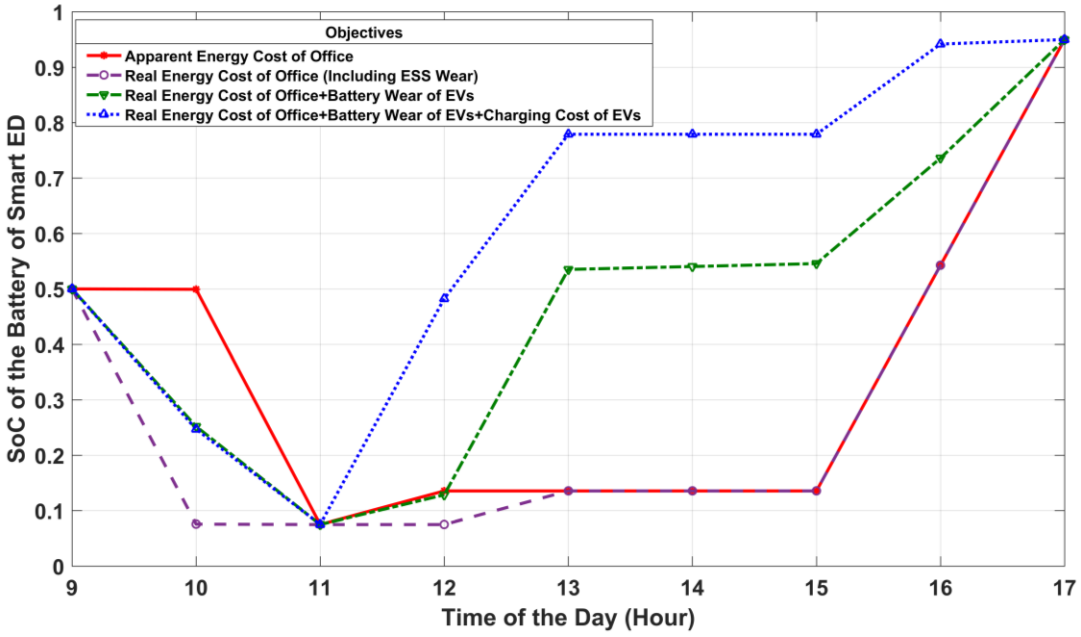

Figure 5.9: SoC variations of the battery of Smart ED for one day, under four different battery scheduling strategies

Now, the four scenarios are evaluated for a one-month sample period. To obtain the monthly test conditions, the daily load of the office which was acquired from [140] was varied with a gaussian distribution and 10% standard deviation. The PV irradiance, as well as the daily time-of-use energy prices, were also obtained from [102] and [141], respectively. Battery degradation, payable and total costs of the system operator and EV users will be studied in this section. Figure 5.10 and Table 5.2 show how large the capacity loss of a local energy storage system could become when its degradation is not addressed, as in a basic cycling strategy that merely considers the net energy cost. In fact, the capacity loss of ESS in the conventional case was almost 70% more than that of the other scenarios. The other three cases show insignificant wear differences as in those cases the SoC variations of ESS have high similarities.

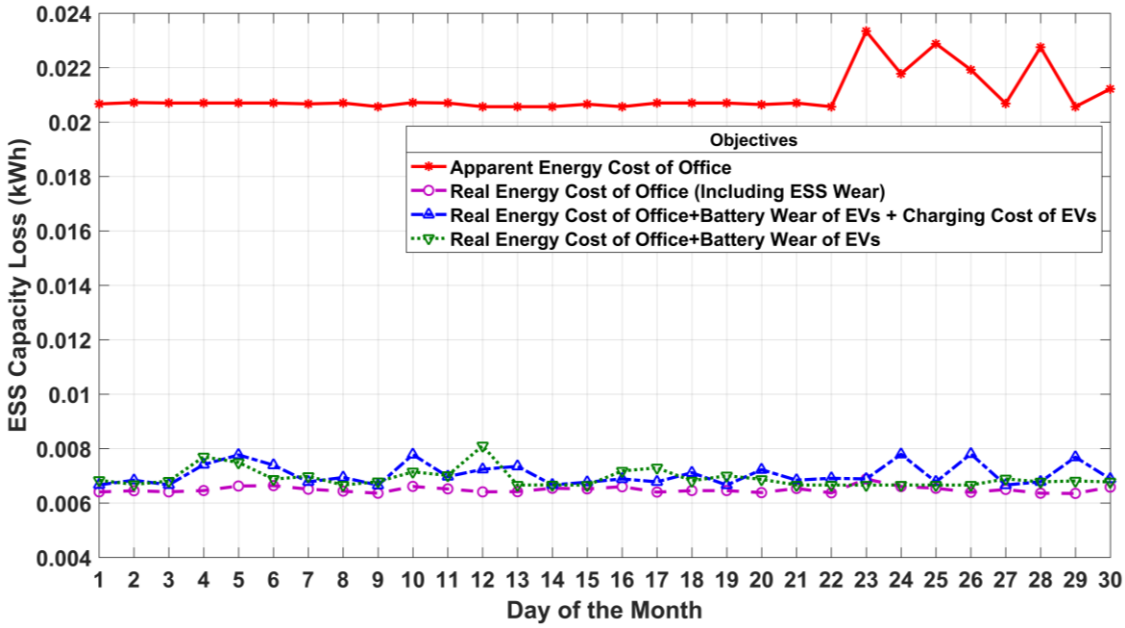

Figure 5.10: Daily capacity loss of ESS for one month, under four different battery scheduling strategies

Table 5.2: Capacity loss of office ESS for one month

Objective Set	Cost	Cost & ESS Deg	Cost & ESS+EV Deg	Cost & ESS+EV Deg & Charging Cost of EVs
Monthly Capacity Loss of ESS (kWh)	0.6295	0.1946	0.2073	0.2114

The payable cost of the system operator (e.g., business owner) is shown in figure 5.11 and table 5.3. It is seen that the minimum apparent cost is achieved when "cost" is the sole objective function of the problem. By incorporating other objective functions such as degradation of ESS and EVs, the apparent cost slightly increases. However, it is important to know that a slightly lower payable cost is achieved at a significantly larger real price. This graph also shows that as long as the ESS degradation is taken into account, incorporation of the EV battery wear does not increase the energy cost for the office in a meaningful way. Interestingly, the inclusion of EV battery wear only raised the apparent cost of office by 0.13%. This is important as it shows that overlooking the capacity

loss of the EV battery could not improve the revenues for the office considerably, however, it could significantly increase the costs for the EV users.

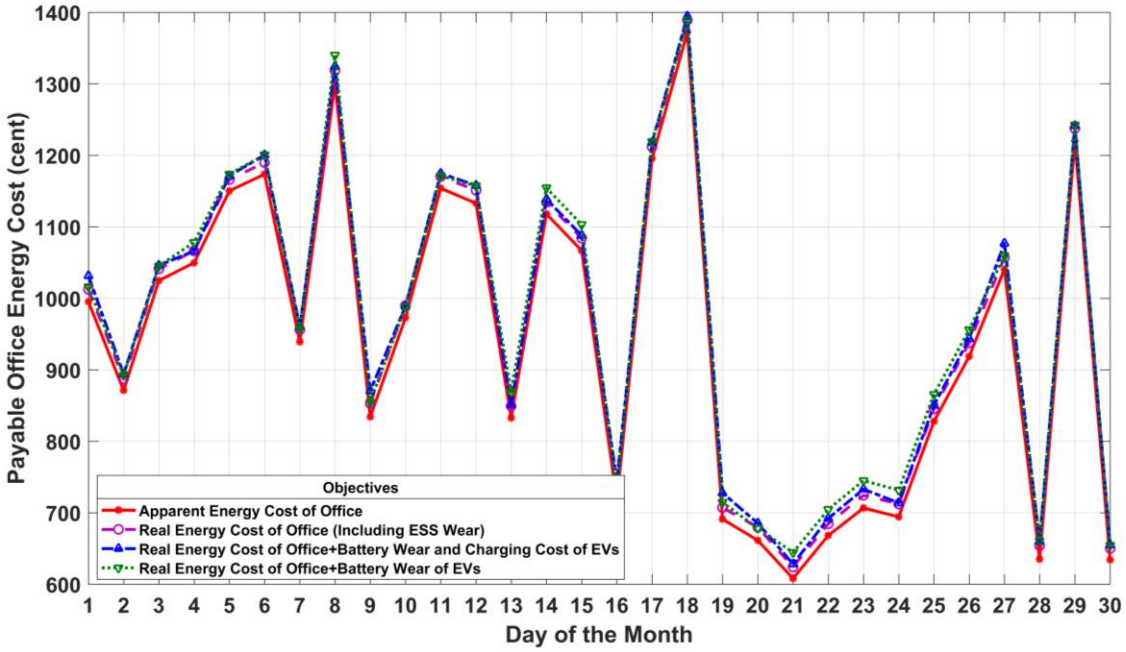

Figure 5.11: Daily energy cost of office for one month, under four different battery scheduling strategies

Table 5.3: Energy cost of office for one month

Objective Set	Cost	Cost & ESS Deg	Cost & ESS+EV Deg	Cost & ESS+EV Deg & Charging Cost of EVs
Payable Monthly Cost of Office ($)	282.06	287.16	289.99	289.26

The real net energy cost of the office which is demonstrated in figure 5.12 and table 5.4 also shows the impact of not including the ESS degradation into account, as the basic case shows the largest costs against its original intent. Only by including ESS wear in case 2, the monthly cost decreased by 11.7%. Another factor that could be taken into account in the total cost of the office is the operation cost of the PV system. To calculate the daily cost associated with the use of the PV system that will be added to the real daily cost, we have to calculate the Levelized Cost of Energy (LCOE)

for the PV system. This is the ratio of the total cost of the system by the total energy that is expected to be produced during the warrantied period as presented in equation (5.20). In this regard, first, we have to estimate the cost of the PV system. Assuming that the system has no cost of repair and maintenance during its lifetime, we employ the PV price of 2.4 $/W for Ontario, Canada which is taken from [143]. Therefore, the price of the 10 kW PV system will be $24000. Now, we have to specify how much energy will be produced in the total warrantied lifetime of the system. By using the PVWatts simulation tool [144], it was calculated that the annual generation of a regular 10 kW PV system is around 13050 kWh. The LCOE is obtained by the equation below assuming the warrantied lifetime of the system is 25 years.

$$LCOE = \frac{Total\ cost\ over\ lifetime}{Total\ generated\ energy\ over\ lifetime} \tag{5.20}$$

The calculated LCOE is 0.0735 dollars per kWh. Therefore, we could estimate the cost of the PV system per every day by using the equation (5.21). Table 5.4 provides the real cost of the office if the cost of the PV system is also considered.

$$\Gamma_{PV} = LCOE \times E_{PV,day\ n} \tag{5.21}$$

Where Γ_{PV} represents the cost associated with the operation of the PV system on day n and $E_{PV,day\ n}$denotes the generated energy of the PV system on day n.

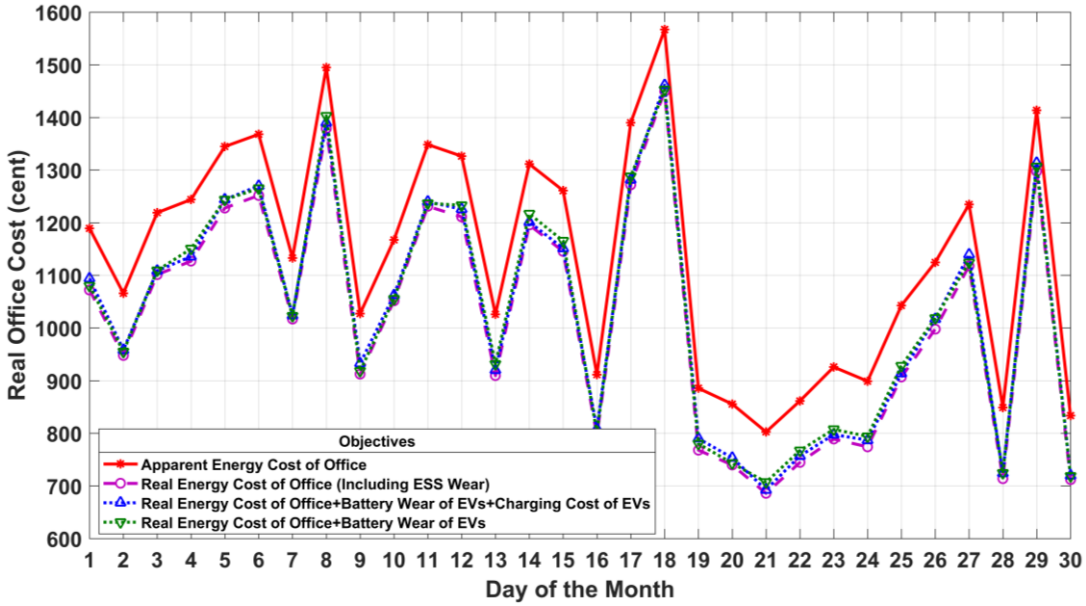

Figure 5.12: Daily real cost of office for one month, under four different battery scheduling strategies

Table 5.4: Real cost of office for one month

Objective Set	Cost	Cost & ESS Deg	Cost & ESS+EV Deg	Cost & ESS+EV Deg & Charging Cost of EVs
Real Monthly Cost of Office ($)	341.24	305.46	309.48	309.14
Real Monthly Cost of Office Including the Cost of PV ($)	412.06	376.28	380.30	379.96

Figure 5.13 provides a comparison between the consumed and feed-in energy of the building under the four studied scenarios. The largest amount of energy transaction with the grid occurs in the basic case as in this case, the energy system merely tends to achieve the minimum apparent energy cost by the maximum deployment of the microgrid components. The addition of ESS wear to the objective set lowered the total energy transaction by 8%. Also, by incorporating EV battery wear in the objectives the total transferred energy is further reduced by another 4% compared to case 2. This lower transferred energy is accompanied by less battery operation which leads to lower battery degradation and consequently lower cost of operation.

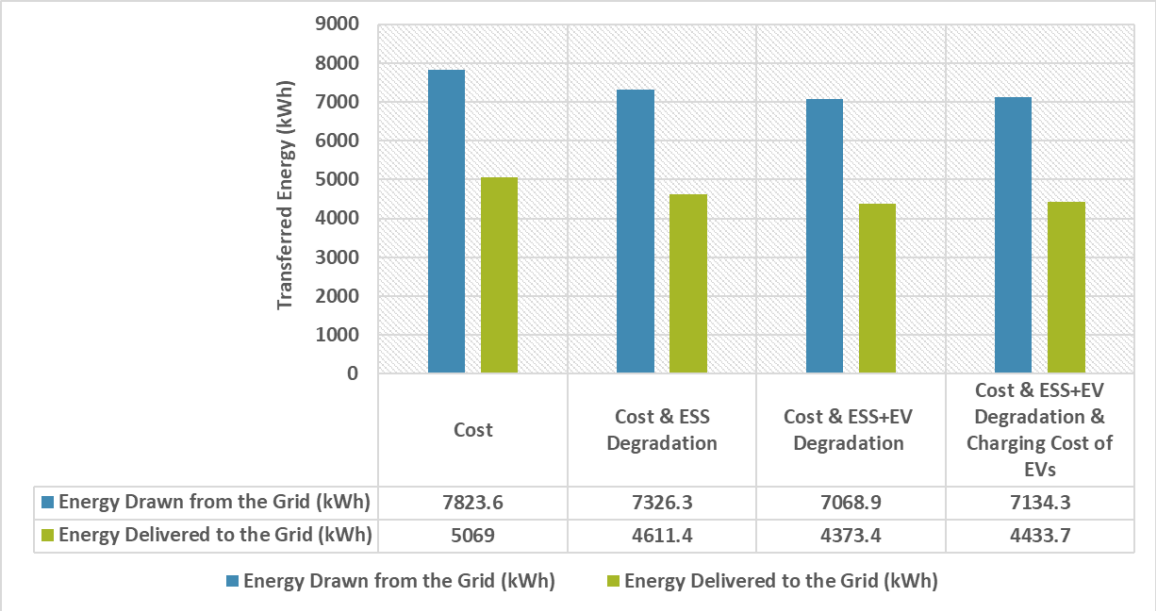

Figure 5.13: Monthly transferred energy of microgrid with the grid, under four different battery scheduling strategies

By taking into account the degradation of every single EV battery in the objective functions, the EV owners will benefit from a lower capacity loss of their batteries. Figure 5.14 shows the daily degradation chart over a month for one of the EVs (Tesla Model 3). It is seen that cases 1 and 2 that disregard the health of EV batteries lead to considerably larger wear rates, while cases 3 and 4 managed to save the battery capacities largely. A general comparison of the capacity losses of ESS and EV batteries has been provided in table 5.5. The data shows that by including the degradation factor of EVs into the models, the capacity loss of EVs decreased in the range of 13% to 27%. However, addressing the wear rate for ESS saved its capacity loss by around 70%. This significant impact on the SoH of ESS as compared to EVs can be attributed to the fact that, unlike EVs, the ESS does not have any commitment to become fully charged by a certain time. This commitment will lower the freedom of EV batteries in cycling events, while ESS can be freely cycled throughout the day for the best possible outcomes. Hence, different cycling strategies could impact ESS to a larger extent compared to EVs.

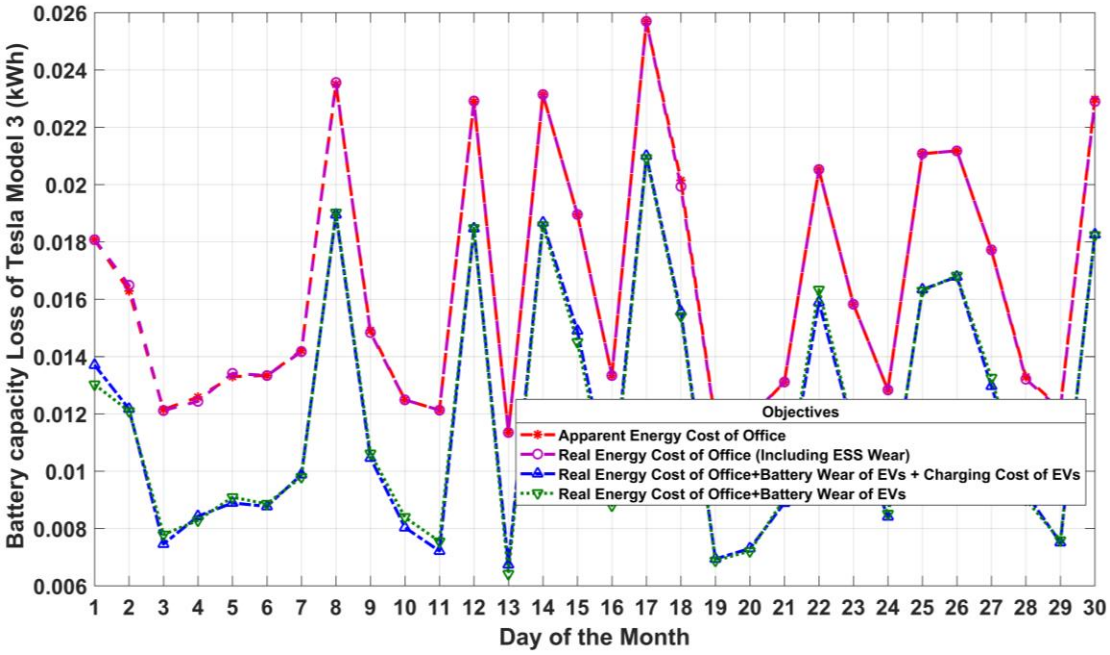

Figure 5.14: Daily capacity loss of the battery of Tesla Model 3 for one month, under four different battery scheduling strategies

Table 5.5: Capacity loss of ESS and EVs for one month

Monthly Capacity Loss (kWh)	Case 1	Case 2	Case 3	Case 4
ESS	0.6295	0.1946	0.2073	0.2114
Smart-ED	0.2072	0.2076	0.1794	0.1796
BMW-i3 (60Ah)	0.2808	0.2810	0.2405	0.2443
Nissan-Leaf	0.3649	0.3643	0.3063	0.3091
Opel-Corsa e	0.3452	0.3450	0.2564	0.2570
Tesla-Model 3	0.4927	0.4924	0.3582	0.3583
Tesla-Model S	0.8296	0.8295	0.6636	0.6641

Figure 5.15 and Table 5.6 illustrate the apparent or payable costs for EV owners under the four UC strategies. It shows that the incorporation of battery degradation, in general, will lower the apparent costs. This is due to the fact that consideration of battery wear will prevent unnecessary energy transactions with the grid which is essentially practiced to achieve the lowest energy expenses. In the studied scenarios, lowering the energy transactions through the involvement of EV battery

degradation showed to have a much larger impact on the payable cost of EV owners compared to the incorporation of "charging cost".

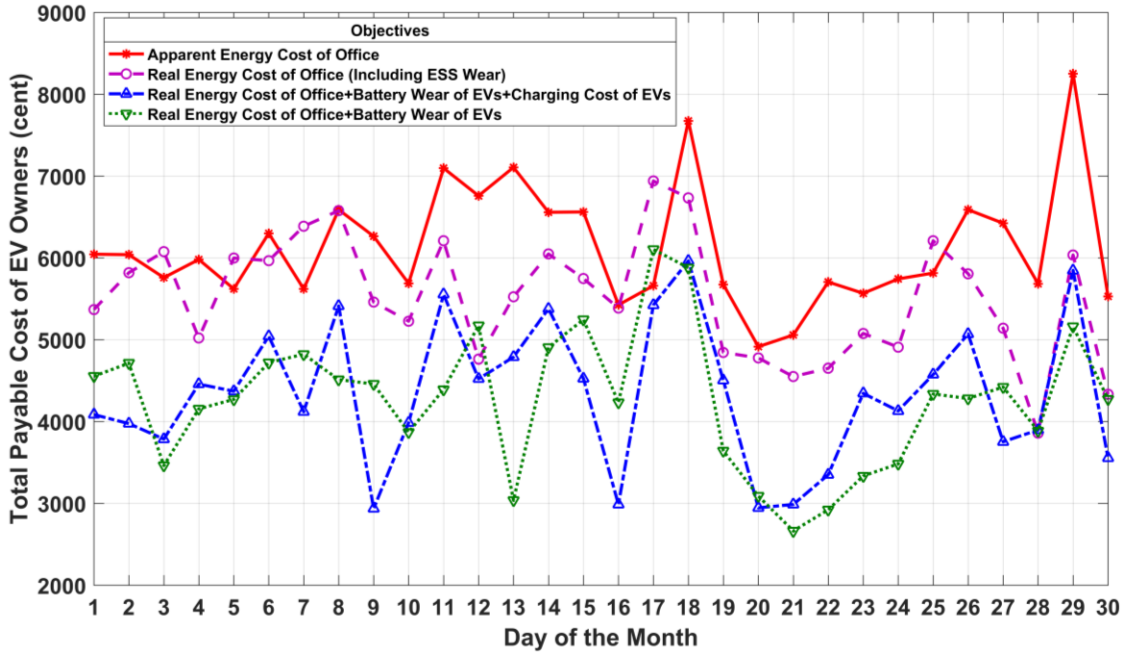

Figure 5.15: Daily total payable cost of EV owners for one month, under four different battery scheduling strategies

Table 5.6: Payable cost of EV owners for one month

Objective Set	Cost	Cost & ESS Deg	Cost & ESS+EV Deg	Cost & ESS+EV Deg & Charging Cost of EVs
Monthly Payable Cost for EV owners Combined ($)	1837	1654	1302	1280

Observing the real cost of EV owners as shown in figure 5.16 and table 5.7 again shows that the main factor to reduce the real expenses for EV users is addressing the health of their batteries in the problem. It is worth noting that depending on several factors such as energy tariffs (both buy and sell), battery prices, and the financial agreements between the company and EV owners, the real costs for EV owners could change in favor of case 3 or case 4. For example, in a scenario where the feed-in energy prices or the company's payment for V2B/V2G service is considerably

high, it may turn out that a more intense discharging regime is in favor of the EV owners even though it leads to higher degradation rates. In the investigated scenarios, the energy tariffs, as well as the company's monetary compensation for discharging EVs, were not sufficiently competitive in comparison with the battery prices to make it affordable for EV owners to make real financial gains from participating in a V2B service. In other words, in this case study, the battery degradation showed to be much more capable of impacting the real cost of an EV owner compared to the energy cost and revenues. However, different input data such as energy fees and battery prices could impact these results. The total costs for every single EV are also provided in figure 5.17. This figure shows that after the size of battery which determines how much energy it requires and directly impacts the costs, the battery scheduling strategy determines the final costs for EV owners.

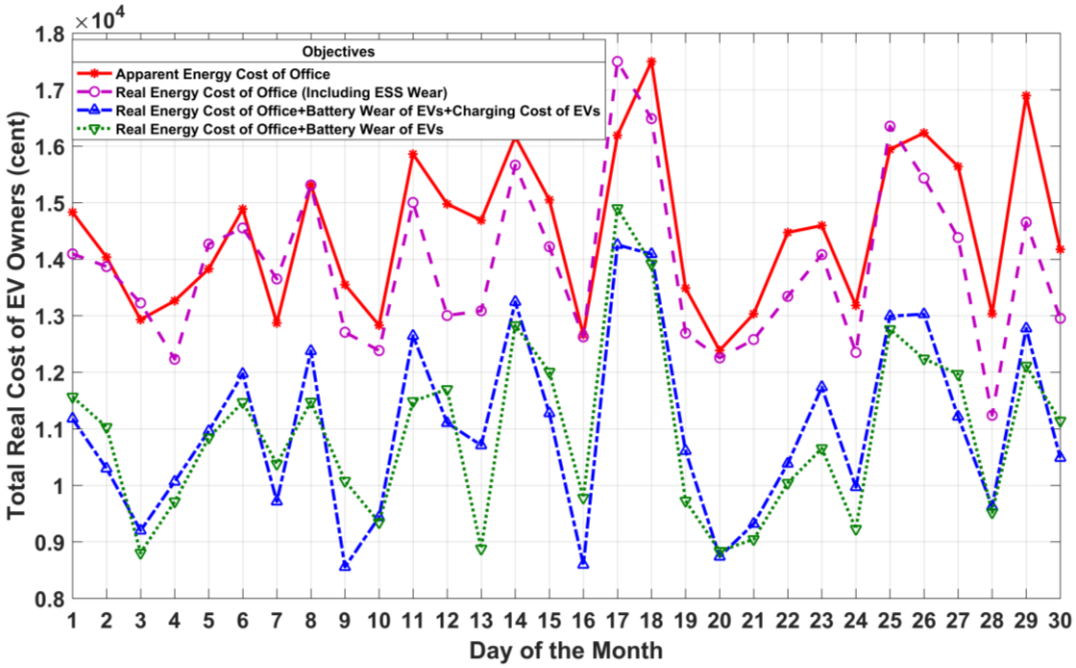

Figure 5.16: Daily real cost of EV owners for one month, under four different battery scheduling strategies

Table 5.7: Real cost of EV owners for one month

Objective Set	Cost	Cost & ESS Degradation	Cost & ESS+EV Degradation	Cost & ESS+EV Degradation & Charging Cost of EVs
Monthly Real Cost for EV owners Combined ($)	4345	4162	3274	3305

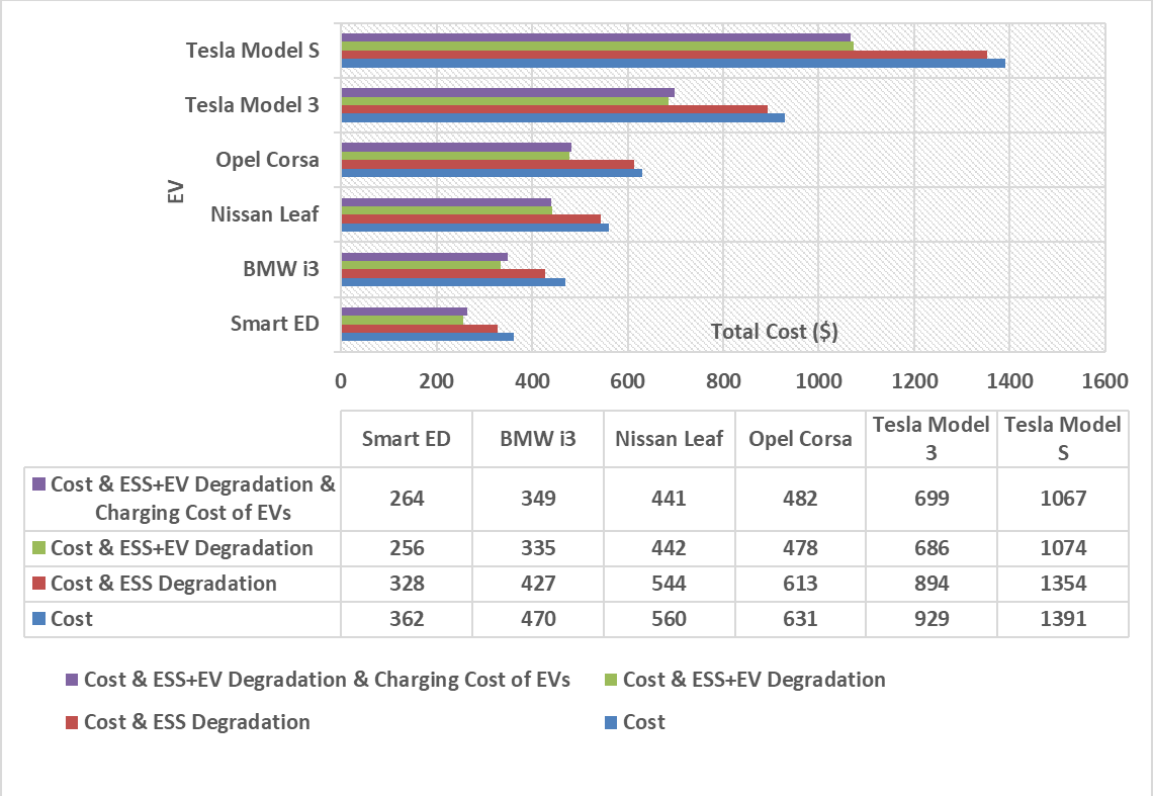

Figure 5.17: Total Monthly cost of every EV, under four different battery scheduling strategies

Grid operators and grid infrastructure are also other entities that could benefit from these UC strategies. Different UC approaches undermine the amount of power drawn from the grid during different times of the day as shown in figure 5.18. As before, the conventional approach led to the worst results in terms of peak power. The average daily peak power was considered as an index for evaluating the daily peak power of the building which is given in table 5.8. The basic case showed more than 21% larger average compared to the next large case which was case 2. Case 2 also causes

13% larger peak powers compared to cases 3 and 4 as it leads to more energy intake from the grid. However, the peak power difference in cases 3 and 4 was negligible as they do not have a significant difference in the amount of energy consumption from the grid.

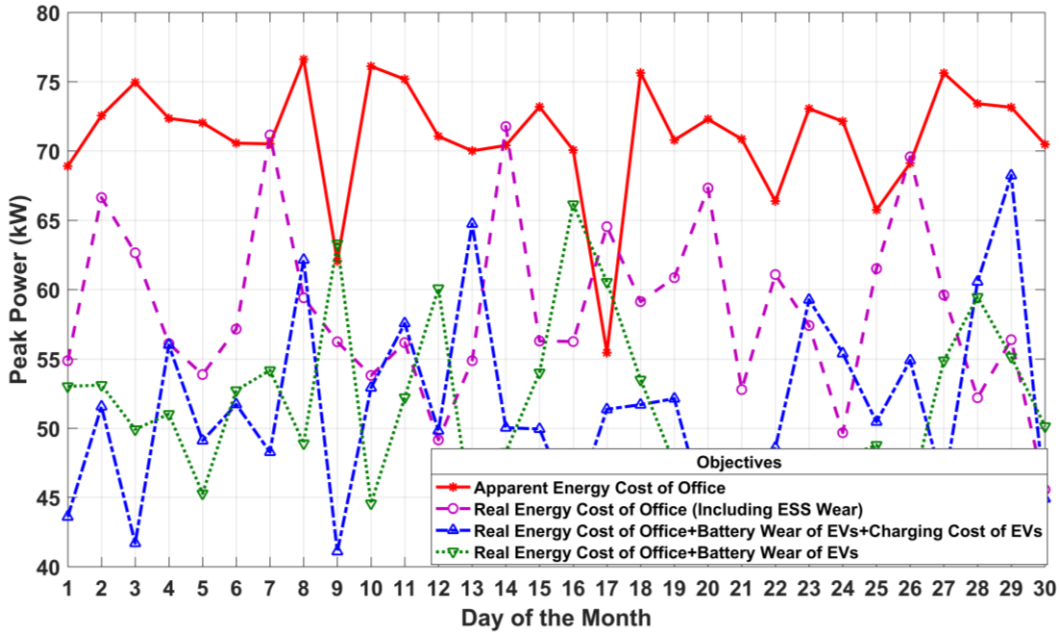

Figure 5.18: Daily peak power of office for one month, under four different battery scheduling strategies

Table 5.8: Average daily peak power of office for one month

Objective Set	Cost	Cost & ESS Deg	Cost & ESS+EV Deg	Cost & ESS+EV Deg & Charging Cost of EVs
Average Daily Peak Power of the Office building in a Month (kW)	71.02	58.46	51.44	51.55

When it comes to providing V2B or V2G service by electric vehicles, a common concern of EV owners is whether or not participating in these services is beneficial for them. There is always this legit concern that participating in a V2B/V2G service may degrade the battery's lifetime more than it could be financially beneficial. However, this concern can be addressed by utilizing the proposed UC algorithm. As a matter of fact, the proposed UC model can generate many useful data such as

capacity loss, cost of capacity loss, charging cost, discharged energy of batteries, discharging revenue of batteries, capacity loss caused by discharging events, payable, and real costs associated with cycling the batteries. This information can provide real insight for the users, helping them to employ their desirable cycling strategies. In this regard, to evaluate the worthwhileness of providing V2B service for EVs in this case study, a merit factor for evaluating the profitability of V2B service during any period has been defined as below.

$$\mathrm{Z}_{EV_m} = \frac{\mathrm{X}_{EV_m}}{\Upsilon_{EV_m}} \tag{5.22}$$

Where, Z_{EV_m} represents the discharge profitability factor for the m_{th} EV, X_{EV_m} denotes the discharging revenue of the m_{th} EV and Υ_{EV_m} is the discharge-associated cost of the m_{th} EV.

Then, this profitability factor was calculated for the six EVs of the case study and the results are provided in table 5.9. Higher compensations paid by the business owner for using the energy of EV batteries could lead to larger profitability factors and consequently, make participation in V2B service more appealing for EV owners.

Table 5.9: Profitability of V2B service for electric vehicles

V2B $\mathbf{Z}_{EV_m}$	Smart ED	BMW i3	Nissan Leaf	Opel Corsa	Tesla Model 3	Tesla Model S
Case 1	1.41	1.43	1.52	2.46	2.66	1.94
Case 2	1.29	1.30	1.34	2.16	2.34	1.70
Case 3	1.28	1.31	1.43	2.29	2.47	1.80
Case 4	1.26	1.30	1.41	2.28	2.46	1.79

Some other useful data regarding the revenues of office and EV owners are provided in table 5.10. Delivered energy to the grid is one of the items listed in this table. We can see that in case 1, the revenue from delivering energy to the grid is at the highest level followed by case 2. Case 4 shows

slightly higher energy transfer as achieving the best energy cost for EV owners is one of the objectives of that case. Regarding the revenue of EV owners from selling energy to the company, it is at the maximum level when the basic objective is in effect and the EV batteries are employed maximally. Case 1 also leads to the maximum revenue for the office from charging EVs, however, in the other cases that consider the battery wear and especially in cases 3 and 4, the office's revenue from charging EVs is at the lowest rate as EVs tend to limit their energy transactions and avoid unnecessary cycling attempts [142].

Table 5.10: Delivered energy to the grid, total V2B revenues, and office revenue from charging EVs for one month

Revenue ($)	Cost	Cost & ESS Deg	Cost & ESS+EV Deg	Cost & ESS+EV Deg & Charging Cost of EVs
Energy delivered to the grid	879	800	758	769
Combined V2B revenue of EV users	1642	1453	1522	1512
Office revenue from charging EVs	1837	1654	1280	1302

Chapter 6: Conclusion and Future Work

6.1.1 Conclusion

The optimal cycling of electric vehicle batteries and energy storage systems in different behind-the-meter applications was investigated in this thesis in the framework of mixed-integer programming (MIP). In this regard, different MIP models were developed to address the battery scheduling problem for household and workplace microgrids where EV and ESS are expected to be optimally cycled in cooperation with PV generation aiming at minimizing the costs and emissions. In order to minimize these two objectives realistically, battery degradation is a crucial factor to be incorporated into the optimization problems. Neglecting the battery degradation which has been traditionally practiced in many battery scheduling research works, could increase the capacity losses to the extent that any unscheduled or "scheduled" battery operation could end up largely detrimental and costly. Therefore, in this work, a battery degradation model was introduced to be employed in the MIP-based unit commitment (UC) models.

Chapter 1 as the introductory chapter was dedicated to the introduction of the research area including but not limited to the scope of work and the research contributions. In chapter 2, after introducing the concept of mixed-integer programming, a day-ahead mixed-integer-linear programming (MILP) battery scheduling model was presented for a residential unit with EV, ESS, PV array, controllable and non-controllable loads that form an AC-bus microgrid and work in a bidirectional market under dynamic pricing schemes. Then, the model was solved in the traditional fashion where the cost of energy was the sole objective function of the problem. The main applicable outcomes of this optimization problem were the "seemingly efficient" operation schedule of the EV battery, ESS, and controllable loads. The outcomes of this conventional UC model were later used for comparison with more sophisticated UC models in the next chapters.

Chapter 3 was focused on the battery degradation issue, battery degradation models, and incorporation of a wear model into a MIP UC problem. In this regard, first, the factors that can damage the Li-ion batteries as well as the main types of wear modeling approaches and the major semi-empirical wear models were introduced in this chapter. However, as optimal operation of batteries in microgrids normally necessitates consistent charging and discharging attempts between random SoCs, typical semi-empirical models cannot be incorporated into MIP-based UC models to address the battery degradation issue. Hence, a technology-agnostic semi-empirical battery wear model was introduced in this chapter that could address the irregular cycling of batteries. This model estimates the capacity loss of battery caused by DoD during an irregular half cycle with consideration of the initial and final SoCs of half-cycles and can be directly incorporated into a MIP model in its discrete version. The wear model employs the cycle life-DoD (*N(D)*) chart of batteries which is accessible for different battery chemistries.

Due to the highly nonlinear nature of a wear coefficient factor in the introduced wear model, a curve-fitting technique was suggested for simplifying the complex function of the wear coefficient to a simpler version so it can be handled by typical MIP solvers. Also, due to the dependence of *N(D)* on the C-rate and temperature of batteries during the measurement process, the impact of these two parameters was also discussed in this chapter. Next, the battery wear model was incorporated into the MIP model of chapter 2 in the context of new MIP wear constraints and objective functions. The carbon footprint of a microgrid was also discussed where energy consumption and battery wear were introduced as the two main sources of carbon footprint. As a result, seven different UC objective sets were introduced to the model, including minimization of apparent cost, battery degradation, emission, and combinations of these objectives. Therefore, the modified MIP UC model was then solved with those sets of objective functions for the same home example in one-day and one-month terms. Cost, battery degradation, and carbon footprint of the building were studied extensively to better understand how incorporating battery degradation

directly into the MIP model can affect the results. The carried-out case study demonstrated that by considering the battery degradation, the real monthly costs associated with the operation of a household microgrid could be decreased by 79%. Also, the monthly carbon footprint and capacity loss of batteries were reduced by 31% and 82% respectively.

Chapter 4 was dedicated to studying how intra-hourly scheduling resolution could impact the battery wear compared to the hourly resolution. In this regard, based on the previous MIP model, a dual-stage algorithm was proposed that scheduled batteries in a residential microgrid with hourly resolution in the first stage and 5-minute resolution in the second stage. Both cases were investigated while battery degradation was and was not taken into account in the MIP model. This study was carried out first using numerical simulation and then by using a controller-hardware-in-the-loop (C-HIL) setup, developed based on Typhoon-HIL 402 platform. The C-HIL results demonstrated that the capacity loss caused by hourly scheduling of EV battery was 72% of that of intra-hourly scheduling while this ratio was 33% for ESS. These results showed that smaller battery scheduling resolutions could lead to higher DoD-associated battery degradation. Also, under the 5-minute resolution, ignoring the battery wear led to a 62% and 118% rise in the capacity loss for EV battery and ESS respectively. As a result, the inclusion of the battery wear model demonstrated it could mitigate the degradation by preventing the batteries from cycling with large DoDs and going around extreme SoCs unless it is totally cost-efficient.

UC strategies in microgrids with multiple beneficiaries was the subject of chapter 5, where a UC model was produced and studied for a workplace with PV, ESS, and multiple EV chargers that serve the business and EV owners. Four different UC strategies were investigated and compared which benefited the business and EV owners to different extents. These strategies include the conventional UC model which only takes into account the apparent energy cost of a business owner, a scenario that aims at minimizing the real cost of a business owner, and two other scenarios that also take into account the interest of EV owners. The results showed that addressing the battery

wear managed to lower the costs of the microgrid operator and EV owners by 10.5% and 24% respectively. The capacity fade of electric vehicles decreased by 27% whereas ESS experienced a 69% decrease in capacity loss. These results could be helpful for microgrid operators in public places such as companies, universities, etc., to implement UC strategies in a fair fashion for the maximum benefit of themselves and the EV owners.

In conclusion, the MIP unit commitment models provided in this work could assist the residential and commercial microgrid operators to schedule the operation of stationary and automotive batteries and achieve minimal cost, carbon footprint, and capacity loss of all the involved batteries thanks to the provided battery degradation model.

6.1.2 Future Work

The relevant future research suggested by this work can be categorized into two areas as mentioned in the following.

- With regards to the certainty of the input variables, the BTM unit commitment problem can be investigated in the context of stochastic optimization, to address the random nature of the inputs such as solar irradiance, load, EV commuting times, and grid tariffs. This approach could be more robust towards the impact of input uncertainties as compared to the undertaken deterministic approach.
- Regarding the battery degradation model, the impact of the C-rate and temperature on the capacity loss could also be taken into account in the UC problem. By addressing these factors in the wear model and providing their corresponding MIP components, it may be feasible to use the upgraded UC model to schedule the EV batteries in fast-charging stations where EV batteries are more prone to be degraded by large charging currents and their thermal effects.

References

[1] Tushar, W., Yuen, C., Huang, S., Smith, D. B., & Poor, H. V. (2016). Cost minimization of charging stations with photovoltaics: An approach with EV classification. *IEEE Transactions on Intelligent Transportation Systems*, *17*(1), 156–169. https://doi.org/10.1109/tits.2015.2462824

[2] Saldaña, G., San Martin, J. I., Zamora, I., Asensio, F. J., & Oñederra, O. (2019). Electric vehicle into the grid: Charging methodologies aimed at providing ancillary services considering battery degradation. *Energies*, *12*(12), 2443. https://doi.org/10.3390/en12122443

[3] Salvatti, G., Carati, E., Cardoso, R., da Costa, J., & Stein, C. (2020). Electric Vehicles Energy Management with V2G/G2V multifactor optimization of smart grids. *Energies*, *13*(5), 1191. https://doi.org/10.3390/en13051191

[4] Kikusato, H., Mori, K., Yoshizawa, S., Fujimoto, Y., Asano, H., Hayashi, Y., Kawashima, A., Inagaki, S., & Suzuki, T. (2019). Electric vehicle charge–discharge management for utilization of photovoltaic by coordination between home and Grid Energy Management Systems. *IEEE Transactions on Smart Grid*, *10*(3), 3186–3197. https://doi.org/10.1109/tsg.2018.2820026

[5] Chandra Mouli, G. R., Kefayati, M., Baldick, R., & Bauer, P. (2019). Integrated PV charging of EV fleet based on energy prices, V2G, and offer of reserves. *IEEE Transactions on Smart Grid*, *10*(2), 1313–1325. https://doi.org/10.1109/tsg.2017.2763683

[6] Wu, X., Hu, X., Moura, S., Yin, X., & Pickert, V. (2016). Stochastic control of Smart Home Energy Management with plug-in Electric Vehicle Battery Energy Storage and Photovoltaic Array. *Journal of Power Sources*, *333*, 203–212. https://doi.org/10.1016/j.jpowsour.2016.09.157

[7] Kudoh, Y., Motose, R., Tahara, K., & Genchi, Y. (2013). A potential CO2 reduction of vehicle to home system from Life Cycle Perspective. *2013 World Electric Vehicle Symposium and Exhibition (EVS27)*. https://doi.org/10.1109/evs.2013.6914789

[8] Chaudhari, K., Ukil, A., Kumar, K. N., Manandhar, U., & Kollimalla, S. K. (2018). Hybrid optimization for economic deployment of ESS in PV-integrated EV charging stations. *IEEE Transactions on Industrial Informatics*, *14*(1), 106–116. https://doi.org/10.1109/tii.2017.2713481

[9] Turker, H., & Bacha, S. (2018). Optimal minimization of plug-in electric vehicle charging cost with vehicle-to-home and vehicle-to-grid concepts. *IEEE Transactions on Vehicular Technology*, *67*(11), 10281–10292. https://doi.org/10.1109/tvt.2018.2867428

[10] Salpakari, J., Rasku, T., Lindgren, J., & Lund, P. D. (2017). Flexibility of electric vehicles and space heating in net zero energy houses: An optimal control model with thermal dynamics and battery degradation. *Applied Energy*, *190*, 800–812. https://doi.org/10.1016/j.apenergy.2017.01.005

[11] Kandasamy, N. K., Kandasamy, K., & Tseng, K. J. (2017). Loss-of-life investigation of EV batteries used as smart energy storage for commercial building-based Solar Photovoltaic Systems. *IET Electrical Systems in Transportation*, *7*(3), 223–229. https://doi.org/10.1049/iet-est.2016.0056

[12] Alahyari, A., Fotuhi-Firuzabad, M., & Rastegar, M. (2014). Incorporating customer reliability cost in PEV charge scheduling schemes considering vehicle to home capability. *IEEE Transactions on Vehicular Technology*, 1–1. https://doi.org/10.1109/tvt.2014.2352413

[13] Erdinc, O., Paterakis, N. G., Mendes, T. D., Bakirtzis, A. G., & P. S. Catalao, J. (2015). Smart Household Operation Considering bi-directional EV and ESS utilization by real-time pricing-based dr. *IEEE Transactions on Smart Grid*, *6*(3), 1281–1291. https://doi.org/10.1109/tsg.2014.2352650

[14] Pal, S., & Kumar, R. (2018). Electric vehicle scheduling strategy in residential demand response programs with neighbor connection. *IEEE Transactions on Industrial Informatics*, *14*(3), 980–988. https://doi.org/10.1109/tii.2017.2787121

[15] Lopez, K. L., Gagne, C., & Gardner, M.-A. (2019). Demand-side management using Deep Learning for smart charging of electric vehicles. *IEEE Transactions on Smart Grid, 10*(3), 2683–2691. https://doi.org/10.1109/tsg.2018.2808247

[16] Van Roy, J., Leemput, N., Geth, F., Buscher, J., Salenbien, R., & Driesen, J. (2014). Electric vehicle charging in an office building microgrid with Distributed Energy Resources. *IEEE Transactions on Sustainable Energy*, *5*(4), 1389–1396. https://doi.org/10.1109/tste.2014.2314754

[17] Tushar, M. H., Zeineddine, A. W., & Assi, C. (2018). Demand-side management by regulating charging and discharging of the EV, ESS, and utilizing renewable energy. *IEEE Transactions on Industrial Informatics*, *14*(1), 117–126. https://doi.org/10.1109/tii.2017.2755465

[18] Ajao, A., Pourbabak, H., & Su, W. (2017). Operating cost optimization of interconnected nanogrids considering bidirectional effect of V2G and v2h. *2017 North American Power Symposium (NAPS)*. https://doi.org/10.1109/naps.2017.8107364

[19] Mbungu, N. T., Naidoo, R. M., Bansal, R. C., & Vahidinasab, V. (2019). Overview of the optimal smart energy coordination for microgrid applications. *IEEE Access*, *7*, 163063–163084. https://doi.org/10.1109/access.2019.2951459

[20] Knueven, B., Ostrowski, J., & Watson, J.-P. (2020). On mixed-integer programming formulations for the unit commitment problem. *INFORMS Journal on Computing*. https://doi.org/10.1287/ijoc.2019.0944

[21] Deckmyn, C., Van de Vyver, J., Vandoorn, T. L., Meersman, B., Desmet, J., & Vandevelde, L. (2017). Day-ahead unit commitment model for Microgrids. *IET Generation, Transmission & Distribution, 11*(1), 1–9. https://doi.org/10.1049/iet-gtd.2016.0222

[22] Byrne, R. H., Nguyen, T. A., Copp, D. A., Chalamala, B. R., & Gyuk, I. (2018). Energy Management and optimization methods for GRID Energy Storage Systems. *IEEE Access, 6*, 13231–13260. https://doi.org/10.1109/access.2017.2741578

[23] Paterakis, N. G., Erdinc, O., Pappi, I. N., Bakirtzis, A. G., & Catalao, J. P. (2016). Coordinated operation of a neighborhood of smart households comprising electric vehicles, energy storage and distributed generation. *IEEE Transactions on Smart Grid*, *7*(6), 2736–2747. https://doi.org/10.1109/tsg.2015.2512501

[24] Justo, J. J., Mwasilu, F., Lee, J., & Jung, J.-W. (2013). AC-microgrids versus DC-microgrids with Distributed Energy Resources: A Review. *Renewable and Sustainable Energy Reviews*, *24*, 387–405. https://doi.org/10.1016/j.rser.2013.03.067

[25] Al-Tameemi, Z. H., Lie, T. T., Foo, G., & Blaabjerg, F. (2021). Control strategies of DC Microgrids Cluster: A Comprehensive Review. *Energies*, *14*(22), 7569. https://doi.org/10.3390/en14227569

[26] Guerrero, J. M., Vasquez, J. C., & Teodorescu, R. (2009). Hierarchical control of droop-controlled DC and AC microgrids — a general approach towards standardization. *2009 35th Annual Conference of IEEE Industrial Electronics*. https://doi.org/10.1109/iecon.2009.5414926

[27] Nejabatkhah, F., & Li, Y. W. (2015). Overview of power management strategies of Hybrid AC/DC Microgrid. *IEEE Transactions on Power Electronics*, *30*(12), 7072–7089. https://doi.org/10.1109/tpel.2014.2384999

[28] Naghibi, B., Masoum, M. A., & Deilami, S. (2018). Effects of V2H integration on optimal sizing of renewable resources in smart home based on Monte Carlo Simulations. *IEEE Power and Energy Technology Systems Journal*, *5*(3), 73–84. https://doi.org/10.1109/jpets.2018.2854709

[29] Abdulgalil, M. A., Khalid, M., & Alismail, F. (2019). Optimal sizing of battery energy storage for a grid-connected microgrid subjected to wind uncertainties. *Energies*, *12*(12), 2412. https://doi.org/10.3390/en12122412

[30] Elsaraiti, M., & Merabet, A. (2022). Solar power forecasting using Deep Learning Techniques. *IEEE Access*, *10*, 31692–31698. https://doi.org/10.1109/access.2022.3160484

[31] Lago, J., Marcjasz, G., De Schutter, B., & Weron, R. (2021). Forecasting Day-Ahead electricity prices: A review of state-of-the-art algorithms, best practices and an open-access benchmark. *Applied Energy*, *293*, 116983. https://doi.org/10.1016/j.apenergy.2021.116983

[32] Lodwick, W., Jamison, D., & Russell, S. (n.d.). A comparison of fuzzy, stochastic and deterministic methods in linear programming. *PeachFuzz 2000. 19th International Conference of the North American Fuzzy Information Processing Society - NAFIPS (Cat. No.00TH8500)*. https://doi.org/10.1109/nafips.2000.877445

[33] Cardoso, G., Stadler, M., Chehreghani Bozchalui, M., Sharma, R., Marnay, C., Barbosa-Povoa, A., & Ferrao, P. (2013). Stochastic programming of vehicle to building interactions

with uncertainty in pevs driving for a medium office building. *IECON 2013 - 39th Annual Conference of the IEEE Industrial Electronics Society*. https://doi.org/10.1109/iecon.2013.6700407

[34] Norouzi, M., Aghaei, J., Pirouzi, S., Niknam, T., Fotuhi-Firuzabad, M., & Shafie-khah, M. (2021). Hybrid stochastic/robust flexible and reliable scheduling of secure networked microgrids with Electric Springs and electric vehicles. *Applied Energy*, *300*, 117395. https://doi.org/10.1016/j.apenergy.2021.117395

[35] Chen, Q., Liu, N., Hu, C., Wang, L., & Zhang, J. (2017). Autonomous Energy Management Strategy for solid-state transformer to integrate PV-assisted EV charging station participating in ancillary service. *IEEE Transactions on Industrial Informatics*, *13*(1), 258–269. https://doi.org/10.1109/tii.2016.2626302

[36] Paterakis, N. G., Erdinc, O., Bakirtzis, A. G., & Catalao, J. P. (2015). Optimal household appliances scheduling under day-ahead pricing and load-shaping demand response strategies. *IEEE Transactions on Industrial Informatics*, *11*(6), 1509–1519. https://doi.org/10.1109/tii.2015.2438534

[37] Pickering, B., Ikeda, S., Choudhary, R., & Ooka, R. (2016, May). Comparison of metaheuristic and linear programming models for the purpose of optimising building energy supply operation schedule. In *Proceedings of the 12th REHVA World Congress, Aalborg, Denmark* (pp. 22-25)

[38] González Vayá, M., Baringo, L., Krause, T., Andersson, G., Almeida, P. M. R., Geth, F., & Rapoport, S. (2015). EV aggregation models for different charging scenarios. In *23rd International Conference and Exhibition on Electricity Distribution (CIRED)*

[39] Yao, L., Damiran, Z., & Lim, W. H. (2017). Optimal charging and discharging scheduling for electric vehicles in a parking station with photovoltaic system and Energy Storage System. *Energies*, *10*(4), 550. https://doi.org/10.3390/en10040550

[40] Wang, S., Guo, D., Han, X., Lu, L., Sun, K., Li, W., Sauer, D. U., & Ouyang, M. (2020). Impact of battery degradation models on energy management of a grid-connected DC microgrid. *Energy*, *207*, 118228. https://doi.org/10.1016/j.energy.2020.118228

[41] Vallem, V. V., & Kumar, A. (2020). *retracted* : Optimal energy dispatch in microgrids with renewable energy sources and demand response. *International Transactions on Electrical Energy Systems*, *30*(5). https://doi.org/10.1002/2050-7038.12328

[42] Shemami, M. S., Alam, M. S., & Asghar, M. S. J. (2017). Load shedding mitigation through plug-in electric vehicle-to-home (V2H) system. *2017 IEEE Transportation Electrification Conference and Expo (ITEC)*. https://doi.org/10.1109/itec.2017.7993371

[43] Olivares, D. E., Mehrizi-Sani, A., Etemadi, A. H., Canizares, C. A., Iravani, R., Kazerani, M., Hajimiragha, A. H., Gomis-Bellmunt, O., Saeedifard, M., Palma-Behnke, R., Jimenez-Estevez, G. A., & Hatziargyriou, N. D. (2014). Trends in Microgrid Control. *IEEE Transactions on Smart Grid*, *5*(4), 1905–1919. https://doi.org/10.1109/tsg.2013.2295514

[44] Vermeer, W., Chandra Mouli, G. R., & Bauer, P. (2020). Real-time building smart charging system based on PV forecast and Li-ion battery degradation. *Energies*, *13*(13), 3415. https://doi.org/10.3390/en13133415

[45] Wu, X., Hu, X., Teng, Y., Qian, S., & Cheng, R. (2017). Optimal integration of a hybrid solar-battery power source into Smart Home nanogrid with plug-in electric vehicle. *Journal of Power Sources*, *363*, 277–283. https://doi.org/10.1016/j.jpowsour.2017.07.086

[46] Wi, Y.-M., Lee, J.-U., & Joo, S.-K. (2013). Electric vehicle charging method for smart homes/buildings with a photovoltaic system. *IEEE Transactions on Consumer Electronics*, *59*(2), 323–328. https://doi.org/10.1109/tce.2013.6531113

[47] Melhem, F. Y., Grunder, O., Hammoudan, Z., & Moubayed, N. (2017). Optimization and Energy Management in smart home considering photovoltaic, wind, and battery storage system with integration of electric vehicles. *Canadian Journal of Electrical and Computer Engineering*, *40*(2), 128–138. https://doi.org/10.1109/cjece.2017.2716780

[48] Eseye, A. T., Lehtonen, M., Tukia, T., Uimonen, S., & Millar, R. J. (2019). Optimal Energy Trading for renewable energy integrated building microgrids containing electric vehicles and energy storage batteries. *IEEE Access*, *7*, 106092–106101. https://doi.org/10.1109/access.2019.2932461

[49] Lin, C.-C., Deng, D.-J., Kuo, C.-C., & Liang, Y.-L. (2018). Optimal charging control of energy storage and electric vehicle of an individual in the internet of energy with energy trading. *IEEE Transactions on Industrial Informatics*, *14*(6), 2570–2578. https://doi.org/10.1109/tii.2017.2782845

[50] Ravichandran, A., Sirouspour, S., Malysz, P., & Emadi, A. (2018). A chance-constraints-based control strategy for microgrids with energy storage and Integrated Electric Vehicles. *IEEE Transactions on Smart Grid*, *9*(1), 346–359. https://doi.org/10.1109/tsg.2016.2552173

[51] van der Meer, D., Chandra Mouli, G. R., Morales-Espana Mouli, G., Elizondo, L. R., & Bauer, P. (2018). Energy Management System with PV power forecast to optimally charge EVs at the workplace. *IEEE Transactions on Industrial Informatics*, *14*(1), 311–320. https://doi.org/10.1109/tii.2016.2634624

[52] Kawashima, A., Sasaki, R., Yamaguchi, T., Inagaki, S., Ito, A., & Suzuki, T. (2015). Energy management systems based on real data and devices for apartment buildings. *IECON 2015 - 41st Annual Conference of the IEEE Industrial Electronics Society*. https://doi.org/10.1109/iecon.2015.7392595

[53] Badawy, M. O., & Sozer, Y. (2017). Power flow management of a grid tied PV-battery system for electric vehicles charging. *IEEE Transactions on Industry Applications*, *53*(2), 1347–1357. https://doi.org/10.1109/tia.2016.2633526

[54] Wang, W., Jiang, X., Su, S., Kong, J., Geng, J., & Cui, W. (2014). Energy management strategy for microgrids considering photovoltaic-energy storage system and electric vehicles. *2014 IEEE Conference and Expo Transportation Electrification Asia-Pacific (ITEC Asia-Pacific)*. https://doi.org/10.1109/itec-ap.2014.6941241

[55] Jiang, W., & Zhen, Y. (2019). A real-time EV charging scheduling for parking lots with PV system and Energy Store System. *IEEE Access*, *7*, 86184–86193. https://doi.org/10.1109/access.2019.2925559

[56] Mao, T., Zhou, B., & Zhang, X. (2019). Accommodating discharging power with consideration of both evs and ESS as commodity based on a two-level genetic algorithm. *IEEE Access*, *7*, 134804–134814. https://doi.org/10.1109/access.2019.2893773

[57] Rafique, M. K., Khan, S. U., Saeed Uz Zaman, M., Mehmood, K. K., Haider, Z. M., Bukhari, S. B., & Kim, C.-H. (2019). An intelligent hybrid energy management system for a smart house considering bidirectional power flow and various EV charging techniques. *Applied Sciences*, *9*(8), 1658. https://doi.org/10.3390/app9081658

[58] Liu, N., Chen, Q., Liu, J., Lu, X., Li, P., Lei, J., & Zhang, J. (2015). A heuristic operation strategy for commercial building microgrids containing evs and PV system. *IEEE Transactions on Industrial Electronics*, *62*(4), 2560–2570. https://doi.org/10.1109/tie.2014.2364553

[59] Turker, H., & Bacha, S. (2015). Application of housing peak shaving (HPS) algorithms with plug-in Hybrid Electric Vehicles (phevs): Impacts on the aging rate of low voltage transformer. *2015 IEEE Transportation Electrification Conference and Expo (ITEC)*. https://doi.org/10.1109/itec.2015.7165759

[60] Li, C., Luo, F., Chen, Y., Xu, Z., An, Y., & Li, X. (2017). Smart Home Energy Management with vehicle-to-home technology. *2017 13th IEEE International Conference on Control & Automation (ICCA)*. https://doi.org/10.1109/icca.2017.8003048

[61] Mahmud, K., Hossain, M. J., & Town, G. E. (2018). Peak-load reduction by coordinated response of photovoltaics, battery storage, and electric vehicles. *IEEE Access*, *6*, 29353–29365. https://doi.org/10.1109/access.2018.2837144

[62] Merabet, A., Al-Durra, A., & El-Saadany, E. F. (2022). Energy Management System for optimal cost and storage utilization of Renewable Hybrid Energy Microgrid. *Energy Conversion and Management*, *252*, 115116. https://doi.org/10.1016/j.enconman.2021.115116

[63] Toosi, H. E., Merabet, A., Ghias, A. M. Y. M., & Swingler, A. (2019). Central Power Management System for hybrid PV/Battery AC-bus microgrid using Typhoon Hil. *2019 IEEE 28th International Symposium on Industrial Electronics (ISIE)*. https://doi.org/10.1109/isie.2019.8781277

[64] Zhu, Z., Lambotharan, S., Chin, W. H., & Fan, Z. (2016). A mean field game theoretic approach to electric vehicles charging. *IEEE Access*, *4*, 3501–3510. https://doi.org/10.1109/access.2016.2581989

[65] Akshya, S., Ravindran, A., Srinidhi, A. S., Panda, S., & Kumar, A. G. (2017). Grid integration for electric vehicle and photovoltaic panel for a smart home. *2017 International Conference on Circuit, Power and Computing Technologies (ICCPCT)*. https://doi.org/10.1109/iccpct.2017.8074358

[66] Ekhteraei Toosi, H., Merabet, A., & Swingler, A. (2020). dual-layer power scheduling strategy for ev-ess-controllable load in bi-directional dynamic markets for low-cost implementation. *International Transactions on Electrical Energy Systems*, *31*(1). https://doi.org/10.1002/2050-7038.12681

[67] Berthold, F., Ravey, A., Blunier, B., Bouquain, D., Williamson, S., & Miraoui, A. (2015). Design and development of a smart control strategy for plug-in hybrid vehicles including vehicle-to-home functionality. *IEEE Transactions on Transportation Electrification*, *1*(2), 168–177. https://doi.org/10.1109/tte.2015.2426508

[68] Ju, C., Wang, P., Goel, L., & Xu, Y. (2018). A two-layer energy management system for microgrids with hybrid energy storage considering degradation costs. *IEEE Transactions on Smart Grid*, *9*(6), 6047–6057. https://doi.org/10.1109/tsg.2017.2703126

[69] Yan, Q., Zhang, B., & Kezunovic, M. (2019). Optimized operational cost reduction for an EV charging station integrated with battery energy storage and PV generation. *IEEE Transactions on Smart Grid*, *10*(2), 2096–2106. https://doi.org/10.1109/tsg.2017.2788440

[70] Eldeeb, H. H., Faddel, S., & Mohammed, O. A. (2018). Multi-objective optimization technique for the operation of grid tied PV powered EV charging station. *Electric Power Systems Research*, *164*, 201–211. https://doi.org/10.1016/j.epsr.2018.08.004

[71] Abronzini, U., Attaianese, C., D'Arpino, M., Di Monaco, M., & Tomasso, G. (2019). Cost minimization energy control including battery aging for Multi-Source EV charging station. *Electronics*, *8*(1), 31. https://doi.org/10.3390/electronics8010031

[72] Wang, T., O'Neill, D., & Kamath, H. (2015). Dynamic Control and optimization of Distributed Energy Resources in a Microgrid. *IEEE Transactions on Smart Grid*, *6*(6), 2884–2894. https://doi.org/10.1109/tsg.2015.2430286

[73] Schoch, J., Gaerttner, J., Schuller, A., & Setzer, T. (2018). Enhancing Electric Vehicle Sustainability through battery life optimal charging. *Transportation Research Part B: Methodological*, *112*, 1–18. https://doi.org/10.1016/j.trb.2018.03.016

[74] Abbasi, M. H., Taki, M., Rajabi, A., Li, L., & Zhang, J. (2019). Coordinated operation of Electric Vehicle Charging and wind power generation as a virtual power plant: A multi-stage risk constrained approach. *Applied Energy*, *239*, 1294–1307. https://doi.org/10.1016/j.apenergy.2019.01.238

[75] Shahkamrani, A., Askarian-abyaneh, H., Nafisi, H., & Marzband, M. (2021). A framework for day-ahead optimal charging scheduling of electric vehicles providing route mapping: Kowloon case study. *Journal of Cleaner Production*, *307*, 127297. https://doi.org/10.1016/j.jclepro.2021.127297

[76] Ghaderi, A., & Nassiraei, A. A. (2015). The economics of using electric vehicles for vehicle to building applications considering the effect of battery degradation. *IECON 2015 - 41st Annual Conference of the IEEE Industrial Electronics Society*. https://doi.org/10.1109/iecon.2015.7392654

[77] Sufyan, M., Rahim, N. A., Muhammad, M. A., Tan, C. K., Raihan, S. R. S., & Bakar, A. H. A. (2020). Charge coordination and battery lifecycle analysis of electric vehicles with V2G implementation. *Electric Power Systems Research*, *184*, 106307. https://doi.org/10.1016/j.epsr.2020.106307

[78] Schneider, S. F., Novak, P., & Kober, T. (2021). Rechargeable batteries for simultaneous demand peak shaving and price arbitrage business. *IEEE Transactions on Sustainable Energy*, *12*(1), 148–157. https://doi.org/10.1109/tste.2020.2988205

[79] Foggo, B., & Yu, N. (2018). Improved battery storage valuation through degradation reduction. *IEEE Transactions on Smart Grid*, *9*(6), 5721–5732. https://doi.org/10.1109/tsg.2017.2695196

[80] Nizami, M. S. H., Hossain, M. J., Amin, B. M. R., & Fernandez, E. (2020). A residential energy management system with bi-level optimization-based bidding strategy for day-ahead bi-directional electricity trading. *Applied Energy*, *261*, 114322. https://doi.org/10.1016/j.apenergy.2019.114322

[81] He, G., Chen, Q., Kang, C., Pinson, P., & Xia, Q. (2016). Optimal bidding strategy of battery storage in power markets considering performance-based regulation and Battery Cycle Life. *IEEE Transactions on Smart Grid*, *7*(5), 2359–2367. https://doi.org/10.1109/tsg.2015.2424314

[82] Farzin, H., Fotuhi-Firuzabad, M., & Moeini-Aghtaie, M. (2016). A practical scheme to involve degradation cost of lithium-ion batteries in vehicle-to-grid applications. *IEEE Transactions on Sustainable Energy*, *7*(4), 1730–1738. https://doi.org/10.1109/tste.2016.2558500

[83] Hoke, A., Brissette, A., Smith, K., Pratt, A., & Maksimovic, D. (2014). Accounting for lithium-ion battery degradation in electric vehicle charging optimization. *IEEE Journal of Emerging and Selected Topics in Power Electronics*, *2*(3), 691–700. https://doi.org/10.1109/jestpe.2014.2315961

[84] Shi, Y., Xu, B., Tan, Y., & Zhang, B. (2018). A convex cycle-based degradation model for battery energy storage planning and Operation. *2018 Annual American Control Conference (ACC)*. https://doi.org/10.23919/acc.2018.8431814

[85] Kolawole, O., & Al-Anbagi, I. (2019). Electric vehicles battery wear cost optimization for frequency regulation support. *IEEE Access*, *7*, 130388–130398. https://doi.org/10.1109/access.2019.2930233

[86] Gonçalves, Sofia.(2018). Feasibility study of an EV management system to provide Vehicle-to-Building considering battery degradation (thesis)

[87] Maheshwari, A., Paterakis, N. G., Santarelli, M., & Gibescu, M. (2020). Optimizing the operation of energy storage using a non-linear lithium-ion battery degradation model. *Applied Energy*, *261*, 114360. https://doi.org/10.1016/j.apenergy.2019.114360

[88] Preger, Y., Barkholtz, H. M., Fresquez, A., Campbell, D. L., Juba, B. W., Romàn- Kustas, J., Ferreira, S. R., & Chalamala, B. (2020). Degradation of commercial lithium-ion cells as a

function of chemistry and cycling conditions. *Journal of The Electrochemical Society*, *167*(12), 120532. https://doi.org/10.1149/1945-7111/abae37

[89] Han, S., Han, S., & Aki, H. (2014). A practical battery wear model for Electric Vehicle Charging Applications. *Applied Energy*, *113*, 1100–1108. https://doi.org/10.1016/j.apenergy.2013.08.062

[90] Wang, Y., Zhou, Z., Botterud, A., Zhang, K., & Ding, Q. (2016). Stochastic coordinated operation of wind and Battery Energy Storage System considering battery degradation. *Journal of Modern Power Systems and Clean Energy*, *4*(4), 581–592. https://doi.org/10.1007/s40565-016-0238-z

[91] Kuang, Y., Hu, M., Dai, R., & Yang, D. (2017). A collaborative decision model for electric vehicle to building integration. *Energy Procedia*, *105*, 2077–2082. https://doi.org/10.1016/j.egypro.2017.03.586

[92] Caner Taskin, Z., & Cole Smith, J. (2008). Tutorial guide to mixed-integer programming models and solution techniques. *Engineering and Management Innovation*. https://doi.org/10.1201/9780849305696.axa

[93] Pisaruk, N. N. (2019). Mixed Integer Programming: Models and Methods. *Minsk: BSU.*

[94] Berthold, T., Hendel, G., & Koch, T. (2016). The Three Phases of MIP Solving.

[95] *CS/ECE/Isye 524: Introduction to optimization - Laurent Lessard*. Laurent Lessard -. (2021, December 20). Retrieved May 10, 2022, from https://laurentlessard.com/teaching/524-intro-to-optimization/

[96] L. L. C. Gurobi Optimization, Gurobi Optimizer Reference Manual. 2020

[97] *Mixed-integer programming (MIP) - A Primer on the Basics*. Gurobi. (2022, January 13). Retrieved May 11, 2022, from https://www.gurobi.com/resource/mip-basics/

[98] Kumar, P.H., & Mageshvaran, R. (2020). Methods And Solvers Used For Solving Mixed Integer Linear Programming And Mixed Nonlinear Programming Problems: A Review. *International Journal of Scientific & Technology Research*, 9, 1872-1882.

[99] Islam, M. S., Mithulananthan, N., & Lee, K. Y. (2018). Suitability of PV and battery storage in EV charging at business premises. *IEEE Transactions on Power Systems*, *33*(4), 4382–4396. https://doi.org/10.1109/tpwrs.2017.2774361

[100] Ferruzzi, G., Graditi, G., Rossi, F., & Russo, A. (2015). Optimal operation of a residential microgrid: The role of Demand Side Management. *Intelligent Industrial Systems*, *1*(1), 61–82. https://doi.org/10.1007/s40903-015-0012-y

[101] *Live prices: ComEd's hourly pricing program*. ComEd. (n.d.). Retrieved May 11, 2022, from https://hourlypricing.comed.com/live-prices/

[102] *Solar radiation - hourly data for Ottawa (kanata - orléans)*. Amateur Weather Statistics for Ottawa (Kanata - Orléans), Ontario. (n.d.). Retrieved May 10, 2022, from https://ottawa.weatherstats.ca/charts/solar_radiation-hourly.html

[103] De Gennaro, M., Paffumi, E., Martini, G., Giallonardo, A., Pedroso, S., & Loiselle-Lapointe, A. (2020). A case study to predict the capacity fade of the battery of electrified vehicles in real-world use conditions. *Case Studies on Transport Policy*, *8*(2), 517–534. https://doi.org/10.1016/j.cstp.2019.11.005

[104] Ortega-Vazquez, M. A. (2014). Optimal scheduling of Electric Vehicle Charging and vehicle-to-grid services at household level including battery degradation and price uncertainty. *IET Generation, Transmission & Distribution*, *8*(6), 1007–1016. https://doi.org/10.1049/iet-gtd.2013.0624

[105] Wang, J., Purewal, J., Liu, P., Hicks-Garner, J., Soukazian, S., Sherman, E., Sorenson, A., Vu, L., Tataria, H., & Verbrugge, M. W. (2014). Degradation of lithium ion batteries employing graphite negatives and nickel–cobalt–manganese oxide + spinel manganese oxide positives: Part 1, aging mechanisms and life estimation. *Journal of Power Sources*, *269*, 937–948. https://doi.org/10.1016/j.jpowsour.2014.07.030

[106] Wang, D., Coignard, J., Zeng, T., Zhang, C., & Saxena, S. (2016). Quantifying electric vehicle battery degradation from driving vs. vehicle-to-grid services. *Journal of Power Sources*, *332*, 193–203. https://doi.org/10.1016/j.jpowsour.2016.09.116

[107] Neubauer, J., Smith, K., Wood, E., & Pesaran, A. (2015). *Identifying and overcoming critical barriers to widespread second use of PEV batteries* (No. NREL/TP-5400-63332). National Renewable Energy Lab.(NREL), Golden, CO (United States).

[108] Zhang, X., Guo, L., Guo, N., Zou, Y., & Du, G. (2021). Bi-level energy management of plug-in hybrid electric vehicles for fuel economy and battery lifetime with intelligent state-of-charge reference. *Journal of Power Sources*, *481*, 228798. https://doi.org/10.1016/j.jpowsour.2020.228798

[109] Xing Jin, Vora, A. P., Hoshing, V., Saha, T., Shaver, G. M., Wasynczuk, O., & Varigonda, S. (2017). Comparison of li-ion battery degradation models for system design and control algorithm development. *2017 American Control Conference (ACC)*. https://doi.org/10.23919/acc.2017.7962933

[110] Bishop, J. D. K., Axon, C. J., Bonilla, D., Tran, M., Banister, D., & McCulloch, M. D. (2013). Evaluating the impact of V2G services on the degradation of batteries in PHEV and EV. *Applied Energy*, *111*, 206–218. https://doi.org/10.1016/j.apenergy.2013.04.094

[111] Shadman Rad, M., Danilov, D. L., Baghalha, M., Kazemeini, M., & Notten, P. H. L. (2013). Adaptive thermal modeling of Li-Ion Batteries. *Electrochimica Acta*, *102*, 183–195. https://doi.org/10.1016/j.electacta.2013.03.167

[112] Millner, A. (2010). Modeling lithium ion battery degradation in electric vehicles. *2010 IEEE Conference on Innovative Technologies for an Efficient and Reliable Electricity Supply*. https://doi.org/10.1109/citres.2010.5619782

[113] Duggal, I., & Venkatesh, B. (2015). Short-term scheduling of thermal generators and battery storage with depth of discharge-based cost model. *IEEE Transactions on Power Systems*, *30*(4), 2110–2118. https://doi.org/10.1109/tpwrs.2014.2352333

[114] Jiang, J., Shi, W., Zheng, J., Zuo, P., Xiao, J., Chen, X., Xu, W., & Zhang, J.-G. (2013). Optimized operating range for large-format lifepo4/graphite batteries. *Journal of The Electrochemical Society*, *161*(3). https://doi.org/10.1149/2.052403jes

[115] Murashko, K., Pyrhonen, J., & Laurila, L. (2013). Three-dimensional thermal model of a lithium ion battery for hybrid mobile working machines: Determination of the model parameters in a pouch cell. *IEEE Transactions on Energy Conversion*, *28*(2), 335–343. https://doi.org/10.1109/tec.2013.2255291

[116] Zhang, C., Jiang, J., Gao, Y., Zhang, W., Liu, Q., & Hu, X. (2016). Polarization based charging time and temperature rise optimization for lithium-ion batteries. *Energy Procedia*, *88*, 675–681. https://doi.org/10.1016/j.egypro.2016.06.097

[117] Jafari, M., Gauchia, A., Zhao, S., Zhang, K., & Gauchia, L. (2018). Electric Vehicle Battery Cycle Aging Evaluation in real-world daily driving and vehicle-to-grid services. *IEEE Transactions on Transportation Electrification*, *4*(1), 122–134. https://doi.org/10.1109/tte.2017.2764320

[118] Gandoman, F. H., Ahmed, E. M., Ali, Z. M., Berecibar, M., Zobaa, A. F., & Abdel Aleem, S. H. (2021). Reliability evaluation of lithium-ion batteries for e-mobility applications from practical and technical perspectives: A case study. *Sustainability*, *13*(21), 11688. https://doi.org/10.3390/su132111688

[119] Tran, V. T., Islam, M. R., Muttaqi, K. M., & Sutanto, D. (2019). An efficient energy management approach for a solar-powered EV battery charging facility to support distribution grids. *IEEE Transactions on Industry Applications*, *55*(6), 6517–6526. https://doi.org/10.1109/tia.2019.2940923

[120] Ekhteraei Toosi, H., Merabet, A., & Swingler, A. (2022). Impact of battery degradation on energy cost and carbon footprint of Smart Homes. *Electric Power Systems Research*, *209*, 107955. https://doi.org/10.1016/j.epsr.2022.107955

[121] *Features & benefits specifications dimensions - batteryspace.com/aa ...* (n.d.). Retrieved May 10, 2022, from https://www.batteryspace.com/prod-specs/NCR18650B.pdf

[122] Hossain, M. A., Mahmud, M. R., & Pota, H. R. (2019). Optimal Energy scheduling of residential building with Battery Cost. *2019 9th International Conference on Power and Energy Systems (ICPES)*. https://doi.org/10.1109/icpes47639.2019.9105626

[123] Vatandoust, B., Ahmadian, A., Golkar, M. A., Elkamel, A., Almansoori, A., & Ghaljehei, M. (2019). Risk-averse optimal bidding of electric vehicles and energy storage aggregator in day-ahead frequency regulation market. *IEEE Transactions on Power Systems*, *34*(3), 2036–2047. https://doi.org/10.1109/tpwrs.2018.2888942

[124] Alam, M. J., & Saha, T. K. (2016). Cycle-life degradation assessment of battery energy storage systems caused by solar PV variability. *2016 IEEE Power and Energy Society General Meeting (PESGM)*. https://doi.org/10.1109/pesgm.2016.7741532

[125] Marano, V., Onori, S., Guezennec, Y., Rizzoni, G., & Madella, N. (2009). Lithium-Ion Batteries Life Estimation for plug-in Hybrid Electric Vehicles. *2009 IEEE Vehicle Power and Propulsion Conference*. https://doi.org/10.1109/vppc.2009.5289803

[126] Omar, N., Monem, M. A., Firouz, Y., Salminen, J., Smekens, J., Hegazy, O., Gaulous, H., Mulder, G., Van den Bossche, P., Coosemans, T., & Van Mierlo, J. (2014). Lithium iron phosphate based battery – assessment of the aging parameters and development of Cycle Life Model. *Applied Energy*, *113*, 1575–1585. https://doi.org/10.1016/j.apenergy.2013.09.003

[127] Elshurafa, & Aldubyan. (2019). State-of-charge effects on standalone solar-storage systems in hot climates: A case study in Saudi Arabia. *Sustainability*, *11*(12), 3471. https://doi.org/10.3390/su11123471

[128] Abronzini, U., Attaianese, C., D'Arpino, M., Di Monaco, M., Genovese, A., Pede, G., & Tomasso, G. (2016). Optimal Energy Control for smart charging infrastructures with ESS and reg. *2016 International Conference on Electrical Systems for Aircraft, Railway, Ship Propulsion and Road Vehicles & International Transportation Electrification Conference (ESARS-ITEC)*. https://doi.org/10.1109/esars-itec.2016.7841427

[129] *Lithium Iron Phosphate Battery – PowerTech systems*. PowerTech Systems - PowerTech Systems. (n.d.). Retrieved May 11, 2022, from https://www.powertechsystems.eu/home/tech-corner/lithium-iron-phosphate-lifepo4/

[130] Wirasanti, P., Srirattanawichaikul, W., & Premrudeepreechacham, S. (2018). Online SOC and battery life estimation: Results from filed test of Electric Bus Transit. *2018 21st International Conference on Electrical Machines and Systems (ICEMS)*. https://doi.org/10.23919/icems.2018.8549487

[131] Wikner, E., & Thiringer, T. (2018). Extending battery lifetime by avoiding high soc. *Applied Sciences*, *8*(10), 1825. https://doi.org/10.3390/app8101825

[132] *Frequently asked questions (faqs) - U.S. energy information administration (EIA)*. Frequently Asked Questions (FAQs) - U.S. Energy Information Administration (EIA). (n.d.). Retrieved May 10, 2022, from https://www.eia.gov/tools/faqs/faq.php?id=74&t=11

[133] Hall, D., & Lutsey, N. (2018). Effects of battery manufacturing on electric vehicle life-cycle greenhouse gas emissions.

[134] Romare, M., & Dahllöf, L. (2017). The life cycle energy consumption and greenhouse gas emissions from lithium-ion batteries.

[135] Newbauer, J., & Pesaran, A. (2010). *NREL's PHEV/EV Li-Ion Battery Secondary-Use Project* (No. NREL/CP-540-48042). National Renewable Energy Lab.(NREL), Golden, CO (United States).

[136] Saxena, S., Le Floch, C., MacDonald, J., & Moura, S. (2015). Quantifying EV battery end-of-life through analysis of travel needs with vehicle powertrain models. *Journal of Power Sources, 282*, 265–276. https://doi.org/10.1016/j.jpowsour.2015.01.072

[137] *Flatirons M2 Daily Raw Data: Field ids - midcdmz.nrel.gov*. (n.d.). Retrieved February 12, 2022, from https://midcdmz.nrel.gov/apps/rawid.pl?site=NWTC;start=20010824;yr=2021;mo=9;dy=4;sort=0

[138] Johnson, G., & Beausoleil-Morrison, I. (2017). Electrical-end-use data from 23 houses sampled each minute for simulating micro-generation systems. *Applied Thermal Engineering*, *114*, 1449–1456. https://doi.org/10.1016/j.applthermaleng.2016.07.133

[139] Typhoon HIL Real-time Hardware-in-the-Loop (HIL) simulation platform, Typhoon HIL Control Center Release 2019.1, Typhoon HIL, Inc. Somerville, Massachusetts, United States

[140] Mikulik, J. (2018). Energy Demand Patterns in an office building: A case study in Kraków (southern Poland). *Sustainability*, *10*(8), 2901. https://doi.org/10.3390/su10082901

[141] *Hydro one*. Hydro One. (n.d.). Retrieved May 10, 2022, from https://www.hydroone.com/rates-and-billing/rates-and-charges/electricity-pricing-and-costs

[142] Toosi, H. E., Merabet, A., Al-Durra, A., & Swingler, A. (2022). Optimal Battery Cycling Strategies in workplaces with Electric Vehicle Chargers, Energy Storage Systems and renewable energy generation. *IET Renewable Power Generation*, *16*(6), 1121–1133. https://doi.org/10.1049/rpg2.12376

[143] Rylan Urban. (2021, December 26). *Cost of solar power in Canada 2021*. energyhub.org. Retrieved May 11, 2022, from https://www.energyhub.org/cost-solar-power-canada/

[144] PVWatts Version 5 Manual. United States: N. p., 2014. Web.